

VOLUME 81

SEPTEMBER 8, 1977

NUMBER 18

JPCA_x

THE JOURNAL OF

PHYSICAL

CHEMISTRY



PUBLISHED BIWEEKLY BY THE AMERICAN CHEMICAL SOCIETY

THE JOURNAL OF PHYSICAL CHEMISTRY

BRYCE CRAWFORD, Jr., Editor
STEPHEN PRAGER, Associate Editor
ROBERT W. CARR, Jr., C. ALDEN MEAD, Assistant Editors

EDITORIAL BOARD: C. A. ANGELL (1973-1977), F. C. ANSON (1974-1978), V. A. BLOOMFIELD (1974-1978), J. R. BOLTON (1976-1980), L. M. DORFMAN (1974-1978), W. E. FALCONER (1977-1978), H. L. FRIEDMAN (1975-1979), H. L. FRISCH (1976-1980), W. A. GODDARD (1976-1980), E. J. HART (1975-1979), W. J. KAUZMANN (1974-1978), R. L. KAY (1977-1981), D. W. McCLURE (1974-1978), K. MYSELS (1977-1981), R. M. NOYES (1973-1977), R. G. PARR (1977-1979), W. B. PERSON (1976-1980), J. C. POLANYI (1976-1980), S. A. RICE (1976-1980), F. S. ROWLAND (1973-1977), R. L. SCOTT (1973-1977), W. A. STEELE (1976-1980), J. B. STOTHERS (1974-1978), F. A. VAN-CATLEDGE (1977-1981), B. WEINSTOCK (1977)

Published by the

AMERICAN CHEMICAL SOCIETY BOOKS AND JOURNALS DIVISION

D. H. Michael Bowen, Director

Marjorie Laflin, Assistant to the Director

Editorial Department: Charles R. Bertsch,
Head; Marianne C. Brogan, Associate
Head; Celia B. McFarland, Joseph E.
Yurvati, Assistant Editors

Magazine and Production Department:
Bacil Guiley, Head

Research and Development Department:
Seldon W. Terrant, Head

Advertising Office: Centcom, Ltd., 25 Sylvan
Road South, Westport, Conn. 06880.

Editorial Department at the ACS Easton
address.

Page charges of \$60.00 per page may be
paid for papers published in this journal.
Payment does not affect acceptance or
scheduling of papers.

Bulk reprints or photocopies of indi-
vidual articles are available. For information
write to Business Operations, Books and
Journals Division at the ACS Washington
address.

Requests for **permission to reprint**
should be directed to Permissions, Books and
Journals Division at the ACS Washington
address. The American Chemical Society and
its Editors assume no responsibility for the
statements and opinions advanced by con-
tributors.

Subscription and Business Information

1977 Subscription rates—including surface
postage

	U.S.	PUAS	Canada, Foreign
Member	\$24.00	\$33.00	\$34.00
Nonmember	96.00	105.00	106.00
Supplementary material	15.00	19.00	20.00

Air mail and air freight rates are avail-
able from Membership & Subscription Ser-
vices, at the ACS Columbus address.

New and renewal subscriptions should
be sent with payment to the Office of the
Controller at the ACS Washington address.
Changes of address must include both old
and new addresses with ZIP code and a recent
mailing label. Send all address changes to the
ACS Columbus address. Please allow six
weeks for change to become effective. **Claims
for missing numbers** will not be allowed if
loss was due to failure of notice of change of
address to be received in the time specified:

if claim is dated (a) North America—more
than 90 days beyond issue date, (b) all other
foreign—more than 1 year beyond issue date;
or if the reason given is "missing from files".
Hard copy claims are handled at the ACS
Columbus address.

Microfiche subscriptions are available
at the same rates but are mailed first class to
U.S. subscribers, air mail to the rest of the
world. Direct all inquiries to Special Issues
Sales, at the ACS Washington address or call
(202) 872-4554. **Single issues** in hard copy
and/or microfiche are available from Special
Issues Sales at the ACS Washington address.
Current year \$4.75. Back issue rates available
from Special Issues Sales. **Back volumes** are
available in hard copy and/or microform.
Write to Special Issues Sales at the ACS
Washington address for further information.
Microfilm editions of ACS periodical pub-
lications are available from volume 1 to the
present. For further information, contact
Special Issues Sales at the ACS Washington
address. **Supplementary material** men-
tioned in the journal appears in the microfilm
edition. Single copies may be ordered directly
from Business Operations, Books and Jour-
nals Division, at the ACS Washington ad-
dress.

	U.S.	PUAS,	Other
		Canada	Foreign
Microfiche	\$2.50	\$3.00	\$3.50
Photocopy			
1-7 pages	4.00	5.50	7.00
8-20 pages	5.00	6.50	8.00

Orders over 20 pages are available only on
microfiche, 4 × 6 in., 24X, negative, silver
halide. Orders must state photocopy or mi-
crofiche if both are available. Full biblio-
graphic citation including names of all au-
thors and prepayment are required. Prices
are subject to change.

© Copyright, 1977, by the American
Chemical Society. No part of this publication
may be reproduced in any form without
permission in writing from the American
Chemical Society.

Published biweekly by the American
Chemical Society at 20th and Northampton
Sts., Easton, Pennsylvania 18042. Second
class postage paid at Washington, D.C. and
at additional mailing offices.

Editorial Information

Instructions for authors are printed in
the first issue of each volume. Please conform
to these instructions when submitting man-
uscripts.

Manuscripts for publication should be
submitted to *The Journal of Physical
Chemistry*, Department of Chemistry, Uni-
versity of Minnesota, Minneapolis, Minn.
55455. Correspondence regarding **accepted
papers and proofs** should be directed to the

American Chemical Society
1155 16th Street, N.W.
Washington, D.C. 20036
(202) 872-4600

Member & Subscription Services
American Chemical Society
P.O. Box 3337
Columbus, Ohio 43210
(614) 421-7230

Editorial Department
American Chemical Society
20th and Northampton Sts.
Easton, Pennsylvania 18042
(215) 258-9111

Notice to Authors last printed in the issue of January 13, 1977

Volume 81, Number 18 September 8, 1977

JPCHAx 81(18) 1701-1794 (1977)

ISSN 0022-3654

- A Kinetic Study of the Gas Phase Formation and Decomposition Reactions of Nitrous Acid
 . . . **E. W. Kaiser*** and **C. H. Wu** 1701
- The Reaction of Thiolane with Hydrogen Atoms at High Temperature. H₂S Elimination from
 Chemically Activated 1-Butanethiol . . . **Osamu Horie,* Kaoru Onuki, and Akira Amano** 1706
- Temperature-Jump Rate Studies of the Association Reactions of Boric and Benzeneboronic Acids
 with Hydroxide Ion **O. Kajimoto, T. Saeki, Y. Nagaoka, and T. Fueno*** 1712
- Thermochemistry of Some Six-Membered Cyclic and Polycyclic Compounds Related to Coal
 . . . **Robert Shaw, David M. Golden,* and Sidney W. Benson** 1716
- Heats of Mixing of Tetraalkyltin Compounds: SnR₄ + SnR'₄
 . . . **Geneviève Delmas-Patterson* and Nguyen Thi Thanh** 1730
- The Partial Molal Volumes of Electrolytes in 0.725 *m* Sodium Chloride Solutions at 25 °C
 . . . **Frank J. Millero,* Arthur L. Laferriere, and Peter V. Chetirkin** 1737 ■
- Solubility of Iodine in Mixed Solvents. A Case Study of Preferential Solvation in Nonpolar and
 Associated Solutions **Koichiro Nakanishi* and Sotō Asakura** 1745 ■
- Photophenomena in Surfactant Media. Quenching of a Water-Soluble Fluorescence Probe by Iodide
 Ion in Micellar Solutions of Sodium Dodecyl Sulfate
 . . . **Frank H. Quina* and Vicente G. Toscano** 1750
- Lipoid pH Indicators as Probes of Electrical Potential and Polarity in Micelles
 . . . **Marta S. Fernández and Peter Fromherz*** 1755
- Hydrogenation of Ethylene over LaNi₅ Alloy **K. Soga,* H. Imamura, and S. Ikeda** 1762
- Interaction of *p*-Nitrosalicylic Acid with Ethylenediamine in the Presence of
 Cetyltrimethylammonium Bromide, Sodium Dodecyl Sulfate, Triton X 100, Polyethylene
 Glycol, and Their Binary Mixtures. A Proton Donor-Acceptor Equilibrium in Micellar Solution
 . . . **S. P. Moulik,* S. Ray, and A. R. Das** 1766
- Observation of Quasilinear Fluorescence Spectra (the "Shpol'skii Effect") in Matrix-Isolated
 Polycyclic Aromatic Hydrocarbons
 . . . **P. Tokousbalides, E. L. Wehry,* and Gleb Mamantov*** 1769
- The Position of the Reaction Site and the Relative Reactivities of Simple Outer- and Inner-Sphere
 Electrode Reactions. The Reduction of Some Cr(III) Amine Complexes at Mercury Electrodes
 . . . **Michael J. Weaver* and Thomas L. Satterberg** 1772
- Upper and Lower Bounds on the Thermal Conductivity of a Random, Two-Phase Material
 . . . **Antonio L. DeVera, Jr., and William Strieder*** 1783
- Superoxide Generation in the Photolysis of Aqueous Cadmium Sulfide Dispersions. Detection
 by Spin Trapping **John R. Harbour* and Michael L. Hair** 1791

11. SEP 25 1977

COMMUNICATIONS TO THE EDITOR

Anion Radical of 2-Chlorothiophene. A σ^* Radical Siro Nagai* and Tomas Gillbro 1793

■ Supplementary and/or miniprint material for this paper is available separately (consult the masthead page for ordering information); it will also appear following the paper in the microfilm edition of this journal.

* In papers with more than one author, the asterisk indicates the name of the author to whom inquiries about the paper should be addressed.

AUTHOR INDEX

Amano, A., 1706	Fueno, T., 1712	Laferriere, A. L., 1737	Ray, S., 1766
Asakura, S., 1745			
Benson, S. W., 1716	Gillbro, T., 1793	Mamantov, G., 1769	Saeki, T., 1712
	Golden, D. M., 1716	Millero, F. J., 1737	Satterberg, T. L., 1772
Chetirkin, P. V., 1737	Hair, M. L., 1791	Moulik, S. P., 1766	Shaw, R., 1716
Das, A. R., 1766	Harbour, J. R., 1791		Soga, K., 1762
Delmas-Patterson, G., 1730	Horie, O., 1706	Nagai, S., 1793	Strieder, W., 1783
DeVera, A. L., Jr., 1783	Ikeda, S., 1762	Nagaoka, Y., 1712	Thanh, N. T., 1730
	Imamura, H., 1762	Nakanishi, K., 1745	Tokousbalides, P., 1769
Fernández, M. S., 1755	Kaiser, E. W., 1701	Onuki, K., 1706	Toscano, V. G., 1750
Fromherz, P., 1755	Kajimoto, O., 1712	Quina, F. H., 1750	Weaver, M. J., 1772
			Wehry, E. L., 1769
			Wu, C. H., 1701

THE JOURNAL OF PHYSICAL CHEMISTRY

Registered in U. S. Patent Office © Copyright, 1977, by the American Chemical Society

VOLUME 81, NUMBER 18 SEPTEMBER 8, 1977

A Kinetic Study of the Gas Phase Formation and Decomposition Reactions of Nitrous Acid

E. W. Kaiser* and C. H. Wu

Chemistry Department, Engineering and Research Staff, Ford Motor Company, Dearborn, Michigan 48121 (Received March 25, 1977)

Publication costs assisted by the Ford Motor Company

The kinetics of the gas phase decomposition and formation reactions of nitrous acid, $2\text{HONO} = \text{NO} + \text{NO}_2 + \text{H}_2\text{O}$ (k_1, k_2), have been investigated in a Pyrex reactor at HONO partial pressures of 0.05–1.0 Torr and total pressures of 5–50 Torr using a mass spectrometer detector. The reactions were determined to be heterogeneous under all surface conditions tested. The best upper limits to the homogeneous rate constants at 300 K were $k_1 \leq 1 \times 10^{-20} \text{ cm}^3/\text{molecule s}$ and $k_2 \leq 4.4 \times 10^{-40} \text{ cm}^6/\text{molecule}^2 \text{ s}$. The kinetics of the heterogeneous reactions were examined, and a rate law is proposed.

I. Introduction

A knowledge of the kinetics of the formation and decomposition of nitrous acid (HONO) via the reactions

$$2\text{HONO} = \text{NO} + \text{NO}_2 + \text{H}_2\text{O} \quad (1)$$


is important in modeling the chemistry of the polluted atmosphere.¹ Studies of the kinetics of reaction 2, carried out using indirect detection techniques, have been published by Wayne and Yost² ($k_2 = 1.2 \times 10^{-34} \text{ cm}^6/\text{molecule}^2 \text{ s}$) and by Graham and Tyler³ ($k_2 = 3.3 \times 10^{-38} \text{ cm}^6/\text{molecule}^2 \text{ s}$). These results are in poor agreement and suggest the presence of a heterogeneous reaction. Recently, values of k_1 ($1 \times 10^{-18} \text{ cm}^3/\text{molecule s}$) and k_2 ($6 \times 10^{-38} \text{ cm}^6/\text{molecule}^2 \text{ s}$) have been determined by Chan et al.⁴ using direct detection of HONO by infrared spectroscopy. The value of Chan et al. agrees with that of Graham and Tyler, leading the former authors to suggest that their results are probably measurements of the homogeneous rate constants. However, Cox and Derwent⁵ have recently reported that the rate of decomposition of HONO at a concentration of 150 ppm is 10–15 ppm/h. This HONO decomposition rate is approximately 200 times slower than that predicted on the basis of the rate constant of Chan et al. and leads to the suspicion that all previous results have been subject to heterogeneous catalysis.

We have, therefore, undertaken a study of these reactions in an attempt to obtain better upper limits to the homogeneous rate constants, k_1 and k_2 , and to achieve a better understanding of the sensitivity of the reactions to surface catalysis. During the course of the experiments, we have also investigated the dependence of reactions 1 and 2 on the initial reactant concentrations.

II. Experimental Section

These experiments were performed in a static Pyrex reactor coupled to a quadrupole mass spectrometer which had an electron impact ion source. This detector permitted direct detection of both reactants and products at their respective parent masses. The reactor contents were directly sampled through a nozzle orifice in the reactor. The continuous sampling was observed to produce a pressure drop of approximately 3%/h in the reactor. This instrument and the fragmentation pattern of HONO have been described in detail previously.⁶

Equilibrium samples of HONO were prepared by mixing measured amounts of NO, NO₂, and H₂O in a 2-L Pyrex storage flask at total pressures ranging from 100 to 900 Torr. These mixtures were allowed to stand for at least 18 h prior to use in order to assure equilibration. The equilibrium HONO concentrations in these storage flasks were then calculated from the following equilibria using

the stated equilibrium constants at 300 K:



The decomposition rate of HONO was studied at 300 K using the following technique. An aliquot (5.5–50 cm³) of an equilibrium HONO mixture prepared as described above was injected into the 750-cm³ reactor. The superequilibrium HONO concentration, which is a result of the sample pressure decrease after injection, then decayed to the new equilibrium concentration determined by the above value of *K*. This method, therefore, provides a direct estimate of the rate of reaction 1. The rate of formation of HONO by reaction 2 was measured by a different technique. These experiments were carried out by pre-mixing measured pressures of NO and H₂O in the reactor and then injecting a known amount of NO₂ to initiate the formation reaction. In all of the above kinetic measurements, the HONO concentration was monitored at its parent mass (47 amu).

III. Results and Discussion

Initially, the effect of surface conditioning on the decomposition rate was studied. Successive measurements of the decay rate were carried out, and after each experiment, the resulting equilibrium mixture was allowed to remain in the reactor for several hours in order to passivate the surface of the reactor. Seasoning of the reaction vessel by this method gradually reduced the observed decomposition rate by approximately a factor of 25 compared to the initial measurements on the clean surface. These experiments proved that the reaction could be surface catalyzed. Ultimately, a rate of decomposition was achieved which was reproducible to ±10% during one day's experiments and to ±25% from day to day. Unless otherwise specified, all of the decomposition rate experiments to be described in succeeding paragraphs were carried out on this well-seasoned surface.

If the decomposition reaction were homogeneous on the well-seasoned surface and proceeded according to reactions 1 and 2, we might expect to observe the following kinetic rate law as used by Chan et al.⁴

$$0.5d(\text{HONO})/dt = -k_1(\text{HONO})^2 + k_2(\text{NO})(\text{NO}_2)(\text{H}_2\text{O}) \quad (\text{A})$$

in which

$$k_2 = k_1K$$

To test the validity of this rate law, HONO decomposition rates were measured using three sample aliquot sizes (5.5, 20, and 50 cm³) with the same initial sample mixture. Equation A predicts that under conditions of Figure 1 the ratio of the initial rate of reaction 1 to that of reaction 2 in a decomposition experiment should be 7.7, 19, and 60 for the 50, 20, and 5.5 cm³ aliquots, respectively. Thus, the rate of reaction 2 would be negligible in the initial stages of the decomposition, and we would expect the initial decay rate to follow essentially a second-order rate law with respect to the HONO concentration. Changing the aliquot size from 5.5 to 50 cm³ will increase the initial HONO concentration by a factor of 9, and this increase can be used to determine whether the initial decomposition rate exhibits a simple second-order dependence on the HONO concentration.

Figure 1 presents typical HONO decomposition curves obtained using these three aliquot sizes. The results are plotted in the form (HONO)/(HONO)₀ as a function of

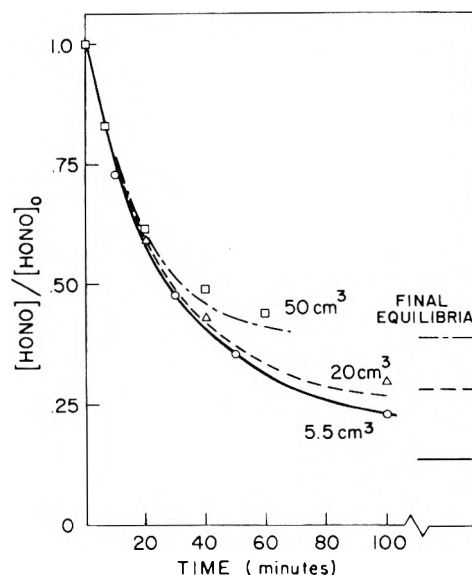


Figure 1. HONO decay rate as a function of sample aliquot size. The experimental data are presented as solid or dashed lines, while the computer generated fits are shown as individual points on these curves. The initial concentrations (Torr) of each compound after injection into the reactor were (for the 5.5 (O, —), 20 (Δ, ---), and 50 (□, ···) cm³ aliquots respectively): NO = 5.3, 18.6, 44.1; NO₂ = 0.37, 1.28, 3.0; H₂O = 0.072, 0.25, 0.59; HONO = 0.12, 0.43, 1.03. The rate constants, *k*₁ (× 10⁻²⁰ cm³/molecule s) and *k*₂ (× 10⁻⁴⁰ cm⁶/molecule² s), used to fit the data were, respectively, *k*₁ = 7.8, 2.3, 1.0; *k*₂ = 34.1, 10.0, 4.38. The calculated final equilibria are also presented.

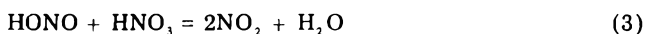
time; (HONO)₀ represents the nitrous acid concentration at *t* = 0. Rate eq A predicts that the observed plot of (HONO)/(HONO)₀ as a function of time for the 50-cm³ aliquot should have an initial slope 9 times greater than that observed for the 5.5-cm³ aliquot. In fact, the initial slopes for all three aliquots are identical. The curves do deviate from one another as the equilibria are approached. The calculated final equilibrium values for each aliquot are also presented in Figure 1 and are in agreement with the experimental data. This indicates that the kinetics cannot be explained by eq A but that the final equilibria are determined by the thermodynamics of reactions 1 and 2. It is likely that the lack of agreement with rate eq A is a result of the fact that the reaction is heterogeneous in the reactor even on the well-seasoned surface as will be discussed later.

The rate of diffusion to the walls could be controlling the heterogeneous reaction rate, resulting in the observed invariance of the slopes in Figure 1 with sample aliquot size since the total pressure also changes. In order to test this hypothesis, the total reactor pressure was varied by addition of N₂ during experiments using the 5.5-cm³ aliquot. Initially, the HONO decay rate was measured by injecting the HONO mixture alone at a total reactor pressure of 5.2 Torr. In the second experiment, the reactor was pressurized to 31 Torr with N₂ immediately after sample injection. Increasing the pressure by a factor of 6 reduced the decomposition rate by a factor of 1.7, indicating that the diffusion rate might be affecting the observed decomposition rate. However, the effect of total pressure on the reaction rate certainly cannot account for the observed invariance of the relative decay rates in Figure 1 over a factor of 9 in sample aliquot size.

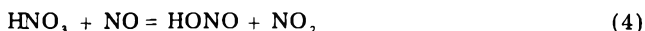
Even though the reaction is heterogeneous and does not obey rate eq A, we can calculate upper limits to the homogeneous rate constants, *k*₁ and *k*₂, by obtaining the best computer simulated fit to the observed data using eq A. The results of such calculations are included as individual points for each expansion aliquot in Figure 1. The smallest

upper limits can be obtained from the 50-cm³ aliquot data, and the fit to the data shows that the best upper limits at 300 K are $k_1 \leq 1 \times 10^{-20}$ cm³/molecule s and $k_2 \leq 4.4 \times 10^{-40}$ cm⁶/molecule² s. These upper limits are approximately 1/100 of the values measured by Chan et al.⁴ but are compatible with the HONO stability reported by Cox and Ferwent.⁵ Note that the computer simulation does not fit the data perfectly, particularly for the larger sample aliquots. This is expected since rate law A is not correct.

Previous experiments⁶ have demonstrated that two other reactions could affect the observed decomposition kinetics. The first of these reactions occurs between HONO and nitric acid, which is expected to reach a small steady state concentration:



The second reaction occurs between HNO₃ and NO by a mechanism which has not been established but possibly occurs via



followed by (3). Values of the forward reaction rates of (3) and (4) were obtained under the experimental conditions present during the decomposition studies.⁶ The reverse rates were estimated from calculated equilibrium constants. Model calculations indicated that the primary effect of these reactions would be to increase the HONO decomposition rate. This increase was calculated to be largest for the 50-cm³ aliquot (50% increase in the initial decay rate) and smallest for the 5.5-cm³ aliquot (6% increase in initial decay rate).

In the above calculations of the upper limits to k_1 and k_2 , reactions 3 and 4 were not included primarily because the reverse of reaction 4 is very speculative. Elimination of these reactions from the mechanism results in an increase in the calculated upper limits to the values of k_1 and k_2 by a factor of 2 or less. Thus, we expect that the upper limits quoted are conservative.

Because the HONO decomposition reaction does not follow rate eq A, we carried out a series of experiments designed to determine the dependence of the initial HONO decay rate on the concentrations of NO, NO₂, H₂O, and HONO. The effect of NO, NO₂, and H₂O concentrations was investigated by adding known amounts of one of these compounds to the reactor prior to the injection of the superequilibrium HONO sample from a 5.5-cm³ aliquot. In each case, a series of measurements of the decay rate with and without the addition of one of the compounds was obtained during one day in order to minimize the effect of surface changes on the rate studies. Representative results of this type are presented in Figures 2 and 3 for the variation of NO₂ and H₂O concentrations, respectively. In the NO₂ study, a different HONO equilibrium mixture, having a lower NO₂ concentration, was used in order to permit a large variation in initial NO₂ while minimizing the change in total pressure.

Figure 2 reveals that changing the NO₂ concentration by a factor of 6 produces very little change in the initial HONO decay rate. The rate was measured three times with and three times without additional NO₂ on the same day. The error bars in the figure show the data scatter observed. The sixfold increase in NO₂ pressure increased the decay rate by approximately 15%, which is only slightly greater than the observed data scatter. Model calculations indicate that this increase can be explained by the presence of reactions 3 and 4. Similar experiments performed with the addition of NO revealed that the initial HONO decay rate decreased by approximately 20% when

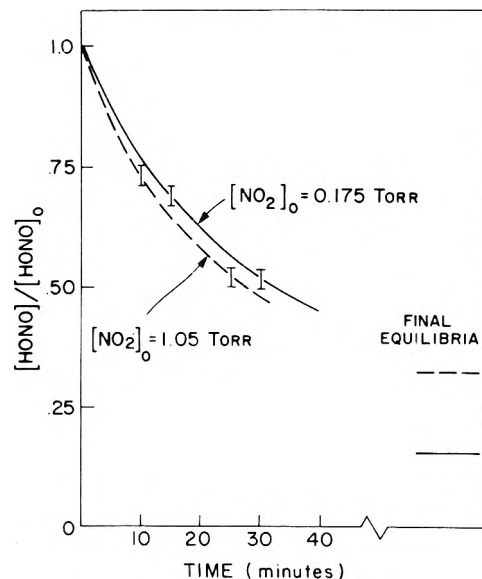


Figure 2. Effect of initial NO₂ concentration on the HONO decay rate (5.5-cm³ aliquot). The initial NO₂ concentrations were 0.175 and 1.05 Torr. The initial concentrations (Torr) of the remaining compounds for both sets of data were NO = 5.78, H₂O = 0.07, and HONO = 0.089. The error bars depict the data scatter observed during three experiments at each NO₂ concentration. The calculated final equilibria are also presented.

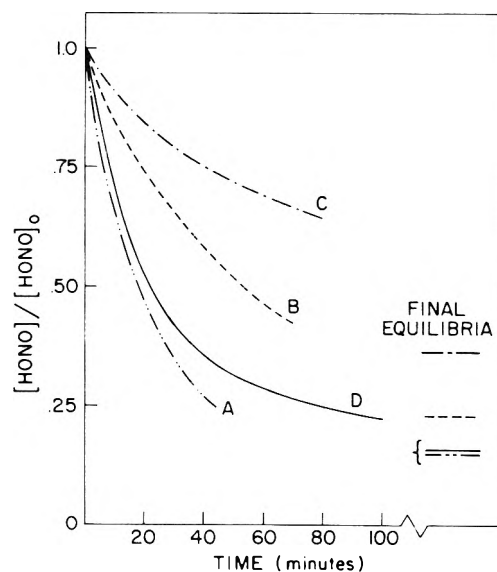


Figure 3. Effect of initial water concentration on the HONO decay rate (5.5-cm³ aliquot). The initial H₂O concentrations in the reactor were 0.07, 0.21, 0.59, and 0.07 Torr for curves A, B, C, and D, respectively. For all curves, the remaining initial concentrations (Torr) were NO = 5.0, NO₂ = 0.35, and HONO = 0.12. The experiments were performed in alphabetical order on one day. The calculated final equilibria are also presented.

NO was increased fourfold. The fact that the total pressure rises from 1.5 to 4.5 Torr when the NO concentration is increased can partially account for this decrease as previously explained. Thus, the effect of NO and NO₂ on the initial decomposition kinetics is small.

Because the reaction does not proceed to completion and because rate eq A has been shown to be incorrect even when modified by the addition of reactions 3 and 4, reaction 2 might be important even in the initial stages of the decomposition. Certainly, the final equilibrium concentration is changed when NO₂ is added as shown in Figure 2. If reaction 2 were important initially, we would expect that a large increase in the initial NO or NO₂ concentrations would result in a large decrease in the initial

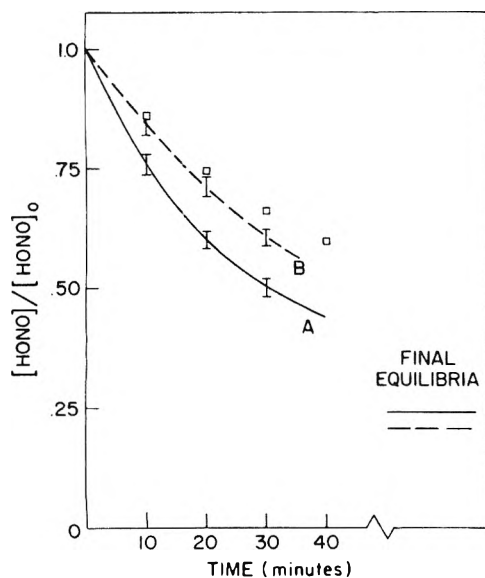


Figure 4. Effect of initial HONO concentration on the HONO decay rate (12.3-cm^3 aliquot). The initial HONO concentrations in the reactor were 0.31 and 0.148 Torr while the initial NO_2 concentrations were 0.92 and 0.17 Torr for curves A and B, respectively. In both experiments, the NO and H_2O concentrations were 13.3 and 0.18 Torr, respectively. The points (\square) show the position of curve B expected if the rate law were second order in HONO concentration. The data scatter observed during four experiments with each mixture are included as error bars. The calculated final equilibria are also presented.

HONO decay rate. The fact that a decrease is not observed provides strong evidence that under our conditions the initial rate of reaction 2 is much smaller than reaction 1 when the sample is injected from a 5.5-cm^3 aliquot. The 5.5-cm^3 aliquot was chosen for the concentration variation experiments in order to maximize the ratio of the initial to the final HONO concentration. This in turn minimizes the initial rate of reaction 2 relative to that of reaction 1.

In contrast to the above results, the effect of adding water vapor to the reactor is very pronounced as shown in Figure 3. Increasing the initial water concentration by a factor of 8 slows the initial decomposition rate by a factor of 4. This effect is reproducible and reversible as shown in the figure and verified during additional experiments. At the high water concentrations, the initial rate of reaction 2 will also be increased and could, therefore, contribute to the observed decrease in the decomposition rate. However, the magnitude of the increase in the rate of reaction 2 should be similar to that observed in the NO and NO_2 studies, and we have shown that this produces a negligible effect on the initial decomposition rate. We have also attempted to fit the data in Figure 3 using eq A with the inclusion of reactions 3 and 4. This rate law predicted only a 12% decrease in the initial HONO decay rate when the water concentration was increased by a factor of 8. Thus, we believe that the observed inverse dependence of the initial HONO decay rate on the water concentration is largely a result of an inverse water dependence in the rate law of reaction 1. This inverse dependence can partially account for the invariance of the initial slopes as a function of sample aliquot size presented in Figure 1. From the data in Figure 3, we calculate that the apparent kinetic order of the water concentration in reaction 1 is -0.6 over the indicated concentration range (0.07–0.56 Torr).

The kinetic order of the HONO concentration could not be easily determined in our experiments because we were using initially equilibrated mixtures as a source of HONO. Thus, changing the initial HONO concentration required significant changes in the concentration of one other

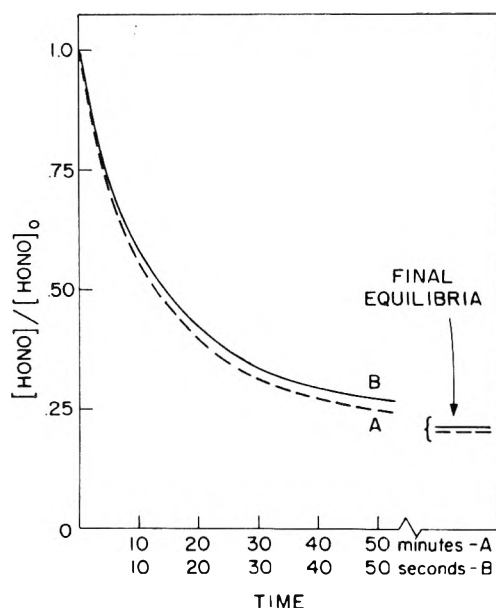


Figure 5. Effect of surface condition on the HONO decay rate (12.3-cm^3 aliquot) using the same initial HONO mixture. Curve A was obtained on the self-seasoned surface while curve B was obtained on the H_3BO_3 coated surface. Note the different time scales for the two curves. The calculated final equilibria are also presented.

reactant. Figure 4 presents data obtained from two sample mixtures differing in both HONO and NO_2 concentration. Four measurements of the decomposition rate were made with each mixture on the same day, and the data scatter is presented as error bars in the figure. The mixture containing low HONO and low NO_2 concentrations, curve B, shows a significantly smaller slope in the figure. The fact that the NO_2 concentration has been reduced by a factor of 5 should produce little effect as discussed previously. The data in Figure 4 show that the kinetic order of HONO is greater than 1 and slightly less than 2. The decay curve to be expected for a second-order dependence relative to curve A is presented as individual points (\square) in the figure.

In order to further investigate the effect of surface catalysis, the reactor was coated with a concentrated solution of H_3BO_3 dissolved in methanol. As shown in Figure 5, the decay rate after this coating procedure was approximately 56 times faster than the rate obtained on the mixture seasoned surface. However, the shape of the decay curves and the final equilibria are identical. This suggests that the reaction is being catalyzed but that the basic mechanism remains the same on both surfaces. Further support for this statement is provided by the observation that the effects of water concentration variation and of variation of sample aliquot size using the H_3BO_3 coated surface are identical with those observed on the self-seasoned surface. These results indicate that reactions 1 and 2 occur only by a heterogeneous mechanism in our reactor under all surface conditions.

The rate of formation of HONO was also directly investigated during this program by premixing measured quantities of NO and H_2O in the reactor and initiating the formation reaction by adding NO_2 . Only limited studies were carried out on the well-seasoned surface. Data obtained from this type of experiment on the well-seasoned surface are presented in Figure 6. Also included in the figure is the best computer-simulated fit to the data using rate eq A. From these data, an upper limit to the value of k_2 can be directly determined. This value $k_2 \leq 5 \times 10^{-39} \text{ cm}^6/\text{molecule}^2 \text{ s}$, is higher than the best upper limit determined from the decomposition studies combined with

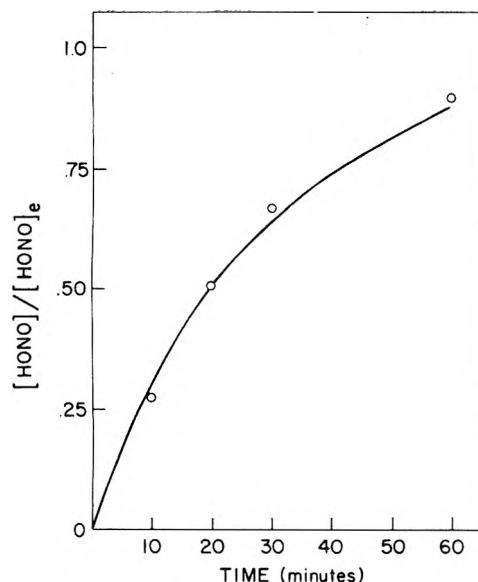


Figure 6. Rate of formation of HONO on the self-seasoned surface. $[\text{HONO}]_e$ represents the final equilibrium HONO concentration (0.056 Torr). The initial concentrations in the reactor (Torr) were $\text{NO} = 6.6$, $\text{NO}_2 = 1.1$, and $\text{H}_2\text{O} = 0.36$. The individual points (O) represent the best computer generated fit to the data using eq A and the rate constants $k_1 = 1.16 \times 10^{-19}$ cm³/molecule s, $k_2 = 5.1 \times 10^{-39}$ cm⁶/molecule² s.

the known equilibrium constants, but it is still a factor of 12 smaller than the value presented by Chan et al.⁴

No experiments were carried out during the formation rate studies to determine the kinetic order of the reactants on the well-seasoned surface. However, extensive measurements were performed on a surface having an activity approximately 15 times greater. We believe that these results also provide good information concerning the kinetic orders on the well-seasoned surface because, in the decomposition studies, we determined that the surface activity does not affect the basic reaction mechanism. Figure 7 presents the results obtained on the active surface by varying the initial water concentration by a factor of 9 while keeping the initial NO and NO₂ concentrations constant. The observed apparent kinetic order of the water concentration over the range 0.25–2.0 Torr is +0.43 as determined from these data. This order is much lower than the order of 2 reported in previous studies of the HONO formation rate carried out using indirect detection methods.^{2,3} Variation of the initial NO and NO₂ concentrations revealed apparent kinetic orders of 0.8 ± 0.2 for NO (3.5–10 Torr) and 1.0 ± 0.2 for NO₂ (0.3–0.8 Torr).⁸

IV. Conclusions

These experiments have shown that rate eq A cannot explain the observed kinetic data even with the addition of reactions 3 and 4. However, we believe that all of the data can be qualitatively explained by a heterogeneous rate law in which the rate-determining step is a reaction between adsorbed and gas phase molecules. The rate expression expected for such a kinetic process is⁹

$$\frac{1}{2} \frac{d(\text{HONO})}{dt} = \frac{-k_1'(\text{HONO})^2 + k_2'(\text{NO})(\text{NO}_2)(\text{H}_2\text{O})}{1 + a(\text{H}_2\text{O}) + b(\text{HONO}) + c(\text{NO}) + d(\text{NO}_2)}$$

in which a , b , c , and d are the adsorption equilibrium constants of the respective gases. If the concentration dependent terms in the denominator are substantially greater than 1, we would predict that the initial HONO

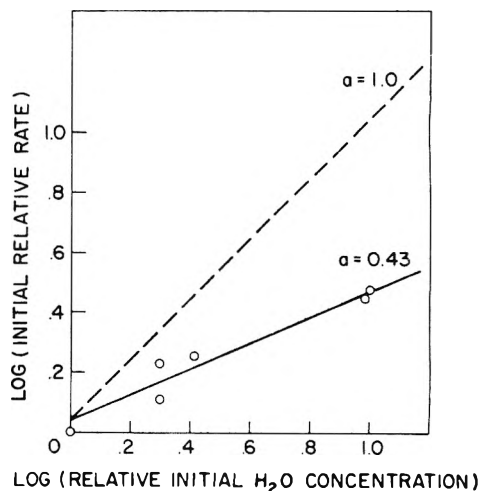


Figure 7. Initial rate of HONO formation relative to that observed at an initial H₂O concentration of 0.25 Torr as a function of initial H₂O concentration. Initial concentrations in the reactor (Torr) were $\text{NO} = 10.0$, $\text{NO}_2 = 0.9$, and $\text{H}_2\text{O} = 0.25\text{--}2.0$. The apparent kinetic order of H₂O is defined as a in the figure. The line for a first-order dependence ($a = 1$) is included for reference.

decomposition rate will be inversely proportional to sample pressure, in agreement with the data obtained during sample aliquot size variation (Figure 1). In addition, if H₂O and HONO are strongly adsorbed on the surface, an inverse water dependence in the initial decomposition rate and an apparent HONO kinetic order less than 2 are expected. Both of these effects are observed (Figures 3 and 4). Furthermore, the rate of the formation reaction should exhibit a water kinetic order less than unity, again in agreement with the observed data (Figure 7). The fact that the apparent kinetic orders of NO and NO₂ are near zero in the decomposition studies and near unity in the formation studies suggests that the term $c(\text{NO}) + d(\text{NO}_2)$ is small. This indicates that neither NO nor NO₂ are strongly adsorbed on the active surface sites.

The results which we have obtained show that the upper limits to the homogeneous rate constants, k_1 and k_2 , are at least a factor of 100 smaller than the best previous determinations and that the reaction is still heterogeneous in our reactor. The fact that the homogeneous rates must be very slow ($k_1 \leq 1 \times 10^{-20}$ cm³/molecule s and $k_2 \leq 4.4 \times 10^{-40}$ cm⁶/molecule² s) suggests that they probably play little role in the chemistry of most air pollution processes. However, the present results indicate that the heterogeneous reactions are extremely sensitive to the condition of the surface. A 100-fold variation in surface activity has been observed in these experiments on a Pyrex surface, and it is possible that other surfaces may be even more active. This surface sensitivity is probably responsible for the large differences in the values of k_1 and k_2 published by other authors. In particular, the results of Chan et al. were obtained in a stainless steel reactor, which might be expected to have a more active surface than either the Tedlar bag used by Cox and Derwent or the seasoned Pyrex reactor used in the present experiments.

Prediction of the effect of the heterogeneous reaction on air pollution chemistry whether in the open air or in exhaust stack gases is, therefore, impossible because of the difficulty of estimating surface area (aerosol, particulate, and fixed surface) and activity. However, rates several orders of magnitude higher than the stated upper limits might be encountered in the polluted atmosphere.

References and Notes

- (1) B. J. Finlayson and J. N. Pitts, *Science*, **192**, 111 (1976), and references therein.

- (2) L. G. Wayne and D. M. Yost, *J. Chem. Phys.*, **19**, 41 (1951).
 (3) R. F. Graham and B. J. Tyler, *J. Chem. Soc., Faraday Trans. 1*, **68**, 683 (1972).
 (4) (a) W. H. Chan, R. J. Ncrdstrom, J. G. Calvert, and J. H. Shaw, *Chem. Phys. Letts.*, **37**, 441 (1976); (b) *Environ. Sci. Technol.*, **10**, 674 (1976).
 (5) R. A. Cox and R. G. Derwent, *J. Photochem.*, **6**, 23 (1976/77).
 (6) E. W. Kaiser and C. H. Wu, *J. Phys. Chem.*, **81**, 187 (1977).
 (7) (a) P. G. Ashmore and B. J. Tyler, *J. Chem. Soc.*, 1017 (1961); (b) C. England and W. H. Corcoran, *Ind. Eng. Chem., Fundam.*, **13**, 373 (1974).
 (8) Similar nonintegral kinetic orders for NO, NO₂, and H₂O have been reported in a recent study of the formation rate of HONO in a Pyrex reactor: L. Zafonte, P. L. Rieger, and J. R. Holmes, Pacific Conference on Chemistry and Spectroscopy, North Hollywood, Calif., Oct 28–30, 1975, Paper No. 79.
 (9) "Comprehensive Chemical Kinetics", Vol. 2, C. H. Bamford and C. F. H. Tipper, Ed., Elsevier, Amsterdam, 1969, pp 41–42.

The Reaction of Thiolane with Hydrogen Atoms at High Temperature. H₂S Elimination from Chemically Activated 1-Butanethiol

Osamu Horie,* Kaoru Onuki, and Akira Amano

Department of Applied Chemistry, Faculty of Engineering, Tohoku University, Aoba, Aramaki, Sendai 980, Japan (Received February 1, 1977)

The reaction of thiolane with hydrogen atoms has been studied over the temperature range 300–580 K at pressures from 2.5 to 10.0 Torr using a conventional discharge-flow apparatus. At room temperature, 1-butanethiol is formed with a high selectivity (~85%), the remaining products being 1-butene, *n*-butane, and C₃ and C₂ hydrocarbons. As the temperature is increased, the selectivity toward 1-butanethiol decreases while that of 1-butene increases. The reaction is considered to proceed by addition of a hydrogen atom to a sulfur atom followed by C–S bond cleavage to form 4-mercapto-1-butyl radicals. Addition of a second hydrogen atom to the radical produces vibrationally excited 1-butanethiol, which then undergoes either collisional stabilization or unimolecular decomposition to 1-butene and hydrogen sulfide. An interpretation by the RRKM theory indicates that the experimental decomposition rate is in accord with a four-center H₂S elimination complex having $A = 2.2 \times 10^{13} \text{ s}^{-1}$ and $E_0 = 51\text{--}55 \text{ kcal/mol}$. The results are shown to be consistent with thermal H₂S elimination data of some alkyl thiols.

Introduction

The reactions of sulfur compounds with hydrogen atoms have so far received minor attention.^{1–4} The reaction of thiirane with hydrogen atoms is characterized by a single-step sulfur atom abstraction to form ethylene and SH radicals.¹ The reaction of thiophene with hydrogen atoms is marked by the absence of sulfur-containing products (except H₂S), which is explained by the initial hydrogen atom addition to carbon atoms adjacent to the sulfur atom followed by the C–S bond cleavage and sulfur atom elimination.³ A preliminary study on thiolane–H reaction indicates that the hydrogen atom initially adds to the sulfur atom, followed by C–S bond dissociation to form 4-mercapto-1-butyl radicals.⁴

All these reactions certainly involve formation and decay of chemically activated species, and bear significant relevance to thermal decompositions of thiols and sulfides. Therefore, the behavior of the energized species pertinent to sulfur compounds is important in the analysis of such reactions. Available data, though very scant,⁵ indicate that thermal decomposition of thiols proceeds by concurrent H₂S elimination and free radical dissociation at the C–S bond, the latter having a higher activation energy.^{6,7} However, neither of these processes have been analyzed in any detail.

The purpose of the present study is (1) to clarify the mechanism of the reaction of thiolane with hydrogen atoms proposed in our previous report,⁴ (2) to interpret the results by the Marcus-Rice unimolecular rate theory, and (3) to correlate the analysis with thermal decomposition of some alkyl thiols.

Experimental Section

The reaction was carried out with the apparatus and procedure similar to those described in our previous

works.^{3,4,8} Basically, the apparatus consisted of discharge-flow reactor, thiolane vaporizer, U-tubes for trapping the products, a flow-control line, and an evacuation unit. The experimental conditions were as follows: temperature 300–580 K, pressure 2.5–10.0 Torr, H₂ flow rate 0.57–0.63 mL NTP/s, N₂ flow rate 2.7–3.0 mL NTP/s. Different conversions were achieved by changing the position of the microwave discharge cavity for generating atomic hydrogen relative to the reaction zone. Accuracy of temperature and pressure measurements was within ±0.5 and ±2%, respectively.

Reaction products were analyzed by gas-liquid chromatography (GLC). C₁–C₄ hydrocarbons were separated at room temperature by a train of three columns in series: 0.75 m DNP/Chromosorb, 0.5 m phenyl isocyanate/silica gel, 8.75 m DMS/Chromosorb. For C₅–C₈ and sulfur compounds, either a 6 m silicone oil/Chromosorb column or a 6 m DNP/Chromosorb column was used at 70 °C. H₂S was qualitatively analyzed on 1.5 m Porapak-Q column at 70 °C with a thermal conductivity detector. The accuracy of the GLC analysis was within ±5% for most compounds, and as large as ±20% for ethane and ethylene due to only partial separation by GLC. Methane was not trapped by the sampling procedure and no attempt was made to analyze for it. The thiolane used was of more than 99.9% purity by GLC analysis, and no further purification was done.

The conversion is based on the amount of the unreacted thiolane C and the reaction products as defined by eq I,

$$B = 100Q/(C + Q) \quad (\text{I})$$

$$Q = [1\text{-C}_4\text{H}_9\text{SH}] + [\text{C}_4] + [\text{C}_3] + 0.5[\text{C}_2] \quad (\text{II})$$

where Q corresponds to the amount of reacted thiolane, eq II, corresponding to the stoichiometry of the reaction

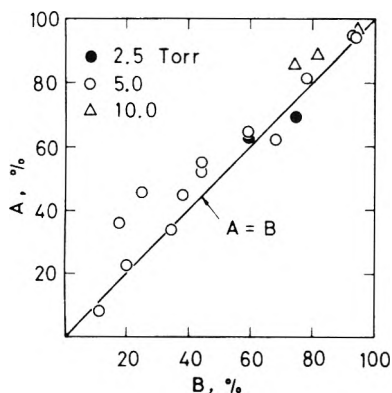


Figure 1. Comparison between the conversions A and B (300 K).

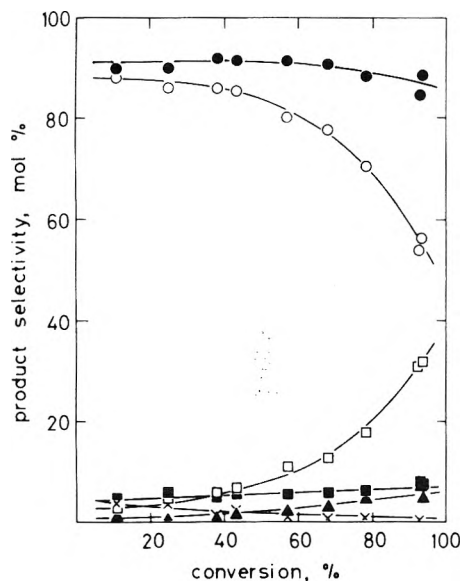


Figure 2. Product selectivity change with conversion (300 K, 5.0 Torr): (O) 1-butanethiol; (■) 1-butene; (□) *n*-butane; (▲) C₃; (X) C₂; (●) the sum of 1-butanethiol and *n*-butane.

to be discussed later. The validity of eq I can be shown by comparison with the usual definition for conversion, $A = 100(C_0 - C)/C_0$, where C_0 is the amount of thiolane of a blank run in which the discharge power is turned off, other conditions being unchanged. The results obtained at 300 K are shown in Figure 1. Both definitions agree well over a wide conversion range. One of the reasons for using B is that fluctuations in C_0 occur due to the variation of the thiolane bath temperature, which is usually kept constant in the range of $-5 \sim -30^\circ\text{C}$.

Results

(1) *Change in Product Selectivity with Conversion at 300 K.* Illustrated in Figure 2 is the change in product selectivity with conversion observed at 300 K and 5.0 Torr. The figure shows that over the whole conversion range the main product is 1-butanethiol. In particular, it represents more than 80% of all the products below 40% conversion. The remaining products are 1-butene, *n*-butane, propylene, propane, ethylene, and ethane. Methane and hydrogen sulfide are not included in the figure. As the conversion is increased, the selectivity toward 1-butanethiol decreases while its decrease is almost exactly counterbalanced by an increase in *n*-butane selectivity. This feature can be seen from the plots representing the sum of 1-butanethiol and *n*-butane selectivities.

Trends in the selectivity-conversion relationship observed at pressures of 2.5 and 10.0 Torr are quite similar to that observed at 5.0 Torr, and will not be described

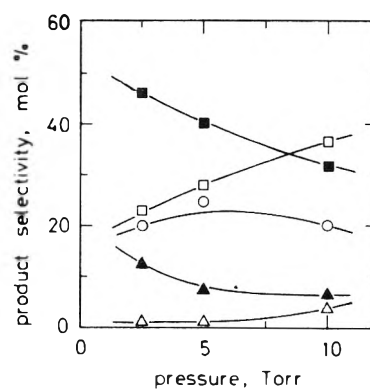


Figure 3. Effect of pressure on hydrocarbon selectivity (300 K, 20% conversion): (■) 1-butene; (□) *n*-butane; (▲) propylene; (Δ) propane; (O) C₂.

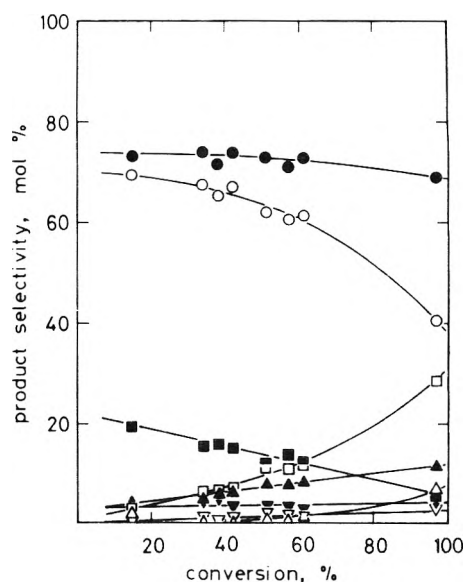


Figure 4. Product selectivity change with conversion (452 K, 5.0 Torr): (O) 1-butanethiol; (■) 1-butene; (□) *n*-butane; (▲) propylene; (Δ) propane; (▼) ethylene; (▽) ethane; (●) the sum of 1-butanethiol and *n*-butane.

further. However, the hydrocarbon selectivity is affected by the change in pressure, as is seen from Figure 3 in which the selectivity of each product with respect to the total hydrocarbon selectivity at 20% conversion is plotted against pressure. In short, the increase in *n*-butane and the decrease in 1-butene are symptoms of a pressure increase.

(2) *Effect of Temperature at 5 Torr.* Illustrated in Figures 4, 5, and 6 are the selectivity-conversion relations observed at a constant pressure of 5.0 Torr and at temperatures of 452, 523, and 580 K, respectively. The results at 452 K show a resemblance to those at 300 K, Figure 2. The products are dominated by 1-butanethiol, and the sum of the thiol and *n*-butane remains nearly constant at about 70% over the entire conversion range. At 523 K, increases in 1-butene and C₃ indicate a marked difference from the lower temperature results. At 580 K, the product distribution pattern undergoes a significant change from that of the lower temperature region, aside from an increased scatter of experimental points. Over most of the conversion range, 1-butene is the major product replacing 1-butanethiol, whose selectivity stays nearly constant at about 20%.

To further clarify the effect of temperature, the selectivity of the products at 20% conversion has been plotted against temperature in Figure 7. Each of the

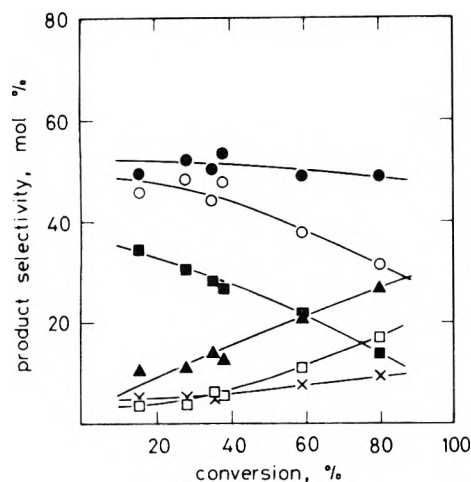


Figure 5. Product selectivity change with conversion (523 K, 5.0 Torr). See caption to Figure 2.

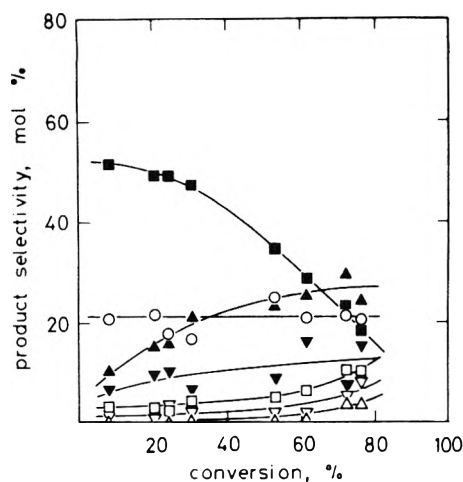


Figure 6. Product selectivity change with conversion (580 K, 5.0 Torr). See caption to Figure 4.

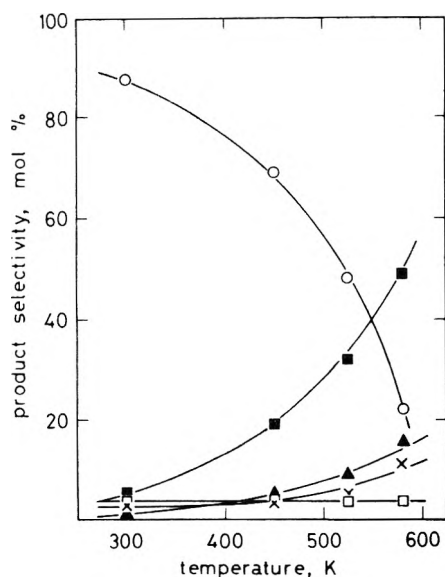


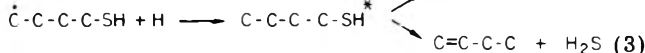
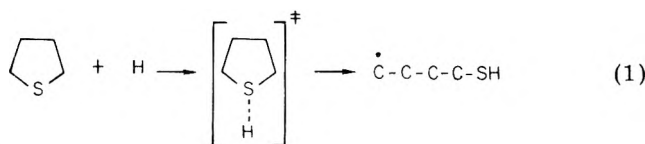
Figure 7. Effect of temperature on product selectivity (5.0 Torr, 20% conversion). See caption to Figure 2.

points in the figure was obtained by interpolations from Figures 2, 4, 5, and 6. The figure clearly shows that the effect of temperature on the selectivity of 1-butanethiol is in the opposite direction to that of 1-butene, which is characteristic of chemical activation systems toward temperature.^{8,9}

No appreciable formation of C_4 hydrocarbons except *n*-butane and 1-butene was observed over the whole experimental conditions. Formation of isobutane was noticed in some runs at 452 K, but the yield was never greater than about 10% of propylene. Combination of methyl and isopropyl radicals may explain the formation of isobutane. Butene isomers other than 1-butene were not observable except for runs with high conversions (more than about 50%) where traces of 2-butene isomers were detected.

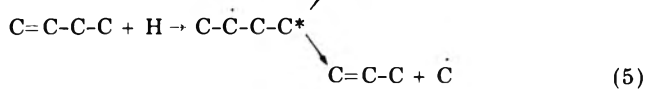
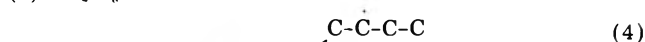
Discussion

(1) *Reaction Mechanism.* A reaction mechanism (eq 1-9) consistent with the experimental findings is proposed. Primary reactions

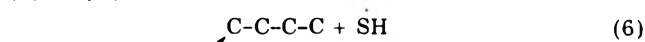


Secondary reactions

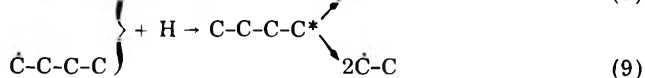
(a) $1-C_nH_{2n}-H$



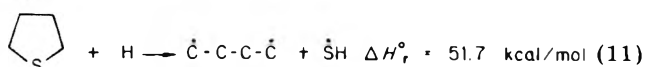
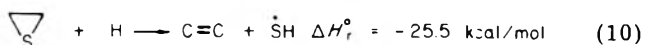
(b) $1-C_nH_{2n}SH-H$



(c) $\dot{\text{C}}-\text{C}-\text{C}-\text{C}$ or $\dot{\text{C}}-\text{C}-\text{C}-\text{C}-\text{H}$



The reaction is initiated by addition of hydrogen atom to sulfur atom to form an activated complex and its decomposition to 4-mercapto-1-butyl radical. The activated complex shown in the scheme is similar to that proposed in the reaction of thiirane with hydrogen atoms,¹ or with methyl radicals,¹⁰ where the initial interaction is presumed to involve the nonbonding 3p orbital of the sulfur atom leading to a symmetrical transition state. It is noted, however, that the thiirane-H reaction (reaction 10) is



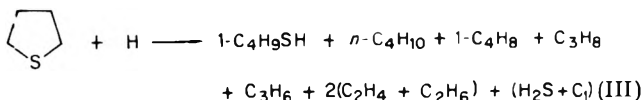
characterized by the complete absence of the addition product of thiol radicals $\dot{\text{C}}\text{H}_2\text{CH}_2\text{SH}$. Unlike the latter case, the thiolane-H reaction is characterized by a high selectivity toward the corresponding addition product, 1-butanethiol. The striking contrast in the observed reactivities between thiirane and thiolane is due largely to the difference in the stabilization of the reaction products. Thus, the analogous sulfur atom abstraction from thiolane (reaction 11) is thought to be highly improbable since the biradical $\dot{\text{C}}-\text{C}-\text{C}-\dot{\text{C}}$ produced would be deprived of π conjugation that is quite manifest in reaction 10. The most probable path out of the activated complex in reaction 1

is, therefore, the cleavage of either of the C-S bonds to form $\dot{C}-C-C-SH$ radicals.

Addition of a hydrogen atom to the radical leads to the formation of vibrationally excited 1-butanethiol (the asterisk indicates the energized state), which undergoes either collisional stabilization to 1-butanethiol (reaction 2) or unimolecular decomposition to 1-butene and hydrogen sulfide (reaction 3). We propose that the latter proceeds through a four-center H_2S elimination complex which is characteristic of well-known HX (X = F, Cl, Br) elimination reactions.¹¹⁻¹³ By postulating the formation of an energized thiol and its subsequent reactions, it is not only possible to explain the formation of the main products but also the change in their selectivities with temperature. This will be discussed later.

If excess hydrogen atoms are present, secondary reactions become important. For 1-butene, they involve the formation of chemically activated *sec*-butyl radicals and their subsequent reactions (reactions 4 and 5). These reactions including the observed effects of temperature have been discussed in detail in our previous work,⁸ and will not be described here. The reactions of 1-butanethiol with hydrogen atoms probably result in the formation of *n*-butane and *n*-butyl radicals, through reactions 6 and 7, respectively. A preliminary study in our laboratory indicates that the reaction of 1-butanethiol with hydrogen atoms at 5 Torr produces three major products, *n*-butane, 1-butene, and propylene in the following selectivities: ~70, ~20, and ~5% at 295 K, and ~25, ~50, and ~7% at 576 K, respectively, both at about 10% conversion. The remaining products besides H_2S are propane, 2-butenes, ethylene, and ethane. *n*-Butyl radicals formed in reaction 7 may either disproportionate into *n*-butane and 1-butene, or react further with hydrogen atoms to yield *n*-butane (reaction 8) or decompose to ethyl radicals (reaction 9).¹⁴

Isomers of 2-butene, which might be the expected products of disproportionation of *sec*-butyl radicals formed in reaction 4, have not been found in any noticeable amount under the entire experimental conditions. In the presence of excess hydrogen atoms, however, the radicals are consumed in a manner similar to *n*-butyl radicals (reactions 8 and 9). Also, the increased decomposition rate of *sec*-butyl radicals at high temperature⁸ may reduce the concentration of stabilized radicals for subsequent reactions. Finally, it should be mentioned that the major part of the C_2 fraction can be accounted for by reaction 9 in view of the predominant formation of 1-butanethiol under most conditions. With these considerations, the stoichiometry of the reaction may be represented by eq III,



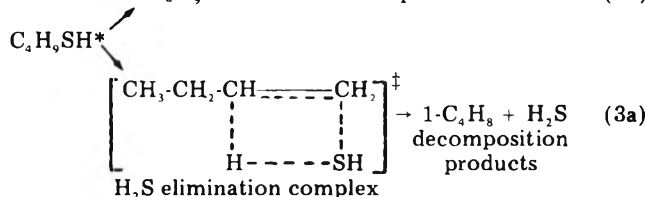
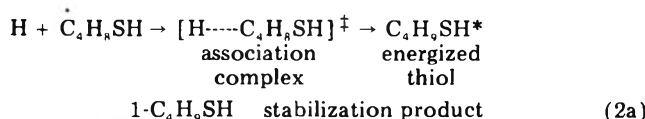
which is basically the same as eq II used in calculating the conversion.

(2) *Interpretation by the Marcus-Rice (RRKM) Unimolecular Rate Theory.* The main reactions proposed in the foregoing paragraph constitute a chemical activation system in which the two competing processes of the energized 1-butanethiol yield distinctive initial products in a relative abundance according to the temperature and pressure at which the reactions are studied. Thus, the present system provides the first instance to which the Marcus-Rice (RRKM) unimolecular rate theory can be applied for analyzing structural details of the reactions involving C-S bond rupture.

Despite the fact that molecular H_2S elimination from thiols has been known for some time,¹⁵⁻¹⁷ notions on the

elimination complex of the thermolysis of thiols are surprisingly sparse. In their study on the thermally induced H_2S elimination from 2-methyl-2-propanethiol and 1-pentanethiol, Thompson et al.^{15,16} concluded that the former proceeds via a free radical mechanism while the latter involves an intramolecular rearrangement. In this latter case, both H and SH were assumed to be eliminated from the same carbon atom, and which was conversely taken as a support for the free radical pathway in the former because of the lack of corresponding hydrogen atoms. By using the toluene carrier method for the pyrolysis of ethanethiol and assuming $A = 10^{13} \text{ s}^{-1}$, Sehon⁶ obtained $E = 48\sim 55 \text{ kcal/mol}$ for the intramolecular H_2S elimination of the type suggested by Thompson. Tsang⁷ appears to be the first to investigate the pyrolysis of thiol under the notion of the four-centered elimination complex similar to that generally accepted for the HX elimination from haloalkanes. Thus, by a shock-tube experiment on 2-methyl-2-propanethiol admixed with propylene radical scavenger, Tsang was able to deduce $k = 10^{13.5} \cdot \exp(-55000/RT) \text{ s}^{-1}$ which is compatible with the four-centered pathway.

The pertinent reaction scheme is rewritten for the purpose of RRKM analysis as follows:



The vibrational model of the four-centered elimination complex is in essence the same as the HCl elimination complex for the chloroethane case.¹⁸ Vibrations involving -SH bonds are taken to be the same as those for -Cl bonds,¹⁹ and vibrations of the alkane part are derived according to Larson.²⁰ The ring frequencies are so estimated as to reflect the A factor of about 10^{13} s^{-1} observed for thermal decomposition of thiols.^{6,7} Vibrational frequencies assigned for the four-center elimination complex are listed in Table I along with those for the association complex and the energized 1-butanethiol molecule. Other relevant molecular parameters are listed in Table II. The energetics of the reaction is determined from the heat of formation of relevant species listed in Table III. The minimum amount of energization, E_{min} , of 98.0 kcal/mol is obtained by assuming that there is no activation barrier for $\text{C}_4\text{H}_8\text{SH}^*$ formation, and that the $\dot{\text{C}}_4\text{H}_8\text{SH}$ radical formed in reaction 1 is thermalized.

The RRKM calculations were performed as described previously.^{8,9} The quantities obtained are the average decomposition rate constant, $\langle k_a \rangle$, and the collision-averaged decomposition rate constant, $\langle k \rangle_{\text{SL}}$, both as a function of temperature and pressure. SL represents the step-ladder model adopted here. The energy step $\Delta E = 2.0 \text{ kcal/mol}$, corresponding to the efficiency of nitrogen, is used in the calculation.

The experimental decomposition rate constant is calculated by the equation $k_{\text{expt}} = \omega(D/S)$, where ω is the collision frequency, and D and S are the relative yield of decomposition and stabilization products, respectively. In this analysis, two extreme cases are considered. Case F assumes that hydrocarbons other than 1-butene are the products of the subsequent reactions of 1-butene alone

TABLE I: Vibrational Models

Vibrations	1-Butanethiol	Association complex	Decomposition complex ^a
C-H str	2860(3) 2935(3) 2950 2960 2880	2860(3) 2935(3) 2950 2960	2860(2) 2935(2) 2950 2960 2880 2890
CH ₂ def, bend	1380 1460(2) 1134 956	1380 1460 1134	1380 1460(2) 1134 956
CH ₃ def, bend	750(2) 789 1297 1304 1290 1244 1250 1081 1455 1466 1449	750(2) 789 1297 1304 1290 1244 1250 1081 1455 1466 1449	750(2) 1297 1304 1081 1466 1244 1250 1455 1450 1290
C-C str	835 970 1058	835 970 1058	835 970
C-C-C bend	432 365	432 365	432 365
C-S str	675	675	
C-C-S bend	350	350	
C-S-H bend	1285(2)	1285(2)	1285(2)
S-H str	2570	2570	2570
C-C tors	212 122(2)	212 122(2)	212 122
C-C...H def		300(2)	
ring vib	C=C str		1324
	C...H str		885
	C...S str		202
	S...H str		1800
	out of plain in-plain puckering		500
Grouped freq	2872(10) 1353(13) 1038(5) 758(5) 381(3) 147(3)	2871(9) 1344(12) 1059(4) 758(5) 346(5) 147(3)	2869(9) 1469(8) 1260(8) 1001(3) 803(4) 429(3) 174(3)

^a $A = 1.1 \times 10^{13} \text{ s}^{-1}$, uncorrected for the statistical factor. The A factor is calculated by $A = (ekT/h) \exp(\Delta S^\ddagger/R)$.

TABLE II: Molecular Parameters

Property	Value
Collision diameter, N_2 , nm	0.385
Collision diameter, $1\text{-C}_4\text{H}_9\text{SH}$, nm	0.593 ^a
Reduced Mass, g/mol	21.36
Statistical factor for decomposition	2

^a Collision diameter of $n\text{-C}_5\text{H}_{12}$ is used. Collision diameters are taken from ref 21.

TABLE III: Heat of Formation at 298 K^a

Species	ΔH_f° , kcal/mol	Species	ΔH_f° , kcal/mol
H	52.1	C-C-C-C-SH	24.9
SH	35.5	C=C-C-C	0.0
H ₂ S	-4.8	C-C-C-C	61.7
Thiolane	-8.0	C=C	12.5
1-C ₄ H ₉ SH	-21.0	Thiirane	20.0

^a Taken or estimated from ref 22 and 23.

(reactions 4 and 5). Thus, with case F, S and D can be defined simply by the following relations:

$$S = [1\text{-butanethiol}] \quad (\text{IV})$$

$$D = 1 - S \quad (\text{V})$$

Case S assumes, on the other hand, that n -butane and C_2 are the products of 1-butane-1-thiol-H reactions (reactions 6 and 7), and that propylene formed through reaction 5. Thus, with case S

$$S' = [1\text{-butanethiol}] + [n\text{-butane}] + 0.5[C_2] \quad (\text{VI})$$

$$D' = [1\text{-butene}] + [\text{propylene}] \quad (\text{VII})$$

The selectivity of each product at zero conversion, obtained by extrapolation to zero conversion, is used in determining D 's and S 's. The values for D , S , D/S , and k_{expt} are listed in Table IV. These two extreme cases correspond to the situations where the reactions of 1-butene with hydrogen atoms are much faster (case F), and much slower (case S) than those of 1-butane-1-thiol with hydrogen atoms. In as much as the rate and its temperature dependence for the latter reactions have not yet been determined, both definitions are amenable to change with temperature.

TABLE IV: Experimental Decomposition Rate Constant k_{expt}

	Temp, K	$10^{-7} \omega, \text{ s}^{-1}$			
		300	452	523	580
Case F	D	12.5	31.0	52.0	78.0
	S	87.5	69.0	48.0	22.0
	D/S	0.142	0.449	1.08	3.54
	$10^{-7} k_{\text{expt}}, \text{ s}^{-1}$	0.94	2.42	5.43	16.8
Case S	D' ^a	6.0	24.5	40.0	56.5
	S'	94.0	73.5	53.0	26.0
	D'/S'	0.064	0.333	0.755	2.17
	$10^{-7} k_{\text{expt}}, \text{ s}^{-1}$	0.420	1.79	3.78	10.3

^a In calculating D' , $[\text{propylene}] = [C_2]$ is used since propane is considered formed from propylene in secondary reactions.

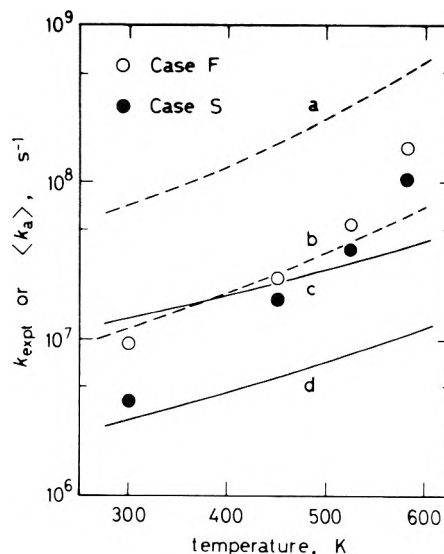


Figure 8. Comparison between experiment and calculations (5.0 Torr): (a) step-ladder model, $E_0 = 51 \text{ kcal/mol}$, $\Delta E = 2.0 \text{ kcal/mol}$; (b) step-ladder model, $E_0 = 55 \text{ kcal/mol}$, $\Delta E = 2.0 \text{ kcal/mol}$; (c) strong-collision model, $E_0 = 51 \text{ kcal/mol}$; (d) strong-collision model, $E_0 = 55 \text{ kcal/mol}$.

A comparison between the theory and experiment is presented in Figure 8. The best overall agreement with

experiments is obtained for strong-collision model with $E_0 = 51$ kcal/mol and for step-ladder model ($\Delta E = 2.0$ kcal/mol) with $E_0 = 55$ kcal/mol. These results together with the A factor of $2.2 \times 10^{13} \text{ s}^{-1}$ for the four-center complex are consistent with the pyrolysis data for H_2S elimination reactions.^{6,7} However, the temperature dependence of k_{expt} is considerably greater than the calculations indicate. The main reason for this difference is that the effect of temperature on the 1-butanethiol-H reaction has not been taken into account in the defining equations for D 's and S 's. Since the reaction of 1-butanethiol with hydrogen atoms will be accelerated by the temperature increase, the concentration of 1-butanethiol used in eq IV will become smaller at higher temperatures than would be the case in the absence of increased thiol consumption under such conditions (case F). Also, the selectivity of 1-butene seems to increase with temperature, as indicated in the preliminary study mentioned above. Therefore, some fraction of 1-butene formed should belong to the stabilization product, with probably an increased share at high temperature. This feature, however, has not been reflected in eq VI and VII (case S). However, elaboration on these discrepancies will not be made until additional kinetic data on the system 1-butanethiol-H become available.

A free radical process initiated by C-S bond dissociation is a possible decomposition path of energized 1-butanethiol as proposed in our preliminary report.⁴ A few calculations using a suitable model for the decomposition complex ($A = 3 \times 10^{13} \text{ s}^{-1}$) suggest that $\langle k_a \rangle$ is of the order of 10^4 (at 300 K) $\sim 10^5$ (at 600 K) s^{-1} . Thus the C-S bond dissociation must be considered to be a negligible path under the present conditions. In thermal reactions, however, the radical process may favorably compete with H_2S elimination since the overall activation energy decreases considerably in forming a free radical chain. This is one of the reasons that pyrolysis of thiols seems complicated.^{6,15-17}

In the chemical activation system, H_2S elimination of thiols can be isolated from the free radical decomposition, enabling the study of the former process which is much less understood than the corresponding haloalkane re-

actions. The reactions of homologues of ring sulfides and their derivatives with hydrogen atoms should provide suitable sources of energized thiols for such investigations. In particular, these reactions are important in elucidating the mechanism of the primary steps in H-sulfide interactions whose difference is so eminently revealed for the two different ring sizes.

References and Notes

- (1) T. Yokota, M. G. Ahmed, I. Safarik, O. P. Strausz, and H. E. Gunning, *J. Phys. Chem.*, **79**, 1758 (1975).
- (2) S. Tsunashima, T. Yokota, I. Safarik, H. E. Gunning, and O. P. Strausz, *J. Phys. Chem.*, **79**, 775 (1975).
- (3) O. Horie, N. H. Hanh, and A. Amano, *Chem. Lett.*, 1015 (1975).
- (4) O. Horie, K. Kawamata, K. Onuki, and A. Amano, *Chem. Lett.*, 753 (1976).
- (5) O. P. Strausz, H. E. Gunning, and J. W. Lown in "Comprehensive Chemical Kinetics", Vol. 5, C. H. Bamford and C. F. H. Tipper, Ed., Elsevier, Amsterdam, 1972, pp 697-731.
- (6) A. H. Sehon and B. deB. Darwent, *J. Am. Chem. Soc.*, **76**, 4806 (1954).
- (7) W. Tsang, *J. Chem. Phys.*, **40**, 1498 (1964).
- (8) O. Horie and N. H. Hanh, *J. Phys. Chem.*, **80**, 1657 (1976).
- (9) "Comprehensive Chemical Kinetics", Horie, and N. H. Hanh, *Int. J. Chem. Kinet.*, **8**, 321 (1976).
- (10) E. Jakubowski, M. G. Ahmed, E. M. Lown, H. S. Sandhu, R. K. Gosavi, and O. P. Strausz, *J. Am. Chem. Soc.*, **94**, 4049 (1972).
- (11) A. Maccoll and P. J. Thomas, *Prog. React. Kinet.*, **4**, 119-148 (1967).
- (12) A. Maccoll, *Chem. Rev.*, **69**, 33 (1969).
- (13) E. W. Swinbourne in "Comprehensive Chemical Kinetics", Vol. 5, C. H. Bamford and C. F. H. Tipper, Ed., Elsevier, Amsterdam, 1972, pp 149-233.
- (14) B. S. Rabinovitch and D. W. Setser, *Adv. Photochem.*, **3**, 1 (1964). See Table XIV, p 58.
- (15) C. J. Thompson, R. A. Meyer, and J. S. Ball, *J. Am. Chem. Soc.*, **74**, 3284 (1952).
- (16) C. J. Thompson, R. A. Meyer, and J. S. Ball, *J. Am. Chem. Soc.*, **74**, 3287 (1952).
- (17) J. L. Boivin and R. MacDonald, *Can. J. Chem.*, **33**, 1281 (1955).
- (18) J. C. Hassler and D. W. Setser, *J. Chem. Phys.*, **45**, 3246 (1966).
- (19) S. Mizushima and T. Shimanouchi, "Infrared Absorption and Raman Effect", Kyoritsu, Tokyo, 1958.
- (20) C. W. Larson, P. T. Chua, and B. S. Rabinovitch, *J. Phys. Chem.*, **76**, 2507 (1972).
- (21) J. O. Hirschfelder, C. F. Curtiss, and R. B. Bird, "Molecular Theory of Gases and Liquids", Wiley, New York, N.Y., 1963.
- (22) S. W. Benson, F. R. Cruickshank, D. M. Golden, G. R. Haugen, H. E. O'Neal, A. S. Rodgers, R. Shaw, and R. Walsh, *Chem. Rev.*, **69**, 279 (1969).
- (23) H. E. O'Neal and S. W. Benson, *Int. J. Chem. Kinet.*, **1**, 221 (1969).

Temperature-Jump Rate Studies of the Association Reactions of Boric and Benzeneboronic Acids with Hydroxide Ion

O. Kajimoto, T. Saeki, Y. Nagaoka, and T. Fueno*

Department of Chemistry, Faculty of Engineering Science, Osaka University, Toyonaka, Osaka 560, Japan (Received March 1, 1977)

The second-order rate constants k for the additions of hydroxide ion toward boric acid $B(OH)_3$ and ring-substituted benzeneboronic acids $XC_6H_4B(OH)_2$ in 0.1 M aqueous KCl medium at 25 and 35 °C were measured by the temperature-jump relaxation method. The reactions were found to be activation-controlled processes with k being of the order of $10^{7-8} M^{-1} s^{-1}$. The empirical activation energy for the boric acid reaction was 4.4 kcal/mol. Benzeneboronic acid showed a greater reactivity than did boric acid. The effects of ring substituents on the reaction rate of benzeneboronic acid proved to obey the Hammett relationship $\log k^X/k^H = \rho_f \sigma$ with $\rho_f = 1.18$ at 35 °C. It is suggested that the π -electronic charge on the boron atom in the acids is a factor governing the relative heights of the activation barrier.

Introduction

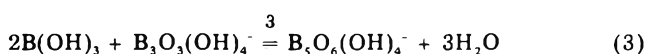
Several workers¹⁻⁵ have demonstrated that boric acid in an aqueous medium undergoes complex equilibria with borate and polyborate ions. In boric acid solutions having a total acid concentration of less than 0.01 M, the equilibrium



is known to be the only important one.^{4,5} At higher acid concentrations, boric acid enters into the formation of polyborate ions¹⁻⁵



and



In the boric acid concentration range 0.06–0.6 M, Eyring et al.⁴ investigated the temperature-jump relaxations of the polymerization equilibria 2 and 3. At pH 7.4, the relaxation times observed were 2–15 ms; the rate constants for forward processes 2 and 3 were 2.8×10^3 and $2.0 \times 10^2 M^{-2} s^{-1}$, respectively, at 25 °C. They noted that, under their conditions, reaction 1 should have a characteristic relaxation time much shorter than the resolving time (10 μ s) of their instrument and that the association reaction would probably be a diffusion-controlled process ($k_1 \approx 10^{10} M^{-1} s^{-1}$).

We have investigated the temperature-jump relaxation of boric acid equilibrium 1 in far more dilute (2×10^{-4} to $1.5 \times 10^{-3} M$) acid solutions. The forward rate constant k_1 has been found to be $1.5 \times 10^7 M^{-1} s^{-1}$ at 25 °C. The activation energy was found to be 4.4 kcal/mol, a result which indicates that the association reaction is "activation controlled".

Motivated by the above finding, we have further studied the reaction rates of several ring-substituted benzeneboronic acids:



where X = *p*-CH₃, *m*-CH₃, H, *m*-CH₃O, *p*-Cl, and *m*-Cl. The rate constants k_4 for the forward processes were found to be of the order of $10^{7-8} M^{-1} s^{-1}$ at 35 °C. The substituent effects on the rates proved to conform to Hammett's

relationship $\log k_4^X/k_4^H = \rho_f \sigma$ with $\rho_f = 1.18$. The equilibrium constants $K_4 = k_4/k_{-4}$ were also correlated with σ ($\rho = 2.00$). Clearly, the electronic effect of substituents plays a dominant role in governing the rate of the forward as well as the backward process of reaction 4.

Experimental Section

Materials. Boric acid of reagent grade was recrystallized from water. Its melting point, 185 °C (with decomposition), checked with the literature datum.

Benzeneboronic acid and its *p*-CH₃, *m*-CH₃, *m*-CH₃O, *p*-Cl, and *m*-Cl derivatives were all synthesized according to the method of Branch et al.^{6,7} Thus, trimethyl borate was allowed to react with appropriate phenylmagnesium bromide at –60 °C, followed by decomposition with dilute sulfuric acid. Benzeneboronic acids thus formed were purified by successive recrystallizations from benzene and water, and dried under a ventilated atmosphere. All the boronic acids were identified by ¹H NMR spectroscopy and elemental analyses. The OH proton chemical shifts (in acetone at 25 °C) were as follow: *p*-CH₃, δ 6.99; *m*-CH₃, δ 7.13; H, δ 7.13; *m*-CH₃O, δ 7.09; *p*-Cl, δ 7.24; and *m*-Cl, δ 7.41. The acids were all subject to dehydration on heating, as reported previously.⁸ Their melting points checked well with the literature data⁸ for anhydrides: *p*-CH₃, 260 °C (lit. 259–260 °C); *m*-CH₃, 162–163 °C (lit. 160–161.5 °C); H, 214 °C (lit. 214–216 °C); *m*-CH₃O, 158 °C (lit. 159 °C); *p*-Cl, ~260 °C (lit. 261–262.5 °C); and *m*-Cl, 183 °C (lit. 179 °C).

Acid Ionization. The ionization constants of boric acid and various benzeneboronic acids in aqueous 0.10 M KCl were determined by the standard procedure described by Albert and Serjeant.⁹ Sample solutions, $1.0 \times 10^{-3} M$ with respect to the acid, were titrated with 0.01 M NaOH under a nitrogen atmosphere. A Hitachi-Horiba pH meter Model F-5 with a scale expander was used for pH measurements. Our pK_a values thus obtained are based on the proton activity in 0.10 M KCl. Hence, they are uniformly greater than the standard concentration-based pK_a values by a constant factor of $-\log \gamma_H = 0.08$, where $\gamma_H = 0.83$ is the activity coefficient of H⁺ in an aqueous KCl solution of ionic strength 0.10 M.¹⁰

Temperature-Jump Experiments. The temperature-jump apparatus constructed in this laboratory is essentially the same as that described by Kresheck et al.¹¹ Details of the specification of our apparatus have been delineated previously.¹² The theoretical temperature rise was calculated to be ca. 7 °C with a rise time of 6 μ s.

The temperature-jump relaxation measurements were carried out with 1.5 mL of each sample solution in the pH range 8.1–8.9. Sample solutions were 0.10 M in KCl and 0.25–1.5 mM in the acid. Temperature jump was effected by discharging a 0.1 μF capacitor charged to 25 kV through a cell. Relaxation courses were traced by monitoring the absorption at 565 nm of cresol red (1.0×10^{-5} M) used as an indicator. Relaxation profiles were recorded on an Iwatsu 5505 oscilloscope and photographed. The relaxation times were evaluated from the slopes of the semi-logarithmic plots of absorbance vs. time. Blank experiments involving only the indicator gave no observable relaxation in the time region (30–400 μs) of interest.

Relaxation Rates. The temperature-jump relaxation observed under our conditions is probably due to the following set of reversible reactions



with the equilibrium constants

$$K_5 = k_5/k_{-5} = [\text{BOH}^-]_e/[\text{B}]_e[\text{OH}^-]_e \quad (7)$$

$$K_6 = k_6/k_{-6} = [\text{In}^{2-}]_e/[\text{HIn}^-]_e[\text{OH}^-]_e \quad (8)$$

where B denotes either boric or benzenboronic acid, and HIn^- is the acid form of the indicator (cresol red) anion. The relaxation equation pertinent to this coupled reaction scheme is

$$-\frac{d}{dt} \begin{pmatrix} \Delta[\text{B}] \\ \Delta[\text{HIn}^-] \end{pmatrix} = \begin{pmatrix} \tau_5^{-1} & k_5[\text{B}]_e \\ k_6[\text{HIn}^-]_e & \tau_6^{-1} \end{pmatrix} \begin{pmatrix} \Delta[\text{B}] \\ \Delta[\text{HIn}^-] \end{pmatrix} \quad (9)$$

where $\Delta[\text{B}]$ and $\Delta[\text{HIn}^-]$ are the respective deviations of instantaneous concentrations of B and HIn^- from equilibrium while τ_5 and τ_6 are the constants defined as

$$\tau_5^{-1} = k_5([\text{B}]_e + [\text{OH}^-]_e) + k_{-5} \quad (10)$$

$$\tau_6^{-1} = k_6([\text{HIn}^-]_e + [\text{OH}^-]_e) + k_{-6} \quad (11)$$

The coupled relaxation time τ of interest is given as the reciprocal of the smaller eigenvalue of the relaxation matrix appearing in eq 9.¹³ Evidently, $\tau_6^{-1} \gg \tau_5^{-1}$, the relaxation time of indicator equilibrium 6 being much shorter¹³ than that of reaction 5. In this limit we can express our relaxation time as

$$\tau^{-1} = \tau_5^{-1} - k_5 k_6 [\text{B}]_e [\text{HIn}^-]_e / \tau_6^{-1} \quad (12)$$

By making use of eq 10 and 11, eq 12 can readily be transformed into

$$\tau^{-1} = k_5 \{ f[\text{B}]_e + [\text{OH}^-]_e + K_5^{-1} \} \quad (13)$$

where f is a quantity defined as

$$f = \left\{ 1 + \frac{K_6[\text{HIn}^-]_e}{1 + K_6[\text{OH}^-]_e} \right\}^{-1} \quad (14)$$

The rate constant k_5 for the forward process of reaction 5 can be obtained from the observed relaxation time τ using eq 13.

The quantity f is exactly what has been referred to as the "indicator correction" factor.¹⁰ The equilibrium constant K_6 is given by

$$K_6 = [\text{In}^{2-}]_e[\text{H}^+]_e/[\text{HIn}^-]_e K_w = K_{\text{HIn}}/K_w \quad (15)$$

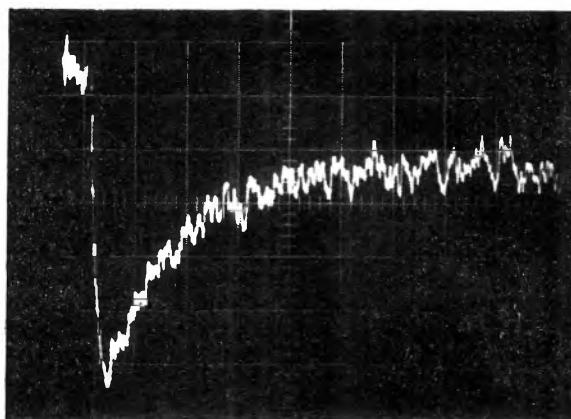


Figure 1. Typical oscillographic record of the relaxational response: ordinate (absorbance at 565 nm), 10 mV/division; abscissa (time), 100 μs /division; boric acid, 1.0×10^{-3} M; cresol red, 1.0×10^{-5} M; medium, 0.10 M KCl; pH, 8.49; temperature, 25 $^\circ\text{C}$; $\tau = 144 \mu\text{s}$. Moving upward on the record corresponds to an increase in the In^{2-} absorption.

where K_w is the ion product of water and K_{HIn} is the ionization constant of HIn^- . At 25 and 35 $^\circ\text{C}$, the $\text{p}K_w$ is 14.00 and 13.68, respectively.¹⁴ The K_{HIn} of cresol red is 8.20 at 25 $^\circ\text{C}$ ¹⁰ and is estimated to be 8.15 at 35 $^\circ\text{C}$. The HIn^- equilibrium concentration can be expressed as

$$[\text{HIn}^-]_e = I_0/(1 + K_6[\text{OH}^-]_e) \quad (16)$$

I_0 being the total concentration of the indicator used. Thus, the factor f is a function of only I_0 and $[\text{OH}^-]_e$ at a given temperature, and tends to decrease with increasing I_0 and decreasing $[\text{OH}^-]_e$. Under the present experimental conditions in which I_0 has been fixed at 1.0×10^{-5} M, f varies from 0.338 to 0.851 at 25 $^\circ\text{C}$ and from 0.513 to 0.929 at 35 $^\circ\text{C}$ as the pH of the sample solution is changed from 8.1 to 8.9.

Results

(A) *Boric Acid.* The equilibrium constant K_1 for reaction 1 in 0.10 M KCl can be evaluated from the acid dissociation constant K_a and the ion product of water K_w in the same medium:

$$K_1 = [\text{B}(\text{OH})_4^-]_e/[\text{B}(\text{OH})_3]_e[\text{OH}^-]_e = K_a/\gamma_{\text{H}} K_w \quad (17)$$

The $\text{p}K_a$ values observed at 25 and 35 $^\circ\text{C}$ were 9.24 and 9.17, respectively. Because in this temperature region the temperature coefficient of K_w exceeds that of K_a , the equilibrium constant K_1 decreases as the temperature is raised.

In the temperature-jump experiments, sample solutions were initially maintained at either 18 or 28 $^\circ\text{C}$. On the temperature jump, equilibrium 1 is shifted to the left to attain a new equilibrium at 25 or 35 $^\circ\text{C}$. Each sample solution gave a single relaxation curve due to the increase in indicator (In^{2-}) absorption. A typical relaxation profile is shown in Figure 1.

In Figure 2, the reciprocals of τ observed at varying total acid concentrations and pH are plotted against $\{[\text{B}(\text{OH})_3]_e + [\text{OH}^-]_e + K_1^{-1}\}$. The regression lines were drawn by forcing them to pass through the origin. The rate constants k_1 are obtained as the slopes of these lines. They are listed in Table I, together with the values for K_1 and $\text{p}K_a$. The uncertainties in the k_1 values indicate the probable errors.

The rate constants observed at the two temperatures permit evaluation of the empirical activation energy E_a . The result was $E_a = 4.4 \pm 2.0$ kcal/mol, where the uncertainty corresponds to the upper and lower limits of E_a which have been evaluated on the basis of the probable error limits for the two k_1 values observed.



The first possibility can be ruled out by the observation that benzenboronic acid admixed with cresol red showed no indication of complex formation. The ultraviolet absorption spectrum of an acid-indicator admixture in water was exactly a superposition of the characteristic absorption spectra for the acid and the indicator. The situation remained true, irrespective of the sample concentrations and the pH of sample solutions.

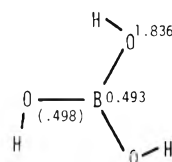
The second possibility, participation of reaction 21, can also be negated on the following grounds. As the pK_a values for boric acid (Table I) show, the dissociation equilibrium constant K_a is greater at higher temperatures. Therefore, if reaction 21 were the primary step to control the temperature-jump relaxation, the relaxation would occur in the direction where the H^+ concentration would be increased. This should accompany a decrease in the OH^- concentration because of the rapid equilibration $H^+ + OH^- \rightleftharpoons H_2O$. The net effect would then be a shift of the indicator equilibrium 6 to the left, resulting in a relaxational decrease of the indicator (In^{2-}) absorption in contradiction to observation.

The rate constants $k_1 = 1.49 \times 10^7$ and $1.90 \times 10^7 M^{-1} s^{-1}$ observed for the reaction of boric acid at 25 and 35 °C gave an activation energy $E_a = 4.4$ kcal/mol. From these results the preexponential factor of k_1 is evaluated to be $2.5 \times 10^{10} M^{-1} s^{-1}$ in this temperature region. The factor would be equal to k_1 itself, if the reaction were a diffusion-controlled process. The rate factor $2.5 \times 10^{10} M^{-1} s^{-1}$ obtained appears to be reasonable; it is of the order of magnitude which is estimated by von Smoluchowsky's equation¹³ for the rate constant of a diffusion-controlled reaction in aqueous solution.

Most likely, boric acid in its ground state is planar in structure and is greatly stabilized by the delocalization of the oxygen lone-pair electrons onto the boron atom. As the interaction between the acid and the incoming hydroxide ion develops, the acid will suffer an increasing deformation from the planar toward tetrahedral conformation. In the meantime, the π -electronic charge which was initially accumulated on the boron atom will be drawn back progressively into the oxygen lone-pair orbitals. The process should naturally be accompanied by a diminishing π conjugation and, hence, by an increasing destabilization of the boric acid moiety. The activation energy observed could be ascribed partly to this destabilization due to the loss in π -conjugation energy.

Benzenboronic acid was found to be more reactive toward hydroxide ion than is boric acid. Since the extent of π -electron delocalization in these reactant acids will be most vividly reflected in the π -electronic charge on the boron atom, such a charge may well be regarded as a measure of the π -conjugation energy loss which should accompany the activation process. Compared in Figure 5 are the π -electronic charge distributions in boric and benzenboronic acids calculated by the CNDO/2 method.¹⁶ The π -charge density on the boron atom is seen to be greater in boric acid than in benzenboronic acid. This is a direct consequence of the greater π -electron-donating character of the hydroxyl group than that of the phenyl group. The greater extent of π -electron accumulation on the boron atom in boric acid would thus provide a greater hindrance to its conformational change as compared with benzenboronic acid. It follows that the former acid should be less reactive than the latter. The conclusion is in harmony with observation, even though the π -electronic charge on the reaction sites may not generally be the only

Boric acid



Benzenboronic acid

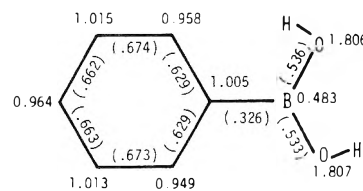


Figure 5. CNDO/2 π -charge distributions in boric and benzenboronic acids. The decimal fractions given in parentheses indicate the π -bond orders.

factor controlling the ionic reactivity of unsaturated compounds.

When the above-described argument is taken to be tenable, the effects of ring substituents on the rate of benzenboronic acid can readily be understood. Thus, the more electron donating a given substituent, the greater will be the π -electronic charge on the boron atom and, hence, the less reactive will be the substituted acid. However, it is yet by no means obvious why the substituent effects should be correlated with Hammett's *original* σ values in particular. The problem could probably be settled satisfactorily by the simple perturbation theory as used previously¹⁷ for the interpretation of the multiplicity of substituent constants.

No matter what the precise implication of the observed substituent effects may be, there is no doubt that the rates of reactions of our study are governed by the electrostatic-structural factor of the reactant acids. From eq 18 and 19, the ratio $\alpha = (\log k_4^X/k_4^H)/(\log K_4^X/K_4^H)$ is calculated to be 0.59. It deserves attention that the Brønsted-type relation¹⁸ holds also for the direct association reaction of Lewis acids with the hydroxide ion. The observed relation is "normal" in the sense that $0 < \alpha < 1$.¹⁹ The results could be taken as an indication that the formation of a coordination bond between the boron atom and the hydroxide ion, and hence the conformational change of the acids as well, should proceed monotonously along the reaction coordinate, with no anomalous mode of interaction developing between substituents and the reaction center.¹⁹

Acknowledgment. The authors are grateful to K. Sakurai for assistance in the temperature-jump experiments.

References and Notes

- (1) N. Ingri, G. Lagerstrom, M. Frydman, and L. G. Sillén, *Acta Chem. Scand.*, **11**, 1034 (1957).
- (2) N. Ingri, *Acta Chem. Scand.*, **16**, 439 (1962).
- (3) N. Ingri, *Acta Chem. Scand.*, **17**, 573, 581 (1963).
- (4) J. L. Anderson, E. M. Eyring, and M. P. Whittaker, *J. Phys. Chem.*, **68**, 1128 (1964).
- (5) R. K. Momii and N. H. Nachtrieb, *Inorg. Chem.*, **6**, 1189 (1957).
- (6) D. L. Yabroff, G. E. K. Branch, and B. Bettman, *J. Am. Chem. Soc.*, **56**, 1850 (1934).
- (7) B. Bettman, G. E. K. Branch, and D. L. Yabroff, *J. Am. Chem. Soc.*, **56**, 1865 (1934).
- (8) M. F. Lappert, *Chem. Rev.*, **56**, 959 (1956).
- (9) A. Albert and E. P. Serjeant, "Ionization Constants of Acids and Bases", Wiley, New York, N.Y., 1962.
- (10) M. H. Miles, E. M. Eyring, W. W. Epstein, and R. E. Ostrund, *J. Phys. Chem.*, **69**, 467 (1965).

- (11) G. C. Kresheck, E. Hamori, G. Davenport, and H. A. Scheraga, *J. Am. Chem. Soc.*, **88**, 246 (1966).
- (12) T. Fueno, O. Kajimoto, Y. Nishigaki, and T. Yoshioka, *J. Chem. Soc. Perkin Trans. 2*, 733 (1973).
- (13) M. Eigen and L. de Maeyer, "Technique of Organic Chemistry", 2nd ed, Vol. 8, Part II, S. L. Friess, E. S. Lewis, and A. Weissberger, Ed., Interscience, New York, N.Y., 1963, Chapter 18.
- (14) H. S. Harned and R. A. Robinson, *Trans. Faraday Soc.*, **36**, 973 (1940).
- (15) L. P. Hammett, "Physical Organic Chemistry", McGraw-Hill, New York, N.Y., 1970, Chapter 7.
- (16) J. A. Pople and D. L. Beveridge, "Approximate Molecular Orbital Theory", McGraw-Hill, New York, N.Y., 1970.
- (17) T. Fueno, T. Okuyama, and J. Furukawa, *Bull. Chem. Soc. Jpn.*, **39**, 569 (1966); T. Fueno, I. Matsumura, T. Okuyama, and J. Furukawa, *ibid.*, **41**, 818 (1968).
- (18) J. N. Bronsted and K. Pedersen, *Z. Phys. Chem.*, **108**, 185 (1924).
- (19) A. J. Kresge, *Chem. Soc. Rev.*, **2**, 475 (1973).

Thermochemistry of Some Six-Membered Cyclic and Polycyclic Compounds Related to Coal

Robert Shaw,

1162 Quince Avenue, Sunnyvale, California 94087

David M. Golden,*

Stanford Research Institute, Menlo Park, California 94025

and Sidney W. Benson

Department of Chemistry, University of Southern California, Los Angeles, California 90007 (Received November 30, 1976)

Publication costs assisted by SRI International

Values are presented for thermochemical properties [$\Delta H_f^\circ_{298}(\text{g})$, $S^\circ_{298}(\text{g})$, $C_p^\circ_{300}(\text{g})$] of some six-membered cyclic and polycyclic compounds. Classes of compounds included are (a) aromatic hydrocarbons containing from one to four rings, (b) hydroaromatic hydrocarbons obtained by adding 1, 2, and 3 (and 4) mol of H_2 to the aromatic hydrocarbons, (c) oxygenated hydrocarbons obtained by substituting O for CH_2 in some of the hydroaromatic hydrocarbons. Many of the values have been estimated by application of group additivity and structural considerations.

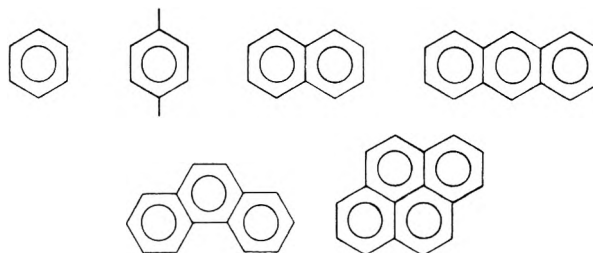
Introduction

The object of this research is to help provide a thermochemical foundation for the liquefaction of coal. An understanding of the thermochemistry of coal will guide strategies for the liquefaction of coal by thermodynamically determining most stable structures and most likely reaction paths. Catalysts accelerate the attainment of thermodynamic equilibrium. The present research is therefore especially appropriate because it is part of an effort¹ to develop homogeneous catalytic hydrocracking processes.

This research was partly motivated by a study of the catalytic hydrogenation of a multi-ring aromatic coal tar constituent (anthracene) by Wisner, Singh, Quader, and Hill,² who report "Bituminous coal is understood to consist primarily of fused ring structures joined together by various types of linkages to form an extensive network. These ring structures are highly aromatic, although considerable quantities of hydroaromatic configurations are present. The size of these structures may vary from one to several rings, an average-sized configuration containing three or four rings."

It is well known that the most abundant heteroatom in coal is oxygen. For example, in Illinois No. 6 coal, oxygen occurs to the extent of one atom per eight or nine carbon atoms. A significant fraction of the oxygen may therefore be in ring structures.

In view of the above considerations, the following six-membered ring structures have been selected for study: (a) aromatic hydrocarbons:



(b) hydroaromatic hydrocarbons, structures obtained by adding 1, 2, and 3 mol of H_2 (without ring opening) to the aromatic hydrocarbons in (a). In the case of anthracene and phenanthrene, 4 mol of H_2 were also added; (c) oxygenated hydrocarbons, structures obtained by substituting O for CH_2 in some of the hydroaromatic compounds in (b).

The thermochemical properties of interest are the following: $\Delta H_f^\circ_{298}(\text{g})$, the standard heat of formation of the ideal gas at 298 K; $S^\circ_{298}(\text{g})$, the standard entropy of the ideal gas at 298 K; (int) $S^\circ_{298}(\text{g})$, the standard intrinsic (corrected for symmetry and optical isomers) entropy of the ideal gas at 298 K; and $C_p^\circ_{300}(\text{g})$, the standard heat

capacity of the ideal gas at 300 K. (The variation in C_p° with temperature may be neglected here.) Using these thermochemical quantities, we can calculate equilibrium constants at any temperature.

It was anticipated that very few measured data would be available. Consequently, the emphasis would be on estimation. Methods of estimation have been developed mainly for the ideal gas state. It is unlikely that equilibrium constants change very much in going from the gas to the liquid phase. For example,^{3,4} for the hydrogenation of benzene to cyclohexane at 298 K, the heat of reaction is -49.2 kcal/mol in the gas phase and -49.0 kcal/mol in the liquid phase. For the same reaction, the entropy change is -86.7 cal/(mol K) in the gas phase and -86.2 kcal/mol in the liquid phase. There is a statistically significant difference in the change of heat capacity.⁵ For the same reaction in the gas phase, the heat capacity is -13.6 cal/(mol K), and in the liquid phase it is -16.1 cal/(mol K). However, the equilibrium constant depends much more on the heat of formation and entropy than on the heat capacity and so using gas phase equilibrium constants for liquids is still a good approximation.

The aromatic compounds have been numbered and named following the practice suggested by the Ring Index⁶ and Chemical Abstracts Index Guide.⁷ For simplicity in naming the hydroaromatic compounds, the prefixes dihydro-, tetrahydro-, etc., have been used, except in the case of the single ring compounds.

Two empirical methods⁸ were used for counting the structures. In the one, an arithmetic approach was used. In dihydronaphthalene, for example, the lowest possible number for the prefix is 1,2-, followed by 1,4-, and so on, up to 4a,8a-. In the other, a double bond in one ring was "frozen" while the double bond was "moved around" in the second ring.

The following literature has been searched for experimental values of the thermochemical properties: Cox and Pilcher,⁹ Stull, Westrum, and Sinke,⁴ and the IUPAC Bulletins¹⁰ since 1969. When choices had to be made, preference was given to Cox and Pilcher's recommendation.

Thermochemical properties were estimated by additivity methods.¹¹⁻¹³ Group values for heats of formation of the hydrocarbons and for entropies and heat capacity of single ring compounds were taken from a paper by Benson, Cruickshank, Golden, Haugen, O'Neal, Rodgers, Shaw, and Walsh.¹¹ Group values for estimating heats of formation of the oxygen compounds were taken from a more recent publication by Eigenmann, Golden, and Benson.¹² The general method used for estimating entropies and heat capacities of polycyclic compounds was developed by O'Neal and Benson.¹³ Briefly, this method depends on making cyclization, unsaturation, and ring-tightening corrections to known values for the corresponding linear compounds.

The uncertainties in the entropies and heat capacities are unlikely to exceed ± 1 cal/(mol K), whereas uncertainties in the heats of formation may vary from ± 0.1 to ± 7 kcal/mol. Estimates of errors have been listed for heats of formation but none for entropies or heat capacities. For consistency, values in the tables have been given to one decimal place.

During the research some group values were revised, and some new ones derived. The results for single ring compounds are listed in Table I. The ring corrections for multiple rings are given in each table as they occur.

Results and Discussion

One Ring. The thermochemical properties of cyclic C_6 compounds are in Table II. All the data were measured

Table I

RING CORRECTIONS FOR SINGLE RING COMPOUNDS DERIVED IN THIS WORK

Ring Correction	$\Delta H_{f,298}^\circ(\text{K})/(\text{Kcal/mol})$	$\text{Int. } S_{298}^\circ(\text{g})/(\text{cal}/(\text{mol K}))$	$C_{p,300}^\circ(\text{K})/(\text{cal}/(\text{mol K}))$
	4.2	24.0	-3.78
	0.1	21.42	-1.64
	1.2	20.0	-4.3
	0.4	18.3	-7.4
		16.94	-8.79

except the entropies and heat capacities of 1,3- and 1,4-cyclohexadiene, which were estimated by O'Neal and Benson.¹³ The heat of formation of 1,4-cyclohexadiene was obtained from the heat of hydrogenation measured by Kistiakowsky, Ruhoff, Smith, and Vaughan.¹⁴

The difference in the heats of formation of 1,3- and 1,4-cyclohexadiene of -0.5 kcal/mol is in excellent agreement with a difference of -0.3 kcal/mol in the heats of hydrogenation in acetic acid solution at 298 K measured by Turner, Mallon, Tichy, Doering, Roth, and Schroder.¹⁵

The difference in free energies of 1,3- and 1,4-cyclohexadiene calculated from Table II is -0.5 kcal/mol at 298 K. This is in excellent agreement with a value of -0.6 kcal/mol measured by Bates, Carnigan, and Staples¹⁶ in *tert*-amyl alcohol solution at 268 K, and with a value of -0.4 kcal/mol measured at 383 K by Doering, Schroder, Trautner, and Staley.¹⁶

Three explanations have been advanced to account for 1,3- and 1,4-cyclohexadiene having heats of formation within 0.5 kcal/mol of each other. First, Bates, Carnigan, and Staples¹⁷ have suggested that 1,4-cyclohexadiene has 2 kcal/mol of stabilization due to interaction of the π electrons of the two double bonds which are closer than they might be in linear 1,4-hexadienes. This postulate is not supported by the heat of hydrogenation data. The heat of hydrogenation of 1,4-cyclohexadiene to cyclohexene is -27.0 kcal/mol, whereas that of cyclohexene to cyclohexane is -28.4 kcal/mol. Second, Turner, Mallon, Tichy, Doering, Roth, and Schroder¹⁵ concluded "that 1,3-cyclohexadiene is devoid of conjugative stabilization and that interaction of the butadiene type is counterbalanced by other factors (possibly π -cloud repulsion) in this planar cisoid system. We do not believe this argument because cyclopentadiene, which is also cisoid, does have the normal strain of C_5 rings with no evidence for π -bond repulsion, and it does have the butadiene stability. Third, Benson¹⁸ has postulated that 1,3-cyclohexadiene is destabilized by H-H repulsion between the two methylene groups which are forced into a gauche position by the conjugated double bond.

The changes in $(\text{int})S_{298}^\circ$ and $C_{p,300}^\circ$ on successive addition of H_2 to benzene contribute little to the free energy change compared with the changes in ΔH_f° . With respect to symmetry numbers, O'Neal and Benson¹³ assigned a value of 1 to the symmetry number of cyclohexene, but there is a rotational axis of symmetry through the plane of the ring at the double bond, and the symmetry of cyclohexene should be 2. In addition, since there are *d* and *l* forms, there is an entropy of mixing of $R \ln 2$. Therefore,

Table II
 THERMOCHEMICAL PROPERTIES OF CYCLIC C₆ COMPOUNDS

Compound	Symmetry No.	No. of Optical Isomers	$\Delta H_f^{\circ}(g)/$ cal (mol K)	$S_{298}^{\circ}(g)/$ (cal/ mol K)	Int. $S_{298}^{\circ}(g)/$ (cal/ mol K)	$Cp_{298}^{\circ}(g)/$ (cal/ mol K)	Reference
Benzene	12	1	19.8	64.3	69.3	19.6	11
			19.8	64.3			4
1,3-Cyclohexadiene	12	1	19.8±0.1	64.3	69.3	19.5	9
			19.8±0.1				Selected
			26.0				11
1,4-Cyclohexadiene	2	1	25.9	70.9	72.3	23.7	4
			25.4±0.2				9
			25.4±0.2				13
			25.4±0.2				See text
1,4-Cyclohexadiene	4	1	26.3	70.9	73.7	24.4	11
			25.9±0.5				See text
			25.9±0.5				13
			25.9±0.5				This work
Cyclohexene	2	1	-0.8	74.3	74.3	25.3	11
			-1.3	74.3			4
			-1.1±0.2	74.3			9
			-1.1±0.2	74.3			13
Cyclohexane	6	1	-29.4	71.3	74.8	25.6	11
			-29.4	71.3			4
			-29.5±0.2	71.3			9
			-29.5±0.2	71.3			13
	6	1	-29.5±0.2	71.3	74.8	25.6	Selected

 Table III
 THERMOCHEMICAL PROPERTIES OF p-DIMETHYL BENZENE AND ITS PRODUCTS ON HYDROGENATION

Compound	Symmetry No.	No. of Optical Isomers	$\Delta H_f^{\circ}(g)/$ (kcal/mol)	$S_{298}^{\circ}(g)/$ (cal/ mol K)	Int. $S_{298}^{\circ}(g)/$ (cal/ mol K)	$Cp_{298}^{\circ}(g)/$ (cal/ mol K)	Reference
1,4-Dimethylbenzene	36	1	4.3	82.8	90.0	30.5	11
			4.3	82.8			4
			4.3±0.2	82.8			9
			4.3±0.2	82.8			Selected
1,4-Dimethyl-1,3-cyclohexadiene	18	1	8.8±1	86.0	91.8	36.0	19
2,5-Dimethyl-1,3-cyclohexadiene	9	1	10.6±1	86.3	90.6	36.4	19
1,4-Dimethyl-1,4-cyclohexadiene	18	1	9.2±1	87.4	93.2	36.7	19
3,6-Dimethyl-1,4-cyclohexadiene	18	1	11.3±1	85.0	90.7	35.7	19
1,4-Dimethyl-1-cyclohexene(exo)	9	2	-16.2±1	90.2	93.2	36.6	19
3,6-Dimethyl-1-cyclohexene(trans)	18	1	-14.4±1	86.7	92.4	35.7	19
Trans-1,4-dimethyl-cyclohexane	18	1	-44.1	87.2	92.9	38.0	11
			-44.1	87.2			4
			-44.1±0.4	87.2			9
	18	1	-44.1±0.4	87.2	92.9	38.0	Selected

the effective symmetry number is one and the ring correction is as stated by O'Neal and Benson. Note that this differs from ref 11.

The heats of formation of the cyclic C₆ compounds were used to derive ring corrections (Table I). These ring

corrections, were obtained by subtracting the sum of the group values from the selected value for the heat of formation of the parent compound. The ring corrections so obtained were used to estimate heats of formation of substituted monocyclic and polycyclic compounds. (In the

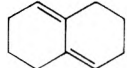
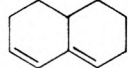
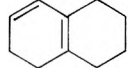
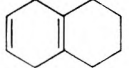
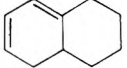
Table IV
 THERMOCHEMICAL PROPERTIES OF NAPHTHALENE (C₁₀H₈) AND DIHYDRONAPHTHALENES (C₁₀H₁₀)

Compound	Sym- metry No.	No. of Optical Isomers	$\Delta H_{f,298}^{\circ}(\text{g})/$ (kcal/mol) ^a	$S_{298}^{\circ}(\text{g})/$ (cal/ mol K)	Int. $S_{298}^{\circ}(\text{g})/$ (cal/ mol K)	$C_{p,298}^{\circ}(\text{g})/$ (cal/ mol K)	Reference
Naphthalene 	4	1	36.1	80.5	83.3		11
			36.1	80.2	83.0	31.9	4
			36.1±0.2				9
	4	1	36.1±0.2	80.4	83.2	31.5	13
					31.9	Selected	
-Dihydronaphthalenes							
1,2- 	1	1	31.6±3				See text
			34.3±2(4.2)	88.1	88.1	35.0	19
				85.4	85.4	34.2	21
			34.3±2	85.4	85.4	34.2	Selected
1,4- 	2	1	34.8±3				See text
			32.9±2(0.1)	88.5	88.5	34.4	19
				86.9	86.9	34.9	21
			32.9±2	86.9	86.9	34.9	Selected
1,5- 	2	1	55.4±2(2)	79.3	80.7	36.8	19
				86.4	87.8	36.6	21
				86.4	87.8	36.6	Selected
1,7- 	1	1	55.4±2(1.1)	78.9	78.9	39.5	19
				89.2	89.2	37.3	21
				87.8	87.8	36.6	Selected
1,8a- 	1	2	55.7±2(2)	80.7	79.3	36.7	19
				88.8	87.4	36.1	21
				88.8	87.4	36.1	Selected
2,3- 	2	1	57.7±2(5.2)	78.5	79.9	37.6	19
				86.0	87.4	36.1	21
				86.0	87.4	36.1	Selected
2,4a- 	1	2	58.9±2(1.1)	81.7	80.3	37.9	19
				90.2	88.8	36.8	21
				86.0	87.4	36.1	Selected
2,6- 	2	1	57.3±2(0.2)	77.3	78.7	40.5	19
				88.4	89.8	38.0	21
				88.4	89.8	38.0	Selected
4a,8a- 	2	cis ^b	60.5±2(2)	80.6	82.0	35.2	19
				80.6	87.4	36.1	21
				80.6	87.4	36.1	Selected

^a Ring corrections are in parentheses.

^b The trans isomer (which has a symmetry number of 2 and 2 optical isomers) is likely to be highly strained and therefore much less stable than the cis isomer.

Chart I

-Hexahydronaphthalene	1,2,3,5,6,7-	1,2,3,7,8,8a-	1,2,3,4,5,6-	1,2,3,4,5,8-	1,2,3,4,4a,5-	Nine others
						
Obsd yield, %	53.7	25.5	14.1	6.4	<1	<1
Est yield, %	29	32	0.3	0.3	32	<2

latter case, the ring corrections were assumed to be additive.) For example, the thermochemical properties of dimethylcyclohexadienes and dimethylcyclohexene in Table III were estimated using ring corrections derived¹⁹ from Table II.

The thermochemical properties of *p*-dimethylbenzene and its products on hydrogenation are in Table III. As in unsubstituted benzene, the addition of the first mole of hydrogen is endothermic. The least endothermic path (by 1 to 2 kcal/mol) is for the hydrogen to add at the carbon atoms that are unsubstituted, in accordance with Markownikoff's principle.

Two Rings. The thermochemical properties of naphthalene and the dihydronaphthalenes are in Table IV. The values for the intrinsic entropy and heat capacity of naphthalene estimated by O'Neal and Benson¹³ give good agreement with those recommended by Stull, Westrum, and Sinke.⁴

No heats of formation in the gas phase have been reported for dihydronaphthalenes, but Cox and Pilcher⁹ list values in the liquid phase for the 1,2 isomer of 18.0 ± 1.5 kcal/mol and for the 1,4 isomer of 21.0 ± 1.5 kcal/mol. The heats of vaporization of the two isomers were estimated using an empirical technique¹¹ and the known

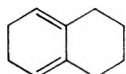
Table V
THERMOCHEMICAL PROPERTIES OF SOME TETRAHYDRONAPHTHALENES (C₁₀H₁₂)

Compound	Sym- metry No.	No. of Optical Isomers	$\Delta H_f^{\circ}(g)/$ (kcal/mol) ^a	$S_{300}^{\circ}(g)/$ (cal/ mol K)	Int. $S_{300}^{\circ}(g)/$ (cal/ mol K)	$Cp_{300}^{\circ}(g)/$ (cal/ mol K)	Reference
-Tetrahydronaphthalenes 1,2,3,4-			6.6	89.2			4
	2	2	7.3±1.3				9
			5.1	88.4	88.4	36.7	19
			7.1				See text
			5.3±0.8	88.1		35.3	22
				88.7		36.3	13
	2	2	6.0±1	88.4	88.4	35.8	Selected
(most stable nonaromatic isomer) 1,2,8,8a-	1	1	31.6±2 (2.2)	83.2	83.2	40.3	19
	1	1		93.2	93.2	39.5	21
	1	1	31.6±2	93.2	93.2	39.5	Selected
(Next most stable nonaromatic isomer) 1,2,3,5-	1	1	31.9±2 (2.2)	84.2	84.2	38.4	19
	1	1		91.4	91.4	39.1	21
	1	1	31.9±2	91.4	91.4	39.1	Selected
(Least stable nonaromatic isomer) 1,4,4a,7	1	2	39.8 (1.3)	90.0	88.6	37.7	19
	1	2		93.8	92.4	39.4	21
	1	2	39.8	93.8	92.4	39.4	Selected

^a Ring correction is in parentheses.

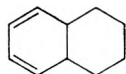
boiling points,²⁰ respectively. The heats of formation of 1,2- and 1,4-dihydronaphthalene are, therefore, 31.6 and 34.8 kcal/mol. The results are in contrast with 1,3- and 1,4-cyclohexadienes which have heats of formation that differ by only 0.5 kcal/mol.

Ring corrections for the nonaromatic rings are made by adding the ring corrections of the single rings with one exception. If a multi-ring compound contains a 1,3 conjugated double bond pair as in 1,3-cyclohexadiene, the full correction of 4.2 kcal/mol was added only if four hydrogen atoms were opposite the double bond pair, viz:

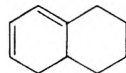


correction = 4.2 kcal/mol

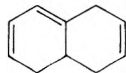
Otherwise the correction for 1,3 conjugation was taken as 1 kcal/mol, viz:



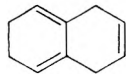
correction = 1 kcal/mol



correction = 1 kcal/mol



correction = 1 + 1.2 = 2.2 kcal/mol



correction = 4.2 + 1.2 = 5.4 kcal/mol

The reasoning here is that the exceptionally large correction factor in 1,3-cyclohexadiene arises in large part from the eclipsing of the four opposite H atoms. When there are no longer four such H atoms, the correction of 1 kcal/mol is probably correct to better than ±2 kcal/mol.

The entropies and heat capacities of 1,2- and 1,4-dihydronaphthalene were estimated as follows. The entropy and heat capacity of *n*-butylbenzene were estimated using group additivity.¹¹ The change in entropy of *n*-butylbenzene on cyclization was estimated using O'Neal and Benson's method.¹³

No measurements have been reported for the thermochemical properties of the nonaromatic dihydronaphthalenes. The heats of formation were estimated (see Table III) using group values.^{11,18} The polycyclic ring corrections for heats of formation are listed in the tables. For example, the ring correction for 1,5-dihydronaphthalene was taken to be the sum of two 1,3-cyclohexadiene ring corrections. The heats of formation of the seven nonaromatic dihydronaphthalenes range from 55.4 to 60.5 kcal/mol. Even the most stable nonaromatic isomer, 2,3-dihydronaphthalene, is more than 18 kcal/mol less stable than the aromatic isomers. The least stable isomer, 4a,8a-dihydronaphthalene, has hydrogen atoms on both bridgehead carbon atoms. The entropies and heat capacities were calculated using O'Neal and Benson's method.²¹ Ring corrections for heats of formation are a small fraction of the total, and so errors in the ring corrections are not significant. However, ring corrections for entropies are large, and adding them for two rings introduces a big uncertainty, which is reflected in the sizable difference between entropies calculated by the two methods.

There are 18 tetrahydronaphthalenes. One isomer, tetralin, is aromatic. Its thermochemical properties are in Table V. Frye and Weitkamp²³ measured the equilibrium constant for the hydrogenation of naphthalene to tetralin as a function of temperature between 575 and 730 K. A value of 7.1 kcal/mol for $\Delta H_f^{\circ}(g)$ for tetralin was calculated from Frye and Weitkamp's equilibrium constant at 624 K by use of values from Table IV for the entropy and heat capacity of naphthalene, from Table V for the entropy of tetralin, from Stull, Westrum, and Sinke⁴ for the heat capacity at 300 and 600 K for naphthalene, and from O'Neal and Benson's method for estimates of the heat capacity of tetralin at 300 and 600 K. This value is in good agreement with the other results.^{4,10,13,19,22}

The thermochemical properties of the 17 nonaromatic tetrahydronaphthalenes were estimated.^{19,21} The heats of formation range from 32 to 40 kcal/mol. They are more than 25 kcal/mol less stable than tetralin.

Table VI
 THERMOCHEMICAL PROPERTIES OF HEXAHYDRONAPHTHALENES (C₁₀H₁₄)

Compound	Sym- metry No.	No. of Optical Isomers ^a	$\Delta H_f^{\circ}(g)/$ (kcal/mol) ^b	$S_{298}^{\circ}(g)/$ (cal/ mol K)	Int. $S_{298}^{\circ}(g)/$ (cal/ mol K)	$Cp_{298}^{\circ}(g)/$ (cal/ mol K)	Reference
-Hexahydronaphthalenes							
1,2,3,4,4a,5-	1	2	7.6±2 (1)	91.6	90.2	40.5	19 21
1,2,3,4,4a,7-	1	2	10.8±2 (0.1)	92.8	91.4	40.9	19 21
1,2,3,4,4a,8a-	1 cis 2 trans	2 1(1)	9.2±2 (1)	89.6	89.6	39.6	19 21
1,2,3,4,5,6-	1	1	11.0±2 (5.4)	90.6	90.6	40.2	19 21
1,2,3,4,5,8-	2	1	11.2±2 (1.3)	90.8	92.2	40.2	19 21
1,2,3,4,6,7-	2	1	10.2±2 (4.2)	89.1	90.5	40.2	19 21
1,2,3,5,6,7-	2	1	8.4±2 (2.4)	93.2	94.6	40.1	19 21
1,2,3,5,6,8a-	1	2	12.8±2 (2.4)	95.4	94.0	39.8	19 21
1,2,3,5,8,8a-	1	2	13.3±2 (2.4)	95.6	94.0	39.8	19 21
1,2,3,7,8,8a-	1	2	9.4±2 (2.4)	95.6	94.0	39.8	19 21
1,2,4a,5,6,8a-	2 cis 1 trans	0(2) 1(1)	14.4±2 (2.4)	94.0	94.0	39.8	19 21
1,2,4a,5,8,8a-	1 cis 1 trans	0(2) 2	14.2±2 (2.4)	95.6	94.0	39.8	19 21
1,2,4a,7,8,8a-	1 cis 1 trans	0(1) 1	14.0±2 (2.4)	94.0	94.0	39.8	19 21
1,4,4a,5,8,8a-	2 cis 2 trans	0(1) 1	13.9±2 (2.4)	94.0	94.0	39.8	19 21

^aThe number in parentheses is the number of isomers not counted because, from consideration of molecular models, they are likely to be too strained.

^bThe number in parentheses is the ring correction.

Thermochemical properties of the hexahydronaphthalenes are in Table VI. The heats of formation range from 8.7 to 13.9 kcal/mol. These values are all more endothermic than that for 1,2,3,4-tetrahydronaphthalene, as a result of the loss of the aromatic stabilization.

The intrinsic entropies of the hexahydronaphthalenes were calculated as follows. The intrinsic entropy of 1-*n*-butyl-1,3-cyclohexadiene was estimated by group additivity to be 110.68 cal/(mol K). That of 5-*n*-butyl-1,3-cyclohexadiene was estimated to be 109.47 cal/(mol K), and gave an average for the two of 110.1 cal/(mol K). Cyclization involves the loss of a methyl and three large group rotors equal to 19.9, and subtraction of 19.9 gave 90.2 cal/(mol K) for 1,2,3,4,4a,5-hexahydronaphthalene.

The intrinsic entropies of 1- and 3-*n*-butyl-1,4-cyclohexadienes were estimated by group additivity to be 112.08 and 110.47 cal/(mol K), respectively, and gave an average of 111.28 cal/(mol K). 19.9 was subtracted for cyclization and gave 91.4 cal/(mol K) for 1,2,3,4,4a,7-hexahydronaphthalene.

The intrinsic entropy of 5-*n*-butyl-1,3-cyclohexadiene was estimated to be 109.47 cal/(mol K). 19.9 was sub-

tracted for cyclization and gave 89.6 cal/(mol K) for 1,2,3,4,4a,8a-hexahydronaphthalene.

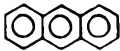
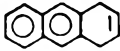
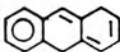
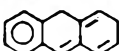
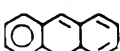
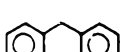
The intrinsic entropies of 1- and 2-*n*-butylcyclohexadienes were estimated to be 110.68 and 110.37 cal/(mol K), respectively, and gave an average of 110.52 cal/(mol K). 10.9 was subtracted for cyclization and gave 90.6 cal/(mol K) for 1,2,3,4,5,6-hexahydronaphthalene.

The intrinsic entropy of 1-*n*-butyl-1,4-cyclohexadiene is 112.08 cal/(mol K) (see above). 19.9 was subtracted for cyclization and gave 92.2 cal/(mol K) for 1,2,3,4,5,8-hexahydronaphthalene.

The intrinsic entropy of 2-*n*-butyl-1,3-cyclohexadiene is 110.37 cal/(mol K) (see above). 19.9 was subtracted for cyclization and gave 90.5 cal/(mol K) for 1,2,3,4,6,7-hexahydronaphthalene.

The intrinsic entropy of 1- and 3-*n*-butylcyclohexene were estimated to be 114.06 and 112.85 cal/(mol K), respectively, and gave an average of 113.45 cal/(mol K). The following corrections were added: -19.9 for cyclization, -0.4 for loss of 2 H, and +1.4 for tightness (a consequence of O'Neal and Benson's assignment¹³ of a symmetry number of 1 for cyclohexene). The result was that the intrinsic

Table VII
 THERMOCHEMICAL PROPERTIES OF ANTHRACENE (C₁₄H₁₀) AND AROMATIC DIHYDROANTHRACENES (C₁₄H₁₂)

Compound	Sym- metry No.	No. of Optical Isomers	$\Delta H_f^{\circ}(g)/$ (kcal/mol) ^a	$S_{298}^{\circ}(g)/$ (cal/ mol K)	Int. $S_{298}^{\circ}(g)/$ (cal/ mol K)	$C_p^{\circ}(g)/$ (cal/ mol K)	Reference
Anthracene 			55.2				11
			55.2±1.1				9
	4	1		94.6	97.4	44.4	21
	4	1		92.5	95.3	44.4	24
	4	1	55.2±1.1	92.5	95.3	44.4	Selected
-Dihydroanthracenes (aromatic)							
1,2- 	1	1	50.9±2(4.2)	100.6	100.6	47.2	19 21
1,4- 	2	1	49.7±2(0.1)	100.6	102.0	47.9	19 21
1,10- 	1	1	64.5±2(2)	104.8	104.8	49.2	19 21
2,9- 	1	1	66.4±2(2.1)	104.8	104.8	50.0	19 21
4a,10- 	1	2	64.6±2(2)	106.2	104.8	49.2	19 21
9,10- 			40.0±2(0.1)				19
			38.2±1.1				9
	4	1		99.2	102.0	47.8	21
	4	1	38.2±1.1	99.2	102.0	47.8	Selected

^aThe ring correction is in parentheses.

entropy of 1,2,3,5,6,7-hexahydronaphthalene was estimated to be 94.6 cal/(mol K).

The intrinsic entropies of 3- and 4-*n*-butylcyclohexene were estimated to be 112.85 and 112.86 cal/(mol K), respectively, and gave an average of 112.86 cal/(mol K). Corrections of -19.9 for cyclization, -0.4 for loss of 2 H, and +1.4 for tightness gave 94.0 cal/(mol K) for 1,2,3,5,6,8a-hexahydronaphthalene.

The intrinsic entropy of 4-*n*-butylcyclohexene was estimated to be 112.86 cal/(mol K). -18.9 was added for cyclization, loss of 2 H, and tightness, and gave 94.0 cal/(mol K) for 1,2,3,5,8,8a-hexahydronaphthalene.

By inspection, the intrinsic entropies of the remaining hexahydronaphthalenes were taken to be 94.0 cal/(mol K). Bates, Carnighan, and Staples¹⁷ have measured the relative stabilities of the hexahydronaphthalenes. Equilibrium mixtures were prepared by heating 1,2,3,7,8,8a- or 1,2,3,4,5,8-hexahydronaphthalene with potassium *tert*-amyl oxide in *tert*-amyl alcohol at 457 K for 24 h. They found an equilibrium distribution of isomers as shown in Chart I. The estimates correctly predict that two of the three most stable isomers are 1,2,3,5,6,7- and 1,2,3,7,8,8a-hexahydronaphthalene. This comparison indicates that the methods described herein are useful for the more stable isomers. The discrepancy of approximately 4 kcal/mol between the two stable isomers and the others may, in fact, be that our use of the group C_d-C_d-H, which is taken directly from 1,3-butadiene, may render the stable isomers relatively more stable. In the absence of specific confirming data, such as the heat of hydrogenation of 1,2,3,5,6,7-hexahydronaphthalene, we will continue to use this group in the larger compounds tabulated later. The error, if any, is less important in the larger compounds since this group does not occur in the more stable (i.e., more aromatic) isomers.

Three Rings. There are two hydrocarbons that have three six-membered rings and that are completely aromatic. The compounds are anthracene and phenanthrene.

The thermochemical properties of anthracene are in Table VII. The heat of formation has been measured previously;⁴ the entropy and heat capacity were estimated.²⁴

We have identified 16 dihydroanthracenes. The thermochemical properties of the six isomers that contain at least one aromatic ring are in Table VII. The heat of formation of the most stable isomer, 9,10-dihydroanthracene, has been measured.⁴ The next most stable isomer is 1,2-dihydroanthracene. Its heat of formation is 10 kcal/mol more than the 9,10 isomer. The heats of formation of the nonaromatic isomers range from 90 to 100 kcal/mol. They are 50 to 60 kcal/mol more than the 9,10 isomer.

We have identified 80 tetrahydroanthracenes, of which 15 contain at least one aromatic ring. The thermochemical properties of the 15 aromatic isomers were estimated. The most stable isomer (1,2,3,5-tetrahydroanthracene) has two aromatic rings, see Table VIII. Its heat of formation is 18 kcal/mol less than the next most stable isomer which has only one aromatic ring. Of the isomers having only one aromatic ring, 1,2,9,9a-tetrahydroanthracene, which has benzene ring on the outside of the three rings, is the most stable, whereas 1,2,5,6- and 1,2,7,8-tetrahydroanthracenes, which have the benzene ring in the middle, are the least stable.

We have identified 99 isomeric hexahydroanthracenes, of which 7 are aromatic. The thermochemical properties of the 7 aromatic isomers are in Table IX. The difference between the most and least stable of the isomers is 4.1 kcal/mol. The two most stable isomers have structures that have conjugative interactions similar to that in styrene. There are two isomeric aromatic octahydroanthracenes. Their thermochemical properties are very similar (see Table IX).

The thermochemical properties of phenanthrene are in Table X. The heat of formation was measured; the entropy and heat capacity were estimated.²⁴

Table VIII
THERMOCHEMICAL PROPERTIES OF SOME AROMATIC TETRAHYDROANTHRACENES (C₁₄H₁₄)

Compound	Symmetry No.	No. of Optical Isomers	$\Delta H_f^{\circ}(g)/$ (kcal/mol) ^a	$S_{298}^{\circ}(g)/$ (cal/mol K)	Int. $S_{298}^{\circ}(g)/$ (cal/mol K)	$CP_{298}^{\circ}(g)/$ (cal/mol K)	Reference	
-Tetrahydroanthracenes								
(Most stable isomer)								
1,2,3,4-		2	1	22.3±2(1.2)	102.4	103.8	49.2	19 21
(Next most stable isomer)								
1,2,9,9a-		1	1	41.7±2(2.2)	106.6	106.6	50.6	19 21
(Least stable isomer)								
1,2,5,6-		4	1	48.9±2(8.4)	102.4	103.8	50.0	19 21
1,2,7,8-		2	1	48.9±2(8.4)	102.4	103.8	50.0	19 21

^a The ring correction is in parentheses.

Table IX
THERMOCHEMICAL PROPERTIES OF AROMATIC HEXA- AND OCTAHYDRO-ANTHRACENES (C₁₄H₁₆ AND C₁₄H₁₈)

Compound	Symmetry No.	No. of Optical Isomers	$\Delta H_f^{\circ}(g)/$ (kcal/mol) ^a	$S_{298}^{\circ}(g)/$ (cal/mol K)	Int. $S_{298}^{\circ}(g)/$ (cal/mol K)	$CP_{298}^{\circ}(g)/$ (cal/mol K)	Reference	
Aromatic hexahydro-anthracenes								
1,2,3,4,4a,10-		1	2	16.8±2(1)	107.0	105.6	51.0	19 21
1,2,3,4,5,6-		1	1	20.2±2(5.4)	105.6	105.6	52.0	19 21
1,2,3,4,5,8-		2	1	18.9±2(1.3)	107.0	108.4	54.2	19 21
1,2,3,4,9,10-		2	1	18.2±2(1.3)	105.6	107.0	52.8	19 21
1,2,3,9,9a,10-		1	2	20.3±2(2.4)	109.8	108.4	52.8	19 21
1,2,4a,9,9a,10-		1	cis 2 trans 2	21.0±2(2.4)	109.8	108.4	52.8	19 21
1,4,4a,9,9a,10-		1	cis 1 trans 2	20.8±2(2.4)	108.4	108.4	52.8	19 21
Aromatic octahydro-anthracenes								
1,2,3,4,4a,9,9a,10-		1	cis 1 trans 2	-7.9±2(1.2)	109.4	109.4	54.2	19 21
1,2,3,4,5,6,7,8-		4	1	-8.2±2(2.4)	107.4	110.2	55.6	19 21

^a The ring correction is in parentheses.

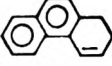
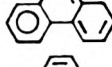
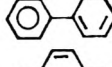
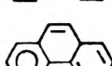
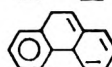
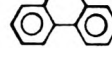
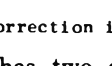
We have identified 28 dihydrophenanthrenes. The thermochemical properties of the 13 isomers that contain at least one aromatic ring are in Table IX. The heats of formation of the isomers that contain two aromatic rings are in the range 41.8–51.3 kcal/mol, compared with 68.4–73.7 kcal/mol for the isomers that contain only one aromatic ring.²⁵ The heat of formation of 9,10-dihydroanthracene has been measured.⁹ It also was estimated using a value of 0.1 kcal/mol for the ring correction of the

partially hydrogenated ring. This value was chosen because it is the same as in 1,4-cyclohexadiene. As in the dihydroanthracenes, the most stable isomer has the benzene rings separated.

9,10-Dihydroanthracene is 3.6 kcal/mol more stable than 9,10-dihydrophenanthrene. This is consistent with the difference between 1,3- and 1,4-cyclohexadienes.

We have identified 123 tetrahydrophenanthrenes of which 25 are aromatic. One isomer (1,2,3,4-tetrahydro-

Table X
THERMOCHEMICAL PROPERTIES OF PHENANTHRENE (C₁₄H₁₀) AND AROMATIC DIHYDROPHENANTHRENES (C₁₄H₁₂)

Compound	Symmetry No.	No. of Optical Isomers	$\Delta H_f^{\circ}(g)/(kcal/mol)^a$	$S_{298}^{\circ}(g)/(cal/mol K)$	Int. $S_{298}^{\circ}(g)/(cal/mol K)$	$C_p^{\circ}(g)/(cal/mol K)$	Reference
Phenanthrene 			49.5				11
			49.5				4
	2	1	49.5±1.1	96.0	97.4	44.4	9
	2	1		93.9	95.3	44.4	21
	2	1	49.5±1.1	93.9	95.3	44.4	24
							Selected
Aromatic Dihydrophenanthrenes							
1,2- 	1	1	50.9±2(4.2)	100.6	100.6	47.0	19 21
1,4- 	1	1	49.4±2(0.1)	102.0	102.0	47.8	19 21
1,9- 	1	1	65.2±2(1.1)	104.4	104.4	47.6	19 21
1,10a- 	1	2	66.5±2(2)	104.4	103.0	47.2	19 21
2,3- 	1	1	67.5±2(5.2)	103.0	103.0	47.2	19 21
2,4a- 	1	2	68.3±2(1.5)	105.8	104.4	47.6	19 21
3,4- 	1	1	50.9±2(4.2)	100.6	100.6	47.0	19 21
3,9- 	1	1	66.1±2(0.2)	105.8	105.8	48.6	19 21
3,10a- 	1	2	69.7±2(1.1)	105.8	104.4	47.8	19 21
4,4a- 	1	2	65.2±2(2)	104.4	103.0	47.2	19 21
4a,9- 	1	2	66.4±2(1.1)	105.8	104.4	47.6	19 21
4a,10a- 	1 cis	2	70.0±2(2)	104.4	103.0	47.2	19 21
	1 trans	2					
9,10- 	2	1	41.8±2(4.2)	99.2	100.6	47.0	19 21

^aThe ring correction is in parentheses.

phenanthrene) has two aromatic rings and is 20–28 kcal/mol more stable than the examples in Table XI which have only one aromatic ring. Other isomers are probably equally unstable.

We have identified 167 hexahydrophenanthrenes. The thermochemical properties of the 11 aromatic isomers are in Table XII. The heats of formation vary from 17.0 to 23.5 kcal/mol. The more stable isomers have the double bond in the same position relative to the aromatic ring as styrene.

The thermochemical properties of the two aromatic octahydrophenanthrenes are very similar (see Table XII).

Four Rings. The measured heat of formation and estimated entropy and heat capacity of pyrene are in Table XIII. The entropy and heat capacity were estimated²⁴ by cyclizing 4-ethylphenanthrene to 4,5-dihdropyrene and then dehydrogenating and tightening the nonaromatic ring.

We have identified one dihydropyrene that has three aromatic rings and seven dihydropyrenes that have two aromatic rings (see Table XIII B). The heat of formation of 4,5-dihdropyrene was estimated from that of phen-

anthrene by adding and subtracting the necessary groups¹⁹ and by assuming that the ring correction was 3 kcal/mol for the nonaromatic ring. The heat of formation of 4,5-dihdropyrene is 2.7 kcal/mol less than that of pyrene. Estimation of the entropy and heat capacity of 4,5-dihdropyrene was discussed above.

We have identified six tetrahydropyrenes that have two aromatic rings (see Table XIV). The heat of formation of 4,5,9,10-tetrahydropyrene was estimated from that of 9,10-dihydrophenanthrene, assuming that the ring correction was 2 kcal/mol.

The entropy and heat capacity of 4,5,9,10-tetrahydropyrene were estimated²¹ from 3,4-dihdropyrene.

We have identified 34 aromatic hexahydropyrenes (see Table XV). Two of the isomers have two aromatic rings, and the remainder have one aromatic ring. The heat of formation of 1,2,3,3a,4,5-hexahydropyrene was estimated from that of 1,2,3,4-tetrahydrophenanthrene assuming a ring correction of 2 kcal/mol. The heat of formation of 1,2,3,6,7,8-hexahydropyrene was estimated from that of naphthalene, assuming that each of the two ring correc-

Table XI
 THERMOCHEMICAL PROPERTIES OF SOME AROMATIC TETRAHYDROPHENANTHRENES (C₁₄H₁₄)

Compound	Symmetry No.	No. of Optical Isomers	$\Delta H_f^{\circ}(g)/$ (kcal/mol) ^a	$S_{298}^{\circ}(g)/$ (cal/mol K)	Int. $S_{298}^{\circ}(g)/$ (cal/mol K)	$Cp_{298}^{\circ}(g)/$ (cal/mol K)	Reference
1,2,3,4-		1	22.3±2(1.2)	103.8	103.8	49.2	19 21
2,3,4,4a-		2	42.0±2(2.2)	108.0	106.6	50.6	19 21
1,4,5,8-		1	49.5±2(0.2)	105.2	106.6	51.4	19 21

^aThe ring correction is in parentheses.

 Table XII
 THERMOCHEMICAL PROPERTIES OF SOME AROMATIC HEXA- AND OCTAHYDROPHENANTHRENES (C₁₄H₁₆ AND C₁₄H₁₈)

Compound	Symmetry No.	No. of Optical Isomers	$\Delta H_f^{\circ}(g)/$ (kcal/mol) ^a	$S_{298}^{\circ}(g)/$ (cal/mol K)	Int. $S_{298}^{\circ}(g)/$ (cal/mol K)	$Cp_{298}^{\circ}(g)/$ (cal/mol K)	Reference
Aromatic hexahydrophenanthrenes							
1,2,3,4,4a,9-	1	2	18.4±2(0.1)	108.4	107.0	52.8	19 21
1,2,3,4,4a,10-	1	2	18.5±2(1)	107.0	105.6	52.0	19 21
1,2,3,4,5,6-	1	1	20.3±2(5.4)	105.6	105.6	52.0	19 21
1,2,3,4,5,8-	1	1	18.9±2(1.3)	107.0	107.0	52.8	19 21
1,3,4,7,8-	1	1	20.3±2(5.4)	105.6	105.6	52.0	19 21
1,2,3,4,9,10-	1	1	19.7±2(5.4)	105.6	105.6	52.0	19 21
1,2,3,9,10,10a-	1	2	18.1±2(2.4)	109.8	108.4	52.8	19 21
1,2,4a,9,10,10a-	1	2	21.4±2(2.4)	109.8	108.4	52.8	19 21
1,4,4a,9,10,10a-	1	2	23.5±2(2.4)	109.8	108.4	52.8	19 21
2,3,4,4a,9,10-	1	2	20.3±2(2.4)	109.8	108.4	52.8	19 21
3,4,4a,9,10,10a-	1	2	21.8±2(2.4)	109.8	108.4	52.8	19 21
Aromatic octahydrophenanthrenes							
1,2,3,4,5,6,7,8-	2	1	-8.2±2(2.4)	108.8	110.2	54.2	19 21
1,2,3,4,4a,9,10,10a-	1	2	-7.1±2(1.2)	110.2	108.8	54.2	19 21

^aThe ring correction is in parentheses.

Table XIII

THERMOCHEMICAL PROPERTIES OF PYRENE (C₁₆H₁₀) AND 4,5-DIHYDROPYRENE (C₁₆H₁₂)

Compound	Sym- metry No.	No. of Optical Isomers	$\Delta H_f^{\circ}(g)/$ (kcal/mol)	$S_{298}^{\circ}(g)/$ (cal/ mol K)	Int. $S_{298}^{\circ}(g)/$ (cal/ mol K)	$C_p^{\circ}(g)/$ (cal/ mol K)	Reference
Pyrene 	4	1	49.9±0.6				9
	4	1	51.6±0.4	96.2	98.9	50.2	24 Selected
-Dihydropyrenes (having 3 aromatic rings) 4,5- 	2	1	47.2±3	104.3	105.7	50.7	See text 21

Table XIV

THERMOCHEMICAL PROPERTIES OF 4,5,9,10-TETRAHYDROPYRENE

Compound	Sym- metry No.	No. of Optical Isomers	$\Delta H_f^{\circ}(g)/$ (kcal/mol)	$S_{298}^{\circ}(g)/$ (cal/ mol K)	Int. $S_{298}^{\circ}(g)/$ (cal/ mol K)	$C_p^{\circ}(g)/$ (cal/ mol K)	Reference
4,5,9,10- Tetrahydropyrene 	4	1	38.5±3	106.1	108.9	53.5	See Text

Table XV

THERMOCHEMICAL PROPERTIES OF AROMATIC HEXAHYDROPYRENES THAT HAVE TWO AROMATIC RINGS

Compound	Sym- metry No.	No. of Optical Isomers	$\Delta H_f^{\circ}(g)/$ (kcal/mol)	$S_{298}^{\circ}(g)/$ (cal/ mol K)	Int. $S_{298}^{\circ}(g)/$ (cal/ mol K)	$C_p^{\circ}(g)/$ (cal/ mol K)	Reference
-Hexahydropyrene (having 2 aromatic rings) 1,2,3,3a,4,5- 	1	2	20.1±3	113.9	112.5	55.6	See text
1,2,3,6,7,8- 	4	1	19.6±3	109.7	112.5	55.6	See text

tions was 2 kcal/mol. The entropy and heat capacity of 1,2,3,3a,4,5-hexahydropyrene was estimated²¹ from those of 3,4-dihydropyrene. The entropy and heat capacity of 1,2,3,6,7,8-hexahydropyrene were assumed to be equal to those of the 1,2,3,3a,4,5 isomer.

Oxygenated Compounds. The thermochemical properties of some oxygenated six-membered cyclic and polycyclic compounds containing one to three rings are in Table XVI. We have studied two compounds that contain a single ring: tetrahydro-2*H*-pyran and 2,5-dimethyl-tetrahydro-2*H*-pyran.

The heat of formation of tetrahydro-2*H*-pyran has been measured.^{4,9} The entropy and heat capacity were estimated²¹ from those of ethyl *n*-propyl ether. Ring corrections were derived from the entropy and heat capacity of tetrahydro-2*H*-pyran and used to estimate the entropy and heat capacity of 2,5-dimethyltetrahydro-2*H*-pyran. The heat of formation of the latter was estimated.¹⁹ The difference between the heat of formation of cyclohexane and tetrahydro-2*H*-pyran is 23.9 kcal/mol,

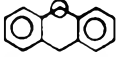
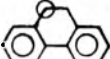
whereas the difference between the dimethyl compounds is 26.1 kcal/mol. There may therefore be a slight stabilizing interaction between the oxygen atom and the methyl group.

For compounds containing two rings, we have estimated the thermochemical properties of the compounds obtained when an oxygen atom is substituted for a methylene group in 1,2- and 1,4-dihydronaphthalene, namely 2*H*-chromene, 4*H*-chromene, and isochromene, and of some compounds obtained when 1 and 2 mol of hydrogen were added to the chromenes and the isochromene.

The heat of formation of 2*H*-chromene and isochromene were estimated by group additivity¹⁹ assuming that the ring corrections were zero. The heat of formation of 4*H*-chromene was estimated by group additivity, assuming that the ring correction was zero, and that the (O-C_B,C_D) group has the same value as the O-C_A group. The latter assumption may introduce a sizable error. For example, the difference between the (O-C_D) and (O-C_B) groups is 7.5 kcal/mol.¹²

Table XVI

THERMOCHEMICAL PROPERTIES OF SOME OXYGENATED SIXMEMBERED CYCLIC AND POLYCYCLIC COMPOUNDS CONTAINING ONE TO THREE RINGS

Compound	Sym- metry No.	No. of Optical Isomers	$\Delta H_f^{\circ}(g)/$ (kcal/mol) ^a	$S_{298}^{\circ}(g)/$ (cal/ mol K)	Int. $S_{298}^{\circ}(g)/$ (cal/ mol K)	$C_p^{\circ}(g)/$ (cal/ mol K)	Reference	
<u>One Ring</u>								
Tetrahydro-2H- pyran			-53.5				11	
			-53.5				4	
		1	1	-53.4±0.2	74.7	74.7	22.2	9
		1	1		74.7	74.7	22.2	21
							Selected	
2,5-Dimethyl tetrahydro-2H- pyran		9 cis	2	-70.2±2	89.6	92.5	32.3	19
		9 trans	2					
<u>Two Rings</u>								
2H-Chromene		1	1	3.8±3 (0)	86.6	86.6	31.8	See text 21
4H-Chromene		1	1	0.2±7 (0)	88.0	88.0	32.5	See text 21
Isochromene		1	1	1.2±3 (0)	86.6	86.6	31.8	See text 21
Chroman		1	1	-21.9±2 (1.2)	89.8	89.8	33.9	19 21
Isochroman		1	1	-18.8±5 (1.2)	89.8	89.8	33.9	19 See text
3,5,6,7-Tetrahydro- 2H-chromene		1	1	-16.7±2 (2.4)	93.0	93.0	37.4	19 21
3,5,6,7-Tetrahydro- 1H-2-benzopyran		1	1	-14.3±2 (2.4)	93.0	93.0	37.4	19 See text
4,6,7,8-Tetrahydro- 3H-2-benzopyran		1	1	-21.5±2 (2.4)	93.0	93.0	37.4	19 See text
<u>Three Rings</u>								
Xanthene				11.6±1.2 13.3				4
		2	1		100.8	102.2	47.8	See text
		2	1	11.6±1.2	100.6	102.0	47.8	See text Selected
6H-Dibenzo[b,d]- pyran				13.1±3				See text
		1	1		100.6	100.6	47.0	See text
		1	1	13.1±3	100.6	100.6	47.0	Selected

^a The ring correction is in parentheses.

The thermochemical properties of chroman and isochroman were estimated. The heats of formation were estimated using group additivity¹⁹ assuming that the ring correction for each isomer was 1.2 kcal/mol as in 3,4-dihydro-2H-pyran.¹² This should be a good approximation for chroman, because the oxygen atom and the double bond are next to each other in both compounds. However, in isochroman, the oxygen atom and double bond are separated by a methylene group, and the approximation may not be as good as for chroman. The uncertainty in the heat of formation of isochroman is, therefore, greater than in chroman.

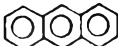
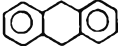
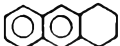
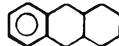
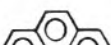
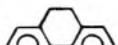
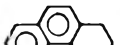
The entropy and heat capacity of chroman was estimated²¹ from those of *n*-propyl cyclohexyl ether. The entropy and the heat capacity of *n*-propyl cyclohexyl ether were estimated using group additivity.¹¹ The entropy and heat capacity of isochroman were assumed to be equal to those of chroman.

The most stable hexahydronaphthalene is the 1,2,3,5,6,7 isomer (see Table VI). We have, therefore, assumed that when 1 mol of hydrogen is added to chroman or isochroman, the double bonds are located as in 1,2,3,5,6,7-hexahydronaphthalene. On hydrogenation, chroman gives

one such compound, and isochroman gives two isomers. The heats of formation of all three compounds were estimated by group additivity,¹⁹ assuming for each compound a total ring correction of 2.4 kcal/mol (1.2 for the -ene ring and 1.2 for the O ring). The heat of formation of 4,6,7,8-tetrahydro-3H-2-benzopyran is 7.2 kcal/mol less than that of 3,5,6,7-tetrahydro-1H-2-benzopyran, suggesting a stabilizing interaction between the oxygen atom and the double bond. The entropy and heat capacity of 3,5,6,7-tetrahydro-2H-chromene were estimated²¹ and assumed equal to those of the other isomers.

The thermochemical properties of the compounds obtained by substituting an oxygen atom for a methylene group in 9,10-dihydroanthracene and in 9,10-dihydrophenanthrene are in Table XVI. The heat of formation of xanthene has been measured.⁴ The heats of formation of both isomers were estimated by adding or subtracting appropriate groups from the corresponding hydrocarbons, 9,10-dihydroanthracene and 9,10-dihydrophenanthrene. These results show that the difference in the heats of formation of the oxygenated compounds is negligible. The entropies and heat capacities of the oxygenated compounds were assumed to be the same as the hydrocarbons obtained

Table XVII
HEATS OF FORMATION ($\Delta H_{f, 298}^{\circ}$ (g)/(kcal/mol)) AND DIFFERENCES (Δ) IN THE HEATS OF FORMATION OF THE MOST STABLE ISOMERS OBTAINED WHEN SUCCESSIVE MOLES OF HYDROGEN ARE ADDED TO SOME SIXMEMBERED CYCLIC AND POLYCYCLIC COMPOUNDS RELATED TO COAL

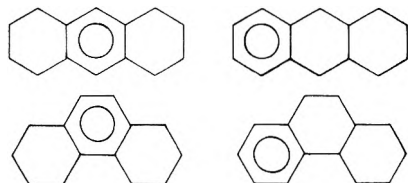
Compound	Δ	+1 Mole H_2	Δ	+2 Moles H_2	Δ	+3 Moles H_2	Δ	+4 Moles H_2
	19.8		26.5		-29.5			
	-5.6	25.4	-1.1	28.4				
	4.3		25.0		-44.1			
	-4.5	8.8	-16.2	27.9				
	36.1		26.9		9.4			
	3.2	32.9	6.0	-3.4				
	55.2		15.9		16.8			
	17.0	38.2	22.3	5.5	24.7		-7.9	
	49.5		19.5		18.1			
	7.7	41.8	22.3	4.2	25.2		-7.1	
	49.9		8.7		19.6			
	2.7	47.2	38.5	18.9				
	0.2		-5.2		-16.7			
	22.1	-21.9	-16.7					
	1.2		-2.7		-21.5			
	20.0	-18.8	-21.5					

by substituting methylene groups for the oxygen atoms.

Conclusions

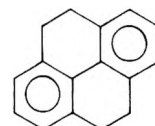
This research provides information that is relevant to three areas of the chemistry of coal, namely, the structure of coal, the thermodynamically most favorable route for hydrogenation, and the comparison of equilibria for hydrogenation with those for hydrocracking.

Structure of Coal. In coal, it is possible that structures having a given molecular formula are present in proportion to their thermodynamic stability. For example, if a coal is known to contain a significant amount of three-ring structures, each with six atoms per ring and with a molecular formula of $C_{14}H_{18}$, then we may conclude from Tables IX and XII that there will be almost equal amounts of the four isomers

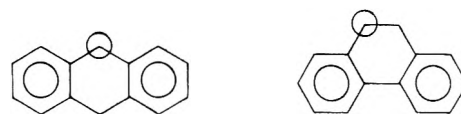


Similarly, if a coal is known to contain a significant amount of hydropyrene structures with a molecular formula of

$C_{16}H_{14}$, then it would be likely (from Table XIV) that the predominant form will have the structure



Finally, if a coal is known to contain a significant amount of dibenzopyran structures, then from Table XVI the structures are equally likely to be

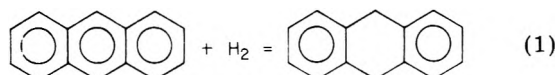


Hydrogenation of Coal. The multi-ring aromatic structures thought to be present in coal are very stable to heat. It is clear that if they are to be broken down to give high yields of liquids, such as benzene, the multi-ring aromatic structures must be hydrogenated. Our results permit us to predict which isomers will be thermodynamically favored when a given structure is hydrogenated and to calculate the amount of heat liberated or consumed during the hydrogenation. The thermodynamically most favorable isomers (neglecting entropy differences) formed

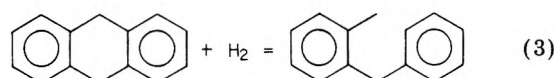
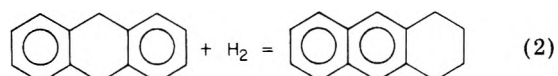
during the successive hydrogenation of the aromatic hydrocarbons are summarized in Table XVII. The results in the earlier tables show that the most important factor in determining which isomer is the most stable is the number of aromatic rings. In the di- and tetrahydronaphthalenes, the difference between an isomer that contains an aromatic ring and one that does not is 27 kcal/mol. In the di- and tetrahydroanthracenes and -hydrophenanthrenes and in the dihydropyrenes, the difference of one aromatic ring is 17.7–20.5 kcal/mol. The next most important factor is the interaction between a double bond and an aromatic ring, as in styrene. This result is based on our estimate that 1,2-dihydronaphthalene is 1.4 kcal/mol less stable than 1,4-dihydronaphthalene. Experimental verification of the size of the interaction by measuring the equilibrium constant between 1,2- and 1,4-dihydronaphthalene would be most welcome.

The addition of 1 mol of hydrogen to a double bond results in a loss of entropy of 31.2 cal/(mol K) at 298 K for a standard state of 1 atm. At 298 K, this corresponds to a gain of 9.3 kcal/mol in free energy. Clearly, a hydrogenation that is endothermic is particularly unfavorable from a thermodynamic point of view. The heats of hydrogenation are in Table XVII. The higher the heat, the more favorable the hydrogenation. Thus, the thermodynamically most favorable hydrogenation is the cyclohexene to cyclohexane, and the least favorable hydrogenation is of chroman to 3,5,6,7-tetrahydro-2*H*-chromene.

Competition between Hydrogenation and Hydrocracking. As mentioned earlier, hydrogen is added to the multi-ring aromatic structures thought to be present in coal to make it easier to break them down into liquid products. Because hydrogen is expensive, it might at times be preferable to hydrocrack an hydroaromatic structure instead of hydrogenating it further. For example, consider anthracene. The addition of 1 mol of hydrogen give 9,10-dihydroanthracene as the most stable product



Further addition of 1 mol of hydrogen gives two possible products, the one of hydrogenation, reaction 2; the other of hydrocracking, reaction 3. The relative amounts of



1,2,3,4-tetrahydroanthracene and of phenyltolylmethane depend directly on the differences in heat of formation and entropy of the two isomers. The present results, together with the thermochemical properties of the corresponding ring-opened products will, therefore, give the equilibrium amounts as a function of temperature of the products of hydrogenation or hydrocracking.

Acknowledgment. This research was performed for the United States Energy Research and Development Administration under Contract E(49-18)-2202. We thank S. E. Stein for many useful discussions, E. F. Meyer for helpful correspondence, and I. S. Shaw and E. Adkins for typing the manuscript.

References and Notes

- (1) Homogeneous Catalytic Hydrocracking Processes for Conversion of Coal to Liquid Fuels: Basic and Exploratory Research SRI Project 4799, ERDA Contract No. E(49-18)-2202 (in progress).
- (2) W. H. Wiser, S. Singh, Q. A. Quader, and G. R. Hill, *Ind. Eng. Chem., Prod. Res. Develop.*, **9**, 350 (1970).
- (3) S. W. Benson, "Thermochemical Kinetics: Methods for the Estimation of Thermochemical Data and Rate Parameters", Wiley, New York, N.Y., 1968.
- (4) D. R. Stull, E. F. Westrum, and G. C. Sinke, "The Chemical Thermodynamics of Organic Compounds", Wiley, New York, N.Y., 1969.
- (5) R. Shaw, *J. Chem. Eng. Data*, **14**, 461 (1969).
- (6) A. M. Patterson, L. T. Capell, and D. F. Walker, "The Ring Index", American Chemical Society, Washington, D.C., 1960.
- (7) Chemical Abstracts Index Guide, **76**, January–June, 1972.
- (8) After the research was completed, W. C. Herndon (private communication) developed another method for counting structures that accurately predicted the number of isomeric dihydronaphthalenes.
- (9) J. D. Cox and G. Pilcher, "Thermochemistry of Organic and Organometallic Compounds", Academic Press, New York, N.Y., 1970.
- (10) Bulletin of Thermodynamics and Thermochemistry, published annually by the International Union of Pure and Applied Chemistry, E. F. Westrum, Jr., Ed., University of Michigan, Ann Arbor, Mich.
- (11) S. W. Benson, F. R. Cruickshank, D. M. Golden, G. R. Haugen, H. E. O'Neal, A. S. Rodgers, R. Shaw, and R. Walsh, *Chem. Rev.*, **60**, 279 (1969).
- (12) H. K. Eigenmann, D. M. Golden, and S. W. Benson, *J. Phys. Chem.*, **77**, 1687 (1973).
- (13) H. E. O'Neal and S. W. Benson, *J. Chem. Eng. Data*, **15**, 266 (1970).
- (14) G. B. Kistiakowsky, J. R. Ruhoff, H. A. Smith, and W. E. Vaughan, *J. Am. Chem. Soc.*, **58**, 146 (1936).
- (15) R. B. Turner, B. J. Mallon, M. Tichy, W. von E. Doering, W. R. Roth, and G. Schröder, *J. Am. Chem. Soc.*, **95**, 8605 (1973).
- (16) W. von E. Doering, G. Schröder, K. Trautner, and S. Staley, Abstracts, 144th National Meeting of the American Chemical Society, Los Angeles, Calif., April 1963, p 14M.
- (17) R. B. Bates, R. H. Carnighan, and C. E. Staples, *J. Am. Chem. Soc.*, **85**, 3030 (1963).
- (18) S. W. Benson, "Thermochemical Kinetics: Methods for the Estimation of Thermochemical Data and Rate Parameters", 2nd ed, Wiley, New York, N.Y., 1976.
- (19) Estimated using group values derived in this work or from ref 11 and 12.
- (20) "Handbook of Chemistry and Physics", 55th ed, Chemical Rubber Publishing Co., Cleveland, Ohio, 1974–1975, p C380.
- (21) Estimated by using O'Neal and Benson's method (ref 13).
- (22) R. H. Boyd, S. N. Sanwal, S. Shary-Tehrany, and D. McNally, *J. Phys. Chem.*, **75**, 1264 (1971).
- (23) C. G. Frye and A. W. Weikamp, *J. Chem. Eng. Data*, **14**, 372 (1969).
- (24) S. E. Stein, D. M. Golden, and S. W. Benson, *J. Phys. Chem.*, submitted for publication.
- (25) NOTE ADDED IN PROOF: Communication by W. D. Good of his recently measured value for the heat of formation of 9,10-dihydrophenanthrene reveals a discrepancy of 5 kcal/mol between his measured value of 36.96 ± 0.38 kcal/mol and our estimated value of 41.8 ± 2 kcal/mol for $\Delta H_f^\circ_{298}(\text{g})$. Our estimated value includes 4.2 kcal/mol of strain energy, an amount based on the assumption that the 1,3-cyclohexadiene structure of the central ring in 9,10-dihydroanthracene will contribute the same "strain" as it does in cyclohexadiene itself, since it was presumed that the strain arises from the adjacent methylene groups being forced into gauche or even eclipsed positions. A similar discrepancy was already encountered for 1,2,3,4,5,6-hexahydronaphthalene where the observed yield in equilibration experiments (Chart 1) corresponds to a compound 3.5 kcal/mol more stable than our estimated value would indicate. Here, too, the estimated value includes the strain energy we had associated with the 1,3-cyclohexadiene structure. In contrast, there is very good agreement of our estimated value for the heat of formation of 1,2,3,4-tetrahydrophenanthracene (22.3 ± 2 kcal/mol) and the recently measured value of Good and co-workers (22.07 ± 0.32 kcal/mol, $\Delta H_f^\circ_{298}(\text{g})$, preliminary value). This latter compound does not contain a 1,3-cyclohexadiene segment, and so our estimate did not include the 4.2 kcal/mol strain energy in question. Thus Good's results substantially add to doubts that the above explanation for the origin of "strain" in 1,3-cyclohexadiene is completely correct. This further emphasizes the need to answer the question more definitively, in order that this ring strain can be correctly taken into account and the group additivity method applied to compounds of this type with the same precision already realized in the estimation of thermochemical data for acyclic compounds.

Heats of Mixing of Tetraalkyltin Compounds: $\text{SnR}_4 + \text{SnR}'_4$

Geneviève Delmas-Patterson* and Nguyen Thi Thanh

Université du Québec à Montréal, Département de Chimie, CP 8888, Montréal, Québec H3C 3P8 (Received July 6, 1976; Revised Manuscript Received June 13, 1977)

Heats of mixing of the tetraalkyltin compounds, $\text{SnR}_4 + \text{SnR}'_4$ ($\text{R} = \text{CH}_3, \text{C}_2\text{H}_5, \text{C}_3\text{H}_7, \text{C}_4\text{H}_9, \text{C}_8\text{H}_{17}, \text{C}_{12}\text{H}_{25}$), have been measured at 25 °C for 14 systems. Heats can be divided into three classes. Class A (six systems) includes only the four shorter members of the series. Class B (seven systems) includes mixtures of a long chain compound with a short chain one. Class C (one system) includes two long chain compounds mixed together. In class A, two systems have exothermic heats and the four others have heats smaller than 60 J/mol. These heats which reflect the balance of free volume and chemical contributions are smaller than those of mixtures of linear alkanes having the same number of carbon atoms. They may be compared to mixtures of branched alkanes. In class B, the large heats, 250–700 J/mol, are attributed to the destruction of the orientational order of SnOct_4 and SnLaur_4 by the globular SnR_4 molecules. The orientational orders of SnOct_4 and SnLaur_4 seem to be larger than that of $n\text{-C}_8$ and $n\text{-C}_{12}$. System C has small heat because of the fitting of octyl and lauryl chains in the solution. Heats of mixing of SnEt_4 and SnPr_4 with SnOct_4 and SnLaur_4 are smaller than expected. This is attributed to the presence of a sterically hindered molecule which brings a negative contribution to the heats. Experimental heats have been compared to several new theories: (a) the Prigogine–Patterson–Flory theory for the free volume term; (b) a simple expression in terms of size and energy difference (Patterson–Despande); (c) an equation of state obtained from Monte Carlo calculation (Singer and Singer); (d) the Snider–Herrington equation of state. Most theories give heats which are too negative. The Monte Carlo calculation gives very good results.

Heats of mixing of nonpolar compounds A and B are recognized to be the sum of several contributions: (1) a positive endothermic heat due to the difference in force field between the two components; (2) a negative exothermic term due to the difference in free volumes between A and B. The first contribution is difficult to calculate but recent theories^{1–3} can predict the free volume term from macroscopic data on the two pure components. Systems for which contribution (1) is small or constant and contribution (2) is changing gradually should be particularly suitable for testing the different models in the theories.

Mixtures of Branched and Linear Alkanes as Test Systems. A large amount of experimental and theoretical work has been done on the series of linear alkanes. One would have expected that for compounds so similar chemically, contribution (2) would be more important than contribution (1) so that the mixture of two alkanes having a large enough difference of chain length would give an exothermic heat. It has been interesting to discover that indeed the mixture of two branched alkanes gives an exothermic heat while the mixture of two linear alkanes gives an endothermic heat. The mixing of a branched and a linear alkane gives a larger heat than the mixing of two linear alkanes when the branched alkane is the shorter of the two.

The endothermic heat obtained in the cases quoted above cannot be explained by contribution (1) or (2). A recent interpretation of these results has been made by Patterson^{4–6} and Delmas;⁵ the chemical change brought about by changing two $-\text{CH}_2-$ in the chain by a $-\text{CH}-$ and a side $-\text{CH}_3$ is negligible compared to the change of shape made in the molecule. As an extreme example, an isomer of n -hexadecane, the very substituted heptamethylnonane has a "fat" globular shape while n -hexadecane is a rather "thin" long molecule. The molecular shape would change the "structure" of the pure liquid. Due to the anisotropy of the molecule, a long n -alkane keeps, in the liquid state, some of the order it had in the solid state; the chains are oriented, one along the other, in order to maximize the van

der Waals interaction along the chain. On the other hand, a branched alkane being a more isotropic molecule would not have such orientational order or correlations of orientations. The relatively large endothermic heats obtained when a long linear alkane is mixed with a branched one would come from a third contribution to the heats, the disordering contribution, which does not exist for a mixture of two branched alkanes.

Macroscopic properties of the liquids such as the melting points or the boiling points cannot be used as indication of structure in the liquid state. However, recent measurements⁷ of thermal pressure coefficients indicate that this property is sensitive to the shape of the molecule.

Nonthermodynamic properties may be indicative of the effect of shape on structure or orientational order in liquids. Bothorel and co-workers⁸ have measured by depolarized Rayleigh scattering an apparent optical anisotropy value γ^2 for the n -alkanes and the branched alkanes. The γ^2 values of long chain alkanes and branched alkanes in the pure state and in solution with a globular nonordered molecule confirm the thermodynamic interpretation of order in long chain and loss of order by such mixing. More details on the comparison of optical and thermodynamical results may be found in ref 6b. Some experimental values of γ^2 will be given later.

Fortunately, the difference between an ordered and nonordered liquid can be shown indirectly by mixing with a well chosen liquid used as a probe. If the probe liquid has the same orientational order as the liquid investigated, the disordering contribution will be small. It will be the same if the probe and the other liquid have no orientational order due to their spherical shape. On the other end, if the shapes of the two molecules mixed are different, i.e., if their "structures" in the pure state are different, it is very likely that a large heat will be observed because the structure of the ordered liquid will be destroyed by the mixing with the nonordered one.

Heats of Mixing of Alkyltin Compounds with Linear and Branched Alkanes.^{5,9} The shorter members of the series (methyl to butyl) have been mixed with linear al-

TABLE I: Physicochemical Parameters for the Pure Components at 25 °C

	$d,^a$ g cm ⁻³	$\alpha^a 10^3,$ K ⁻¹	$P,^b$ J cm ⁻³	$V^*,^e$ cm ³	$s = s/v,$ Å ⁻¹	\bar{v}^e	ξ^f
SnMe ₄	1.2865	1.28	409	107.7	0.96 ^c	1.3023	0.504
SnEt ₄	1.1877	1.00	454	159.0	0.70 ^c	1.2476	0.554
SnPr ₄	1.1013	0.890	579	213.6	0.68 ^c	1.2246	0.579
SnBut ₄	1.0492	0.818	439	271.6	0.61 ^c	1.2090	0.597
SnOct ₄		0.790	486	494.7	0.99 ^d	1.2029	0.604
SnLaur ₄	0.9170	0.775	475	723.6	0.93 ^d	1.1995	0.607

^a Measured in this laboratory. ^b From γ measured in this laboratory by R. Philippe. $P^* = \gamma \bar{v}^2 T$. ^c Calculated as if the molecule were a sphere. ^d Calculated as for an alkane of the same chain length. ^e From $\{[(4/3)\alpha T + 1]/[\alpha T + 1]\}^3$ and V . ^f From eq 16.

kanes to measure the order-breaking ability of globular molecules of different sizes. The heats were large with the linear alkanes due to the heat of chain disordering and very small or exothermic with the branched alkanes. These small heats were an indication of the aliphatic character of the SnR₄ compounds, the Sn atom being protected by the alkyl groups. Heats of mixing of a long chain member of the series, SnLaur₄, were on the contrary about three times larger with the branched alkanes than with the linear alkanes. This was interpreted by the presence of orientational order between the lauryl chains similar to that of the long chain alkanes.

Measurements of the heats of the SnR₄ compounds with the SnR'₄ compounds seemed interesting to us from several points of view; (1) to confirm the results obtained with mixtures with the alkanes, i.e., the globular shape of the shorter members of the series and the orientational order of the long chain derivatives; (2) to test the theories of mixtures of nonpolar globular molecules on the mixtures of the shorter members; and (3) to investigate the presence of the "steric hindrance effect" which has been observed on mixtures containing a sterically hindered hydrocarbon such as the 3,3-diethylpentane^{6b} since there is an analogy of structure between such a compound and the SnR₄ molecules.

This work presents the results of the heats of mixing at 25 °C of 14 mixtures. Of all the possible combinations of the six derivatives (R = CH₃, C₂H₅, C₃H₇, C₄H₉, C₈H₁₇, C₁₂H₂₅) only the SnPr₄ + SnOct₄ was not made, because of difficulties in the supply of sufficiently pure SnOct₄.

Experimental Section

Apparatus. The heats were measured using a tilting Tian Calvet calorimeter. Details of the instruments, the cells, and the calibration can be found in ref 5 and 10. With the reference system cyclohexane + hexane our points agree to within 2% of the published values.¹¹

Chemicals. The tetramethyl, ethyl, and propyl derivatives have been obtained from the K and K Co. (99%). Tetrabutyltin was either from Aldrich or from the K and K Co. The tetraoctyl and tetralauryl derivatives were obtained from the Chemical Procurement Laboratories (College Point, N.Y.). Densities of the compounds were measured as a test of their purity. The experimental heats have been fitted to the equation

$$\Delta h_M = x_1 x_2 (A + Bx_2 + Cx_2^2) \quad (1)$$

where x is the mole fraction. The number of measurements used to determine A , B , and C was only between five and seven due to the high price of the products. The difference between the experimental value and that calculated with the above equation was usually between 0.5 and 1.5% but could reach occasionally 3%.

Parameters for the Pure Components. The densities, expansion coefficients, pressure reduction parameters P^* ,

core volume V^* , and surface to volume ratio s are given in Table I. The surface to volume ratio of the SnR₄ molecules have been calculated as if they were spheres except for SnOct₄ and SnLaur₄ which have been assumed tentatively equal to that of n -octane and n -dodecane. The reduced volumes \bar{v} for the pure components used in the Flory theory and the ξ parameters obtained in the Snider-Herrington theory have been added.

Results and Discussion

Table II summarizes the results for all the systems.

The first two columns of Table II give the maximum of the heats and the concentration of maximum. The next four columns give the concentration dependence of the heat as given by the A , B , and C parameters and the heat per cm³: $\Delta h_V = \Delta h_M / (x_1 V_1^* + x_2 V_2^*)$. The other columns give the calculated values $\Delta h_M(\text{fv})$ and $s_1^{-1} X_{12}$ from the Flory theory.

Qualitative Discussion of the Results. It is assumed that there are four additive contributions to the heat of mixing:

$$\Delta h_M = \Delta h_{\text{chem}} + \Delta h_{\text{fv}} + \Delta h_{\text{dis}} + \Delta h_{\text{sh}} \quad (2)$$

Δh_{sh} , a new contribution associated with the sterically hindered SnR₄ molecules will be discussed further. Δh_{chem} (chemical) and Δh_{fv} (free volume) are small for most of the systems except for those containing SnMe₄. Δh_{dis} exists only for the systems containing SnOct₄ and SnLaur₄. Δh_{fv} and Δh_{sh} are exothermic while Δh_{dis} is endothermic indicative of the destruction of the orientational order of the longer members of the series by the shorter ones. Δh_{chem} is endothermic too. The four systems involving mixtures of SnEt₄ and SnPr₄ with SnOct₄ and SnLaur₄ have heats which are lower than the values for the other members of the series as can be seen in Figure 1E and 1F. This is attributed to the steric hindrance effect.

Extra-Exothermic Effect: Δh_{sh} . Exothermic heats are very rare in nonpolar systems. Prigogine¹ has predicted such heats for systems with large free volume differences. They were shown to occur in many polymeric mixtures^{12,13} for which the chemical difference between the solvent and the polymer is not large enough to compensate the exothermic contribution. One can find exothermic heats in mixtures of branched alkanes⁴ of large free volume differences but they are small (between 0 and -50 J/mol). For most of the systems, endothermic contributions, larger than the free volume one, give a positive heat of mixing. It was a surprise for Mathot¹⁴ and co-workers to find in 1957 a large exothermic heat (-80 J/mol) for the mixture of two alkanes, 3,3-diethylpentane and n -C₈, the magnitude of which could not be explained in terms of free volume differences. Since then, other heats of mixing have been made on systems containing alkanes similar in shape to 3,3-diethylpentane.^{6a,b} The same large exothermic contributions to the heats have been found although 3,3-diethylpentane appears to give the maximum effect. The molecular origin of this effect is not clear yet; it may be

TABLE II: Heats of Mixing and Experimental and Calculated Parameters for Mixtures of Tetraalkyl Compounds $\text{SnR}_1 + \text{SnR}'_4$ at 25 °C

System		Experimental					Calculated		
		$\Delta h_M(\text{max})$, J mol^{-1}	x_2 - (max)	A	B	C	Δh_v , J/cm^3	Flory $\Delta h_M(\text{fv})$, J mol^{-1}	van der Waals $X_{12}S_1^{-1}$, J cm^{-3} Å
(1)	(2)								
A	$\text{SnMe}_4 + \text{SnEt}_4$	-7.4	0.425	-41.40	+34.23	-18.93	-0.057	-18	0.32
	$+ \text{SnPr}_4$	58.0	0.525	85.24	530.10	-468.36	0.352	-39	1.71
	$+ \text{SnBut}_4$	63.5	0.450	252.36	121.76	-241.47	0.348	-63	3.82
	$\text{SnEt}_4 + \text{SnPr}_4$	-21.5	0.450	-99.09	6.67	46.44	-0.117	-5	-0.43
	$+ \text{SnBut}_4$	44.5	0.450	250.51	-229.25	164.13	0.211	-16	1.52
	$\text{SnPr}_4 + \text{SnBut}_4$	18.4	0.375	131.13	-198.02	152.99	0.077	-3	0.46
B	$\text{SnMe}_4 + \text{SnOct}_4$	354	0.350	2529.2	-3406.8	1826.3	1.45	-91	9.4
	$+ \text{SnLaur}_4$	700	0.375	4425.4	-4339.2	1490.3	2.07	-102	17.1
	$\text{SnEt}_4 + \text{SnOct}_4$	220	0.400	1333.8	-1170.3	309.9	0.75	-27	4.2
	$+ \text{SnLaur}_4$	440	0.325	3319.5	-4963.2	2954.1	1.28	-35	5.8
	$\text{SnPr}_4 + \text{SnOct}_4$	326 ^a	0.4				0.50	-8	3.4
	$+ \text{SnLaur}_4$	395	0.375	2521.3	-2676.7	1242.3	0.97	-12	4.8
	$\text{SnBut}_4 + \text{SnOct}_4$	240	0.375	+1655.7	-2129.8	+1264.7	0.67	-1	2.6
	$+ \text{SnLaur}_4$	564	0.400	3378.3	-3237.4	1721.4	1.24	-2	5.7
C	$\text{SnOct}_4 + \text{SnLaur}_4$	142	0.475	596.70	-126.6	75.77		0	6.3

^a Estimated.

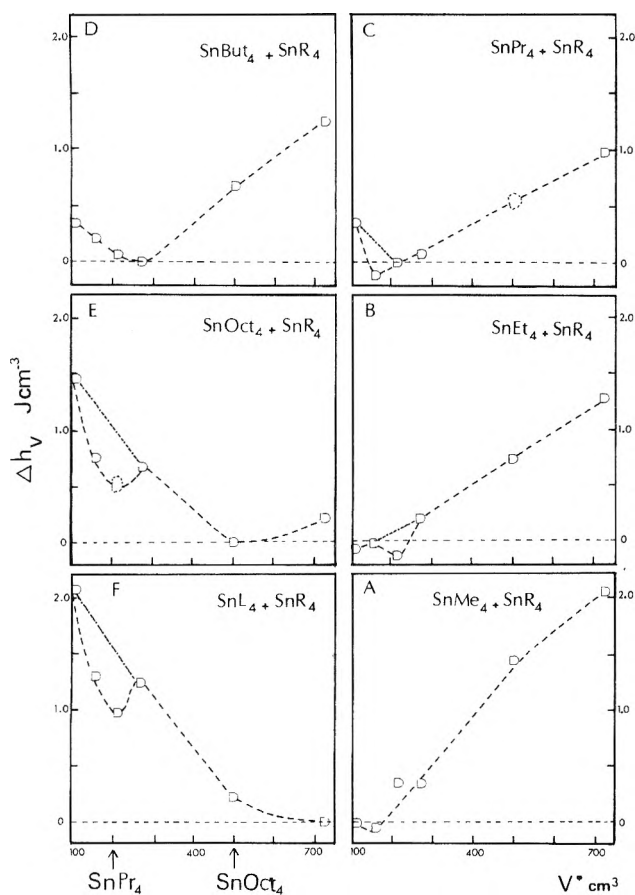


Figure 1. Heats of mixing in J/cm^3 for the $\text{SnR}_4 + \text{SnR}'_4$ systems vs. the core volume of one component. In Figure 1A, the heats of SnMe_4 with the five other members of the series are plotted against V^* for SnEt_4 , SnPr_4 , etc.; in Figure 1B the heats for SnEt_4 with the five other members of the series are plotted against V^* . In Figure 1C to 1F, SnPr_4 , SnBut_4 , SnOct_4 , and SnLaur_4 are, respectively, taken as the first component. This representation in which a system is plotted twice has the advantage of bringing out some features of the heats. For instance, the steric hindrance effect with the lower values is seen with SnEt_4 and SnPr_4 in Figure 1E and 1F but not on Figure 1B and 1C. The dotted line is an estimated value.

due^{6a,b} to some change of accessibility of the second component to the sterically hindered molecule or to a

better packing in solution than in the pure state. These exothermic heats are accompanied in solution by a large negative excess volume.¹⁵ In the case of the SnR_4 molecules, one could have expected that the steric hindrance of the different members of the series would be the same since they have the same structure around the Sn atom. It will be seen that SnEt_4 and SnPr_4 appear to have the most effective steric hindrance effect. The apparent disappearance of the effect when the chain length increases could not be predicted but can be understood; the second component does not reach the sterically hindered part of the molecule when the chain length increases or with the better packing hypothesis, the improvement of packing in solution cannot be very important with long chains attached to a central atom. Densities and expansion coefficients are diminishing very fast along the series because of the diminishing proportion of the heavy Sn atom. One would have expected that steric hindrance, as seen by heats of mixing for SnEt_4 and SnPr_4 , would have given an irregularity in these physical properties along the series. This has not been seen, undoubtedly because the effect of packing or steric hindrance would be smaller than the effect of composition. However it has been rewarding to find such irregularity in the thermal pressure coefficients γ or pressure reduction parameter P^* ($= \gamma \bar{v}^2 T$). The values do not vary smoothly and are indicative of higher cohesive energies for SnEt_4 and SnPr_4 ; as can be seen in Table I, the P^* values are respectively (in J/cm^3) 453 and 579 for SnEt_4 and SnPr_4 while they are 409 and 439 for SnMe_4 and SnBut_4 .⁷

A. *Mixtures of the Four Shorter Members (Six Systems)*. Their heats range from -21.5 to 63.5 J/mol. The trend of the heats when the difference in chain length increases does not follow the trend of the free volume which is calculated by the Flory theory to go from -20 to -70 J/mol for the SnMe_4 - SnEt_4 system to the SnMe_4 - SnBut_4 system. The heats must reflect the fact that the positive or chemical contribution does not vary regularly along the series. The difference of $P_1^* - P_2^*$ is an indication of the magnitude of the positive term. It will be larger for SnMe_4 (P_1^* low) with SnEt_4 and SnPr_4 (P_2^* high) than for SnMe_4 with SnBut_4 (P_1^* and P_2^* low). The almost two identical values of $\text{SnMe}_4 + \text{SnPr}_4$ and $\text{SnMe}_4 + \text{SnBut}_4$ must come from a compensation of free volume

and chemical terms. Two values with SnPr₄ seem too small: that with SnBut₄ is 18.4 and that with SnEt₄ is -21.5. Other measurements have shown that two sterically hindered molecules mixed together with a rather large Δh_{sh} contribution as seems to be the case for the SnEt₄ + SnPr₄ mixture. As was noted before,⁵ the free volume term calculated by the van der Waals model is too large for systems with large differences in expansion coefficients.

B. Mixtures of Long-Chain SnR₄ with Short Chain SnR₄ (Nine Systems). Figure 1A-F shows that the heats for these systems vary between 0.7 and 2.1 J/cm³ while those for the first group are less than 0.4. The value for the system SnPr₄ + SnOct₄ which could not be measured has been estimated in Figure 1C (dotted point) and reported in Figure 1E. These large values reflect the heat of disordering of the long chains. As was noted before with the *n*-alkanes,⁵ they are larger if the order-breaker molecule is smaller. This may be due to a better efficiency of the smaller molecule, whose surface to volume ratio is larger or to the presence of a larger chemical contribution. On Figure 1E and 1F a dotted line was drawn between the butyl and methyl derivatives to emphasize the appearance of an extra-exothermic contribution for SnEt₄ and SnPr₄ mixed with the long-chain compounds SnOct₄ and SnLaur₄. In other graphs, no irregularity is visible except for the already mentioned SnEt₄ + SnPr₄ system which gives a low value for the mixing of two sterically hindered molecules together (Figure 1B and 1C). In Figure 1A, the system SnPr₄ is too high and SnBut₄ is too low but no explanation could be found for this.

Evaluation of the Extra-Exothermic Heat: Δh_{sh} . This heat can be evaluated in Figure 1E and 1F by the difference between the dotted line and the experimental points. The values obtained are quite similar if the second molecule is SnOct₄ or SnLaur₄: 0.50 and 0.52 for SnPr₄ and SnEt₄ on SnLaur₄ and 0.63 and 0.52 for the same on SnOct₄. The values converted to J/mol vary between -165 and -185 for the four systems which represent a very large exothermic contribution. These values compare well with those obtained in a similar way when the sterically hindered molecule is 3,3-diethylpentane and the second molecule *n*-hexadecane (-195 J/mol).^{6b}

Evaluation of the Heat of Chain Disordering for SnOct₄ and SnLaur₄. SnLaur₄. The evaluation is possible if one considers a system in which the order breaker is not volatile and is chemically similar to SnLaur₄. Then, it can be assumed that in eq 2 all the terms are negligible except Δh_{dis} . SnBut₄ fulfills these conditions so that Δh_{dis} from Table I is found to be 1.24 J/cm³. It is interesting to compare this value with those found with other order breakers such as three very branched alkanes. The total heats per cm³ found in ref 9 for SnLaur₄ with br-C₈, br-C₁₂, and br-C₁₆ were respectively 1.22, 1.25, and 1.24 J/cm³; this perfect agreement means that the assumptions of $\Delta h(\text{total}) = \Delta h_{\text{dis}}$ is quite reasonable for the four systems. From these results and the corresponding ones when the ordered liquid is a linear alkane, one can compare the orientational order of an alkane chain in C₁₂, free to move in the liquid, with that which is attached to three others by the Sn atom. From the heats given in ref 5 for SnBut₄ and the linear alkanes, the value found here for the SnLaur₄ would correspond to the orientational order for *n*-C₁₅. This would indicate that there is more orientational order in long chain SnR₄ than in the linear alkane having the same chain length. Orientational order near that of the *n*-hexadecane for the SnLaur₄ is confirmed by the heats of *n*-C₁₆ with three branched alkanes: br-C₈ (1.28), br-C₁₂ (1.30), br-C₁₆ (1.11) in J/cm³.

SnOct₄. The heat of mixing per cm³ of SnOct₄ and SnBut₄ is 0.67 J/cm³. From the same considerations and in particular from the value of the heat of mixing of SnBut₄ with *n*-C₁₂ (0.87 J/cm³) or of br-C₁₂ with *n*-C₁₂ (0.71 J/cm³), one can conclude that the order in the octyl chains of SnOct₄ is considerably higher than the order in the *n*-octane and is rather near that of *n*-C₁₁ or *n*-C₁₂.

Orientalional Order and the Bothorel *J* Parameter. Bothorel and collaborators⁸ measured the anisotropic Rayleigh scattering on pure solvents and on solutions. The determination of the apparent anisotropy γ^2 in the pure state and in various spherical molecule solvents allows the definition of a parameter *J*:

$$J = [\gamma^2(\text{pure})/\gamma^2(\text{soln})] - 1 \quad (3)$$

which is a measure of the orientational order. If a liquid has orientational order, its $\gamma^2(\text{soln})$ in a solvent made of globular molecules will be smaller than in the pure state. If the solvent and solute can correlate their orientations, $\gamma^2(\text{soln})$ is more like $\gamma^2(\text{pure})$. As an example, the values of γ^2 in Å⁶ for *n*-C₁₆ in the pure state and at infinite dilution in various solvents are the following: 26.14, 21.18 (in *n*-C₆), 18.87 (in *n*-C₆), 11.24 (in CCl₄). On the other hand, γ^2 for br-C₁₆ hardly changes in the pure state or in different solvents, 8.15, 9.57 (in *n*-C₆), 6.70 (in CCl₄), since the lateral groups give a globular shape to the molecule and so prevent the molecule from having orientational order. Unfortunately, it has not been possible to measure γ^2 values for SnOct₄ and SnLaur₄ because of the presence of some fluorescent impurities in the pure liquids. The order breaker qualities of SnMe₄ and SnEt₄ are confirmed by the low γ^2 values of *n*-C₁₆ at infinite dilution in these solvents: 13.49 for SnMe₄ and 12.60 for SnEt₄. They were measured by P. Tancrede in Bothorel's laboratory (Bordeaux, France).

C. Mixture of Two Long Chain Compounds. SnOct₄ and SnLaur₄. The heat (0.25 J/cm³) is remarkably small for the large size difference of the two compounds. It is very similar to the heat of *n*-C₁₀ with SnLaur₄ (0.28) or of two long alkanes: 0.23 for *n*-C₁₀ + *n*-C₁₆. There are enough correlations of orientations in the shorter SnOct₄ to fit the ordered lauryl chains in the solution. The structure of the solution should be similar to that of the pure liquids.

Comparison with Theories

The experimental heats have been compared with the free volume theory, where a van der Waals model is used for the energy.² They are also compared with the hard sphere model theories and Monte Carlo calculations.

Free Volume Theory. The free volume term is given by the expression

$$\Delta h_{\text{fv}}/x_1x_2[x_1U_1^* + x_2U_2^*] = X_1\tilde{T}_1 + X_2\tilde{T}_2 - \tilde{T}_s \quad (4)$$

where $U^* = P^*V^*$ and the \tilde{T} are the pure solvent and solution reduced temperatures. For the pure components, \tilde{v} is obtained from the expansion coefficient by $\tilde{v}^{1/3} = ((4/3)\alpha T + 1)/(\alpha T + 1)$, $V^* = \tilde{v}/V$. X is the energy fraction: $X_1 = x_1U_1^*/(x_1U_1^* + x_2U_2^*)$. The solution reduced volume is obtained by an energy fraction average of the \tilde{v}^{-1} . $P^* = \gamma\tilde{v}^2T$ where γ is the thermal pressure coefficient. $\tilde{T} = \tilde{v}^{-1}(1 - \tilde{v}^{-1/3})$. The size of h_{fv}^E depends on the curvature of $\tilde{v}(\tilde{T})$ and the recipe to obtain \tilde{T}_s . The values become more and more negative when the difference in expansion coefficients of pure components increases. The X_{12} parameter, which depends on the non-free-volume part of the heats, is obtained from Δh_{expt} by the formula:

$$\Delta h_{\text{expt}} - \Delta h_{\text{fv}}/(x_1 U_1^* + x_2 U_2^*) = (X_{12}/P_1^*)f(\bar{v})\psi_1\theta_2 \quad (5)$$

$f(\bar{v})$ is not very different from unity. ψ_1 and θ_2 , the contact energy fraction and the surface fraction, are used rather than the mole fraction. X_{12} has the units of energy per cm^3 . The parameter $s_1^{-1}X_{12}$ has been tabulated in the last column of Table II since the multiplication by s_1^{-1} makes it independent of the choice of 1 and 2.

In the class A systems, the large value of X_{12} found for the $\text{SnMe}_4 + \text{SnBut}_4$ system is just due to a compensation for the too large calculated value of the free volume term (-63 J). It is interesting to see on one example that the extra-exothermic contribution Δh_{sh} is large enough to make negative the value of X_{12} for the $\text{SnEt}_4 + \text{SnPr}_4$ system. For the class B systems, large values of X_{12} reflect the heat contribution of the orientational order in the long chain destroyed by the mixing. A plot of X_{12} vs. the volume of the second component would give graphs similar to those obtained in Figure 1. In particular for the $\text{SnLaur}_4 + \text{SnR}'_4$ graph, one finds a minimum for the $\text{SnEt}_4 + \text{SnLaur}_4$ and $\text{SnPr}_4 + \text{SnLaur}_4$ mixtures indicating a negative contribution in X_{12} due to the steric hindrance effect. Very large values of X_{12} for the $\text{SnMe}_4 + \text{SnLaur}_4$ and $\text{SnMe}_4 + \text{SnOct}_4$ systems come from the too large calculated free volume term.

More Recent Theories. A. Simple Approximation for Δh_M in a Function of the Size and Energy Difference of the Two Components. Instead of the random mixture theory which was giving large positive heats of mixing for mixtures of molecules with large size differences, Rowlinson and co-worker have proposed a new van der Waals mixing rule. Patterson and co-workers¹⁷ have shown that it can give a simple expression for Δh_M in terms of the size difference (ϕ) and the energy difference (θ) between the two components and the deviation from the Berthelot combining rule (k_{12}):

$$\Delta h_M \propto 2(1 - k_{12}) - \theta\phi/2 \quad (6)$$

For these systems ϕ and θ have been obtained from the pressure and volume reduction parameters:

$$\begin{aligned} \phi &= V_2^*/V_1^* - 1 \\ \theta &= P_2^*V_2^*/P_1^*V_1^* - 1 \end{aligned} \quad (7)$$

$$\epsilon_{12} = k_{12}(\epsilon_{11}\epsilon_{12})^{1/2}$$

Equation 6 predicts Δh_M which are negative if $k_{12} = 1$ and become positive for decreasing values of k_{12} . For a given k_{12} , the heats become more and more negative when the size difference between the two components increases. For the class A systems, in which the molecules can be considered as globular, values of ϕ and θ may be found in Table III. As the $\Delta h_M(\text{expt})$ follow a trend inverse to that of $\phi\theta$, a term depending on P^*/s , i.e., on energy vs. surface area, have been added. s is the surface to volume ratio of the molecule calculated as if it were a sphere. Equation 8 of ref 17 has been added to eq 6 to give Δh_M :

$$\frac{\Delta h_M}{x_1x_2(-U + TC_p)} = \left[1 - \left(\frac{P_2^*/s_2}{P_1^*/s_1} \right)^{1/2} \right]^2 + 2(1 - k_{12}) \left(1 + \frac{P_2^*/s_2}{P_1^*/s_1} \right) - \frac{\phi\theta}{2} \quad (8)$$

Table III gives the results of the calculation starting with the negative term in eq 8, the positive term which depends on the difference in energy by unit surface of the two components, and the deviation of the Berthelot rule for the energies ($k_{12} = 0.98$). One sees that the positive term

TABLE III: Calculated Heats from the Size and Energy Difference for the Class A Mixtures of $\text{SnR}'_4 + \text{SnR}'_4$

System	(1)	(2)	$V_2^*/V_1^* - 1 = \phi$	$P_2^*V_2^*/P_1^*V_1^* - 1 = \theta$	$\phi\theta/2$	$1 - \left(\frac{P_2^*/s_2}{P_1^*/s_1} \right)^{1/2}$	$1 - \left(\frac{P_2^*/s_2}{P_1^*/s_1} \right)$	Total	Δh_M^a	k_{12} to calc Δh_M
$\text{SnBut}_4 + \text{SnMe}_4$			-0.603	-0.625	0.188	0.042	0.064	-0.080	-301	0.950
$\text{SnEt}_4 + \text{SnPr}_4$			-0.414	-0.393	0.081	0.007	0.073	-0.001	-3.7	0.976
$\text{SnPr}_4 + \text{SnMe}_4$			-0.213	-0.138	0.015	0	0.079	0.064	240	0.995
$\text{SnEt}_4 + \text{SnMe}_4$			-0.496	-0.564	0.139	0.047	0.064	-0.027	-102	0.976
$\text{SnEt}_4 + \text{SnMe}_4$			-0.255	-0.296	0.037	0.006	0.074	0.042	159	0.993
$\text{SnEt}_4 + \text{SnMe}_4$			-0.322	-0.382	0.061	0.024	0.068	0.032	116	0.989

^a From $-U + TC_p = 30000 \text{ J}$ and eq 8.

which depends on the difference in energy by unit surface gives to Δh_M the right trend in function of the difference in chain length but it does not vary fast enough to compensate the term in $\phi\theta$; the term in k_{12} hardly varies with the system. The values of Δh_M obtained with $-U + TC_P = 30000$ are still more negative for systems with large size differences; the last column gives the k_{12} values necessary to fit the heats. Values of k_{12} further away from 1 are needed for systems having large size differences to compensate the negative term in $\theta\phi$. This is perhaps not very reasonable for systems which appear so similar chemically.

B. Use of a State Equation Generated by the Monte Carlo Calculation Method. The simplest description for a solution is that of a pure liquid (one-fluid model) for which the parameters of size σ_m and energy ϵ_m are some average of that of the components.

Excess thermodynamic properties such as the heats can be obtained from either a model or experimental values of the energy for a reference component and the size and energy difference parameters. Keeping, in the expansion, only the terms in squares of the parameters, one obtains¹⁸

$$\frac{\Delta h_M}{x_1 x_2} = \frac{-\Delta\epsilon}{x_1 x_2 \epsilon_{12}^0} (-U + TC_P) - 2\delta^2 T^2 \frac{dC_P}{dT} \quad (9)$$

The first term corresponds to Δh_{chem} , the second to Δh_{iv} . $\Delta\epsilon$ is a function of the two parameters η and δ

$$\eta = (\sigma_{11}/\sigma_{12}^0) - 1 \quad (10)$$

$$\delta = \epsilon_{11}/\epsilon_{12}^0 - 1$$

σ is the hard sphere diameter; the liquid 1 is compared to a reference liquid which follows the Berthelot-Lorentz rules:

$$\epsilon_{12}^0 = \epsilon_{11}^{1/2} \epsilon_{22}^{1/2} \quad (11)$$

$$\sigma_{12}^0 = (\sigma_{11} + \sigma_{22})/2$$

From the Monte Carlo calculations, Singer and Singer¹⁹ give the following expression for h :

$$\Delta h = RT^* [-8.6961 + 0.3042\tilde{T} + 0.7854\tilde{T}^2] \quad (12)$$

From the first and second derivative of h one can obtain C_P and dC_P/dT needed in eq 9. After some simple arrangement, the expression to calculate Δh_M is:

$$\Delta h_M/x_1 x_2 RT = (\delta - 2\eta)^2 [(8.6961/\tilde{T}) + 0.7854\tilde{T}] - 2\delta^2 [1.5708\tilde{T}] \quad (13)$$

Using the Flory combining rule $(\delta - 2\eta)^2$ has been used for $-\Delta\epsilon/\epsilon_{12}^0$. In eq 13, \tilde{T} is that of the reference liquid.

Parameters for the Pure Components. The reduced volume and reduced temperature are obtained for αT and the two equations $\alpha T = (-0.1648\tilde{T} - 0.4130\tilde{T}^2)(1.068 - 0.1648\tilde{T} - 0.2065\tilde{T}^2)^{-1}$ and $\tilde{v} = (1.068 - 0.1648\tilde{T} - 0.2065\tilde{T}^2)^{-1}$. The size parameter σ can be calculated from \tilde{v} and the molar volume. The ϵ are kT/\tilde{T} and ϵ_{12}^0 is from eq 11. Table IV gives for eight systems the pure component reduced temperatures \tilde{T}_1 and \tilde{T}_2 , the parameters σ_{12} , ϵ_{12} , and \tilde{T}_{12} corresponding to the reference liquid, and the difference parameters η and δ . $\Delta h_M(\text{calcd})$ and $\Delta h_M(\text{expt})$ are reported in the next columns.

It seems that the agreement is very good; the trend of the heats is followed by every system. It is even surprising that the large heats due to the destruction of orientational order in the long chains are obtained to a good approximation. This satisfying agreement is due to the fact that the state equation calculated from the Monte Carlo simulation does not give an exaggerated value of the term dC_P/dT so that the free volume term does not become too large when the size difference increases. On the other

TABLE IV: Calculated Heats Using the Monte Carlo Simulated Equation of State and the Snider-Herrington Theory

System	\tilde{T}_i		σ_{12}^0 , Å	$\epsilon_{12}^0/k K^{-1}$	Monte Carlo, $\Delta\epsilon/\epsilon_{12}^0 = (\eta - 2\delta)^2$	\tilde{T}_{12}	η	δ	$h^E(\text{calcd})$	$h^E(\text{expt})$	Snider Herrington		
	(1)	(2)									$k_{12} = 1.0$ $h^E(\text{calcd})$	$k_{12} = 0.985$ $h^E(\text{calcd})$	Fitted to Δh_M k_{12}
SnMe ₄ + SnEt ₄	0.710	0.628	6.622	446.26	0.6681	0.6681	-0.059	-0.059	35	-7	-249	178	0.992
+ SnPr ₄	0.710	0.585	6.581	462.38	0.6448	0.6448	-0.092	-0.092	153	58	-699	-245	0.975
+ SnBut ₄ ^a	0.710	0.560	6.880	472.59	0.6305	0.6305	0.154	0.126	274	63	-1184	-717	0.960
SnEt ₄ + SnPr ₄	0.628	0.585	6.981	491.64	0.6064	0.6064	-0.051	-0.034	40	-21	-115	432	0.997
+ SnBut ₄ ^a	0.628	0.560	7.281	502.50	0.5930	0.5930	0.091	0.059	137	44	-371	205	0.990
SnPr ₄ + SnBut ₄ ^a	0.585	0.560	7.640	520.60	0.5724	0.5724	0.039	0.022	30	18	-75.9	565	0.997
SnMe ₄ + SnOct ₄											-1346	-907	0.950
+ SnLaur ₄											-1035	-623	0.935
SnEt ₄ + SnOct ₄											-81.5	469	0.997
+ SnLaur ₄											-602	1123	1.01
SnPr ₄ + SnOct ₄											396	1025	1.00
+ SnLaur ₄											1292	1894	1.020
SnBut ₄ + SnOct ₄	0.550	0.560	8.800	536.92	0.5550	0.5550	-0.097	-0.009	342	240	626	1315	1.008
+ SnLaur ₄	0.540	0.560	9.460	541.86	0.5499	0.5499	-0.160	-0.018	918	564	1707	2375	1.025
SnOct ₄ + SnLaur ₄											317	1044	1.005

^a For this system the calculations were made with (1) = SnBut₄.

hand, the chemical term obtained from $(-U + TC_p)$ does not vary too much with the size of the molecules and $(\delta - 2\eta)^2$ is a good balance of the size and energy difference.

C. *Comparison with the Snider-Herrington Theory.* A new equation of state was developed by Snider and Herrington²⁰ and applied successfully to mixtures of simple liquids

$$p/nkT = \chi(\xi) - (an/kT) \quad (14)$$

p is the pressure, n is the number density ($= N_{AV}/V$)

$$\xi = (1/6)\pi r^3 n \quad (15)$$

$$\chi(\xi) = (1 + \xi + \xi^2)/(1 - \xi)^3$$

r is the hard-sphere diameter and a an energy multiplied by volume parameter. r and a for the pure components are obtained from ξ . Snider and Herrington obtained ξ from the heat of vaporization. Since these heats were not available for the SnR₄ compounds, the expansion coefficients were used instead. The following equation is derived from eq 7a of ref 20:

$$\alpha T = [(1 + \xi + \xi^2)(1 - \xi)] / [-1 + 4(\xi + \xi^2 + (\xi^3/2))] \quad (16)$$

eq 14 and 15 may be generalized for a mixture. The solution hard sphere diameter being $r_m^3 = x_1 r_1^3 + x_2 r_2^3$. a_m and ξ_m are given by eq 8 and 9, cf. ref 20. A deviation from the geometrical rule can be introduced as in eq 7:

$$\frac{a_{12}/kT}{r_m^3} = k_{12} \left(\frac{a_{11}/kT}{r_1^3} \right)^{1/2} \left(\frac{a_{22}/kT}{r_2^3} \right)^{1/2}$$

Δh_M is given by the differences between the $\chi(\xi)$ for the solution and the $\chi(\xi)$ for the pure liquids since p/nkT can be neglected.

$$\Delta h_M = RT[-\chi(\xi_m) + x_1 \chi(\xi_1) + x_2 \chi(\xi_2)]$$

$$\chi(\xi_m) = (1 + \xi_m + \xi_m^2)/(1 - \xi_m)^3 - f((r_1 - r_2), x_1)$$

One sees that the excess heats will be very sensitive to the curvature of the function $\chi(\xi)$.

The three last columns of Table IV give the results of the calculations for the SnR₄ mixtures. The ξ values for the pure components were given in Table I. One sees that the values of $\Delta h_M(\text{calcd})$ are too negative for the class A systems. This can be due to the fact that the curvature of the function $\chi(\xi)$ is changing fast when ξ increases. This will exaggerate the magnitude of the heats. The difference

of size between the two components makes Δh_M more negative but if the size difference is larger than 3, a large positive contribution comes in; large positive heats are indeed predicted even with $k_{12} = 1$ for three of the six systems with SnOct₄ and SnLaur₄. For the three other systems the free volume term or term coming from the difference between ξ_1 and ξ_2 is too negative to be compensated by the size difference term. The next two columns give the values of the heats for $k_{12} = 0.985$ and the value of k_{12} needed to fit the $\Delta h_M(\text{expt})$. It is likely that the trend of variation of k_{12} (fitted) with the systems does not have a physical meaning but reflects the corrections to the theory which must be large when ξ increases.

Acknowledgment. We thank Dr. Philippe for the measurement of γ , Dr. Jambon for writing the computing programs in the Snider-Herrington theory, and the National Research Council for financial assistance.

References and Notes

- (1) I. Prigogine (with the collaboration of A. Bellemans and V. Mathot), "The Molecular Theory of Solutions", North-Holland Publishing Co., Amsterdam, 1957.
- (2) P. J. Flory, R. A. Orwoll, and A. Vrij, *J. Am. Chem. Soc.*, **86**, 3507, 3515 (1964).
- (3) D. Patterson and G. Delmas, *Discuss. Faraday Soc.*, **49**, 98 (1970).
- (4) V. T. Lam, P. Picker, D. Patterson, and P. Tancrede, *J. Chem. Soc., Faraday Trans. 2*, **70**, 1465 (1974).
- (5) G. Delmas and S. Turrell, *J. Chem. Soc., Faraday Trans. 2*, **70**, 572 (1974).
- (6) (a) P. Tancrede, P. Bothorel, and D. Patterson, *J. Chem. Soc., Faraday Trans. 2*, **73**, 29 (1976); (b) P. Tancrede, P. Bothorel, P. de Saint-Romain, and D. Patterson, *J. Chem. Soc., Faraday Trans. 2*, **73**, 15 (1976).
- (7) G. Delmas and R. Philippe, *Can. J. Chem.*, to be published.
- (8) (a) P. Bothorel, *J. Colloid Sci.*, **27**, 529 (1968); (b) P. Bothorel, C. Clement, and P. Maraval, *C. R. Acad. Sci.*, **264**, 568 (1967); (c) P. Bothorel and G. Fourche, *J. Chem. Soc., Faraday Trans. 2*, **69**, 441 (1973); (d) P. Bothorel, C. Such, and C. Clement, *J. Chim. Phys.*, **10**, 516 (1972); (e) H. Quinones and P. Bothorel, *C. R. Acad. Sci.*, **277**, 133 (1973).
- (9) G. Delmas and Ng. T. Thanh, *J. Chem. Soc., Faraday Trans. 1*, **71**, 1172 (1975).
- (10) P. Tancrede and G. Delmas, *Europ. Polym. J.*, **9**, 199 (1973).
- (11) S. Murakami and G. C. Benson, *J. Chem. Thermodyn.*, **1**, 559 (1969).
- (12) G. Delmas, D. Patterson, and T. Somcynski, *J. Polym. Sci.*, **57**, 79 (1962).
- (13) D. W. Dreifus and D. Patterson, *Trans. Faraday Soc.*, **67**, 631 (1971).
- (14) (a) I. Prigogine and V. Mathot, *J. Chem. Phys.*, **18**, 765 (1950); (b) V. Mathot, *Bull. Soc. Chim. Belg.*, **59**, 111 (1950).
- (15) G. Delmas and Cl. Jambon, "Excess Volumes on the SnR₄ + SnR'₄ Systems", to be published.
- (16) G. Turrell, D. Richon, and D. Patterson, *Chem. Phys.*, **16**, 61 (1976).
- (17) D. D. Deshpande and D. Patterson, *J. Phys. Chem.*, **77**, 1679 (1973).
- (18) D. Patterson, *Pure Appl. Chem.*, **47**, 305 (1976).
- (19) J. V. L. Singer and K. Singer, *Mol. Phys.*, **24**, 357 (1972).
- (20) N. S. Snider and T. M. Herrington, *J. Chem. Phys.*, **47**, 2248 (1967).

The Partial Molal Volumes of Electrolytes in 0.725 *m* Sodium Chloride Solutions at 25 °C

Frank J. Millero,* Arthur L. Laferrere, and Peter V. Chetirkin

The Rosenstiel School of Marine and Atmospheric Science, University of Miami, Miami, Florida 33149 (Received February 22, 1977)

Publication costs assisted by the National Science Foundation and the Office of Naval Research

The apparent molal volumes of 29 electrolytes have been determined in the medium 0.725 *m* NaCl from precise density measurements at 25 °C. The values of ϕ_V have been extrapolated to infinite dilution by using a least-squares fit of the data and by using Young's rule. The two methods yield values of \bar{V}^{*0} in 0.725 *m* NaCl that agree to within 0.2 cm³ mol⁻¹. The experimentally determined values of \bar{V}^{*0} are compared to those predicted from binary solution data by using the ionic strength principle, Young's rule, and the specific interaction model. The values of \bar{V}^{*0} predicted by using the specific interaction model and Young's rule are similar and in better agreement (± 0.3 cm³ mol⁻¹) with the experimental results than those predicted by using the ionic strength principle (± 0.4 cm³ mol⁻¹). For electrolytes without a common cation (Na⁺) or anion (Cl⁻), the specific interaction model gives the best estimates. The volumes of mixing the electrolytes with a common cation (NaX + NaCl) and anion (MCl + NaCl) at *I* = 0.725 determined from our results correlate very well with the enthalpies of mixing and various properties of the uncommon ion (M⁺ and X⁻).

Introduction

In recent years a number of workers have developed¹⁻⁵ and used⁶⁻¹¹ various ionic interaction models to estimate the activity coefficients of electrolytes in various ionic media (e.g., seawater). Progress has also been made in using these models to estimate the effect of pressure on the activity coefficients or the partial molal volumes of electrolytes in ionic media.¹²⁻¹⁷ Owen and Brinkley¹² estimated the partial molal volumes (\bar{V}) of electrolytes in seawater by assuming the \bar{V} 's were equivalent to the values in binary solutions at the ionic strength of seawater (~ 0.725 *m*). They defined 0.725 *m* NaCl as being equivalent to "sea salt" and estimated the \bar{V} of electrolytes in sea salt from the measurements of Wirth.¹⁸ In recent years, we have examined the \bar{V} 's of electrolytes in 0.725 *m* NaCl¹³⁻¹⁵ and seawater,¹³⁻¹⁵ by using a simple hydration model.¹³ We have interpreted the deviations from this model in terms of ion pairing.¹³⁻¹⁵ Lee¹⁹ has measured the \bar{V} 's of electrolytes in NaCl solutions and also showed how Young's rule^{23,24} could be used to estimate the partial molal volumes. Leyendekkers¹⁷ has recently used these methods to estimate the partial molal volumes of electrolytes in seawater. In a recent paper, we have used the specific interaction model¹⁶ to estimate the \bar{V} of electrolytes in NaCl and seawater solutions. At present it is difficult to state with certainty which of these methods gives the most reliable estimates for the partial molal volumes of electrolytes in an ionic media because of the paucity of reliable experimental data.

In the present paper we will present our experimental results for measurements of 29 electrolytes in 0.725 *m* NaCl. We will use these experimental results to examine the most reliable method that can be used to estimate the partial molal volumes of electrolytes in an ionic media.

Experimental Section

The density measurements were made with a vibrating densimeter that is described in detail elsewhere.²⁵ The densimeter measures the relative densities of aqueous solutions ($d - d^0$) to a precision of $\pm 3 \times 10^{-6}$ g cm⁻³.^{25,26} The densimeter was calibrated by using ion-exchanged water and dry nitrogen. The reliability of the densimeter was checked by measuring the densities of standard

seawater solutions weight evaporated or diluted with water. The measured densities agree on the average to ± 2 ppm²⁶ with the values calculated from the equation of state of seawater.²⁷

The temperature of the densimeter is controlled to ± 0.001 °C and set to ± 0.005 °C with a platinum resistance thermometer (calibrated by the National Bureau of Standards on the 1968 IPTS temperature scale) and a G-2 Mueller bridge.

All of the salts used were Baker reagent grade. The salts that did not decompose were heated in vacuo at 110 °C for at least 1 h. Stock solutions of these salts (KBr, LiCl, RbCl, CsCl, NaI, KI, NaBr, KCl, NaNO₃, KNO₃, Na₂CO₃, K₂CO₃, Na₂SO₄, K₂SO₄, NaF, KHCO₃, NaHCO₃, NH₄Cl, and NH₄Br) were made by weight in 0.725 *m* NaCl. Approximately 1 *m* stock solutions of the electrolytes that could not be dried (HCl, NaOH, KOH, KF, MgCl₂, CaCl₂, SrCl₂, and BaCl₂) were made. The molalities of these solutions were determined by measuring the density (HCl, NaOH, KOH, MgSO₄, and KF) or by titrating with AgNO₃ (MgCl₂, CaCl₂, SrCl₂, and BaCl₂). The NaCl was added to these solutions to make them 0.725 *m* NaCl. Dilute solutions of the salt mixtures (salt and NaCl) were prepared by adding a weighted amount of 0.725 *m* NaCl.

Duplicate density measurements were made on most of the solutions. The two measurements agreed on the average to ± 3.5 ppm which represents the precision of the measurements. The density of the NaCl medium for all of the experiments was $1.025810 \pm 0.000002_5$ g mL⁻¹. This density is equivalent to a molality of 0.72525 ± 0.00006 mol (kg of H₂O)⁻¹ as determined from the relationship $10^3(d - d^0) = 1.011 + 38.227 m$ (valid from 0.7 to 0.8 *m*). The combined error in density was ~ 6 ppm. This error is equivalent to an error of ± 0.006 cm³ mol⁻¹ at 1.0 *m* and ± 0.06 cm³ mol⁻¹ at 0.1 *m* in the apparent molal volumes of the electrolytes.

Results and Calculations

The densities at 25 °C for the various electrolytes (NaF, KF, HCl, LiCl, NaCl, KCl, RbCl, CsCl, NH₄Cl, MgCl₂, CaCl₂, SrCl₂, BaCl₂, NaBr, KBr, NH₄Br, NaI, KI, NaOH, KOH, NaNO₃, KNO₃, NaHCO₃, KHCO₃, Na₂CO₃, K₂CO₃, Na₂SO₄, K₂SO₄, and MgSO₄) at various molalities (*m*₃) in

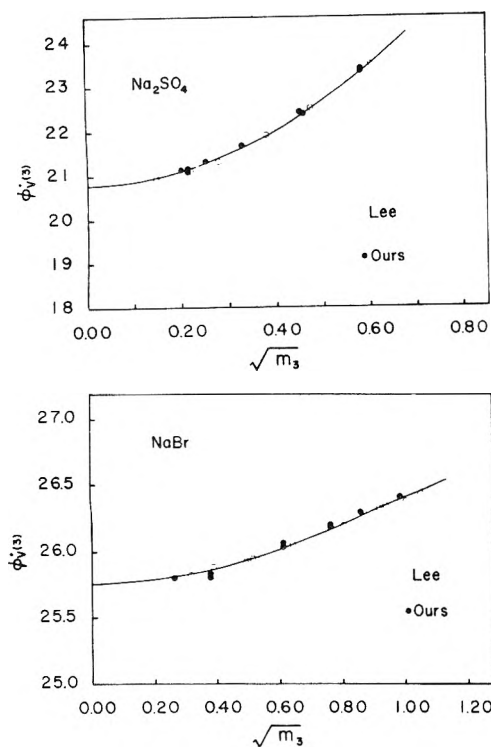


Figure 1. The apparent molal volumes of Na_2SO_4 and NaBr in 0.725 m NaCl at 25°C plotted vs. the square root of molality.

0.725 m NaCl are given in Tables I-XXIX.²⁸ As with binary solutions, it is convenient to examine the volume properties of ternary electrolyte solutions in terms of the apparent molal volume (ϕ_v). If one of the electrolytes 3 is considered to be dissolving in a solvent of electrolyte 2 in water, one can define the apparent molal volume of 3 in this ionic medium by

$$\phi_v^*(3) = [V_{\text{soln}} - V_{\text{med}}]/n_3 \quad (1)$$

where V_{soln} and V_{med} are the volumes of the solution and medium, and n_3 is the number of moles of electrolyte 3. For a molal solution the volume of the solution and the medium are given by

$$V_{\text{soln}} = [1000 + m_2M_2 + m_3M_3]/d \quad (2)$$

$$V_{\text{med}} = [1000 + m_2M_2]/d_2 \\ = 1000/d_0 + m_2\phi_v(2) \quad (3)$$

where m_i is the molality and M_i is the molecular weight of solute i , d is the measured density of the mixed solution, d_2 is the density of the medium, d_0 is the density of water,²⁹ and $\phi_v(2)$ is the apparent molal volume of the medium. Substituting eq 2 and 3 into eq 1 gives

$$\phi_v^*(3) = \frac{1000(d_2 - d)}{dd_2m_3} + \frac{M_3}{d} + \frac{m_2M_2}{m_3d} - \frac{m_2M_2}{m_3d_2} \quad (4)$$

The values of $\phi_v^*(3)$ determined from eq 4 are given in Tables I-XXIX.²⁸ The variation of the $\phi_v^*(3)$ vs. $m_3^{1/2}$ for a 1-1 electrolyte (NaBr), three 2-1 electrolytes (Na_2SO_4 , CaCl_2 , MgCl_2), and the 2-2 electrolyte MgSO_4 are shown in Figures 1 and 2 along with the results of Lee.¹⁹ These values of $\phi_v^*(3)$ have been fitted to the equation

$$\phi_v^*(3) = \phi_v^{*0}(3) + Am_3^{1/2} + Bm_3 \quad (5)$$

The values of the coefficients $\phi_v^{*0}(3) = \bar{V}_3^{*0}$, the infinite dilution partial molal volume, A and B determined by a weighted least-squares fit of the data are given in Table

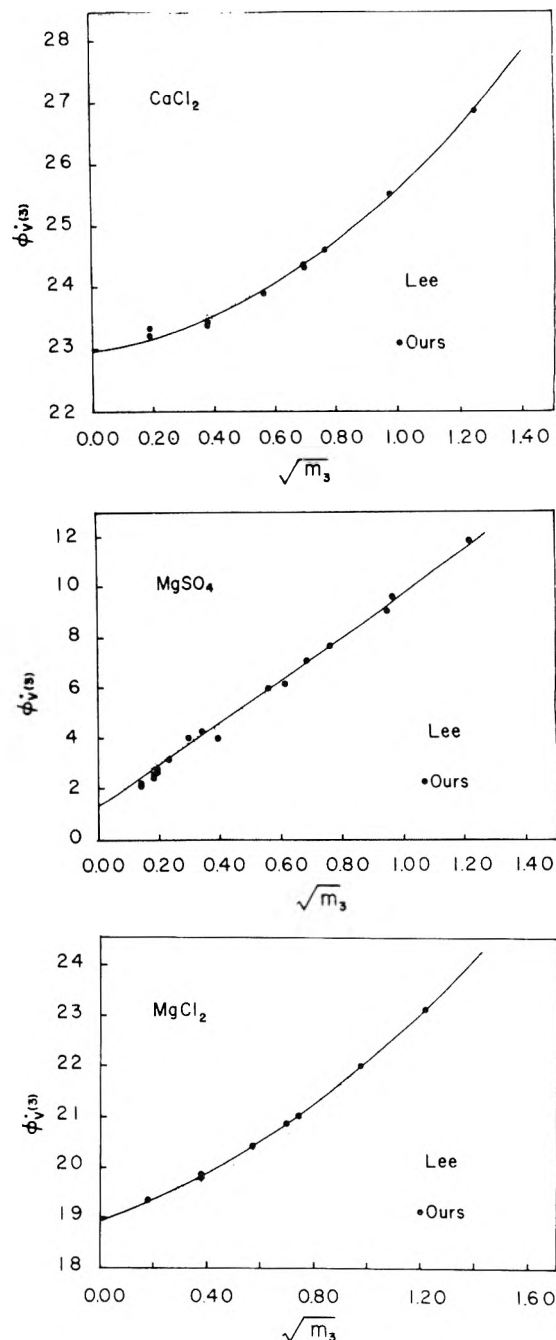


Figure 2. The apparent molal volumes of CaCl_2 , MgSO_4 , and MgCl_2 in 0.725 m NaCl at 25°C plotted vs. the square root of molality.

XXX along with the standard deviations.

The partial molal volume of electrolyte 3 in the medium can be determined from

$$\bar{V}_3^* = (\partial V_{\text{soln}}/\partial m_3) = \phi_v^*(3) \\ + m_3[\partial \phi_v^*(3)/\partial m_3] \quad (6)$$

The differentiation of eq 5 gives

$$\bar{V}_3^* = \bar{V}_3^{*0} + 1.5Am_3^{1/2} + 2Bm_3 \quad (7)$$

where \bar{V}_3^{*0} is the infinite dilution partial molal volume of electrolyte 3 in the medium. Although the $\phi_v^*(3)$ data for the electrolytes studied can be fitted to eq 5 with standard deviations less than $0.1\text{ cm}^3\text{ mol}^{-1}$, the errors in \bar{V}_3^{*0} are slightly larger (as much as $\pm 0.2\text{ cm}^3\text{ mol}^{-1}$ for 2-1 and 2-2 electrolytes). To test the extrapolation procedure, we have made volume measurements on solutions formed by adding weighted amounts of NaCl to 0.725 m NaCl . The ex-

TABLE XXX: Coefficients of Eq 5 for Various Electrolytes in 0.725 *m* NaCl at 25 °C^a

Electrolyte	ϕ_V^{*0}	<i>A</i>	<i>B</i>	σ
NaF	0.303	-0.015	1.630	0.02
KF	10.612	0.336	0.883	0.01
HCl	19.606	0.028	0.198	0.01
LiCl	19.192	0.595	-0.178	0.02
NaCl	19.080	0.056	0.701	0.01
KCl	29.343	0.339	0.557	0.01
RbCl	34.654	0.608		0.04
CsCl	41.742	0.758		0.03
NH ₄ Cl	37.905	0.208	0.372	0.02
MgCl ₂	18.942	1.754	1.408	0.03
CaCl ₂	22.973	0.689	1.931	0.05
SrCl ₂	23.169	1.967	1.593	0.03
BaCl ₂	28.917	1.474	1.959	0.04
NaBr	25.620	0.521	0.299	0.03
KBr	36.165	0.208	0.526	0.03
NH ₄ Br	44.715	0.011	0.295	0.02
NaI	36.917	0.343	0.215	0.02
KI	47.424	0.625		0.03
NaOH	-2.417	0.647	1.178	0.04
KOH	7.896	0.796	0.860	0.04
NaNO ₃	30.549	0.428	0.567	0.02
KNO ₃	40.861	0.445	0.501	0.01
NaHCO ₃	26.772	0.699	1.155	0.02
KHCO ₃	37.200	0.491	1.310	0.01
Na ₂ CO ₃	1.945	1.616	1.398	0.03
K ₂ CO ₃	22.599	1.261	1.188	0.06
Na ₂ SO ₄	20.794	0.186	2.340	0.05
K ₂ SO ₄	41.239	2.191	4.739	0.04
MgSO ₄	1.608	7.081	1.007	0.09

^a The values of ϕ_V^* have the units of $\text{cm}^3 \text{mol}^{-1}$. Since the values of ϕ_V^* at 1 *m* are ten times more reliable than at 0.1 *m* for a given error in density; the values of ϕ_V^* have been weighted by the factor 10 *m*.

trapolated value of $\phi_V^{*0} = 18.08 \text{ cm}^3 \text{mol}^{-1}$ for NaCl agrees very well with the value of $\bar{V} = 18.06 \text{ cm}^3 \text{mol}^{-1}$ at 0.725 *m* calculated from apparent molal volume data.

The volume properties of these ternary electrolyte solutions can also be examined in terms of the mean apparent molal volume defined by

$$\Phi_{V(2,3)} = [V_{\text{soln}} - V_{\text{H}_2\text{O}}]/(m_2 + m_3) \quad (8)$$

where $V_{\text{H}_2\text{O}} = 1000/d_0$ is the volume of water in the solution and $m_2 + m_3$ is the total molality of electrolytes in solution. Substitution of eq 2 into eq 8 gives

$$\Phi_{V(2,3)} = \frac{1000(d_0 - d)}{d_0 d(m_2 + m_3)} + \frac{m_2 M_2 + m_3 M_3}{(m_2 + m_3)d} \quad (9)$$

This equation can be simplified by defining the total molality, $m_T = m_2 + m_3$ and mean molecular weight, $M_T = (m_2 M_2 + m_3 M_3)/(m_2 + m_3)$

$$\Phi_{V(2,3)} = \frac{1000(d_0 - d)}{d_0 d m_T} + \frac{M_T}{d} \quad (10)$$

The values of $\Phi_{V(2,3)}$ for the various electrolyte mixtures calculated from eq 9 at various molalities are also given in Tables I-XXIX.²⁸ The variation of the $\Phi_{V(2,3)}$ vs. m_3 for a 1-1 electrolyte (NaBr), three 2-1 electrolytes (Na₂SO₄, MgCl₂, CaCl₂), and the 2-2 electrolyte MgSO₄ are shown in Figures 3 and 4 along with the results of Lee.¹⁹

From the two definitions of $\phi_V^*(3)$ and $\Phi_{V(2,3)}$, one can relate these two quantities by

$$\phi_V^*(3) = \frac{m_2 + m_3}{m_3} \Phi_{V(2,3)} - \frac{m_2}{m_3} \phi_V(2) \quad (11)$$

$$\Phi_{V(2,3)} = \frac{m_2}{m_2 + m_3} \phi_V(2) + \frac{m_3}{m_2 + m_3} \phi_V^*(3) \quad (12)$$

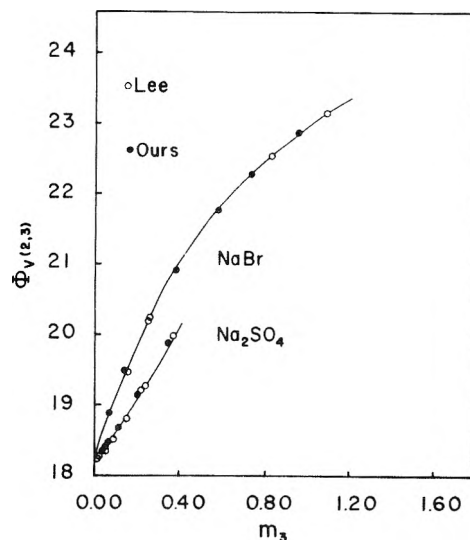


Figure 3. The mean apparent molal volumes of NaBr and Na₂SO₄ in 0.725 *m* NaCl at 25 °C plotted vs. molality.

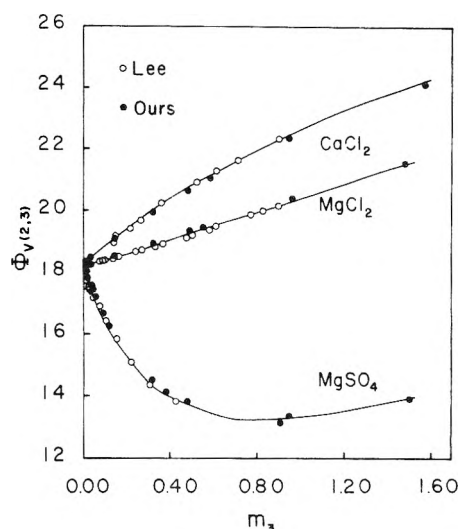


Figure 4. The mean apparent molal volumes of CaCl₂, MgCl₂, and MgSO₄ in 0.725 *m* NaCl at 25 °C plotted vs. molality.

The \bar{V}_3^* can also be determined from the concentration dependency of $\Phi_{V(2,3)}$. By differentiating eq 11 with respect to m_3 and substituting into eq 6, we have

$$\bar{V}_3^* = \Phi_{V(2,3)} + (m_2 + m_3) [\partial \Phi_{V(2,3)} / \partial m_3] \quad (13)$$

Since $\Phi_{V(2,3)} = \phi_V(2)$ and $(m_2 + m_3) = m_3$ at $m_3 = 0$, the limiting partial molal volume \bar{V}_3^{*0} is given by

$$\bar{V}_3^{*0} = \phi_V(2) + m_2 [\partial \Phi_{V(2,3)} / \partial m_3]_{m_3=0} \quad (14)$$

The derivative $\partial \Phi_{V(2,3)} / \partial m_3$ can be obtained¹⁹ from the concentration dependence of $\Phi_{V(2,3)}$

$$\Phi_{V(2,3)} = \phi_V(2) + A' m_3 + B' m_3^2 + \dots \quad (15)$$

At $m_3 = 0$ the derivative of $\partial \Phi_{V(2,3)} / \partial m_3$ equals A' , and the partial molal volume is given by

$$\bar{V}_3^{*0} = \phi_V(2) + m_2 A' \quad (16)$$

The values of \bar{V}_3^{*0} calculated from eq 16 are not very reliable¹⁹ because the value determined for A' is quite dependent upon the degree used to fit the data and reliable values of $\Phi_{V(2,3)}$ in dilute solutions are not available.

TABLE XXXI: Coefficients for Eq 21 for Various Electrolytes in Water at 25 °C

Electrolyte	$\phi_V^0(i)$	A_i	B_i	σ	Ref
NaF	-2.371	1.839	0.561	0.02	30, 31, 32
KF	7.844	1.724	0.509	0.03	31, 33, 34
HCl	17.854	1.460	-0.307	0.02	18b, 35-37
LiCl	16.961	1.700	-0.198	0.02	31, 33, 38-40
NaCl	16.613	1.811	0.094	0.02	18b, 19, 38, 40-43
KCl	26.850	1.839	0.087	0.02	18a, 31, 38, 41, 44-45
RbCl	31.940	1.818	0.191	0.02	31, 38
CsCl	39.166	1.843	0.162	0.02	31, 38
NH ₄ Cl	35.815	1.717	-0.147	0.02	40
MgCl ₂	14.522	3.155	0.106	0.03	19, 36, 40, 46
CaCl ₂	17.858	3.611	-0.117	0.03	19, 36, 40, 41, 46
SrCl ₂	17.975	3.941	-0.038	0.05	40, 46, 47
BaCl ₂	23.208	4.576	-0.360	0.04	36, 40, 41, 46
NaBr	23.504	1.689	0.076	0.02	19, 31, 32, 39, 48, 49
KBr	33.725	1.403	0.480	0.02	31, 39, 41
NH ₄ Br	42.521	1.965	-0.498	0.02	40, 48
NaI	35.018	1.593	-0.126	0.03	31, 39, 49
KI	45.229	1.645	0.044	0.02	31, 39, 41
NaOH	-5.246	2.048	0.984	0.05	31, 50
KOH	4.929	1.809	0.987	0.05	40
NaNO ₃	27.805	2.586	-0.292	0.05	40, 51
KNO ₃	37.979	3.103	-0.712	0.05	36, 40
NaHCO ₃	23.118	3.662	-0.115	0.05	40, 52
KHCO ₃	33.427	3.691	-0.024	0.07	40
Na ₂ CO ₃	-6.195	7.710	-0.383	0.05	40, 44, 52
K ₂ CO ₃	14.526	5.525	0.371	0.05	40
Na ₂ SO ₄	11.559	6.750	0.087	0.03	19, 36, 44
K ₂ SO ₄	32.024	7.464	-0.285	0.03	18a, 36, 40
MgSO ₄ ^a	-7.198	17.765	-18.462	0.05	19, 40

^a For MgSO₄ the terms $12.316I^{3/2} - 3.054I^2$ must be added to eq 21 to fit the data.

Another method that can be used to determine the \bar{V}_3^{*0} of the electrolytes in the medium is to use Young's rule^{23,24}

$$\phi_V(2,3) = \frac{m_2}{m_2 + m_3} \phi_V'(2) + \frac{m_3}{m_2 + m_3} \phi_V'(3) + \frac{\Delta V_m}{m_2 + m_3} \quad (17)$$

where $\phi_V'(2)$ and $\phi_V'(3)$ are the apparent molal volumes of electrolytes (2) and (3) in binary solutions at the ionic strength of the mixture ($I = w_2m_2 + w_3m_3$, where w_i is a valence factor equal to 1.0, 3.0, and 4.0, respectively, for 1-1, 2-1, and 2-2 electrolytes) and ΔV_m is the volume of mixing the two electrolyte solutions at the same ionic strength. By combining eq 12 and 17, we obtain

$$\phi_V^*(3) = (m_2/m_3)[\phi_V'(2) - \phi_V(2)] + \phi_V'(3) + (\Delta V_m/m_3) \quad (18)$$

The partial molal volume of electrolyte (3) can be obtained from eq 18 by differentiation and substitution into eq 6

$$\bar{V}_3^* = \phi_V'(3) + m_3 \left[\frac{\partial \phi_V'(3)}{\partial m_3} \right] + m_2 \left[\frac{\partial \phi_V'(2)}{\partial m_3} \right] + \left(\frac{\partial \Delta V_m}{\partial m_3} \right) \quad (19)$$

The value of \bar{V}_3^* at $m_3 = 0$ can be evaluated from

$$\bar{V}_3^{*0} = [\phi_V'(3)]_{m_3=0} + m_2 \left[\frac{\partial \phi_V'(2)}{\partial m_3} \right]_{m_3=0} + \left[\frac{\partial \Delta V_m}{\partial m_3} \right]_{m_3=0} \quad (20)$$

To evaluate \bar{V}_3^* as well as calculate ΔV_m from eq 17, the apparent molal volumes of the electrolytes studied in pure

water^{18,19,30-52} (from 0 to 1 *m*) were fitted to equations of the form

$$\phi_V'(i) = \phi_V^0(i) + A_i I^{1/2} + B_i I \quad (21)$$

The values of $\phi_V^0(i)$, A_i , and B_i for the various electrolytes are given in Table XXXI. The first two terms of eq 20 are given by

$$[\phi_V'(3)]_{m_3=0} = \phi_V^0(3) + A_3 m_2^{1/2} + B_3 m_2 \quad (22)$$

$$m_2 \left[\frac{\partial \phi_V'(2)}{\partial m_3} \right]_{m_3=0} = w_3 \left[B_2 m_2 + \frac{A_2}{2} m_2^{1/2} \right] \quad (23)$$

The value of $\phi_V'(3)$ at $m_3 = 0$ is just the value of $\phi_V(3)$ in itself at the ionic strength of the NaCl medium (0.725 *m*). The value of $m_2[\partial \phi_V'(2)/\partial m_3]$ at $m_3 = 0$ is simply equal to $\bar{V}_2 - \phi_V(2) = m_2[\partial \phi_V(2)/\partial m_2]$ for NaCl (0.839) at 0.725 *m* times the valence factor w_3 for the added solute. If $\Delta V_m = 0$, the \bar{V}_3^{*0} is simply given by

$$\bar{V}_3^{*0} = \phi_V^0(3) + A_3 m_2^{1/2} + B_3 m_2 + w_3 [B_2 m_2 + (A_2/2)m_2^{1/2}] \quad (24)$$

To calculate $(\partial \Delta V_m / \partial m_3)_{m_3=0}$, one must examine the concentration dependence of ΔV_m . The volume of mixing electrolyte solutions at a constant ionic strength have been studied by a number of workers.⁵³⁻⁵⁷ For the mixing of two 1-1 electrolytes at a constant ionic strength, the ΔV_m is given by

$$\Delta V_m = y_3(1 - y_3)[v_0 + v_1(1 - 2y_3)] \quad (25)$$

where $y_3 = m_3/(m_2 + m_3)$, $(1 - y_3) = y_2 = m_2/(m_2 + m_3)$, and v_0 and v_1 are adjustable parameters related to ionic interactions. The differentiation of eq 25 with respect to m_3 , evaluated at $m_3 = 0$ gives

$$\left[\frac{\partial \Delta V_m}{\partial m_3} \right]_{m_3=0} = \frac{v_0}{m_2} + \frac{v_1}{m_2} \quad (26)$$

Since the measurements made in this study were made at

TABLE XXXII: Values of $(\partial \Delta V_m / \partial m_3)$ at $m_3 = 0$ for Mixing Various Electrolytes with NaCl at 25 °C and $I = 0.725 m$

Electrolyte	$(\partial \Delta V_m / \partial m_3)_{m_3=0}$	Electrolyte	$(\partial \Delta V_m / \partial m_3)_{m_3=0}$
NaF	-0.18	NH ₄ Br	-0.02 ₃
KF	0.17	NaI	-0.13
HCl	-0.04 ₂	KI	-0.07 ₉
LiCl	-0.02 ₅	NaOH	0.39
NaCl	0.00	KOH	0.11
KCl	0.02 ₇	NaNO ₃	-0.01 ₀
RbCl	0.16	KNO ₃	-0.01 ₈
CsCl	0.11	NaHCO ₃	-0.12
NH ₄ Cl	-0.07 ₃	KHCO ₃	-0.13
MgCl ₂	-0.64	Na ₂ CO ₃	-0.66
CaCl ₂	-0.45	K ₂ CO ₃	0.68
SrCl ₂	-0.66	Na ₂ SO ₄	0.82
BaCl ₂	-0.42	K ₂ SO ₄	0.73
NaBr	-0.07 ₀	MgSO ₄	-2.26
KBr	0.10		

changing ionic strengths, it is not possible to fit the values of ΔV_m calculated from eq 17 to eq 25. We have subsequently fitted the values of ΔV_m calculated from

$$\Delta V_m = (m_2 + m_3)[\Phi_V(2,3) - \gamma_2 \phi_V'(2) - \gamma_3 \phi_V'(3)] \quad (27)$$

to equations of the form

$$\Delta V_m = A + Bm_3 + Cm_3^2 + \dots \quad (28)$$

The values of $(\partial \Delta V_m / \partial m_3)$ at $m_3 = 0$ (B in eq 28) evaluated from the experimental results are given in Table XXXII. It should be pointed out that the values of $(\partial \Delta V_m / \partial m_3)$ at $m_3 = 0$ are equal to $(v_0 + v_1)/m_2$. For most of the 1-1 electrolytes studied $(\partial \Delta V_m / \partial m_3)_{m_3=0}$ is less than 0.2 cm³ mol⁻¹; while for the 2-1 electrolytes the values are less than 0.7 cm³ mol⁻¹. The value of $(\partial \Delta V_m / \partial m_3)_{m_3=0}$ for MgSO₄ is quite large, probably due to ion pairing effects.⁵⁸

The values of \bar{V}^{*0} calculated from eq 20 using the values of $\Delta \partial V_m / \partial m_3$ at $m_3 = 0$ are given in Table XXXIII along with those obtained from eq 7. The results of \bar{V}^{*0} obtained by the two methods agree to within 0.2 cm³ mol⁻¹ for all of the electrolytes studied (which we feel is the maximum error). We will use the average values of \bar{V}^{*0} obtained by these two methods in all of our further calculations.

The reliability and internal consistency of our values of \bar{V}^{*0} can be determined by examining the additivity of the various salt pairs. For the difference between Na⁺ and K⁺, our results give $\bar{V}^{*0}(\text{Na}^+) - \bar{V}^{*0}(\text{K}^+) = -10.36 \pm 0.07$ cm³ mol⁻¹ from the salt pairs NaCl-KCl, NaF-KF, NaBr-KBr, NaI-KI, NaOH-KOH, NaNO₃-KNO₃, NaHCO₃-KHCO₃, $1/2\text{Na}_2\text{CO}_3 - 1/2\text{K}_2\text{CO}_3$, and $1/2\text{Na}_2\text{SO}_4 - 1/2\text{K}_2\text{SO}_4$ (the maximum difference was 0.13 cm³ mol⁻¹). The difference between Cl⁻ and the various anions obtained from our results are: $\bar{V}^{*0}(\text{Cl}^-) - \bar{V}^{*0}(\text{F}^-) = 18.74 \pm 0.04$ cm³ mol⁻¹, $\bar{V}^{*0}(\text{Cl}^-) - \bar{V}^{*0}(\text{Br}^-) = -6.75 \pm 0.11$ cm³ mol⁻¹; $\bar{V}^{*0}(\text{Cl}^-) - \bar{V}^{*0}(\text{I}^-) = -17.99 \pm 0.10$ cm³ mol⁻¹; $\bar{V}^{*0}(\text{Cl}^-) - \bar{V}^{*0}(\text{NO}_3^-) = -11.54 \pm 0.01$ cm³ mol⁻¹; $\bar{V}^{*0}(\text{Cl}^-) - \bar{V}^{*0}(\text{OH}^-) = 21.43 \pm 0.01$ cm³ mol⁻¹; $\bar{V}^{*0}(\text{Cl}^-) - \bar{V}^{*0}(\text{HCO}_3^-) = -7.83 \pm 0.07$ cm³ mol⁻¹; $\bar{V}^{*0}(\text{Cl}^-) - 1/2\bar{V}^{*0}(\text{CO}_3^{2-}) = 18.05 \pm 0.03$ cm³ mol⁻¹; and $\bar{V}^{*0}(\text{Cl}^-) - 1/2\bar{V}^{*0}(\text{SO}_4^{2-}) = -8.68 \pm 0.02$ cm³ mol⁻¹.

These differences can be used along with the values of \bar{V}^{*0} for the various electrolytes to obtain reliable values for various ions. To divide the values of \bar{V}^{*0} for the electrolytes into ionic values, it is necessary to assign a value to one ion. We have selected a value of $\bar{V}^{*0}(\text{Na}^+) = -4.50$ cm³ mol⁻¹ which is obtained from the specific interaction model.¹⁶ The values of \bar{V}^{*0} for various ions in 0.725 *m* NaCl obtained by using this value of $\bar{V}^{*0}(\text{Na}^+)$ are given in Table XXXIV.

TABLE XXXIII: Comparison of the Values of \bar{V}^{*0} for Various Electrolytes in 0.725 *m* NaCl Obtained by Extrapolation and by Using Young's Rule

Electrolyte	\bar{V}^{*0} , cm ³ mol ⁻¹		
	Extrapolation ^a	Young's full equation ^b	Δ^c
NaF	0.30	0.26	0.04
KF	10.61	10.69	-0.08
HCl	19.61	19.67	-0.06
LiCl	19.19	19.08	0.11
NaCl	19.08	19.06	0.02
KCl	29.34	29.35	-0.01
RbCl	34.65	34.63	0.02
CsCl	41.74	41.80	-0.06
NH ₄ Cl	37.91	37.94	-0.03
MgCl ₂	18.94	19.16	-0.22
CaCl ₂	22.97	22.92	0.05
SrCl ₂	23.17	23.16	0.01
BaCl ₂	28.92	28.94	-0.02
NaBr	25.62	25.77	-0.15
KBr	36.17	36.21	-0.04
NH ₄ Br	44.57	44.65	-0.08
NaI	36.92	36.99	-0.07
KI	47.42	47.42	0.00
NaOH	-2.42	-2.34	-0.08
KOH	7.90	7.92	-0.02
NaNO ₃	30.55	30.62	-0.07
KNO ₃	40.86	40.93	-0.07
NaHCO ₃	26.77	26.87	-0.10
KHCO ₃	37.20	37.26	-0.06
Na ₂ CO ₃	1.95	1.95	0.00
K ₂ CO ₃	22.60	22.70	-0.10
Na ₂ SO ₄	20.79	20.71	0.08
K ₂ SO ₄	41.24	41.42	-0.18
MgSO ₄	1.57	1.66	-0.09

^a Extrapolated from the $\phi_V^*(3)$ data by using eq 7 (Table XXX). ^b Calculated from Young's full equation (eq 20) using the values of ϕ_V^0 , A_i , and B_i given in Table XXXI and $(\partial \Delta V_m / \partial m_3)$ at $m_3 = 0$ given in Table XXXII. ^c $\Delta = \bar{V}^{*0}(\text{extrapolated}) - \bar{V}^{*0}(\text{Young's full equation})$.

TABLE XXXIV: The Partial Molal Volumes of Various Ions in 0.725 *m* NaCl at 25 °C

Ion	$\bar{V}^0(\text{M}^{n-})$, cm ³ mol ⁻¹	Ion	$\bar{V}^0(\text{X}^{n-})$, cm ³ mol ⁻¹
H ⁺	-3.92	F ⁻	4.82
Li ⁺	-4.39	Cl ⁻	23.56
Na ⁺	-4.50	Br ⁻	30.31
K ⁺	5.78	I ⁻	41.55
Rb ⁺	11.08	OH ⁻	2.12
Cs ⁺	18.21	NO ₃ ⁻	35.10
NH ₄ ⁺	14.33	HCO ₃ ⁻	31.39
Mg ²⁺	-28.07	CO ₃ ²⁻	11.02
Ca ²⁺	-24.17	SO ₄ ²⁻	29.76
Sr ²⁺	-23.96		
Ba ²⁺	-18.19		

Discussion

A comparison of the partial molal volumes of electrolytes in 0.725 *m* NaCl determined in this study and by other workers is shown in Table XXXV. Our volume results agree very well (to within ± 0.26 cm³ mol⁻¹) with the work of Wirth¹⁸ and Lee.¹⁹ The larger errors for MgCl₂ and MgSO₄ are due to the methods used by Lee in extrapolating the $\phi_V^*(3)$ data. The value of \bar{V}^{*0} for MgCl₂ obtained by fitting Lee's results to eq 5 are in good agreement with our results and also yield an additivity value for MgSO₄ that agrees with our results. The disagreement between our values of \bar{V}^{*0} for Na₂CO₃ and K₂CO₃ and the results of Duedall²⁰ is related to expansibility effects (his measurements were made at 20 °C). Duedall's results for K₂CO₃ and Na₂CO₃ yield differences for the $\bar{V}^*(\text{K}^+) -$

TABLE XXXV: Comparison of the Partial Molal Volumes of Electrolytes in 0.725 *m* NaCl Obtained in this Study and Those Obtained by Other Workers at 25 °C

Electrolyte	\bar{V}^{*0} , cm ³ mol ⁻¹		Δ
	Our results	Lit.	
HCl	19.64	19.64 ^a	0.00
NaCl	19.06	19.05 ^{a,b}	0.01
KCl	29.34	29.32 ^c	0.02
NaBr	25.70	25.79 ^b	-0.09
KBr	36.19	36.34 ^c	-0.15
Na ₂ SO ₄	20.75	20.65 ^b	0.10
K ₂ SO ₄	41.33	41.31 ^c	0.02
MgCl ₂	19.05	19.31 ^b	-0.26
		(19.09) ^b	(-0.04)
CaCl ₂	22.97	23.08 ^b	-0.11
MgSO ₄	1.62	1.88 ^b	-0.25
		(1.64) ^b	(-0.02)
Na ₂ CO ₃	1.95	1.70 ^d	0.25
K ₂ CO ₃	22.65	23.20 ^d	-0.55

^a Wirth,^{18b} estimated by interpolation. ^b Lee.¹⁹ The value for MgSO₄ was obtained by additivity [$\phi_{V^{*0}}(\text{MgSO}_4) = \phi_{V^{*0}}(\text{MgCl}_2) + \phi_{V^{*0}}(\text{Na}_2\text{SO}_4) - 2\phi_{V^{*0}}(\text{NaCl})$]. The values given in parentheses were calculated from Lee's values of $\phi_{V^{*0}}(3)$ by using eq 7. ^c Wirth,^{18a} estimated by interpolation. ^d Duedall²⁰ at 20 °C.

$\bar{V}^*(\text{Na}^+) = 10.75 \text{ cm}^3 \text{ mol}^{-1}$ which is $\sim 0.4 \text{ cm}^3 \text{ mol}^{-1}$ larger than found in this study. Since the differences in the expansibilities of Na⁺ and K⁺ are small at an ionic strength of 0.725 *m*, this comparison indicates that Duedall's \bar{V}^{*0} for K₂CO₃ at 20 °C may be too high. To summarize, these comparisons indicate that our values of \bar{V}^{*0} are reliable to $\pm 0.1 \text{ cm}^3 \text{ mol}^{-1}$ for 1-1 electrolytes and $\pm 0.2 \text{ cm}^3 \text{ mol}^{-1}$ for 2-1 electrolytes.

The partial molal volume of an electrolyte in an ionic medium can be estimated by a number of methods.¹²⁻¹⁷ Most of the methods are based on various models for ionic interactions.^{1-10,59} The most direct method is the use of the ionic strength principle.¹² This method essentially states that the partial molal volume of an electrolyte in an ionic medium is equal to the value in pure water at the ionic strength of the medium. The method is related to Harned's rule² for the trace activity coefficient of an electrolyte (γ_3) in a mixed electrolyte solution

$$\log \gamma_3 = \log \gamma_3' + \alpha_{23} m_2 \quad (29)$$

where γ_3' is the value of γ_3 in pure water at the ionic strength of the mixture of molality m_2 and α_{23} is an interaction coefficient. By assuming the Harned coefficient α_{23} is independent of pressure, we obtain

$$\bar{V}_3^{*0} = \bar{V}_3' = \phi_{V^0}(3) + 1.5A_3 m_2^{1/2} + 2B_3 m_2 \quad (30)$$

The partial molal volumes of electrolytes determined in this study are compared in Table XXXVI with those calculated from eq 30.

For electrolytes with a common anion (Cl⁻), the ionic strength principle predicts values for \bar{V}^{*0} that agree on the average to $\pm 0.23 \text{ cm}^3 \text{ mol}^{-1}$ (maximum difference of 0.58 $\text{cm}^3 \text{ mol}^{-1}$). For electrolytes with a common cation (Na⁺) the deviations are larger $\pm 0.48 \text{ cm}^3 \text{ mol}^{-1}$ (maximum difference of 1.18 $\text{cm}^3 \text{ mol}^{-1}$). For electrolytes without a common cation or anion the predicted values agree with the measured values on the average to $\pm 0.41 \text{ cm}^3 \text{ mol}^{-1}$ (maximum difference of 1.29 $\text{cm}^3 \text{ mol}^{-1}$). The values of \bar{V}^{*0} for various ions estimated by using the ionic strength principle (from the values for electrolytes with a common cation or anion) are compared with the measured values in Table XXXVII. For cations the predicted \bar{V}^{*0} 's agree with the measured values to $\pm 0.22 \text{ cm}^3 \text{ mol}^{-1}$ and for anions

TABLE XXXVI: Comparisons of the Measured and Calculated Values of \bar{V}^{*0} of Electrolytes in 0.725 *m* NaCl at 25 °C

Electrolyte	$\bar{V}^{*0}(\text{measd}) - \bar{V}^{*0}(\text{calcd})$, cm ³ mol ⁻¹		
	Ionic strength	Young's rule	Specific interaction
HCl	0.37	-0.07	-0.13
LiCl	0.33	0.05	0.05
NaCl	0.00	0.00	0.00
KCl	0.02	0.02	0.03
RbCl	0.10	0.17	0.20
CsCl	0.02	0.08	0.09
NH ₄ Cl	0.13	-0.09	-0.04
MgCl ₂	0.35	-0.75	-0.75
CaCl ₂	0.58	-0.49	-0.41
SrCl ₂	0.21	-0.66	-0.67
BaCl ₂	0.40	-0.43	-0.38
	± 0.23	± 0.26	± 0.25
NaF	-0.51	-0.16	-0.15
NaCl	0.00	0.00	0.00
NaBr	-0.07	-0.14	-0.16
NaI	0.08	-0.17	-0.21
NaOH	-1.18	-0.43	-0.37
NaNO ₃	-0.09	-0.04	0.13
NaHCO ₃	-0.81	-0.17	0.23
Na ₂ CO ₃	-1.15	-0.66	-0.99
Na ₂ SO ₄	0.44	0.86	0.51
	± 0.48	± 0.29	± 0.31
NH ₄ Br	0.30	-0.06	-0.15
KF	-0.13	0.13	-0.03
KBr	-0.02	0.08	0.08
KI	0.03	-0.08	0.01
KOH	-0.76	-0.11	-0.33
KNO ₃	0.02	-0.05	0.18
KHCO ₃	-0.88	-0.16	0.39
K ₂ CO ₃	0.49	0.59	-0.83
K ₂ SO ₄	0.20	0.65	0.60
MgSO ₄	-1.29	-2.30	-0.27
	± 0.41	± 0.42	± 0.29

TABLE XXXVII: Comparison of the Measured and Calculated Values of \bar{V}^{*0} of Ions in 0.725 *m* NaCl at 25 °C

Ion	$\bar{V}^{*0}(\text{measd}) - \bar{V}^{*0}(\text{calcd})$, cm ³ mol ⁻¹		
	Ionic strength	Young's rule	Specific interaction
H ⁺	0.37	0.07	-0.13
Li ⁺	0.32	0.07	0.05
Na ⁺	0.00	0.00	0.00
K ⁺	0.01	0.02	0.03
Rb ⁺	0.10	0.17	0.20
Cs ⁺	0.01	0.08	0.09
NH ₄ ⁺	0.09	-0.12	-0.07
Mg ²⁺	0.34	-0.75	-0.72
Ca ²⁺	0.58	-0.49	-0.34
Sr ²⁺	0.21	-0.66	-0.67
Ba ²⁺	0.40	-0.43	-0.38
	± 0.22	± 0.26	± 0.24
F ⁻	0.46	-0.11	-0.11
Cl ⁻	0.00	0.00	0.00
Br ⁻	0.04	-0.03	-0.05
I ⁻	0.18	-0.07	-0.11
OH ⁻	-1.18	-0.43	-0.37
NO ₃ ⁻	-0.08	-0.03	0.14
HCO ₃ ⁻	-0.74	-0.10	0.30
CO ₃ ²⁻	-1.10	-0.61	-0.92
SO ₄ ²⁻	0.46	0.88	0.52
	± 0.47	± 0.25	± 0.28

the predicted \bar{V}^{*0} 's agree with the measured values to $\pm 0.47 \text{ cm}^3 \text{ mol}^{-1}$. The better agreement for cations is

related to the fact that most cations do not have strong interactions with Cl⁻ ions. The larger deviations for the anions can be related to the volume changes for the formation of various ion pairs with Na⁺.¹⁶

The use of Young's rule to estimate the \bar{V}^{*0} was discussed earlier. The method assumes that the volume of mixing two electrolyte solutions is zero. The partial molal volumes of electrolytes and ions determined in this study are compared with those calculated from eq 24 in Tables XXXVI and XXXVII. For electrolytes with a common anion, the differences are $\pm 0.26 \text{ cm}^3 \text{ mol}^{-1}$; for electrolytes with a common cation, the differences are $\pm 0.29 \text{ cm}^3 \text{ mol}^{-1}$; and for electrolytes with uncommon ions, the differences are $\pm 0.42 \text{ cm}^3 \text{ mol}^{-1}$. The predicted values for cations and anions agree, respectively, on the average to ± 0.26 and $\pm 0.25 \text{ cm}^3 \text{ mol}^{-1}$. Overall, the predicted values of \bar{V}^{*0} using Young's rule are better than using the ionic strength principle.

The use of the specific interaction model to estimate the \bar{V}^{*0} of electrolytes and ions in ionic media has been discussed elsewhere.¹⁶ In using the specific interaction model one assumes that specific short-range interactions in solutions of constant ionic strength are limited to ions of opposite charge only.⁵⁹ The partial molal volumes of electrolytes in water are represented by¹⁶

$$\bar{V}(\text{MX}) = \bar{V}^0(\text{MX}) + \frac{S_V I^{1/2}}{1 + I^{1/2}} + 2\nu_M \nu_X B_{\text{MX}}[\text{MX}] \quad (31)$$

where S_V is the Debye-Hückel limiting slope ($=2.802w$ at 25 °C), ν_M is the number of cations and ν_X is the number of anions formed when MX completely dissociates, [MX] is the molality of MX, and B_{MX} is the volume specific interaction parameter which is a function of ionic strength.¹⁶ The partial molal volumes of electrolytes and ions are predicted by using the equations¹⁶

$$\bar{V}^*(\text{MX}) = \bar{V}^0(\text{MX}) + \frac{2.802wI^{1/2}}{1 + I^{1/2}} + \nu_M \sum_X B_{\text{MX}}[X] + \nu_X \sum_M B_{\text{MX}}[M] \quad (32)$$

$$\bar{V}^*(\text{M}^+) = \bar{V}^0(\text{M}^+) + \frac{2.802wI^{1/2}}{1 + I^{1/2}} + \sum_X B_{\text{MX}}[X] \quad (33)$$

$$\bar{V}^*(\text{X}^-) = \bar{V}^0(\text{X}^-) + \frac{2.802w'I^{1/2}}{1 + I^{1/2}} + \sum_M B_{\text{MX}}[M] \quad (34)$$

where the interaction coefficients B_{MX} are at the ionic strength of the mixture and $w' = Z^{1/2}$ (0.5 for $Z = \pm 1$ and 2.0 for $Z = \pm 2$). In a 0.725 *m* NaCl solution the values of $\bar{V}^*(\text{MX})$, $\bar{V}^*(\text{M}^+)$, and $\bar{V}^*(\text{X}^-)$ are determined from

$$\bar{V}^*(\text{MX}) = \bar{V}^0(\text{MX}) + 1.289w + \nu_M B_{\text{MCl}}(0.725) + \nu_X B_{\text{NaX}}(0.725) \quad (35)$$

$$\bar{V}^*(\text{M}^+) = \bar{V}^0(\text{M}^+) + 1.289w' + B_{\text{MCl}}(0.725) \quad (36)$$

$$\bar{V}^*(\text{X}^-) = \bar{V}^0(\text{X}^-) + 1.289w' + B_{\text{NaX}}(0.725) \quad (37)$$

The values of \bar{V}^{*0} for various electrolytes and ions calculated from eq 35–37 are compared with the measured values in Tables XXXVI and XXXVII. For electrolytes with a common anion, the predicted values agree on the average to $\pm 0.25 \text{ cm}^3 \text{ mol}^{-1}$; with a common cation, the differences are $\pm 0.31 \text{ cm}^3 \text{ mol}^{-1}$; and with both uncommon cations and anions, the differences are $\pm 0.29 \text{ cm}^3 \text{ mol}^{-1}$. The values of \bar{V}^{*0} predicted from the specific interaction model are much better than those estimated by using the

TABLE XXXVIII: Comparison of the Values of v_0 with the Values of RTh_0 for Common Cation and Anion Mixing of Electrolytes with NaCl

	v_0	RTh_0
Common Cation		Cl-X Interactions
F	-0.13	
Cl	0.00	0.0
Br	-0.05	3.2 ^{60,61,62}
I	-0.09	
OH	-0.28	
NO ₃	-0.07	12.4 ^{60,61,62}
HCO ₃	-0.09	
CO ₃	-0.48	
SO ₄	0.59	-27 ^{60,61,67}
Common Anion		Na-M Interactions
H	-0.03	124 ^{60,69}
Li	-0.02	84 ^{60,61,62,65,68}
Na	0.00	0.0
K	0.02	-38 ^{60,61,62,68}
Rb	0.12	-50 ^{60,61}
Cs	0.08	-35 ^{60,61}
NH ₃	-0.05	
Mg	-0.46	172 ⁶³
Ca	-0.33	137 ⁶⁶
Sr	-0.48	
Ba	-0.30	85.3 ⁶⁶

ionic strength principle and slightly better than those estimated by using Young's rule. If MgSO₄ is eliminated from the comparisons, the specific interaction model and Young's rule are nearly equivalent. This is clearly demonstrated by examining the estimates for the values of \bar{V}^{*0} (Table XXXVII) for cations and anions. In summary, these comparisons indicate that the specific interaction model and Young's rule (without ΔV_m) predict better values of \bar{V}^{*0} in 0.725 *m* NaCl than the ionic strength principle.

The failure of Young's rule and the specific interaction model to predict more reliable values is due to the fact that the interactions between like charged ions are not considered. To improve these estimations, one must have some knowledge of the volume of mixing the various electrolyte solutions with NaCl at an ionic strength of 0.725. Since the values of \bar{V}^{*0} are additive, only the volumes of mixing various electrolytes with a common cation (Na⁺) and anion (Cl⁻) need to be considered. Although the values of $v_0 \approx m_2(\partial\Delta v_m/\partial m_3)_{m_3=0}$ determined from our results have large errors, it is possible to examine how the values of v_0 are related to other excess thermodynamic properties for the same systems. The enthalpies of mixing electrolytes containing a common cation and anion with NaCl at $I = 1.0$ have been studied by Young and co-workers,^{60,61} Wood and co-workers,⁶²⁻⁶⁷ and Stern and co-workers.^{68,69} A comparison of our estimated values of v_0 and the enthalpy interaction¹ term RTh_0 (at $I = 0$) is given in Table XXXVIII and Figure 5. As is quite apparent from these comparisons, the values of v_0 correlate very well with RTh_0 . As found in enthalpy studies by other workers^{60,61} for common anion mixtures, the cations can be divided into two groups (H⁺, Li⁺, NH₄⁺, Mg²⁺, Ca²⁺, Sr²⁺, Ba²⁺), and (K⁺, Rb⁺, Cs⁺). The mixing of Na⁺ with the so-called "structure making" cations (H⁺, Li⁺, NH₄⁺, Mg²⁺, Ca²⁺, Sr²⁺, and Ba²⁺) produces a decrease in volume; while the mixing with the "structure breaking" cations (K⁺, Rb⁺, and Cs⁺) produces an increase in volume.

The effect of water structural interactions on ion-ion interactions was first suggested by Frank and Robinson.⁷⁰ Gurney⁷¹ with his cosphere model made further developments of these ideas. Desnoyers et al.³¹ developed a general rule that relates these ionic structural interactions in terms of the Gurney cospheres. They³¹ state that, "two

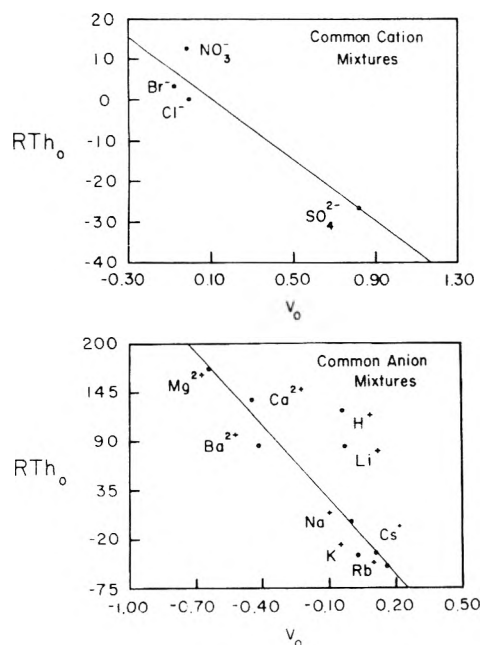


Figure 5. The enthalpy interaction term (RTh_0) plotted vs. the volume interaction term (v_0) for mixing NaCl with electrolytes containing a common cation (NaX) and a common anion (MCl) at 25 °C.

solutes will attract each other if their structural influences, or their tendencies to orient water molecules, are compatible with each other; conversely, an incompatibility in these structural influences or tendencies will result in repulsive forces". The mixing of two electrolytes of the same structural form (i.e., two "structure making" electrolytes) causes a repulsion with a decrease in volume and an increase in enthalpy. The mixing of two electrolytes of opposite structural forms (i.e., a "structure making" and "structure breaking" electrolyte) causes an attraction with an increase in volume and a decrease in enthalpy. As is clearly demonstrated in the comparisons given in Table XXXVIII and shown in Figure 5, our results are in agreement with the predictions of the structural interaction model of Desnoyers.³¹ Although the sign of ΔV_m or v_0 can be predicted from this structural interaction model, it is not possible to predict the magnitude of the volume changes. There also is no unambiguous way of selecting whether an ion is a "structure breaker or maker".⁷² If the structural concepts are valid, one might expect a correlation between excess thermodynamic properties with properties related to structure such as molal entropies, volumes, and expansibilities.^{73,74} Leyendekkers¹⁷ for example has developed a correlation between $(\partial\Delta V_m/\partial m_3)_{m_3=0}$ and entropy for mixtures of electrolytes in seawater. The functional form¹⁷ of the correlation for anions, however, is quite complex ($\partial\Delta V_m/\partial m_3$ is a cubic function of entropy).

We have attempted to correlate the values of v_0 to various thermodynamic properties of the uncommon ions, such as S^0 , the partial molal entropy; E^0 , the partial molal compressibility; K_S^0 , the partial molal adiabatic compressibility; b_v , the Redlich-Rosenfeld molal volume deviation parameter, and $\bar{V}^0(\text{ion}) - \bar{V}^0(\text{cryst})$, the differences between the partial molal volume of an ion and the crystal molal volume ($2.52r^3$, where r is the crystal radius). The linear correlation of v_0 vs. $\bar{V}^0(\text{ion}) - \bar{V}^0(\text{cryst})$ for the common cations and anions is shown in Figure 6. The values of v_0 for the common anion mixtures show a linear correlation with these thermodynamic properties. [The standard errors in v_0 are 0.10, 0.16, 0.13, 0.07, and 0.07 $\text{cm}^3 \text{mol}^{-1}$, respectively, for the correlations with S^0 , E^0 , K_S^0 , b_v , and $\bar{V}^0(\text{ion}) - \bar{V}^0(\text{cryst})$.] The values of v_0 for the

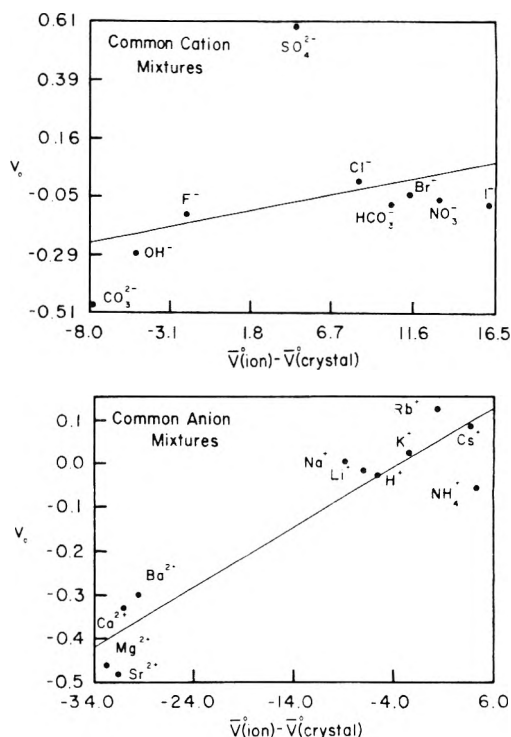


Figure 6. The volume interaction term (v_0) plotted vs. the difference between the partial molal volume of the uncommon ion at infinite dilution, $\bar{V}^0(\text{ion})$, and the crystal molal volume, $\bar{V}^0(\text{cryst})$.

common cation mixtures do not correlate as well with the thermodynamic properties of the uncommon anion. [The standard errors in v_0 are 0.27, 0.24, 0.28, 0.28, and 0.26 $\text{cm}^3 \text{mol}^{-1}$, respectively, for linear correlations with S^0 , E^0 , K_S^0 , b_v , and $\bar{V}^0(\text{ion}) - \bar{V}^0(\text{cryst})$.] If the $\text{SO}_4^{2-}\text{Cl}^-$ mixtures are not used, the correlations improve considerably. [The standard errors in v_0 are 0.11, 0.10, 0.07, 0.11, 0.09 $\text{cm}^3 \text{mol}^{-1}$, respectively, for correlations with S^0 , E^0 , K_S^0 , b_v , and $\bar{V}^0(\text{ion}) - \bar{V}^0(\text{cryst})$.]

Although these correlations may be fortuitous, the results do indicate that the volume of mixing electrolyte solutions with common anions and cations are related to the water-ion interactions of the uncommon ion. In our future work we plan to make direct volume of mixing measurements of NaCl solutions with other electrolytes (with and without a common ion) as a function of ionic strength and temperature in an attempt to elucidate these structural interactions.

Acknowledgment. The authors wish to acknowledge the support of the Office of Naval Research (N00014-75-C-0173) and the Oceanographic Branch of the National Science Foundation (OCE73-00351-A01) for this study. We also wish to thank Chris Woodhouse and Francis Gombar for their help in the computer fitting of the data.

Supplementary Material Available: Tables I-XXIX, listings of density, $\phi_v^*(3)$, and $\Phi_v(2,3)$ for the various electrolytes studied (29 pages). Ordering information is available on any current masthead page.

References and Notes

- (1) H. L. Friedman, *J. Chem. Phys.*, **32**, 1134 (1960).
- (2) H. S. Harned and R. S. Robinson, "Multicomponent Electrolyte Solutions", Pergamon Press, Oxford, 1968.
- (3) G. Scatchard, *J. Am. Chem. Soc.*, **90**, 3124 (1968); **91**, 2410 (1969); G. Scatchard, R. M. Rush, and J. S. Johnson, *J. Phys. Chem.*, **74**, 3786 (1970).
- (4) R. H. Wood and P. J. Reilly, *Annu. Rev. Phys. Chem.*, **21**, 287 (1970); P. J. Reilly and R. H. Wood, *J. Phys. Chem.*, **73**, 4292 (1969); P. J. Reilly, R. H. Wood, and R. A. Robinson, *ibid.*, **75**, 1305 (1971).
- (5) K. S. Pitzer, *J. Phys. Chem.*, **77**, 268 (1973).
- (6) R. A. Robinson and R. H. Wood, *J. Solution Chem.*, **1**, 481 (1972).

- (7) M. W. Watson, R. H. Wood, F. J. Millero, *ACS Symp. Ser.*, No. 18 (1975).
- (8) F. J. Millero in "The Sea", Vol. 5, E. D. Goldberg, Ed., Wiley-Interscience, New York, N.Y., 1974; *Annu. Rev. Earth Planet. Sci. Lett.*, 2, 101 (1974); *ACS Symp. Ser.*, No. 18 (1975); *Thalassia Jugosl.*, 11, 53 (1975).
- (9) M. Whitfield in "Chemical Oceanography", Vol. 1, 2nd ed, J. P. Riley and G. Skirrow, Ed., Academic Press, New York, N.Y., 1975; *Deep-Sea Res.*, 21, 57 (1973); *Mar. Chem.*, 1, 251 (1973); 3, 197 (1975); *Geochim. Cosmochim. Acta.*, 39, 1545 (1975).
- (10) J. V. Leyendekkers, *Anal. Chem.*, 43, 1835 (1971); *J. Phys. Chem.*, 75, 946 (1971); *Mar. Chem.*, 1, 75 (1973).
- (11) K. S. Pitzer and J. J. Kim, *J. Am. Chem. Soc.*, 96, 5701 (1974).
- (12) B. B. Owen and S. R. Brinkley, Jr., *Chem. Rev.*, 29, 461 (1941).
- (13) F. J. Millero, *Limnol. Oceanogr.*, 14, 376 (1969); *J. Phys. Chem.*, 73, 2417 (1969); *Chem. Rev.*, 71, 147 (1971); *Geochim. Cosmochim. Acta.*, 35, 1089 (1971).
- (14) F. J. Millero and R. A. Berner, *Geochim. Cosmochim. Acta.*, 36, 92 (1972).
- (15) G. K. Ward and F. J. Millero, *Geochim. Cosmochim. Acta.*, 39, 1595 (1975).
- (16) F. J. Millero, *Geochim. Cosmochim. Acta.*, 41, 215 (1977).
- (17) B. B. Leyendekkers, *Mar. Chem.*, 2, 89 (1974).
- (18) (a) H. E. Wirth, *J. Am. Chem. Soc.*, 59, 2549 (1937); (b) 62, 1128 (1940).
- (19) J. Lee, Ph.D. Dissertation, Yale University, University Microfilm, Ann Arbor, Mich., No. 66-4906; *Abstr.* B27, 131 (1966).
- (20) I. W. Duedall, *Geochim. Cosmochim. Acta.*, 36, 729 (1972).
- (21) I. W. Duedall and P. K. Weyl, *Limnol. Oceanogr.*, 12, 52 (1967).
- (22) A. Poisson and J. Chanu, *Limnol. Oceanogr.*, 21, 853 (1976).
- (23) T. F. Young, *Recl. Chem. Prog.*, 12, 81 (1951).
- (24) T. F. Young and M. B. Smith, *J. Phys. Chem.*, 58, 716 (1954).
- (25) P. Picker, E. Tremblay, and C. Jolicoeur, *J. Solution Chem.*, 3, 377 (1974).
- (26) F. J. Millero, D. Lawson, and A. Gonzalez, *J. Geophys. Res.*, 81, 1177 (1976).
- (27) F. J. Millero, A. Gonzalez, and G. K. Ward, *J. Mar. Res.*, 34, 61 (1976).
- (28) See paragraph at end of text regarding supplementary material.
- (29) G. S. Kell, *J. Chem. Eng. Data*, 20, 97 (1975).
- (30) F. J. Millero, *J. Phys. Chem.*, 71, 4567 (1967).
- (31) J. E. Desnoyers, M. Arel, G. Perron, and C. Jolicoeur, *J. Phys. Chem.*, 73, 3346 (1969).
- (32) B. E. Conway and L. H. Laliberte, *J. Phys. Chem.*, 72, 4317 (1968).
- (33) W. Geffcken, *Z. Phys. Chem.*, A155, 1 (1931).
- (34) N. M. Burns, *Can. J. Chem.*, 51, 3123 (1973).
- (35) O. Redlich and J. Bigeleisen, *J. Am. Chem. Soc.*, 64, 758 (1942).
- (36) L. A. Dunn, *Trans. Faraday Soc.*, 62, 2348 (1966).
- (37) F. J. Millero, E. V. Hoff, and L. A. Kahn, *J. Solution Chem.*, 1, 309 (1972).
- (38) F. Vaslow, *J. Phys. Chem.*, 70, 2286 (1966).
- (39) A. F. Scott, *J. Phys. Chem.*, 35, 2315 (1931).
- (40) F. J. Millero, P. V. Chetirkin, and A. Gonzalez, unpublished results.
- (41) L. A. Dunn, *Trans. Faraday Soc.*, 64, 2951 (1968).
- (42) L. A. Dunn, *Trans. Faraday Soc.*, 64, 1898 (1968).
- (43) F. J. Millero, *J. Phys. Chem.*, 74, 356 (1970).
- (44) W. Geffcken and D. Price, *Z. Phys. Chem.*, B26, 81 (1934).
- (45) F. H. Spedding, M. J. Pikal, and B. O. Ayres, *J. Phys. Chem.*, 70, 2440 (1966).
- (46) G. Perron, J. E. Desnoyers, and F. J. Millero, *Can. J. Chem.*, 52, 3738 (1974).
- (47) A. Krus, *Z. Phys. Chem.*, B34, 1 (1936).
- (48) J. E. Desnoyers and M. Arel, *Can. J. Chem.*, 45, 359 (1967).
- (49) F. Vaslow, *J. Phys. Chem.*, 73, 3745 (1969).
- (50) L. G. Hepler, J. M. Stokes, and R. H. Stokes, *Trans. Faraday Soc.*, 61, 20 (1965).
- (51) R. A. Robinson, *J. Am. Chem. Soc.*, 59, 84 (1937).
- (52) G. Perron, J. E. Desnoyers, and F. J. Millero, *Can. J. Chem.*, 53, 1134 (1975).
- (53) H. E. Wirth, R. E. Lindstrom, and J. N. Johnson, *J. Phys. Chem.*, 67, 2339 (1963).
- (54) H. E. Wirth and A. Lo Surdo, *J. Chem. Eng. Data*, 13, 226 (1968).
- (55) H. E. Wirth and W. L. Mills, *J. Chem. Eng. Data*, 13, 102 (1968).
- (56) W. Y. Wen and K. Nara, *J. Phys. Chem.*, 71, 3907 (1967); 72, 1137 (1968).
- (57) W. Y. Wen, K. Nara, and R. H. Wood, *J. Phys. Chem.*, 72, 3048 (1968).
- (58) F. J. Millero and W. L. Masterton, *J. Phys. Chem.*, 78, 1287 (1974).
- (59) E. A. Guggenheim, *Phil. Mag.*, 19, 588 (1935).
- (60) T. F. Young, Y. C. Wu, and A. A. Krawetz, *Discuss. Faraday Soc.*, 24, 27, 77, 80 (1957).
- (61) Y. C. Wu, M. B. Smith, and T. F. Young, *J. Phys. Chem.*, 69, 1868, 1873 (1965).
- (62) R. H. Wood and R. W. Smith, *J. Phys. Chem.*, 69, 2974 (1965).
- (63) R. H. Wood, J. D. Patton, and M. Ghamkhar, *J. Phys. Chem.*, 73, 346 (1969).
- (64) R. F. Srna and R. H. Wood, *J. Phys. Chem.*, 79, 1535 (1975).
- (65) R. H. Wood, D. E. Smith, H. K. W. Chen, and P. T. Thompson, *J. Phys. Chem.*, 79, 1532 (1975).
- (66) R. H. Wood and M. Ghamkhar, *J. Phys. Chem.*, 73, 3959 (1969).
- (67) R. B. Cassel and R. H. Wood, *J. Phys. Chem.*, 78, 1924 (1974).
- (68) J. H. Stern and C. W. Anderson, *J. Phys. Chem.*, 68, 2528 (1964).
- (69) J. H. Stern and A. A. Passchier, *J. Phys. Chem.*, 67, 2420 (1963).
- (70) H. S. Frank and A. L. Robinson, *J. Chem. Phys.*, 8, 933 (1940).
- (71) R. W. Gurney, "Ionic Processes in Solution", Dover Publication, New York, N.Y., 1953.
- (72) A. Holtzer and M. F. Emerson, *J. Phys. Chem.*, 73, 26 (1969).
- (73) F. J. Millero in "Biophysical Properties of Skin", H. R. Eiden, Ed., Wiley-Interscience, New York, N.Y., 1971.
- (74) F. J. Millero in "Water and Aqueous Solutions", R. A. Horne, Ed., Wiley-Interscience, New York, N.Y., 1972.

Solubility of Iodine in Mixed Solvents. A Case Study of Preferential Solvation in Nonpolar and Associated Solutions

Koichiro Nakanishi* and Sotō Asakura

Department of Industrial Chemistry, Kyoto University, Kyoto 606, Japan (Received July 29, 1976; Revised Manuscript Received April 25, 1977)

Publication costs assisted by Kyoto University

The solubilities of iodine have been measured at 288.15, 298.15, and 308.15 K in the following seven binary mixed solvents: $n\text{-C}_6\text{H}_{14}$ + $c\text{-C}_6\text{H}_{12}$, $c\text{-C}_6\text{H}_{12}$ + C_6H_6 , C_6H_6 + $\text{C}_6\text{H}_5\text{CH}_3$, $c\text{-C}_6\text{H}_{12}$ + EtOH , $n\text{-C}_7\text{H}_{16}$ + EtOH , C_6H_6 + EtOH , and EtOH + H_2O . The entropy of solution of iodine ΔS_{soln} has been evaluated at 298.15 K as a function of the mole fraction of one solvent x in mixed solvents. A distinct maximum or minimum in the ΔS_{soln} vs. x relation for such associated solutions as EtOH + H_2O or $c\text{-C}_6\text{H}_{12}$ + EtOH was found to be parallel with the anomalies in the diffusivity of iodine in the same solvent systems. A thermodynamic analysis of the solubility data based primarily on the regular solution theory was given.

Introduction

Our recent studies on the diffusivity of iodine in binary mixed solvents¹⁻³ have revealed that the temperature reduced isoviscous diffusion coefficient $D_{11}^0 \eta_{23}/T$ vs. mole fraction of mixed solvents x_2 relation^{4,5} deviates negatively from the additivity with respect to x_2 , whenever the

difference in the interactions of two solvents with iodine is nonnegligible. Such a relative decrease in diffusivity suggests that the stability of iodine complexes in these mixed solvents might be greater than those in pure solvents. The entropy of solution ΔS_{soln} of iodine which may be obtained from the temperature dependence of the

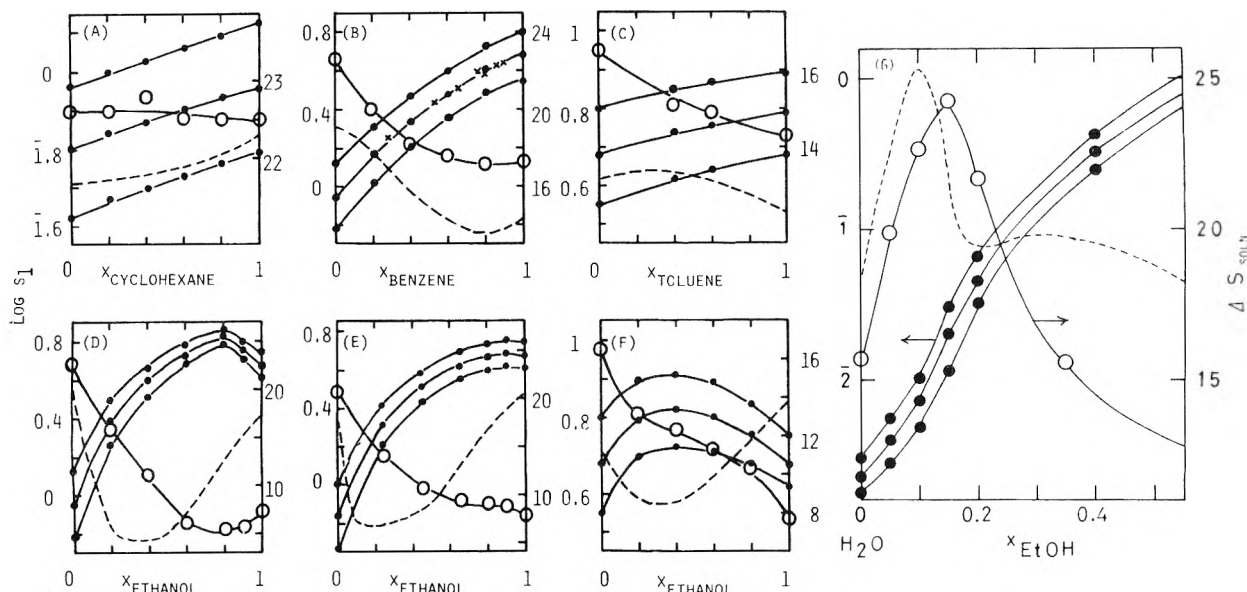


Figure 2. Solubility s_1 , entropy of solution ΔS_{soln} , and reduced isoviscous diffusion coefficient $D_{11}^0 \eta_{23}/T$ of iodine in mixed solvents: (●) $\log s_1$ (this work); (X) $\log s_1$ (ref 8); (O) ΔS_{soln} , (---) $D_{11}^0 \eta_{23}/T$. (A) $n\text{-C}_6\text{H}_{14} + c\text{-C}_6\text{H}_{12}$, (B) $c\text{-C}_6\text{H}_{12} + \text{C}_6\text{H}_6$, (C) $\text{C}_6\text{H}_6 + \text{C}_6\text{H}_5\text{CH}_3$, (D) $c\text{-C}_6\text{H}_{12} + \text{EtOH}$, (E) $n\text{-C}_7\text{H}_{16} + \text{EtOH}$, (F) $\text{C}_6\text{H}_6 + \text{EtOH}$, (G) $\text{EtOH} + \text{H}_2\text{O}$.

saturated solubility s_1 of solid iodine will serve as a measure of the complex stability.⁶ Data are available for the solubility of iodine in several nearly ideal solutions^{7,8} and in aqueous solutions.⁹ We had therefore planned to measure s_1 as a function of temperature in various types of binary mixed solutions. For this purpose, we have already designed a novel solubility apparatus and made a preliminary measurement.¹⁰

In this paper, we present the solubility data in seven binary solutions which we believe to be representative of the combination of different types of interactions with iodine. The data reveal that there is a parallelism between ΔS_{soln} and $D_{11}^0 \eta_{23}/T$ and that both preferential solvation and disintegration of hydrogen bonding structures in associated liquids may be equally responsible for the complicated behavior of iodine solubility in ethanol solutions.

Experimental Section

Materials. Iodine used in this study was a Merck doubly-sublimated reagent or JIS (Japan Industrial Standard) guaranteed reagent. Organic solvents were also JIS guaranteed reagents. Water used as a solvent was from a commercial sample specially prepared for quantitative analytical use. These materials were used without further purifications.

Apparatus and Procedure. Several different solubility apparatus have been described by Hildebrand and co-workers.¹¹ Our new apparatus¹⁰ shown in Figure 1 (available as supplementary material) was designed to ensure complete transfer of saturated solutions for the analysis at temperatures higher than room temperature. During the measurements, it was placed on a water-sealed magnetic stirrer immersed in a double thermostat which was controlled within ± 0.03 °C. Solutions saturated with iodine were allowed to stand for a few hours under agitation to attain solubility equilibrium.¹² The saturated iodine solutions were then transferred from the apparatus to a flask by using a hypodermic syringe and the sampling container, diluted with water, and titrated with sodium thiosulfate solutions, the concentration of which was $1/20$ N except for the water-rich region of aqueous ethanol solutions. The solubility was determined at 288.15, 298.15 and 308.15 K. The sampling of saturated solutions was

first done at the highest temperature and then repeated in order of decreasing temperature.

Results and Discussion

Solubility. The solubilities of iodine s_1 (mol %) in seven binary mixed solvents at three temperatures are given in Table I. The solubility data in pure solvents reported by Hildebrand et al.^{6,11a,13} are also included in the table. Reasonable agreements were obtained with each other. Figure 2 illustrates the dependence of s_1 on the molar composition of mixed solvents. While the s_1 vs. x_2 curves for nonpolar solutions exhibit simple and monotoneous changes, those for ethanol solutions show maximum solubility. Purkayastha and Walkley⁸ have reported s_1 data for $c\text{-C}_6\text{H}_{12} + \text{C}_6\text{H}_6$ solutions at 298.15 K. As seen in Figure 2b, the present data agree quite well with theirs. The s_1 vs. x_2 curve for an aqueous ethanol solution has no maximum, but there is an inflection point in the water-rich region. This last observation has also been reported by Mikhailov et al.,⁹ though there are nonnegligible disagreements between the two data.

Entropy of Solution. In Table I are also given the values for $R(d \log s_1/d \log T)$ at 298.15 K estimated from the temperature dependence of s_1 . This quantity corresponds to the entropy of isothermal transfer of iodine into infinitely dilute solution from the pure solid. Since the solubility of iodine is sometimes fairly large in the present case, the activity correction must be made to obtain accurate values for the entropy of solution ΔS_{soln} (cf. ref 6 and footnote a of Table I). However, we may use the uncorrected values in Table I as ΔS_{soln} in the following qualitative discussion. These approximate ΔS_{soln} values are plotted in Figure 2 against x_2 , though the use of volume fraction ϕ_2 , instead of x_2 , is preferred in the framework of the solubility parameter theory.⁶

Iodine forms charge-transfer complexes with various kinds of organic solvents.¹⁴ We call them complexing solvents, while those solvents which dissolve iodine to form violet solution are classified as noncomplexing. Based on this fact, the following qualitative interpretations may be given to the plots in Figure 2. There are observed four types of composition dependence of ΔS_{soln} upon x_2 . They are (a) linear dependence, (b) the presence of a minimum point, (c) s-shaped curve, and (d) the presence of a

TABLE I: Solubility and Entropy of Solution of Iodine in Binary Mixed Solvents

Mixed solvent	s_1 (mol %)/ ΔS_{soln}^a	x_2									
		0	0.05	0.1	0.15	0.2	0.4	0.6	0.8	0.9	1
c-C ₆ H ₁₂ (2) + n-C ₆ H ₁₄ (3)	s_1 (288.15 K)	0.417				0.466	0.494	0.535	0.575		0.613
	s_1 (298.15 K)	0.623				0.686	0.736	0.794	0.854		0.901
	s_1 (308.15 K)	0.915				0.988	1.06	1.15	1.23		1.33
	ΔS_{soln} (298.15 K)	22.6				22.6	22.8	22.5	22.5		22.5
C ₆ H ₆ (2) + c-C ₆ H ₁₂ (3)	s_1 (288.15 K)	0.613				1.05	1.60	2.24	3.06		3.56
	s_1 (298.15 K)	0.901				1.48	2.19	3.04	4.09		4.78
	s_1 (308.15 K)	1.33				2.06	2.98	4.01	5.41		6.32
	ΔS_{soln} (298.15 K)	22.5				20.0	18.2	17.5	17.1		17.2
C ₆ H ₅ CH ₃ (2) + C ₆ H ₆ (3)	s_1 (288.15 K)	3.56				4.17	4.17	4.38		4.83	
	s_1 (298.15 K)	4.78				5.47	5.47	5.68		6.21	
	s_1 (308.15 K)	6.32				7.07	7.07	7.38		7.98	
	ΔS_{soln} (298.15 K)	17.2				15.1	14.9			14.3	
EtOH(2) + c-C ₆ H ₁₂ (3)	s_1 (288.15 K)	0.613				1.87	3.22	4.75	6.01		4.15
	s_1 (298.15 K)	0.901				2.47	3.96	5.17	6.78		4.69
	s_1 (308.15 K)	1.33				3.13	4.59	5.90	7.26		4.71 ^e
	ΔS_{soln} (298.15 K)	22.5				15.7	10.8	7.4	5.8		7.7
EtOH(2) + n-C ₇ H ₁₆ (3)	s_1 (288.15 K)	0.464				1.61 ^f	2.65 ^g	3.56 ^h	3.97		4.15
	s_1 (298.15 K)	0.693				2.04 ^f	3.13 ^g	4.11 ^h	4.57		4.69
	s_1 (308.15 K)	0.988				2.55 ^f	3.79 ^g	4.84 ^h	5.37		5.62
	ΔS_{soln} (298.15 K)	20.6				13.8 ^f	10.6 ^g	9.2 ^h	9.0		7.7
EtOH(2) + C ₆ H ₆ (3)	s_1 (288.15 K)	3.56				5.00	5.28	5.15	4.79		4.15
	s_1 (298.15 K)	4.78				6.30	6.56	6.19	5.68		4.69
	s_1 (308.15 K)	6.32				7.86	8.14	7.86	6.85		5.62
	ΔS_{soln} (298.15 K)	17.2				13.1	12.3	11.3	10.3		7.7
EtOH(2) + H ₂ O(3)	s_1 (288.15 K)	0.0018	0.0028	0.0048	0.014	0.032	0.253	0.835	2.02		4.15
	s_1 (298.15 K)	0.0023	0.0040	0.0074	0.021	0.046	0.333	1.01	2.34		4.69
	s_1 (308.15 K)	0.0030	0.0055	0.0104	0.031	0.066	0.429	1.27	2.91		5.62
	ΔS_{soln} (298.15 K)	15.7	19.9	22.7	24.3	21.7	15.6	12.4	10.9		7.7

^a cal deg⁻¹ mol⁻¹. Strictly-speaking, ΔS_{soln} could not be determined by the solubility measurement alone, unless we know the temperature and composition dependences of the activity coefficient from other independent measurements. Instead we may evaluate approximate ΔS_{soln} values from the following equations: $\Delta S_{\text{soln}} = R(\partial \ln s_1/\partial T)_{\text{sat soln}}$, $p(\partial \ln a_1/\partial \ln x_2)_{p,T}$; $(\partial \ln a_2/\partial \ln x_2)_{p,T} = 1 - 2(\delta_2 - \delta_3)V_2^2V_3^2x_2^2x_3^2/RT(V_2x_2 + V_3x_3)^3$, where δ and V are respectively the solubility parameter and molar volume of the solvents. This calculation is based on the assumption that the solubility parameter theory is still a reasonable approximation even for such associated solutions as used here in the case when we attempt to make the activity correction. The largest deviation from the ideal solubility is seen in EtOH + c-C₆H₁₂ solution with $x_{\text{EtOH}} = 0.8$. In this case, the activity correction factor is 0.902 and the estimated ΔS_{soln} value from the above equations is 5.23, which is to be compared with 5.8 in this table. This is the largest correction to be applied to the present data. ^b Reference 13b. ^c Reference 13a. ^d Reference 11a. ^e Reference 13a. ^f $x_2 = 0.237$. ^g $x_2 = 0.452$. ^h $x_2 = 0.650$. ⁱ Reference 6.

maximum point. Type (a) includes such mixed solvents as those consisting of two noncomplexing solvents or of two complexing solvents whose interactions with the solute (I_2) are of comparable strength. The binary solvent systems, *n*-hexane + cyclohexane and benzene + toluene, are typical examples. The combination of one complexing solvent with a noncomplexing solvent forms the second group, type (b). The minimum point in the ΔS_{soln} vs. x_2 relation seems to occur irrespective of whether the complexing solvent is associated or not. However, this minimum is most distinct in cyclohexane + ethanol solutions. In the case of cyclohexane + benzene solutions, only a shallow minimum is observed, but the ΔS_{soln} vs. x_2 curve has a definite negative deviation from the mole fraction average. In this connection, it is rather unexpected that the ΔS_{soln} vs. x_2 relation has no minimum in *n*-heptane + ethanol solutions. However, if we compare the ΔS_{soln} vs. ϕ_2 relation of this mixed solvent with that of cyclohexane + ethanol, we will find that the general pattern of composition dependence is common to both solvent system. Perhaps two important observations are that the stability of iodine complexes seems to be promoted by dilution with noncomplexing solvents and that the addition of a strong complexing solvent to noncomplexing solutions causes a rapid decrease in ΔS_{soln} . In the third case, type (c), where there is a distinct difference between the complexities in the interactions of iodine with solvents, the ΔS_{soln} vs. x_2 plot is s-shaped. Of the systems studied here, this behavior is observed only for the benzene + ethanol solutions. Type (d), which involves the presence of a maximum in ΔS_{soln} , is associated with aqueous solutions where the changes in "water structure" is the source of the many peculiar behaviors in physicochemical properties.

Enthalpy of Solution. The enthalpy of solution ΔH_{soln} of iodine may be obtained either from a plot of $\log s_1$ against $1/T$ or simply from the relation, $\Delta H_{\text{soln}} = T\Delta S_{\text{soln}}$.⁶ The ΔH_{soln} value is the sum of two terms

$$\Delta H_{\text{soln}} = \Delta H_{\text{fusion}} + \bar{H}_1 \quad (1)$$

where ΔH_{fusion} is the enthalpy of fusion of iodine and \bar{H}_1 is the partial molar enthalpy of iodine in saturated solution. The ΔH_{fusion} value at 298.15 K is estimated to be 3.01 kcal/mol,¹⁵ while the ΔH_{soln} values range from the largest value, 6.78 kcal/mol, for iodine in cyclohexane to the smallest value, 1.73 kcal/mol, for iodine in cyclohexane + ethanol solution with $x_2 = 0.8$. Thus iodine will mix endothermically with cyclohexane, while showing exothermic mixing with ethanol or ethanol-rich solutions.

Diffusivity vs. Stability of Iodine Complexes. Also included in Figure 2 is the $D_{11}^0 \eta_{23}/T$ vs. x_2 plot,¹⁻³ indicated by a dashed line. We see that there is generally a close parallelism between ΔS_{soln} vs. x_2 and the $D_{11}^0 \eta_{23}/T$ vs. x_2 relations. Thus the anomalous behavior in diffusivity can be explained at least partly by such thermodynamic effects (retardation of diffusional motion of I_2 due to increased complex stability). One exceptional discrepancy from this parallelism is observed in $C_6H_6 + EtOH$ solutions. No minimum was found to exist in the ΔS_{soln} vs. x_2 relation, which may be expected from the $D_{11}^0 \eta_{23}/T$ vs. x_2 plot. Perhaps the iodine complexes in these solutions will involve two solvents. In the ethanol-rich region, the I_2 -EtOH complexes may be predominant as in $c-C_6H_{12} + EtOH$ solutions. This is because partial disintegration of the hydrogen-bonded polymeric structure of ethanol by benzene molecules would result in a stabilization of the I_2 -EtOH complex. This is reflected by the rapid decrease in ΔS_{soln} with the addition of ethanol to benzene. On the other hand, the contribution of the I_2 - C_6H_6 complex in benzene-rich solutions will become comparable to that due

to the I_2 -EtOH complex. This may reduce the stability of iodine complexes and the overall effect will be an s-shaped ΔS_{soln} vs. x_2 curve.

Thermodynamic Analysis. The iodine + binary mixed solvent system may be regarded as a kind of ternary systems and the present s_1 data constitute a part of the isotherms on the iodine liquidus surface which spreads from the melting point of iodine in ternary phase diagram. General patterns of this kind of ternary phase diagram can well be described by the ternary regular solution approximation.¹⁶ Thus the activity coefficient γ_1 of iodine may be given by an equation of the type

$$RT \ln \gamma_1 = [A_{12}r^2 + A_{13} + (A_{12} + A_{13} - A_{23})r] (1 - x_1)^2 / (1 + r)^2 \quad (2)$$

where A_{ij} is the exchange energy of the i - j pair and the pseudo-binary consisting of iodine and a mixed solvent is specified by a r value where r is given by x_2/x_3 .¹⁶ It was found that maximum or minimum solubility can be expressed by eq 2 with an appropriate combination of three A_{ij} values. Along with this approach, the previous analysis of Wood et al.⁷ has used a more elaborate treatment based on Wohl's generalized excess free energy equation.

The ideal solubility of iodine at 298.15 K has been estimated to be 0.258.⁶ Thus γ_1 is always larger than unity for all the systems studied and it may be possible to apply the regular solution theory and its extended version⁶ to the present data. Hildebrand has suggested the following extension of his theory to mixed solvents: the solubility parameter δ_M of mixed solvent should be given by

$$\delta_M = (\delta_2\phi_2 + \delta_3\phi_3) / (\phi_2 + \phi_3) \quad (3)$$

where δ_i is the solubility parameter of solvent i . Recently, Walkley⁸ proposed a refined theory by taking into account preferential solvation of one solvent to iodine. With a concept of effective volume fraction ϕ^* defined by

$$\phi_2^* / \phi_3^* = (\phi_2 / \phi_3) (\delta_1 - \delta_3)^2 / (\delta_1 - \delta_2)^2 \quad (4)$$

their equation for δ_M can be written as

$$\delta_M = \frac{\phi_2 \delta_2 (\delta_1 - \delta_3)^2 + \phi_3 \delta_3 (\delta_1 - \delta_2)^2}{\phi_2 (\delta_1 - \delta_3)^2 + \phi_3 (\delta_1 - \delta_2)^2} \quad (5)$$

This equation could reproduce almost perfectly their s_1 data in $c-C_6H_{12} + C_6H_6$ solutions at 25 °C.

We will propose an alternate equation for calculating the apparent solubility parameter of mixed solvents. Walkley cited an idea presented by Christian.¹⁷ This idea suggests that the local fraction of solvents in the neighborhood of the solute should differ from the overall composition and the latter may be converted to the former by multiplying it with a Boltzmann factor with the enthalpy of complex formation ΔH_{ij} between solute and solvent as the energy term. If this is directly taken into account, the following equation may be derived:

$$\delta_M = \frac{\phi_2 \delta_2 \exp(-\alpha \Delta H_{13}/RT) + \phi_3 \delta_3 \exp(-\alpha \Delta H_{12}/RT)}{\phi_2 \exp(-\alpha \Delta H_{13}/RT) + \phi_3 \exp(-\alpha \Delta H_{12}/RT)} \quad (6)$$

where a correction factor α is taken somewhat arbitrary to be 1/3, in accordance with that in the Wilson-Renon type equations for the excess free energy.¹⁸ Figure 3 illustrates the validity of eq 6 by comparing the δ_M values calculated by eq 3, 5, and 6 with the experimental δ_M values from I_2 in $c-C_6H_{12} + C_6H_6$ solutions.¹⁹ The value for the enthalpy of complex formation of I_2 - C_6H_6 in CCl_4 , 1.32 kcal/mol,²⁰ is used as ΔH_{12} , and ΔH_{13} is assumed to be zero. Note that both eq 5 and 6 give practically the same results,

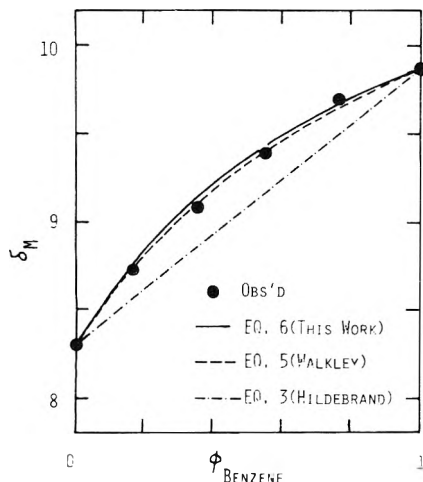


Figure 3. Experimental test of eq 3, 5, and 6 for I_2 - c - C_6H_{12} + C_6H_6 at 298.15 K.

while eq 3 completely fails. On the other hand, the above three equations gave an equally good fit to the experimental δ_M values for the case of I_2 in n - C_6H_{14} + c - C_6H_{12} solutions where there is no detectable preferential solvation. However, eq 5 and 6 still show a slightly better agreement with experimental data.

Preferential Solvation in Associated Solutions. Except for the aqueous ethanol solution, the solubility of iodine exhibits a maximum at an intermediate composition of mixed solution for all the three systems containing ethanol. This phenomena can never be explained only by preferential solvation. When mixed with ethanol (or with other associated liquids), the disintegration of the hydrogen bonding structure in ethanol should need extra positive enthalpy for the iodine molecule to form I_2 -EtOH complexes. This enthalpy will become smaller if ethanol is diluted, in advance, with nonpolar or weakly polar solvents. Under these circumstances, complex formation between iodine and ethanol will be energetically more favorable and the equilibrium of the process



will shift to the right.

We can treat as below the problem quantitatively within the framework of the regular solution theory.²¹ The following two assumptions must be made.

1. In mixed solvents containing ethanol, iodine is supposed to dissolve into a ternary solvent, the components of which are associated polymeric ethanol, free monomeric ethanol, and the other solvent.

2. The average value of the solubility parameter of ethanol, $\bar{\delta}_2$, which is determined by the ratio of two ethanol species, is composition dependent. Since no free ethanol is actually present in the pure liquid state, the δ_2 value estimated from the s_1 value in ethanol is assumed to be that for associated ethanol. Then, by substituting δ_2 with $\bar{\delta}_2$, eq 6 can be used to calculate the δ_M values in mixed solvents containing ethanol, provided that $\bar{\delta}_2$ is known once as a function of ϕ_2 .

However, let us first examine this variation of $\bar{\delta}_2$ with ϕ_2 from experimentally determined δ_M values. If we adopt as the ΔH_{12} value the enthalpy of complex formation between iodine and ethanol in CCl_4 , 2.10 kcal/mol,²² then the experimental $\bar{\delta}_2$'s are obtained for three mixed solvent systems as in Figure 4. The $\bar{\delta}_2$ value for the C_6H_6 + EtOH solution increases exponentially with the addition of benzene into ethanol, while the $\bar{\delta}_2$ vs. ϕ_2 relation for n - C_7H_{16} + EtOH and especially for c - C_6H_{12} + EtOH solutions is s-shaped. It is well established from spectroscopic

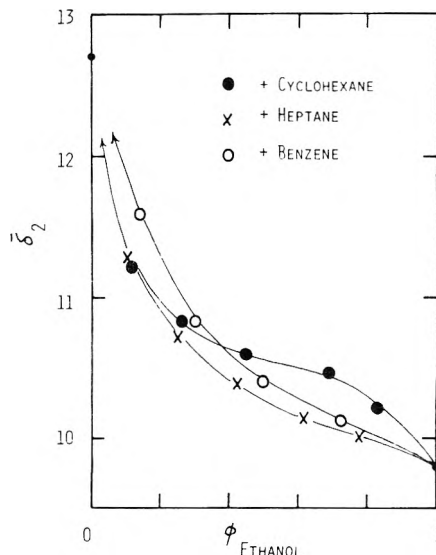


Figure 4. Average values of $\bar{\delta}_2$ for three ethanol containing solutions. The $\bar{\delta}_2$ values have been calculated by eq 6 with experimental δ_M and $\alpha = 1/3$ at 298.15 K.

and thermodynamic studies that the fraction of free monomeric alcohol decreases rapidly with an increase in the total fraction of alcohol in the alcohol + hydrocarbon solutions and that essentially no free molecules of alcohol are present in the alcohol-rich region. Therefore, the present analysis suggests that the variation of $\bar{\delta}_2$ with ϕ_2 is not completely parallel with that of the monomer fraction of alcohol. We may conclude with a little imagination that partial disintegration of the associated alcohol structure is sufficient to favor complex formation of iodine with alcohol, and that, even among saturated hydrocarbons, there should be an appreciable difference in the ability to destroy the structure of the alcohol. As far as the present data are concerned, cyclohexane seems to be the most powerful diluent to ethanol.

It is interesting to estimate the limiting value of $\bar{\delta}_2$ at $\phi_2 = 0$ from the extrapolation of the $\bar{\delta}_2$ vs. ϕ_2 relation. Since data at very low ϕ_2 are lacking, we may tentatively assume that our $\bar{\delta}_2$ vs. ϕ_2 curves converge at $\phi_2 = 0$ to a δ_2 value of 12.7.²³ Incidentally this is just the thermodynamical value for the solubility parameter of ethanol.²⁵

It is clear from the above analysis that, with the lack of accurate knowledge about the state of association of ethanol, we must abandon at present any attempt to predict accurately the s_1 values in associated mixed solvents. However, the following equation may be used to calculate $\bar{\delta}_2$:

$$\bar{\delta}_2 = [1 - \exp(-k\phi_2)]\delta_2 + \exp(-k\phi_2)\delta_2' \quad (7)$$

where δ_2' is the solubility parameter of free ethanol (= 12.7) and k is arbitrary taken as 3.0.²⁶ By combining eq 6 and 7, the δ_M and s_1 values can be reproduced reasonably well except for the ethanol-rich region.²⁸

In conclusion, the solid solubility data in mixed solvents will make an important contribution to the interpretation of various physical and chemical behaviors for which preferential solvation with or without solvent association is responsible.

Acknowledgment. The authors wish to acknowledge the assistance of Mr. K. Matsuda for some of the solubility measurements. They are also grateful to Dr. H. Touhara and Professor N. Watanabe for interest and discussions.

Supplementary Material Available: A description of the apparatus for solubility determinations and plots of

the experimental test of eq 6, Figures 1 and 5 (2 pages). Ordering information is given on any current masthead page.

References and Notes

- (1) K. Nakanishi and T. Ozasa, *J. Phys. Chem.*, **74**, 2956 (1970).
- (2) K. Nakanishi, T. Ozasa, and K. Ashtani, *J. Phys. Chem.*, **75**, 963 (1971).
- (3) K. Nakanishi and S. Kitajima, *J. Phys. Chem.*, **76**, 2470 (1972).
- (4) Throughout this paper, subscripts 1, 2, and 3 refer to iodine, one solvent, and another less polar solvent, and the superscript 0 refers to infinite dilution.
- (5) D_{11}^0 is the diffusion coefficient of iodine, η_{23} is the viscosity of the solvents, T is the absolute temperature, and x_2 is the mole fraction of the more polar solvent in mixed solvents.
- (6) J. H. Hildebrand, J. M. Prausnitz, and R. L. Scott, "Regular and Related Solutions", Van Nostrand-Reinhold, New York, N.Y., 1970.
- (7) S. E. Wood, B. D. Fine, and L. M. Isaacson, *J. Phys. Chem.*, **61**, 1605 (1957).
- (8) A. Purkayastha and J. Walkley, *Can. J. Chem.*, **50**, 834 (1972).
- (9) V. A. Mikhailov, E. F. Grigoreva, and I. I. Semina, *Zh. Strukt. Khim.*, **9**, 958 (1968).
- (10) K. Nakanishi and S. Asakura, *Chem. Lett. (Jpn.)*, **1**, 493 (1972).
- (11) (a) J. H. Hildebrand and C. A. Jenks, *J. Am. Chem. Soc.*, **42**, 2180 (1920); (b) G. R. Negishi, L. H. Donnally, and J. H. Hildebrand, *J. Am. Chem. Soc.*, **55**, 4793 (1933); (c) D. N. Glew and J. H. Hildebrand, *J. Phys. Chem.*, **60**, 616 (1956).
- (12) In several runs involving aqueous alcohol solutions, the solubility was determined as a function of time to ascertain the establishment of true solubility equilibrium. Although an apparent equilibrium had been attained within 2 h, there was a gradual increase in solubility with time overnight. This may be due to the effects of oxygen and/or carbon dioxide contaminated into the apparatus which was not completely vacuum-tight. In these cases, the solubility was evaluated by an extrapolation of s_1 vs. time (t) plot to $t = 0$.
- (13) (a) J. H. Hildebrand and J. Dymond, *Proc. Natl. Acad. Sci. N. Y.*, **54**, 1001 (1965); (b) J. H. Hildebrand, H. A. Benesi, and L. M. Mower, *J. Am. Chem. Soc.*, **72**, 1017 (1950).
- (14) The charge-transfer complexes involving iodine are well documented in the following references, though the charge-transfer interactions in such systems as those involved in the present study are not fully investigated. (a) L. J. Andrews and R. M. Keefer, "Molecular Complexes in Organic Chemistry", Holden-Day, San Francisco, Calif.,

1964; (b) R. S. Mulliken and W. B. Person, "Molecular Complexes", Wiley-Interscience, New York, N.Y., 1969.

- (15) The value for ΔH_{fusion} at 298.15 K was calculated by the following equation

$$\Delta H_{\text{fusion}} = \Delta H^{\circ}_{\text{fusion}} - (C_p^1 - C_p^s)\Delta T$$

All pertinent data are available in ref 6.

- (16) K. Nakanishi, *Ind. Eng. Chem., Fundam.*, **9**, 449 (1970).
- (17) S. Christian, *J. Am. Chem. Soc.*, **91**, 6514 (1969).
- (18) J. M. Prausnitz, "Molecular Thermodynamics of Fluid-Phase Equilibria", Prentice-Hall, Englewood Cliffs, N.J., 1969.
- (19) In this calculation, the original solubility parameter equation for the activity of the solute was used and the solubility parameter of iodine was assigned to be 14.1.⁶ In order to give the pure solvents s_1 accurately, the pure solvents δ used is not equal to their thermodynamic value.⁶ The following corrected values were used: $n\text{-C}_6\text{H}_{14}$, 8.0 (7.3); $n\text{-C}_7\text{H}_{16}$, 8.1 (7.4); $c\text{-C}_6\text{H}_{12}$, 8.3 (8.2); C_6H_6 , 9.9 (9.2); $\text{C}_6\text{H}_5\text{CH}_3$, 10.2 (8.9); EtOH , 9.8 (12.7-13.0). The number in parentheses is the thermodynamic value.⁶ See also ref 8.
- (20) R. M. Keefer and L. J. Andrews, *J. Am. Chem. Soc.*, **77**, 2164 (1955).
- (21) Since the solubility parameter theory is originally based on the dispersion interaction and geometric-mean approximation, the following treatment must be regarded as a conventional bypass to the problem of the combining rule in interactions between unlike molecules.
- (22) P. A. D. de Maine, *J. Chem. Phys.*, **26**, 1192 (1957).
- (23) This kind of extrapolation will become somewhat ambiguous because, in a very dilute region of complexing solvent, the solubility of iodine may change discontinuously.²⁴ Therefore, this value should be regarded as an apparent value which may be used only as a terminal point for δ_2 .
- (24) G. Kortüm and M. Kortüm-Seiler, *Z. Naturforsch.*, **59**, 544 (1950).
- (25) A. F. M. Barton, *Chem. Rev.*, **75**, 731 (1975).
- (26) Equation 7 has no theoretical basis, rather it is of intuitive nature. As is well known, the fraction of monomeric species of alcohols in nonpolar solutions decreases rapidly as the mole fraction of alcohol increases.²⁷ We observe that this change may be expressed by an exponential curve. Equation 7 was derived with the assumption that the change of δ_2 with ϕ_2 may be analogous to that of the monomer fraction.
- (27) A classical example of this kind of plot may be Figure 26.1 in I. Prigogine and R. Defay, "Chemical Thermodynamics", Longmans, Green and Co., London, 1954.
- (28) The results of this calculation are shown in Figure 5 (available as supplementary material).

Photophenomena in Surfactant Media. Quenching of a Water-Soluble Fluorescence Probe by Iodide Ion in Micellar Solutions of Sodium Dodecyl Sulfate

Frank H. Quina*¹ and Vicente G. Toscano

Laboratório de Fotoquímica, Instituto de Química, Universidade de São Paulo, Caixa Postal 20.780, São Paulo, Brasil (Received December 20, 1976)

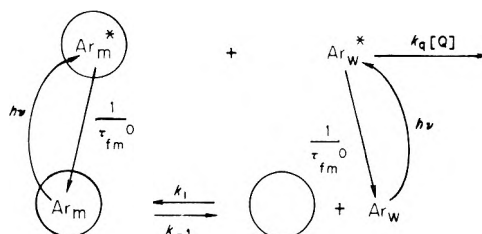
Publication costs assisted by the CNPq-NAS Program of Postgraduate Research and Teaching in Brazil

Data for the quenching of the water-soluble fluorescence probe sodium 4-(1-pyrene)butyrate (1) by the iodide ion in micellar solutions of sodium dodecyl sulfate (SDS) are analyzed in terms of a two-reactive-state (aqueous and micellar probe) model in which only one of the states (aqueous probe) is quenchable. The results are in accord with the model and permit evaluation of the equilibrium constant for partitioning of 1 between the aqueous and micellar phases.

Introduction

A number of studies indicates that ionic quenchers localized in the aqueous phase fail to quench the fluorescence of aromatics incorporated in the micellar phase when the ion and the micelle surface are like-charged. Thus, the fluorescence of anthracene incorporated in micellar sodium dodecyl sulfate (SDS) is unquenched by the iodide ion (I^-),^{2,3} the fluorescence of naphthalene incorporated in SDS is unquenched by the bromide ion,⁶ and the fluorescence of anthracene incorporated in aqueous cetyltrimethylammonium bromide (CTAB) is unquenched by pyridinium chloride.³ In this

Scheme I



paper, we examine this lack of quenching in a quantitative fashion and demonstrate that it may be used to determine

equilibrium constants for the incorporation of water-soluble fluorescence probes into the micellar phase.

The Model

If one considers an aqueous solution of an ionic micelle-forming detergent D containing a like-charged ionic quencher Q localized in the aqueous phase and a quenchable fluorescence probe Ar which partitions between the aqueous and micellar phases, one has the system depicted in Scheme I. At the instant of excitation, both excited micellar ($A_{r_m}^*$) and aqueous ($A_{r_w}^*$) probes are created. If the micellar entry and exit rates for the probe are slow relative to the photophysical events being observed, $A_{r_m}^*$ should decay independent of the external Q concentration with a rate $1/\tau_{fm}^0$. $A_{r_w}^*$ should decay according to Stern-Volmer kinetics (eq 1), where τ_{fw}^0 and

$$\phi_{fw}^0/\phi_{fw} = 1 + k_q \tau_{fw}^0 [Q] \quad (1)$$

ϕ_{fw}^0 are the fluorescence lifetime and quantum yield in the absence of Q, ϕ_{fw} the quantum yield in the presence of Q, and k_q the fluorescence quenching rate constant.

The system in Scheme I is similar to the common kinetic situation in homogeneous solution photochemistry⁷ in which two reactive states, only one of which is quenchable, give rise to the same product (in this case fluorescence). The fundamental difference is that the excited states are generally formed sequentially in homogeneous solution and are formed simultaneously in the excitation process in the micellar solution. However, by careful excitation of the micellar system at an isosbestic point for the aqueous and micellar absorptions of the probe and by determination of the fluorescence yields over the entire band of the emission spectra (when differences exist), the micellar system becomes entirely analogous to the two-reactive-state situation in homogeneous solution. Under these conditions, the total emission yield (ϕ_f^0) in the absence of Q is given by eq 2, where a and b are the fractions ($a +$

$$\phi_f^0 = a\phi_{fm}^0 + b\phi_{fw}^0 \quad (2)$$

$b = 1$) of micellar and aqueous probe, respectively, and ϕ_{fm}^0 is the apparent fluorescence quantum yield of the micellar probe. The yield (ϕ_f) in the presence of Q is given by eq 3. Combining eq 1–3 gives eq 4, which relates the overall

$$\phi_f = a\phi_{fm}^0 + b\phi_{fw} \quad (3)$$

$$\frac{\phi_f^0}{\phi_f^0 - \phi_f} = \left[\frac{a\phi_{fm}^0}{b\phi_{fw}^0} + 1 \right] \left[1 + \frac{1}{k_q \tau_{fw}^0 [Q]} \right] \quad (4)$$

quenching behavior to the concentration of Q.

Equation 4 predicts that plots of $\phi_f^0/(\phi_f^0 - \phi_f)$ vs. $[Q]^{-1}$ should be linear with intercept/slope ratios equal to the Stern-Volmer quenching constant ($k_q \tau_{fw}^0$, eq 1) determined in the absence of D. If the ratio of apparent fluorescence quantum yields of the probe in the micellar and aqueous phases (ϕ_{fm}^0/ϕ_{fw}^0) is known and reasonable values for the critical micelle concentration (cmc) and mean aggregation number (N) of D are available, the intercept can be used to calculate a/b and thus the equilibrium constant (K_{eq}) for the incorporation of the probe into the micellar phase (eq 5).

$$K_{eq} = \frac{k_1}{k_{-1}} = \frac{a}{b} \left[\frac{[D]_t - [cmc]}{N} - a[Ar]_t \right]^{-1} \quad (5)$$

Experimental Section

Materials. 4-(1-Pyrene)butyric acid (Eastman) was used as received. The excitation and emission spectra of aqueous solutions of the sodium salt were wavelength

independent, indicating the absence of extraneous fluorescent impurities. SDS (BDH specially pure grade), shown to be free from inorganic sulfate, free alcohol, and higher analogues (by GLPC of ether extracts following acid hydrolysis), was used as received. Water was doubly distilled in glass. Sodium carbonate, sodium hydroxide, sodium dihydrogen phosphate, sodium thiosulfate, and sodium chloride were analytical reagent grade materials. Sodium iodide (extra pure dry) was obtained from Merck, Darmstadt.

Apparatus. Fluorescence spectra were recorded on a Hitachi-Perkin-Elmer MPF-4 spectrophotometer in the ratio mode. Absorption spectra were recorded on a Cary 17 spectrophotometer. Absorption measurements at fixed wavelength (equilibrium constant determination) were made with a Zeiss DMR 10 spektralphotometer coupled to a Fluke Model 8200A digital voltmeter. Fluorescence lifetimes were determined with a TRW Model 31B nanosecond spectral source (D₂ lamp, Corning CS 7-54 and 7-39 excitation filters and CS 3-74 emission filter) with Model 32A decay time computer coupled to a Tektronix Type 7704A oscilloscope.

Methods. Fluorescence Quenching. A concentrated stock solution of 1 (ca. 10^{-3} M) was prepared by dissolving a weighed quantity of the corresponding acid in a slight excess of aqueous sodium carbonate, followed by quantitative dilution with 0.010 M pH 8 phosphate buffer (sodium dihydrogen phosphate adjusted with NaOH). The concentrated stock was rediluted with buffer to provide a dilute stock solution of 1 (ca. 10^{-4} M). The fluorescence stock solutions were prepared as follows: (1) appropriate aliquots of the dilute stock of 1 and of freshly prepared stock solutions of SDS in pH 8 buffer were added to a 25-mL volumetric flask; (2) taking into account the subsequent dilutions in the fluorescence measurements, the contributions to the free sodium ion concentration from the buffer and the detergent eq 6 were summed and appropriate additions of NaCl made to normalize the ultimate free Na⁺ contribution from the fluorescence stock to 0.020 M; (3) the solution was diluted to the mark with buffer. Aliquots (3.00 mL) of the fluorescence stock were added to 1-cm square quartz fluorescence cuvetts. After recording the fluorescence spectrum (327-nm excitation), 100 μ L of one of the following was added: 2.48 M NaCl (to give a final free Na⁺ of 0.10 M in 3.1 mL), 2.48 M NaI (freshly prepared and containing a trace of sodium thiosulfate to prevent I₂ formation), or appropriate mixtures of 2.48 M NaCl and NaI, and the fluorescence spectrum rerecorded. This procedure permitted internal correction for small difference in the fluorescence cells. Corrected fluorescence intensity ratios, $I_f^0/(I_f^0 - I_f)$, at a number of isoemissive points were averaged and the data plotted according to eq 4.

K_{eq} of 1 by Absorption. Aliquots (3.00 mL) of a solution of 1 (2×10^{-5} M) in 0.10 M NaCl were added to 1-cm path length quartz absorption cells. After measuring the absorbance at fixed wavelength, successive aliquots of a concentrated stock solution of SDS were added and the absorbance remeasured. After applying corrections for the blank and for dilution, the data were plotted according to the following equation:

$$\frac{1}{A_t - A_w^0} = \frac{1}{A_m^0 - A_w^0} \left[1 + \frac{N}{K_{eq}([SDS]_t - cmc)} \right]$$

where A_w^0 is the absorbance in the absence of SDS, A_t the absorbance (corrected for dilution) in the presence of SDS, and A_m^0 the limiting absorbance upon complete incorporation of 1 in the micellar phase.

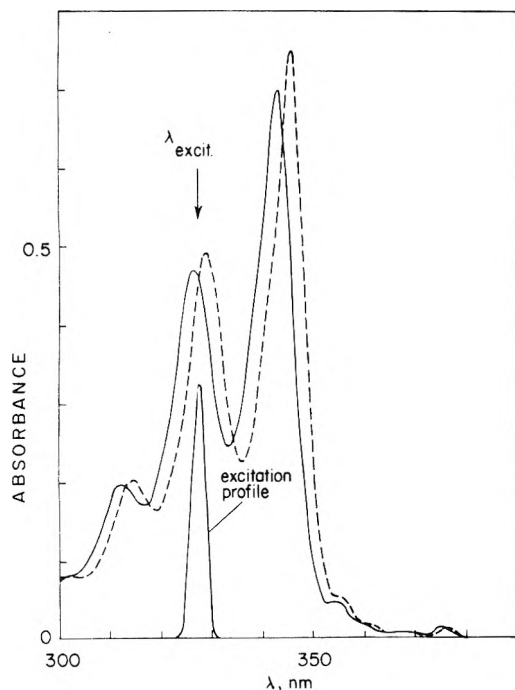


Figure 1. Absorption spectrum of **1** (2×10^{-5} M, 1 cm path) in 0.10 M aqueous NaCl (—) and in the presence of 0.090 M SDS (---, free $\text{Na}^+ = 0.10$ M).

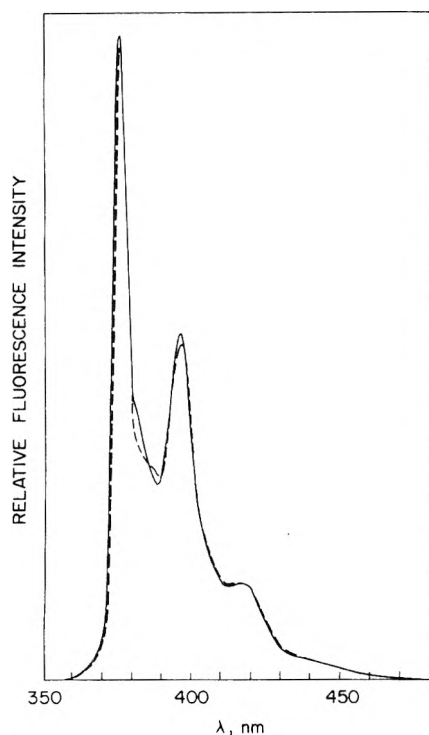
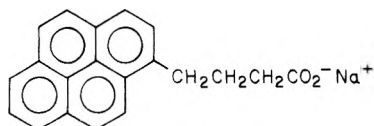


Figure 2. Emission spectrum of **1** (2×10^{-5} M, excitation at 327 nm) in 0.10 M aqueous NaCl (—) and in the presence of 0.090 M SDS (---, free $\text{Na}^+ = 0.10$ M).

Results

The anionic micelle-forming detergent SDS and the anionic quencher I^- were chosen for this study. The fluorescent probe selected was the sodium salt of 4-(1-pyrene)butyric acid (**1**). The absorption and emission



1

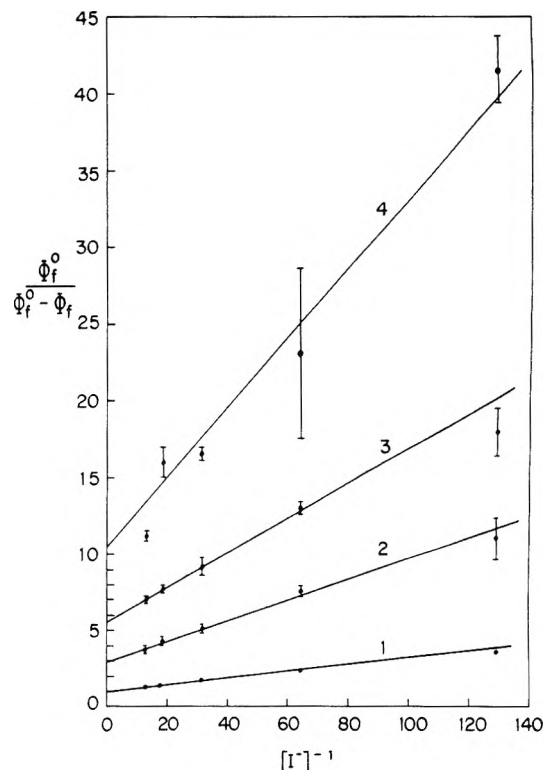


Figure 3. Plots of the data according to eq 4 for the quenching of the fluorescence of **1** (1.05×10^{-5} M) by I^- : curve 1, absence of SDS; curve 2, 0.0097 M SDS; curve 3, 0.0194 M SDS; curve 4, 0.0387 M SDS. The line drawn for 0.0387 M SDS is the calculated line for $K_{eq} = 24\,000 \text{ M}^{-1}$ and $k_q\tau_{fw}^0 = 47 \text{ M}^{-1}$.

spectra of **1** in aqueous solution and in the presence of 0.09 M SDS (>95% incorporation of **1** in the micellar phase) are presented in Figures 1 and 2.

In the initial stages of this study, it became apparent that the micellar properties and the partitioning of **1** between the aqueous and micellar phases were extremely sensitive to ionic strength. The appropriate manner in which to estimate the ionic strength of a micellar solution is not at all clear. However, it seemed reasonable to us that the micellar properties and the partitioning of **1** should be determined largely by the concentration of sodium ions free in the aqueous phase. We thus adopted the expediency of maintaining the free sodium ion concentration constant at 0.10 M for all solutions. Taking the cmc to be 1.5×10^{-3} M under these conditions⁸ and the degree of micellar ionization (α) to be about 0.2,¹¹ the free sodium ion concentration due to the detergent was calculated from eq 6. Appropriate additions of NaCl and NaI were then

$$[\text{Na}^+]_D = \text{cmc} + \alpha([\text{D}]_t - \text{cmc}) \quad (6)$$

made to give a final free sodium ion concentration of 0.10 M in all solutions.

The Stern-Volmer constant ($k_q\tau_{fw}^0$) for the quenching of **1** by I^- in the absence of SDS, determined from both fluorescence intensities and lifetimes, is 47 M^{-1} . With the fluorescence lifetime of 90 ± 5 ns in the absence of I^- , the calculated quenching rate constant (k_q) is $5.2 \times 10^8 \text{ M}^{-1} \text{ s}^{-1}$.

Data for the quenching by I^- in the presence of SDS (excitation at the 327-nm isosbestic, Figure 1) are presented in Figure 3 and Table I. The intercept/slope ratios in the presence of SDS are in reasonable agreement with the value of the Stern-Volmer quenching constant determined in the absence of SDS.

The calculation of the equilibrium constant for the incorporation of **1** requires a knowledge of the ratio

TABLE I: Data for the Quenching of the Fluorescence of 1 (1.05×10^{-5} M) by I^-

SDS, M	Intercept ^a	Intercept/slope, ^a M ⁻¹	K_{eq} , ^b M ⁻¹
0	1.00	47	
0.0097	3.0	44	23700
0.0145	4.1	35	22600
0.0194	5.6	50	24100
0.0290	8.5	40	25200
			24000 ± 1500

^a From plots of eq 4. ^b Calculated from eq 5.

ϕ_{fm}^0/ϕ_{fw}^0 for 1 and of the mean aggregation number (\bar{N}) of SDS under the conditions employed. From relative emission spectra of 1 in the absence of SDS and in the presence of 0.09 M SDS (>95% incorporation of 1 in the micellar phase) with excitation at the isosbetic points at 343, 327, and 313 nm, the ratio ϕ_{fm}^0/ϕ_{fw}^0 was determined to be 0.98 ± 0.02 . Literature values of \bar{N} for SDS in the presence of 0.10 M NaCl are 93.4,^{12,13} 95,¹⁰ and 88.^{13,14} The data of Mazer et al.¹⁵ are consistent with an \bar{N} of about 30 for 0.069 M SDS at 25 °C in the presence of 0.15 M NaCl. An aggregation number of 88 was employed in the calculation of K_{eq} . The K_{eq} value of 24000 ± 1500 M⁻¹ determined from the fluorescence data according to eq 5 (Table I) is in good agreement with the value of 24500 ± 2000 M⁻¹ determined independently from absorption spectroscopy (plots of absorption data for 346 and 278 nm provided a value of $K_{eq}/\bar{N} = 280 \pm 20$ M⁻¹).

One of the basic assumptions of the model employed here is that the micellar entry and exit rates for the probe are slow in relation to the time scale of the fluorescence event being observed. Since $K_{eq} = k_1/k_{-1}$ and k_1 can be estimated to be of the order of 2.5×10^{10} M⁻¹ s⁻¹ in the absence of charge repulsions with the micellar surface,¹⁶ an upper limit of about 10^6 s⁻¹ can be put on the exit rate (k_{-1}) of micellar 1. For micelle concentrations of the order of 2×10^{-4} M, an upper limit of about 5×10^6 s⁻¹ can be put on the rate of entry of excited aqueous 1 into the micellar phase. Since like-charge repulsions would be expected to decrease k_1 significantly,¹⁷ it is not unreasonable to expect that the micellar entry and exit rates for 1 are slow relative to the rate of decay of excited 1 (ca. 10^7 s⁻¹). In the presence of 0.02 and 0.03 M SDS, the fluorescence decay of 1 consists of two components due to emission from micellar and aqueous 1. In the presence of 0.08 M I^- , which quenches about 80% of the excited aqueous 1, the lifetime of the aqueous component was reduced to a point which allowed direct determination of the lifetime of the micellar component. At 0.08 M SDS, the aqueous component is small (>95% incorporation of 1 in the micellar phase), allowing ready determination of the decay time of micellar 1 in the presence and absence of I^- . The lifetime data (Table II) provide no evidence for partitioning of excited 1 during its lifetime or for a change in the lifetime of micellar 1 under any of these conditions.

Discussion

The data for the quenching of 1 by I^- in SDS solutions are fully in accord with the expectations of eq 4 and 5 and thus of the model upon which they were based. The use of eq 5 implicitly assumes the following: (1) the concentration of multiply occupied micelles is small relative to that of singly occupied micelles; (2) the intermicellar (free) detergent monomer concentration is constant above the cmc; (3) the mean micellar aggregation number is insensitive to the detergent concentration.

TABLE II: Fluorescence Lifetime Data for 1 (2×10^{-5} M)

SDS, M	I^- , M	τ_{fw} , ns	τ_{fm} , ns
0	0	90 ± 5	
0	0.080	18.5 ± 1	
0.020	0.080		120 ± 5
0.030	0.080		120 ± 5
0.080	0		120 ± 5
0.080	0.080		120 ± 5

Accepting a Poisson distribution²⁰ of micellar 1 among the micelles of SDS ($\bar{N} = 88$), we calculate that the error due to multiple occupation is at most 8% at the lowest concentration of SDS employed (and proportionately smaller at the higher SDS concentrations). The lack of a significant increase in the K_{eq} values at the lower SDS concentrations is consistent with minimal effects of multiple occupation. At low SDS concentrations (5.8×10^{-3} M) and higher concentrations of 1 (3×10^{-5} M and above), weak excimer emission, indicative of multiple occupation,²⁰ could be detected.

In calculating K_{eq} , we have used the cmc of SDS in 0.01 M NaCl as an approximation to the intermicellar monomer concentration at detergent concentrations above the cmc. In the absence of added salt, the free SDS monomer concentration decreases with increasing SDS concentration in a manner which is consistent with the charged phase separation model for micelle formation.^{21,22} According to this model, the intermicellar SDS monomer concentration above the cmc should be dependent on the intermicellar sodium ion activity, which is in turn related to the concentration of added salt plus the contribution due to micellar dissociation.²¹ The compensation for micellar dissociation via eq 6, which was arrived at on an empirical basis, is thus a reasonable approximation to the maintenance of a constant intermicellar sodium ion activity. The maintenance of such a constant intermicellar activity is also necessary in order to ensure that the rate constant (k_q) for the quenching of the fluorescence of 1 by I^- in the intermicellar aqueous phase be constant.^{23,24} It should be noted that, for detergents with millimolar cmcs, any micellar parameter extrapolated to the cmc will of necessity be dependent on the total concentration of added salt, contributions from the micellar phase being unimportant at the cmc.

The relative constancy of \bar{N} under our conditions may be justified simply on the basis of the weak dependence of \bar{N} on the added NaCl concentration. The data of Mysels and Princen,^{13,14} for example, indicate a change in \bar{N} for SDS (extrapolated to the cmc) from 80 to 88 to 101 as the NaCl concentration is increased from 0.05 to 0.10 to 0.20 M. The data of Mazer et al.¹⁵ for 0.069 M SDS at 25 °C indicate a change in \bar{N} from about 80 at 0.15 M NaCl to about 120 at 0.30 M NaCl. Moreover, the maintenance of relatively constant intermicellar sodium and SDS monomer ion activities should further serve to minimize changes in the mean micellar aggregation number.

The solubilization site of 1 must surely be in or near the Stern layer of the SDS micelle. A localization of the chromophore of 1 in or near the Stern layer is supported by the lifetime and absorption data. Vaughan and Weber²⁵ have shown that the fluorescence lifetime of 1 in deoxy-glycerol-water mixtures increases with decreasing water content (from ca. 125 ns in water to ca. 175 ns in glycerol). In addition there is a concomitant shift in the absorption maximum of 1 from 342 nm (pure H₂O) toward 346 nm as the water content is decreased. The fluorescence lifetime (163 ± 5 ns) and λ_{max} (344.5 nm) of micellar 1 in degassed SDS solutions correspond to an environment for 1 roughly equivalent to that of 20–40 wt % of H₂O in

glycerol. Such an environment is not at all unreasonable for incorporation of I in or near the Stern layer of SDS.¹⁹

Since quenching of the fluorescence of excited micellar I by I⁻ would have to occur in or near the Stern layer, the failure to observe such quenching implies that the equilibrium concentration of I⁻ in the vicinity of the Stern layer is sufficiently small to make quenching improbable on a time scale of the order of a few hundred nanoseconds. In addition, diffusional arrival of I⁻ at the Stern layer during the lifetime of excited micellar I must also be effectively retarded by the repulsive electrostatic field due to the net micellar surface charge.

The lack of correlation between the ratios of fluorescence lifetimes ($\tau_{fm}^0/\tau_{fw}^0 = 1.3 \pm 0.1$) and of apparent fluorescence quantum yields ($\phi_{fm}^0/\phi_{fw}^0 = 0.98 \pm 0.02$) for I in the micellar and aqueous phases is intriguing. A similar ratio of fluorescence lifetimes obtains in degassed solutions ($\tau_{fm}(\text{degassed}) = 163 \pm 5$ ns, $\tau_{fw}(\text{degassed}) = 128 \pm 5$ ns, $\tau_{fm}^0/\tau_{fw}^0 = 1.3 \pm 0.1$) and the validity of the apparent fluorescence quantum yield ratio is supported by the independent determination of K_{eq} from absorbance data. The radiative rate constant (k_f) of pyrene is known to be relatively insensitive to the solvent when corrected for refractive index differences.²⁶ The integrated absorption intensities²⁷ for aqueous and micellar I in the region of the $S_0 \rightarrow S_1$ absorption indicate at most a 10% decrease in k_f in the micellar phase in the absence of other factors. Since we have no reason to expect the intervention of a process involving purely static quenching of I in the micellar phase, we suggest that this lack of correlation might be due to an optical effect in the micellar phase and that quantum yield data for molecules incorporated in the micellar phase be treated with some reserve. Two possibilities for such an effect, both requiring that the micellar "refractive index" be higher than that of water, are readily apparent. One is a simple geometric effect similar to that encountered in the determination of fluorescence quantum yields in homogenous solution;²⁸ thus, the emitted photon is refracted at the micelle-water interface, resulting in an apparent decrease in the quantum yield of emission from micellar I. The other possibility is that, due to the small micellar radius, partial reflection of the emitted photon at the micelle-water interface affects (retards) the radiative rate constant of micellar I. Effects of this type on the emission of molecules incorporated in fatty acid monolayer assemblies have been described and analyzed by Kuhn and co-workers.²⁹

Acknowledgment. The Laboratório de Fotoquímica is supported by funds from the Brazilian Conselho Nacional de Desenvolvimento Científico e Tecnológico (CNPq) and the U.S. National Academy of Sciences (NAS). We wish to thank Professor Hernan Chaimovich for a critical

reading of the manuscript and Cecília Lopes for invaluable technical assistance.

References and Notes

- (1) CNPq-NAS Fellow.
- (2) V. A. Ponomareva and E. E. Zaev, *Zh. Prikl. Spektrosk.*, **21**, 844 (1974); *Chem. Abstr.*, **82**, 64815v (1974).
- (3) H. J. Pownall and L. C. Smith, *Biochemistry*, **13**, 2594 (1974). Although these authors refer to their solutions as being micellar in nature, at the detergent concentration employed (1.0 M) CTAB^{4,5} is well into the middle soap region of the detergent-water phase diagram and the SDS micelles are highly rodlike,⁶ even in the absence of added salt. Attempts to reproduce the quenching of anthracene fluorescence by KI in CTAB at a true micellar concentration (0.01 M CTAB) resulted in copious opalescent precipitation at KI concentrations as low as 2×10^{-3} M.
- (4) F. Reiss-Husson and V. Luzzati, *J. Phys. Chem.*, **68**, 3504 (1964).
- (5) P. Ekwall, L. Mandell, and P. Solyom, *J. Colloid Interface Sci.*, **519** (1971).
- (6) R. R. Hautala, N. E. Schore, and N. J. Turro, *J. Am. Chem. Soc.*, **95**, 5508 (1973).
- (7) M. D. Shetlar, *Mol. Photochem.*, **5**, 331 (1973), and references cited therein.
- (8) Literature values for the cmc of SDS in the presence of 0.1 M NaCl are 1.49×10^{-3} M⁹ and 1.48×10^{-3} M¹⁰.
- (9) P. Mukerjee, K. J. Mysels, and P. Kapauuan, *J. Phys. Chem.*, **71**, 4166 (1967).
- (10) M. F. Emerson and A. Holtzer, *J. Phys. Chem.*, **71**, 1898 (1967).
- (11) L. Romsted, Ph.D. Thesis, Indiana University, Bloomington, Ind., 1975.
- (12) H. F. Huisman, *Proc. Kon. Ned. Akad. Wetensch., Ser. B*, **67**, 407 (1964).
- (13) D. Stigter, *J. Colloid Interface Sci.*, **47**, 473 (1974).
- (14) K. J. Mysels and L. H. Princen, *J. Phys. Chem.*, **63**, 1696 (1959).
- (15) N. A. Mazer, G. B. Benedek, and M. C. Carey, *J. Phys. Chem.*, **80**, 1075 (1976).
- (16) This is the rate constant for entry of CH₂I₂ into micelles of SDS: P. P. Infelta, M. Grätzel, and J. K. Thomas, *J. Phys. Chem.*, **78**, 190 (1974).
- (17) Compare, for example, rates of monomer exchange for ionic surfactants.^{18,19}
- (18) E. A. G. Aniansson, S. N. Wall, M. Almgren, H. Hoffman, I. Kielman, W. Ulbricht, R. Zana, J. Lang, and C. Tondre, *J. Phys. Chem.*, **80**, 905 (1976).
- (19) J. H. Fendler and E. J. Fendler, "Catalysis in Micellar and Macromolecular Systems", Academic Press, New York, N.Y., 1975.
- (20) (a) R. C. Dorrance and T. F. Hunter, *J. Chem. Soc., Faraday Trans. 1*, **70**, 1572 (1974); (b) U. Khuanga, B. K. Selinger, and R. McDonald, *Aust. J. Chem.*, **29**, 1 (1976).
- (21) T. Sasaki, M. Hattori, J. Sasaki, and K. Nukina, *Bull. Chem. Soc. Jpn.*, **48**, 1397 (1975).
- (22) B. J. Birch and D. E. Clarke, *Anal. Chim. Acta*, **61**, 159 (1972); **67**, 387 (1973).
- (23) V. Balzani, L. Moggi, M. F. Manfrin, F. Bolletta, and G. S. Laurence, *Coord. Chem. Rev.*, **15**, 321 (1975).
- (24) J. N. Demas and J. W. Addington, *J. Am. Chem. Soc.*, **98**, 5800 (1976).
- (25) W. M. Vaughan and G. Weber, *Biochemistry*, **9**, 464 (1970).
- (26) J. B. Birks, "Photophysics of Aromatic Molecules", Wiley-Interscience, New York, N.Y., 1970, pp 309-312.
- (27) The integrated absorption intensity is related to the radiative rate constant k_f . See, for example, ref 26, pp 84-88.
- (28) J. N. Demas and G. A. Crosby, *J. Phys. Chem.*, **75**, 991 (1971).
- (29) (a) H. Kuhn, D. Möbius, and H. Bücher, "Physical Methods of Chemistry", Vol. 1, Part 3B, A. Weissburger and B. Rossiter, Ed., Wiley, New York, N.Y., 1972, p 588; (b) K. H. Tews, *Ann. Phys.*, **29**, 97 (1973); (c) K. H. Tews, *Z. Naturforsch. A*, **29**, 712 (1974); (d) K. H. Tews, *J. Lumin.*, **9**, 223 (1974).

Lipoid pH Indicators as Probes of Electrical Potential and Polarity in Micelles¹Marta S. Fernández² and Peter Fromherz*

Max-Planck-Institut für Biophysikalische Chemie, D 3400, Göttingen-Nikolausberg, West Germany (Received January 14, 1977)

Two types of fluorescent pH indicators, a hydroxycoumarin and an aminocoumarin dye, are incorporated by means of long paraffinic chain substituents to neutral, anionic, and cationic micelles. The apparent pK values for the dyes in the micelles are compared to the pK values in aqueous solution. Shifts of the apparent pK are found for charged as well as for uncharged micelles, being different for the two indicators. A comparison of the pK shifts of the indicators in neutral micelles to pK shifts in a series of mixed solvents of different dielectric constant (ϵ) leads us to attribute the shifts in the neutral system to a reduced polarity at the micelle surface for which a value of $\epsilon \approx 32$ is estimated. With respect to charged micelles this polarity effect is responsible for part of the apparent pK shift. It may be revealed by comparing the results for the two indicator types. The value of the effective dielectric constant is found to be similar to that in the neutral micelle. The remaining part of the apparent pK shift may be taken as a measure of the electrical potential at the surface of the charged micelles. Some examples of potential measurements for various counterions are presented. A thermodynamical section attempts to present clear definitions of (and relations between) terms as "apparent pK ", "interfacial pK ", "interfacial pH", and "acidity function".

1. Introduction

For a measurement of the electrical potential at the surface of a charged membrane or a similar interface one requires a probe of molecular size which does not disturb the system itself. Hartley and Roe suggested in 1940 the use of pH indicators adsorbed to charged micelles.³ They attributed the "apparent" shift of pK detectable in the micellar solutions, as compared to pure aqueous solutions, to a change of the "local interfacial" proton activity $a_{H^+}^i$ at the surface of charged micelles as compared to that in bulk water $a_{H^+}^w$. They related this pH shift to an interfacial potential Ψ by Boltzmann's law according to eq 1, where F is Faraday's constant, R is the general gas

$$a_{H^+}^i = a_{H^+}^w e^{-F\Psi/RT} \quad (1)$$

constant, and T is the temperature. However, the equilibrium of an indicator, bound to a surface, may be affected not only by an electrostatic potential, but in addition by a different local environment, e.g., by a lower dielectric constant as compared to bulk water. Accordingly, Mukerjee and Banerjee pointed out in 1964 that the apparent shift of pK includes a shift of the "intrinsic" pK , such that an electrical potential or "local pH shift" is related only to a difference of the "apparent" pK^a and this unknown intrinsic "interfacial" pK^i according to⁴

$$pK^a - pK^i = -F\Psi/2.3RT \quad (2)$$

In fact Tong and Gleesmann observed in 1957 pK shifts of several phenols and naphthols even in neutral micelles.⁵ On the other hand, Montal and Gitler compared in 1973 the effect of charged and uncharged micelles on the pK of well-known indicator dyes as umbelliferone, bromthymol blue, and methyl red and found that the pK 's were affected only by the charged micelles whereas they were not "significantly modified by the neutral ones".⁶

In order to obtain a strong fixation of a pH-sensitive chromophore to a membrane system the first lipoid pH indicator, heptadecylumbelliferone, was introduced in 1973 as applied to monomolecular films of lipids and tensides.^{7,8} The pK shifts were found to be considerably larger for charged interfaces than those reported by Montal and Gitler and, in addition, remarkable shifts in neutral monolayers were detected. In order to calculate an electrostatic potential for the charged systems the apparent

pK^a_0 in a neutral monolayer was taken as a reference according to⁹

$$pK^a - pK^a_0 = -F\Psi/2.3RT \quad (3)$$

This procedure identifies the interfacial pK^i of eq 2 with the apparent pK^a_0 and implies that the environmental effect on the intrinsic pK is similar in the charged and uncharged interface.

The present paper now intends to provide a more detailed discussion of the lipoid pH indicator method, by comparing two conjugate lipoid pH indicators, the substituted umbelliferone and an analogous aminocoumarin. At first the various pK 's which appear in the study of an interfacial acid-base equilibrium are characterized. Thereafter the titrations of the two indicators in charged and uncharged micelles are described. It is shown how the observable shifts of "apparent" pK^a may be partitioned explicitly into a component due to the electrical potential and a component caused by a change of polarity. This procedure provides a well-founded basis for the application of lipoid pH indicators as probes of the interfacial potential in membrane systems. In addition by comparing the shift of the interfacial intrinsic pK^i to the pK shift measured in nonpolar nonaqueous solvents an estimation of the effective interfacial dielectric constant can be derived, exhibiting the indicators as probes of interfacial polarity.

2. Theory

In the following discussion of acid-base equilibria two particular reaction types are considered: (I) the disso-



ciation of a molecular acid A ; and (II) the dissociation of a cation acid A^+ . In a titration experiment of a pH indicator, which is bound to a membrane (m) in its acidic and basic form, one measures the proton activity in the bulk aqueous phase (w) (e.g., by a glass electrode) and the ratio of acid and base concentration in the membrane (e.g., by optical techniques). The acid-base reaction is characterized by the "apparent" pK^a according to eq 4, i.e., by

$$pK^a = -\log(c_{B^m}^m/c_{A^m}^m)a_{H^+}^w \quad (4)$$

the bulk pH, for which the indicator in the membrane is

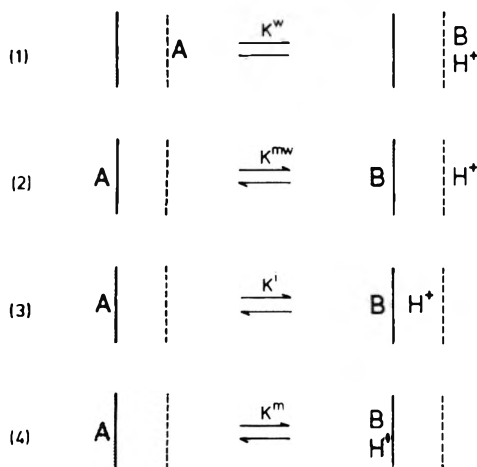


Figure 1. The different types of equilibria which may be considered in the case of an acid-base reaction $A \rightleftharpoons B + H^+$ at a membrane surface. The hatched areas represent the membrane (m), the zone between the membrane and the dotted line denotes the aqueous phase just at the membrane/water interface (i), and the area right of the dotted line is the bulk water phase (w). (1) symbolizes the dissociation within the bulk water phase as characterized by the equilibrium constant K^w (eq 5). (2) symbolizes the dissociation of membrane-bound acid into a membrane-bound base and a proton in the bulk aqueous phase as characterized by the equilibrium constant K^{mw} (eq 10) which corresponds essentially to the apparent equilibrium constant K^a . (3) symbolizes the dissociation of membrane-bound acid into membrane-bound base and a proton in the water near the interface, as characterized by the "interfacial" equilibrium constant K^i (eq 6). (4) symbolizes the dissociation within the nonaqueous medium of the membrane as characterized by the equilibrium constant K^m (eq 8).

50% dissociated. As a reference one observes the corresponding reaction in water (Figure 1-1), characterized by a pK^w as obtained from the reactant activities in water according to eq 5, where all activities are products of

$$pK^w = -\log \frac{a_B^w a_{H^+}^w}{a_A^w} = \frac{1}{2.3RT} (\mu_{H^+}^{ow} + \mu_B^{ow} - \mu_A^{ow}) \quad (5)$$

concentrations and activity coefficients with $a_i = c_i f_i$. The pK^w is proportional to the standard Gibbs' free energy ΔG^{ow} of the indicator dissociation in water with $pK^w = \Delta G^{ow}/2.3RT$. Resolving ΔG^{ow} into the single standard chemical potentials in water, μ^{ow} , one obtains the second part of eq 5.

Let us consider now the titration of an indicator which is bound to a *neutral* membrane surface. Here the bulk proton activity observed, $a_{H^+}^w$, may be assumed to be equal to the activity in water near the interface, $a_{H^+}^i$. The apparent pK^a_0 in the neutral membrane corresponds then essentially to an "interfacial" pK^i referring to the proton dissociation into the aqueous phase, the indicator remaining in the nonaqueous membrane, which may be expressed by the standard free energy of this two-phase reaction (Figure 1-3) according to

$$pK^i = -\log \frac{f_B^m c_B^m}{f_A^m c_A^m} a_{H^+}^i = \frac{1}{2.3RT} (\mu_{H^+}^{ow} + \mu_B^{om} - \mu_A^{om}) \quad (6)$$

The standard chemical potentials are referred to water for the proton but to the nonaqueous membrane medium for acid and base. The interfacial pK^i and the apparent pK^a_0 in a neutral membrane differ only by the effect of the activity coefficients of acid and base referred to the

membraneous medium, i.e., by $\log f_B^m/f_A^m$. However, this correction disappears at low indicator concentrations if the actual condition of the neutral membrane is considered as a reference standard state.

The interfacial pK^i differs from the aqueous pK^w by the free energy required to transfer *acid and base* from water to the nonaqueous medium of the membrane (Figure 1-1 and 1-3). Using the notation $\Delta pK^i = pK^i - pK^w$ one obtains

$$\Delta pK^i = \frac{1}{2.3RT} (\mu_B^{om} - \mu_B^{ow}) - \frac{1}{2.3RT} (\mu_A^{om} - \mu_A^{ow}) \quad (7)$$

A positive difference of the chemical potentials, $\mu^{om} - \mu^{ow}$, may arise in particular for the charged indicator species by a reduced dielectric constant of the membrane as compared to water. In reaction I the base B^- is charged, such that the equilibrium may be shifted to the left with a positive ΔpK^i , whereas in the case of reaction II the charged acid A^+ is affected, such that the equilibrium is shifted to the right with a negative ΔpK^i as expressed by eq 7.

Note that the pK^i referring to a two-phase reaction differs not only from the aqueous pK^w as discussed above, but also from the pK^m which characterizes the dissociation reaction *within* the nonaqueous medium (Figure 1-4) as defined by

$$pK^m = -\log \frac{a_B^m}{a_A^m} a_{H^+}^m = \frac{1}{2.3RT} (\mu_{H^+}^{om} + \mu_B^{om} - \mu_A^{om}) \quad (8)$$

The difference of pK^i and pK^m is due to the work required to transfer the proton from water to the membrane, which is the so called "primary medium effect" of the proton (cf. eq 7 and 8). The pK^m cannot be measured for a membrane system. However, this type of pK is used to characterize an acid-base reaction in *bulk* nonaqueous solvents. Thus the pK shift caused by the location of the indicator in a nonaqueous membrane, the ΔpK^i , cannot be identified with a pK shift caused by a reduction of the polarity of a bulk medium, the ΔpK^m . The two shifts are related by

$$\Delta pK^i - \Delta pK^m = -\frac{1}{2.3RT} (\mu_{H^+}^{om} - \mu_{H^+}^{ow}) \quad (9)$$

Let us consider now an indicator bound to the surface of an *electrically charged* membrane. It is assumed generally, that an "outer" electrostatic potential exists at the aqueous side of the membrane/water boundary created by the separation of the fixed membrane charges and the counterions, as described e.g., by the Gouy-Chapman theory of the diffuse double layer. In this case the dissociation of the membrane-bound acid into membrane bound base and into a proton in the bulk water phase (Figure 1-2) depends not only on the free reaction energy of dissociation across the boundary, but in addition on the electrostatic energy difference of the proton between the interface and the bulk water. Introducing the standard chemical potentials of the proton in water, and of acid and base in the charged membrane, one obtains

$$pK^{mw} = -\log \frac{f_B^m c_B^m}{f_A^m c_A^m} a_{H^+}^w = \frac{1}{2.3RT} (\mu_{H^+}^{ow} + \mu_B^{om} - \mu_A^{om}) - \frac{F}{2.3RT} \Psi \quad (10)$$

(The equation is based on the equality of the electrochemical potentials of all species throughout the whole system including the equilibrium of the dissociation reaction itself.) This pK^{mw} of the total two phase reaction and the directly observable apparent pK^a (eq 4) differ by the effect of the activity coefficients of acid and base, $\log f_B^m/f_A^m$. However, pK^{mw} and pK^a may be identified at low indicator concentrations if the actual membrane environment itself is considered as a reference standard state of the reaction. The difference of the total pK^{mw} and the reference pK^w is due to the energy required to bring acid and base from bulk water to their actual location in the membrane, which includes the electrostatic energy for the transfer of the charged indicator species, B^- and A^+ respectively, from the bulk phase to the interface. Combining eq 10 and 5 one obtains for $\Delta pK^{mw} = pK^{mw} - pK^w$ eq 11 where ΔpK^i is defined by eq 7.¹⁰ The total shift

$$\Delta pK^{mw} = \Delta pK^i - \frac{F}{2.3RT} \Psi \quad (11)$$

of pK^{mw} of a membrane-bound indicator is partitioned into a pK shift ($pK^i - pK^w$), whereby the peculiar nature of the "interphase" pK^i has to be considered, and into an electrostatic potential contribution, which may be considered as a shift of "local pH" derivable from the potential Ψ by eq 1. Note that the latter component affects all types of acid-base equilibria in the same direction, whereas the first part depends on the reaction type, especially on the charge type of the dissociation, as mentioned above.

Two remarks have to be added concerning the nature of these two components.

(a) A priori the location of an indicator in a membrane is unknown. If it is located inside of the surface dipole layer (of polar head groups and oriented water) the total electrostatic potential between bulk water and the indicator location is an "inner" potential which includes the "outer" potential mentioned and the potential difference created by the oriented dipole layer.¹⁴ If in such a case the potential in eq 11 is considered to be this inner potential, the interfacial pK^i comprises the dissociation across the membrane/water boundary at constant potential, which is apparently a virtual process. In such a case the general eq 11 has to be applied also for an indicator in a neutral membrane.

(b) Near a charged membrane the ionic concentration may be quite large due to the attraction of the counterions by the surface charges. Thus there may exist not only an energy difference for the charged species between bulk water and the interface, which is due to an electrostatic potential, but in addition a component due to ionic polarization. If the actual condition of the charged interface is taken as a reference standard state, this contribution of direct interaction of the charged indicator species with the counterions and the interfacial charges themselves is comprised in the pK^i . On the other hand, it is possible as well to describe this ionic polarization by the activity coefficients of the charged indicator species, $f_{A^+}^m$ and $f_{B^-}^m$ respectively, such that the pK^i describes the interfacial dissociation without ionic interaction, which is apparently a virtual process.

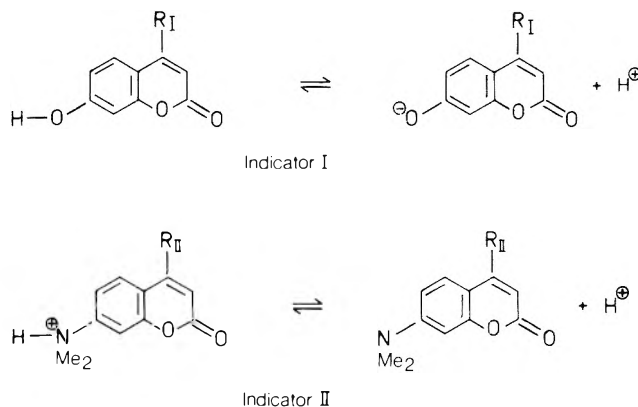
The somewhat artificial partitioning of the measurable shifts of "apparent" pK^a of an indicator in a charged membrane as compared to the pK^w in bulk water is justified, if there exists an experimental way to reveal from indicator measurements an indicator-independent term, which may be assigned to an electrostatic potential as calculated in theoretical treatments. It is the purpose of

the subsequent sections to show that such a result can be achieved by combining a pair of indicators of reaction type I and II.

An application of the preceding equations, however, requires independent measurements of the apparent pK^a of a membrane-bound indicator and of the pK^w of the indicator in bulk aqueous solution. If the indicator is distributed in equilibrium between the bulk aqueous phase and the membrane (and in intermediate regions of the diffuse double layer) at comparable concentrations, it is possible to extract the pK^a of the membrane bound molecules only by an independent determination of this distribution. This problem may be by-passed by the application of indicator chromophores in two chemical forms, one being substituted with a long paraffinic chain which binds the chromophore strongly to a membrane system by hydrophobic interaction, and one being substituted with a short chain such that the chromophore is easily water soluble.⁷ A direct evaluation of the pK^a shift of the membrane-bound lipid indicator with respect to the pK^w of the water soluble chromophore implies an identical effect of the substituent on the chemical potentials to acid and base. In that case the additional hydrophobic parts in the chemical potentials cancel in eq 7. I.e., all equations remain valid if the differences of pK and of chemical potentials are referred to the chromophores alone.

3. Experimental Section

Two types of coumarin dyes are applied as pH indicators in the present study (indicators I and II). The two similar



chromophores differ in the charge type of dissociation. The first being a molecular acid and the second a molecular base. They have similar spectroscopic properties: When excited by light of 366 nm, the basic forms emit a blue fluorescence around 450 nm, whereas the acidic forms are not affected. Since these coumarin dyes are stronger acids in the excited state the relative fluorescence intensity is a direct measure of the dissociation degree $c_B/(c_B + c_A)$ in the ground state.^{15,16}

In order to achieve a strong binding of the chromophores to micelles and to avoid any interference of a binding equilibrium onto the apparent pK 's, dyes with long paraffinic chain substitution in position 4 are applied for the determination of the micellar apparent pK^a values ($R_I = -C_{11}H_{23}$; $R_{II} = -C_{17}H_{35}$). These lipid dyes are insoluble in water but easily solubilized by micellar solutions of detergents. The aqueous pK^w of the indicators is determined using the chainless or methyl-substituted chromophores.

The two indicators are studied in micellar solutions of cetyltrimethylammonium bromide (CTAB, Merck, Darmstadt), sodium dodecyl sulfate (SDS, Schwarz & Mann, Orangeburg, N.Y.), and polyoxyethylene isoocetyl

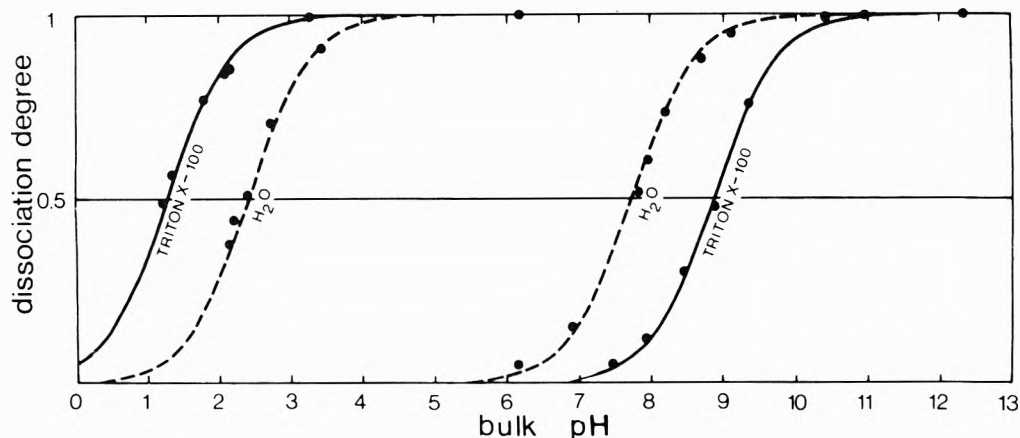


Figure 2. Dissociation degree of pH-indicator acid vs. bulk pH. The figure compares the titration of hydroxycoumarin (indicator I) and aminocoumarin (indicator II) hydrophobically bound to neutral micelles in a 5 mM solution of polyoxyethylene isooctyl phenyl ether (Triton X-100) and dissolved in water. The two curves at low pH refer to aminocoumarin; the two curves at high pH refer to hydroxycoumarin.

phenyl ether (Triton X-100, Serva, Heidelberg). The detergent concentrations, unless otherwise noted, are 24 mM for CTAB and SDS and 5 mM for Triton X-100 as in the study of Montal and Gitler⁶ on the chainless umbelliferone. Titrations of the hydroxycoumarin indicator have been performed in the presence of 1 mM Tris buffer. The ratio of the number of detergent molecules, compared to the number of solubilized dye molecules, is chosen to be large (>400:1) such that there is less than one indicator molecule available per micelle, considering the aggregation numbers of these micelles.¹⁷ The pH is determined by a glass electrode (Ingold, Frankfurt) relative to NBS standard solutions (Schott, Mainz).

Titrations of the indicators in nonaqueous solvents are carried out using a series of dioxane-water mixtures containing 0, 20, 45, 70, and 82 wt % dioxane, corresponding to dielectric constants of 78.36, 60.79, 38.48, 17.69, and 9.53.¹⁸ The method of Van Uitert and Haas¹⁹ is employed to obtain proton concentrations from the readings of the glass electrode. The procedure involves the previous calibration of the glass electrode in the different mixtures to obtain a correction factor. This calibration allows elimination of the combined and undistinguishable contributions of primary medium effect and liquid junction potential from the pH readings. The ionic activity coefficients for solutes, referred to the respective solvent mixture at infinite dilution, are approximated by using the tabulated mean activity coefficients of hydrochloric acid.²⁰

4. Results and Discussion

(a) *The Polarity Shift of pK in Neutral Micelles.* Figure 2 compares the titrations of the hydroxycoumarin and the aminocoumarin in Triton X-100 and in water. The "apparent" pK^a in the neutral micelle differs from the pK^w for both indicators, the ΔpK^a_0 being of similar value but opposite sign (cf. Table I). These features correspond to the arguments presented in section 2, that in a neutral membrane ΔpK^a is determined essentially by the energy difference of the charged indicator species between the aqueous and the nonpolar medium (eq 7). The positive $\Delta pK^a_0 = \Delta pK^i$ of hydroxycoumarin (indicator I) may be assigned to the destabilization of the charged phenolate base, whereas the negative ΔpK^a_0 of aminocoumarin (indicator II) may reflect the destabilization of the charged ammonium acid in the low polarity medium of the micelle.

In order to test this interpretation and to estimate the value of the dielectric constant at the location of the micelle-bound chromophore, the indicators are titrated in a series of media of known dielectric constant. The values

TABLE I: pK Values of the Hydroxycoumarin Indicator I and of the Aminocoumarin Indicator II in Micellar Solutions of Cetyltrimethylammonium Bromide (CTAB, 24 mM), Polyoxyethylene Isooctyl Phenyl Ether (Triton X-100, 5 mM), and Sodium Dodecyl Sulfate (SDS, 24 mM)^a

	Indicator I			Indicator II		
	CTAB	Triton X-100	SDS	CTAB	Triton X-100	SDS
pK^a	6.35	8.85	11.15	1.25	3.55	
$pK^a - pK^w$	-1.4	+1.1	+3.4	-1.1	+1.2	
$pK^a - pK^a_0$	-2.5		+2.3		+2.3	
		CTAB	Triton X-100	SDS		
$1/2 [\Delta pK^a_I - \Delta pK^a_{II}]$			+1.1	+1.1		
$1/2 [\Delta pK^a_I + \Delta pK^a_{II}]$			0.0	+2.3		

^a The pK^a shifts in the second row are referred to the aqueous pK^w , which is for indicator I $pK^w_I = 7.75$ and for indicator II $pK^w_{II} = 2.35$. The pK^a shifts in the third row are referred to the pK^a in Triton X-100, pK^a_0 . The values in this row, as well as the differences of the $\Delta pK^a = pK^a - pK^w$ referring to both indicators in the fourth and fifth row, are used for the calculation of electrical potential and polarity (cf. eq 13, 14, and 15).

of $\Delta pK^m = pK^m - pK^w$ (cf. eq 8) for a series of water/dioxane mixture are plotted in Figure 3 (dotted lines) vs. the dielectric constant of those media. Lowering the dielectric constant leads to a large increase of pK^m for dye I, yet only a slight change of pK^m for dye II, as is to be expected from the ionic character of the dissociation reactions: By the dissociation of dye I two ions are created which is an unfavorable process in a medium of low dielectric constant, whereas in the dissociation of dye II the number of ions remains constant.

In order to make a correct comparison of these bulk media titrations with the micellar titrations, the ΔpK^m values have to be transformed into ΔpK^i values referring to the two-phase reaction, as it is observed in the case of the micelles, according to eq 9. The primary medium effect of the proton may be expressed for each water/dioxane mixture as a "degenerate activity coefficient" of the proton $f^{\circ}_{H^+}$ ²¹ and approximated by the mean degenerate activity coefficient of HCl, f°_{HCl} , for dioxane/water mixtures,²⁰ according to

$$\begin{aligned} \mu^{\circ m}_{H^+} - \mu^{\circ w}_{H^+} &= 2.3RT \log f^{\circ}_{H^+} \\ &\approx 2.3RT \log f^{\circ}_{HCl} \end{aligned} \quad (12)$$

The shifts ΔpK^i for water/dioxane mixtures obtained in

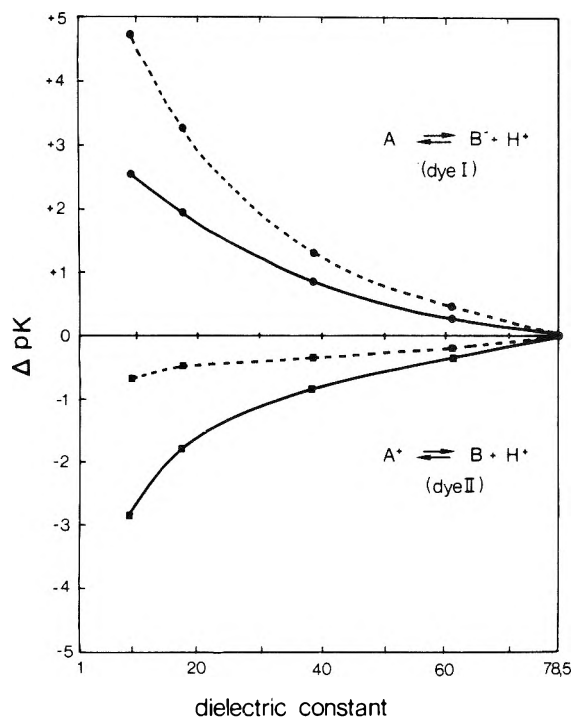


Figure 3. pK shifts of pH indicators in dioxane-water mixtures referred to pure aqueous solutions vs. the dielectric constant of the solvent. The dashed curves represent the shift of pK^m (cf. eq 8) whereas the full curves are the shifts of the "interphase" pK^i (cf. eq 6). The upper two curves refer to hydroxycoumarin (indicator I); the lower two curves refer to aminocoumarin (indicator II). The two types of ΔpK , $pK^m - pK^w$, and $pK^i - pK^w$, differ by the primary medium effect of the proton (eq 9).

this way are plotted in Figure 3 (full lines). It is apparent that a lowering of the dielectric constant leads to pK^i shifts of similar magnitude and opposite sign for the two indicators. This symmetric response is still present even at dioxane concentrations as high as 70% ($\epsilon = 17.69$). Only the points corresponding to 82% dioxane ($\epsilon = 10.49$) are slightly deviating from the symmetric behavior. This is not surprising since large errors can be expected in the pH evaluation at such high dioxane concentrations.

If now the ΔpK^a_0 values of the two indicators in Triton X-100 are compared with the ΔpK^i values of the low polarity media one interpolates from Figure 3 an effective micellar dielectric constant of $\epsilon \approx 32 \pm 1$, independently for both indicator titrations. This value is similar to a rough estimate given for neutral monolayers of, e.g., methyl palmitate.⁷

The main conclusions which may be drawn from the results of this section are the following: (1) The shift of the apparent pK^a in a neutral micelle may be attributed consistently to a change of polarity at the micellar location of the chromophores as compared to bulk water. A contribution of the electrical potential may be excluded, since according to eq 11, such a potential would destroy the symmetric dielectric shift. (2) The effective dielectric constant differs from that of bulk water, but differs also from that expected for the paraffinic core of a micelle ($\epsilon \approx 2-3$). This intermediate dielectric constant indicates that the indicator chromophores are located just in the surface of the micelle. Both conclusions are consistent: If the chromophores are located just in the micelle/water interface in the region of the polar head groups of the tenside and of interfacial water, they are sensitive only to the outer potential, which may be assumed to be zero for a neutral micelle, but not to a potential created by oriented dipoles of the interface. This interfacial location corresponds to the picture proposed for the position of the lipid-pH indicators in lipid monolayers.⁷

(b) *Polarity Shift and Potential Shift of pK in Charged Micelles.* Figure 4 compares the titrations of two indicators in the negatively charged micelles of sodium dodecyl sulfate and in aqueous solution. In both cases the pK^a in the micelles is higher than the pK^w in water, the ΔpK^a of hydroxycoumarin being nearly three times the ΔpK^a of aminocoumarin (Table I). According to eq 11 the shift of apparent pK^a is composed of a pK^i shift and a potential effect. Since a negative outer potential at the micelle surface leads to a positive ΔpK^a for both indicator types, whereas the ΔpK^i may be expected to be of different sign similar to the neutral micelle, the experimental pK^a shifts may be explained qualitatively by the superposition of these two components: For indicator I both effects point into the same direction, leading to large positive ΔpK^a_i , whereas for indicator II a negative ΔpK^i compensates in part the potential shift, leading to a small overall ΔpK^a_{II} .

Two procedures may be used to separate quantitatively the ΔpK^i effect and the outer potential contribution.

(a) The ΔpK^i in the charged system is assumed to be identical with that in the neutral system for each indicator. Substituting then the ΔpK^i in eq 11 by the ΔpK^a_0 one obtains the electrical potential by⁹

$$-F\psi/2.3RT = \Delta pK^a - \Delta pK^a_0 \quad (13)$$

This procedure implies that the effect of the dielectric polarization in the neutral micelle equals the effect of dielectric plus ionic polarization in the charged micelle as

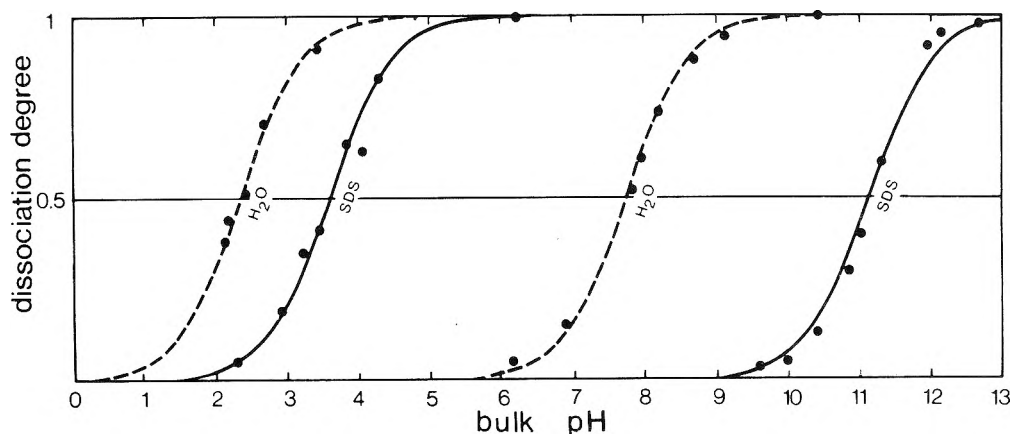


Figure 4. Dissociation degree of pH indicator acid vs. bulk pH. The figure compares the titration of the indicator pair hydroxycoumarin (indicator I) and aminocoumarin (indicator II) hydrophobically bound to negatively charged micelles in 24 mM solution of sodium dodecyl sulfate (SDS) and dissolved in water. The two curves at low pH refer to aminocoumarin; the two curves at high pH refer to hydroxycoumarin.

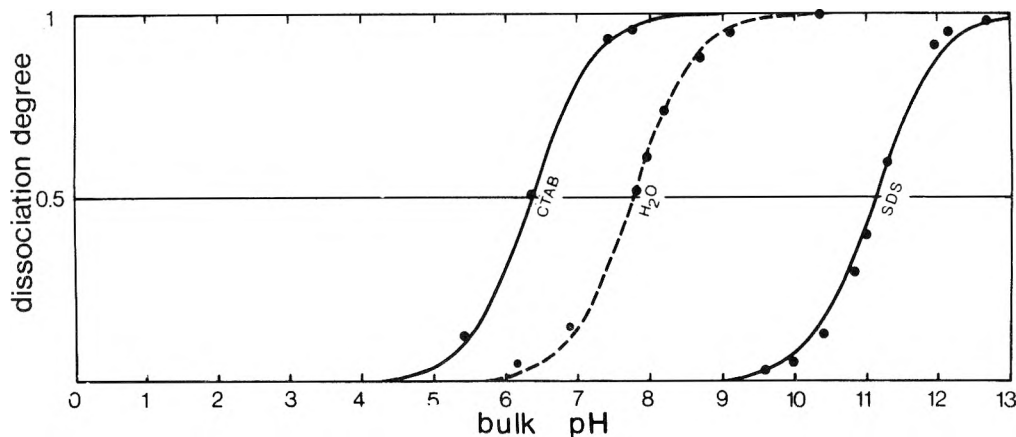


Figure 5. Dissociation degree of pH indicator acid vs. bulk pH. The figure compares the titration of hydroxycoumarin chromophore (*indicator I*) hydrophobically bound to *positively and negatively charged micelles* in 24 mM solutions of cetyltrimethylammonium bromide (CTAB) and of sodium dodecyl sulfate (SDS), respectively, and dissolved in water.

included in the relevant standard chemical potentials (eq 7).

(b) The ΔpK^i is assumed to be of identical magnitude but of opposite sign for the two indicators in the charged micelle. Addition of the ΔpK^a_{I1} and ΔpK^a_{II} removes the ΔpK^i component and reveals the electrical potential according to eq 14. Correspondingly, by subtraction of the

$$-F\psi/2.3RT = 1/2[\Delta pK^a_{I1} + \Delta pK^a_{II}] \quad (14)$$

$$|\Delta pK^i| = 1/2[\Delta pK^a_{I1} - \Delta pK^a_{II}] \quad (15)$$

two ΔpK^a the absolute value of ΔpK^i is obtained (eq 15).²² With respect to the dielectric component the assumption of equal magnitude of pK^i_{I1} and pK^i_{II} is supported over a wide range of polarity by the symmetry of the pK^i shifts found in the nonaqueous solvents. In addition to that, procedure (b) implies an identical ionic polarization for the charged species of the two indicators, B_{I1}^- and A_{II}^+ , respectively. It should be considered that such an assumption is not justified a priori since the relation of a cation and anion to the anisotropic ionic environment at a micellar surface may be different.

Inserting now the experimental pK^a values of the two indicators in SDS (Table I) into eq 14 and on the other hand the pK^a values of both indicators in SDS and in Triton X-100 (Table I) into eq 13 one obtains in all cases an electrical potential of $\Psi = -134$ mV. According to this agreement one calculates from eq 15 for the magnitude of the shift of intrinsic pK^i in SDS a value of $|\Delta pK^i| = 1.1$, which agrees with the shift found in Triton X-100 for both indicators independently (Table I). The coincidence of the two procedures indicates the practical consistency of the assumptions involved.

A similar treatment may be applied in principle also to a positively charged interface. However, in the present case the apparent pK^a of indicator II is shifted to an immeasurable low value. Thus, Figure 5 compares only the titration of hydroxycoumarin in positive micelles made from cetyltrimethylammonium bromide (CTAB) and in negative micelles made from SDS. It is apparent that the ΔpK^a in CTAB is of opposite sign to that in SDS but of less than half in its magnitude. This result corresponds to the interpretation that a positive ΔpK^i of indicator I increases in SDS the shift due to the negative potential, but partially compensates in CTAB the shift due to the positive potential (eq 11). The combination of indicator I/positive interface behaves analogous to the combination of indicator II/negative interface (cf. Figures 4 and 5).²⁴

A quantitative evaluation is possible only according to procedure (a), by assuming for indicator I in CTAB the

same ΔpK^i as in SDS and in Triton X-100. One obtains for the electrical potential using eq 13 and Table I $\Psi = +148$ mV. Thus the positive potential in CTAB is similar in magnitude to the negative potential in SDS, which is consistent to the similar size and aggregation number of these micelles.¹⁷ An attribution of an effective dielectric constant of $\epsilon = 32$ also to the CTAB micelle surface as for SDS and Triton X-100 corresponds to a value of $\epsilon = 36$ estimated by Mukerjee and Ray for dodecylpyridinium micelles.²⁵

The electrical potentials found in this way for SDS micelles (-134 mV) and CTAB ($+148$ mV) are similar to the potentials detected by the lipid-pH indicator in charged monolayers of comparable charge density,⁹ but considerably larger in magnitude than the values detectable by chainless umbelliferone. From the pK^i shifts reported for this indicator by Montal and Gitler⁶ it is possible to calculate potentials of -27 mV for SDS and $+56$ mV for CTAB micelles, respectively. This discrepancy may result from the complete binding of the lipid indicator to micelles compared to the distribution equilibrium of the chainless analogous between micellar and aqueous phase and from the closer binding of the chromophore to the micelle surface by hydrophobic interaction of the long paraffinic side chain and the core of the micelle in the case of the lipid indicators. This explanation is consistent with the remarkable shift of pK^i , indicating a closer approach of the chromophores to the interfacial region of low polarity. This comparison emphasizes the important role played by hydrophobic interactions in the location of amphiphatic compounds in the lipid-water interface.^{26,27}

The main conclusions which may be drawn from the results of this section are as follows. (a) The effective polarity at the location of the hydrophobically bound chromophores in the negatively charged micelle of SDS is similar to that in the neutral micelle of Triton X-100. It corresponds to a bulk dielectric constant of $\epsilon \approx 32$. Whether some ionic polarization component is included here cannot be decided. (b) The value of the effective dielectric constant indicates a similar location of the chromophore in SDS as in Triton X-100, i.e., at the interface between the polar head groups. This location implies that the electrical potential, as obtained after subtracting the shift of intrinsic pK^i , reflects the outer potential at the charged surface of the micelles. (c) The perfect agreement of the mean $|\Delta pK^i|$ for both indicators in SDS with the single ΔpK^i shifts in Triton X-100 supports strongly the assumption that the neutral interface may be taken as a reference state for any similar charged

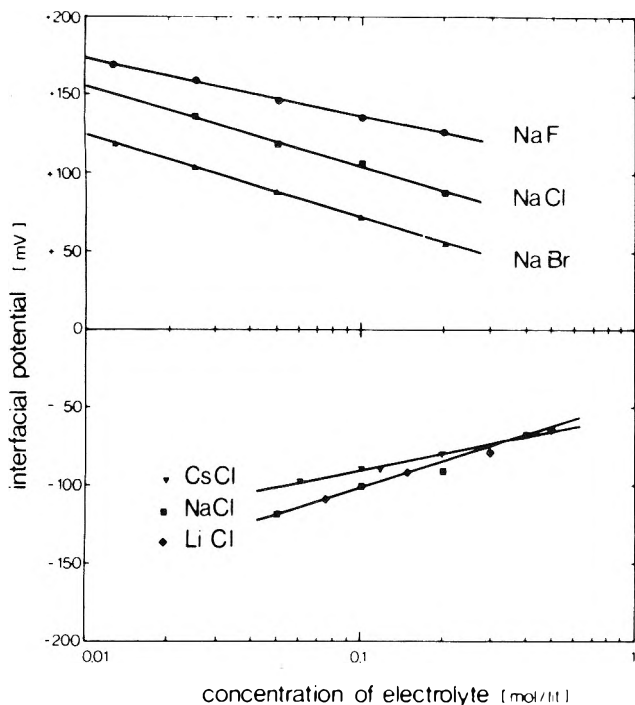


Figure 6. Electrical potential at micelle surface vs. concentration of foreign electrolyte. The upper three curves refer to 2 mM solutions of cetyltrimethylammonium bromide (CTAB), where the potentials are detected by indicator I, using eq 13. The lower three curves refer to 10 mM solutions of sodium dodecyl sulfate (SDS), where the potentials are detected similarly by indicator II.

interface. I.e., the unknown interfacial pK^i in charged systems may be substituted by the apparent pK^a_0 in a neutral system leading to the postulate that the difference $pK^a - pK^a_0$ of a lipid pH indicator reveals the outer electrical potential at the micelles surface.

(c) *Measurements of Interfacial Potentials.* As an example of the use of the lipid pH indicators as potential probes Figure 6 presents the outer potential at the surface of micelles made from CTAB (2 mM) and SDS (10 mM) as a function of salt concentration for several uni-univalent electrolytes, as calculated from eq 13. Dye I and dye II have been used in CTAB and SDS micelles, respectively. Salt concentrations much higher than the detergent critical micellar concentration have been used. In this way the concentration of salt added can be considered to be equal to the total electrolyte concentration.

Only a few short comments shall be made in the present paper concerning these measurements. In the case of CTAB a distinct effect of the different counterions added is observed (F^- , Cl^- , Br^-). The induced reduction of the potential follows the lyotropic series.²⁸ Addition of I^- and SCN^- promotes precipitation of the system. The slopes $d\psi/d \log c$ for NaCl and NaBr (51 mV) are slightly smaller than the theoretical value for a plane electrical double layer (59 mV), while in the case of NaF a value of 36 mV is obtained. Deviations from linearity at low salt concentrations (not represented) are to be expected since all curves must pass through the point corresponding to the pure detergent (without salt added).

For SDS micelles a similar effect of Na^+ and Li^+ on the potentials is found. The slope (55 mV) is similar to the theoretical value for a plane interface. Deviations from linearity are to be expected (as in the case of CTAB) at low salt concentrations, since the curves must pass through the point corresponding to no salt added. K^+ and Rb^+

induce precipitation of the system. Cs^+ leads to a slope of only 32 mV in the range of concentrations studied. At high CsCl concentrations the micellar solution shows a very high viscosity, which may be attributed to the formation of larger aggregates.²⁷ The magnitude of the experimental potentials is lower than the theoretical values obtained from the Gouy-Chapman theory of the diffuse double-layer but larger than the Booth ζ potentials derived from electrophoresis.²⁹ The reduction of the potential as induced by the different cations may be considered to follow Eisenman's serie IV of ionic interaction,³⁰ if one assumes that the instability of micelles in the case of K^+ and Rb^+ is due to efficient reduction of the potential.

References and Notes

- (1) Fourth of a series on lipid pH indicators, for the first three articles, see ref 7-9.
- (2) Research fellow of the Alexander von Humboldt Stiftung. Present address: Department of Bioquímica, Centro de Investigación del I.P.N., P.O. Box 14-740, México 14 D.F.
- (3) G. S. Hartley and J. W. Roe, *Trans. Faraday Soc.*, **36**, 101-109 (1940).
- (4) P. Mukerjee and K. Banerjee, *J. Phys. Chem.*, **68**, 3567-3574 (1964).
- (5) L. K. J. Tong and M. C. Gleesmann, *J. Am. Chem. Soc.*, **79**, 4305-4310 (1957).
- (6) M. Montal and C. Gitler, *Bioenergetics*, **4**, 363-382 (1973).
- (7) P. Fromherz, *Biochem. Biophys. Acta*, **323**, 326-334 (1973).
- (8) P. Fromherz, *Chem. Phys. Lett.*, **26**, 221-224 (1974).
- (9) P. Fromherz and B. Masters, *Biochim. Biophys. Acta*, **356**, 270-275 (1974).
- (10) The shift $pK^{mw} - pK^w$ corresponds to the shift of Hammett's acidity function¹¹ with respect to two media in equilibrium, as studied, e.g., by Bunton and Robinson in 1969 for micellar solutions.^{12,13} Considering the definitions $H^m = pK^w + \log c_B^m/c_A^m$ and $H^w = pK^w + \log c_B^w/c_A^w$ one derives from eq 4 and 5 that $H^m - H^w$ differs from $pK^{mw} - pK^w$ only by activity coefficient corrections of acid and base.
- (11) L. P. Hammett, *Chem. Rev.*, **13**, 61-71 (1935).
- (12) C. A. Bunton and L. Robinson, *J. Phys. Chem.*, **73**, 4237-4241 (1969).
- (13) K. H. Fendler and E. J. Fendler, "Catalysis in Micellar and Macromolecular Systems", Academic Press, New York, N.Y., 1975, p 204 ff.
- (14) E. Lange and H. Göhr, "Thermodynamische Elektrochemie", Hüthig Verlag, Heidelberg, 1962, p 31.
- (15) R. F. Chen, *Anal. Lett.*, **1**, 423-428 (1968).
- (16) K. H. Drexhage in "Dye Lasers", F. P. Schäfer, Ed., Springer-Verlag, Heidelberg, 1973, pp 144-270.
- (17) K. Shinoda, T. Nakagawa, B. Tamamushi, and T. Isemura, "Colloidal Surfactants", Academic Press, New York, N.Y., 1963, pp 20 ff, 117 ff.
- (18) E. J. King, "Acid-Base Equilibria", Pergamon Press, Oxford, 1965, p 252.
- (19) L. G. Van Uitert and C. G. Haas, *J. Am. Chem. Soc.*, **75**, 541-455 (1953).
- (20) H. S. Harned and B. B. Owen, "The Physical Chemistry of Electrolytic Solutions", Reinhold, New York, N.Y., 1943.
- (21) B. Gutbezahl and E. Grunwald, *J. Am. Chem. Soc.*, **75**, 565-574 (1953).
- (22) This addition-subtraction procedure used to reveal the environmental and the electrical potential component in the apparent pK shift corresponds to a similar idea of Bates and Schwarzenbach (1955) concerning the elimination of the primary medium effect from acidity function measurements in nonaqueous solvents in order to reveal the true medium pH.²³
- (23) R. G. Bates and G. Schwarzenbach, *Helv. Chim. Acta*, **38**, 699-716 (1955).
- (24) An asymmetry of ΔpK^a in positive and negative micelles opposite to that seen in Figure 6 is expected for an indicator of type II. Such a feature may be reflected by the acidity function shifts reported by Bunton and Robinson for *N*-methyl-*p*-nitroaniline in CTAB ($H^m - H^w = -1.0$) and SDS ($H^m - H^w = +0.35$).¹²
- (25) P. Mukerjee and A. Ray, *J. Phys. Chem.*, **70**, 2144-2149 (1966).
- (26) M. S. Fernández and J. Cerbón, *Biochim. Biophys. Acta*, **298**, 8-14 (1973).
- (27) M. S. Fernández and J. Cerbón, *Arch. Biochem. Biophys.*, **172**, 721-725 (1976).
- (28) J. T. G. Overbeek in "Colloid Science", Vol. 1, H. R. Kruyt, Ed., Elsevier, Amsterdam, 1952, p 302 ff.
- (29) D. Stigter, R. J. Williams, and K. J. Mysels, *J. Phys. Chem.*, **59**, 330-335 (1955).
- (30) G. Eisenmann in "Membrane Transport and Metabolism", A. Kleinzeller and A. Kotyk, Ed., Academic Press, New York, N.Y., 1961, pp 163-179.

Hydrogenation of Ethylene over LaNi₅ Alloy

K. Soga,* H. Imamura, and S. Ikeda

Research Laboratory of Resources Utilization, Tokyo Institute of Technology, Ookayama, Meguro-ku, Tokyo, Japan (Received November 19, 1976; Revised Manuscript Received May 5, 1977)

Publication costs assisted by the Tokyo Institute of Technology

The hydrogenation of ethylene was kinetically investigated over the LaNi₅H_n catalyst with $n = 0.62, 0.92, 1.5, 2.1,$ and 2.4 as well as over the LaNi₅ catalyst over a temperature range from -60 to -84 °C. It was found that the rate of hydrogenation over the LaNi₅H_n catalyst was far greater than the rate over the LaNi₅ catalyst, and that the hydrogenation over the LaNi₅H_n catalyst took place by using the absorbed hydrogen atoms, not by using gaseous hydrogen. The data obtained led to the conclusion that the rate-determining step of hydrogenation over the LaNi₅H_n catalyst is the migration process of absorbed hydrogen atoms from the bulk of the catalyst to the surface.

Introduction

Some activated intermetallic compounds of transition metals, such as, LaNi₅, PrCo₅, LaCo₅, CeCo₅, etc., absorb appreciable amounts of hydrogen in an atomic form at high pressure and desorb it rapidly at reduced pressure. Taking a convenient equilibrium pressure, these compounds could be used for the storage of hydrogen. From this point of view, a considerable amount of work has been done on the equilibrium properties between hydrogen and these compounds.¹ According to the literature¹ LaNi₅ seems to be the most promising among these compounds for the storage of hydrogen. The physical properties of the LaNi₅-H₂ system were extensively measured by Neuman,² van Vucht et al.,³ and van Mal.⁴

Scarcely any studies have been concerned, however, with the chemical nature of the absorbed hydrogen atom (hydride).

Recently Coon et al. have reported⁵ that these intermetallic compounds catalyze the reaction of carbon monoxide and hydrogen to form methane at high temperature ($250\sim 300$ °C). On the other hand, we have also found that the hydrogenation of ethylene proceeds at high velocity at -78 °C over the LaNi₅ alloy containing a considerable amount of the hydride. Some of the results have already been reported briefly.⁶

This paper reports the detailed results on the hydrogenation of ethylene over LaNi₅ alloy, including a plausible mechanism for the hydrogenation.

Experimental Section

Preparation of LaNi₅H_n. A binary alloy of LaNi₅ was obtained from Moly Corp. The alloy was adequately washed with purified acetone and then it was treated at 450 °C for several hours under vacuum (ca. 4×10^{-5} mmHg). The alloy was exposed to a hydrogen pressure of 100 atm at 450 °C, cooled step-by-step to room temperature, evacuated, and then gradually heated to 450 °C under vacuum. This treatment was repeated until it absorbed hydrogen quite fast. The LaNi₅H_n thus obtained was preserved at room temperature under an atmospheric pressure of hydrogen. The surface area of the LaNi₅ (without hydrogen) thus prepared was 0.87 m²/g measured by the BET method with nitrogen adsorption.

Apparatus and Procedure for the Hydrogenation of Ethylene. The hydrogenation of ethylene was conducted in a conventional gas circulation system having a reaction space of about 440 cm³ effective volume including the reactor. The reactor was a quartz tube about 17 cm long and 2.0 cm in diameter. It was confirmed that the speed

of the circulation pump used in the present system was sufficiently fast.

The research grade ethylene used in this work was obtained from Takachiho Chemical Corp. An ultrahigh purity grade of hydrogen was passed through a spiral type trap immersed in liquid nitrogen. Hydrogen deuteride was the only impurity (0.5%) detected by a mass spectrometer in deuterium obtained from Takachiho Chemical Corp.

About 0.40 g of the LaNi₅H_n prepared according to the procedures described above was supported on glass wool in the reaction tube, and every time immediately before the measurement of the reaction rate it was again treated as follows: The LaNi₅H_n was heated at 400 °C under vacuum (ca. 4×10^{-5} mmHg) for 3 h, exposed to a pressure of hydrogen from 8 to 40 cmHg at 400 °C for 1 h, cooled quickly to -78 °C, kept for 2 h at -78 °C, and then it was quickly adjusted to the reaction temperature. The amount of hydrogen absorbed was estimated from the pressure drop of the gaseous hydrogen. The LaNi₅D_n was also prepared according to the same procedures.

After the temperature of the catalyst (LaNi₅H_n or LaNi₅D_n), which was monitored by a thermometer inserted at the center of the catalyst bed, reached the reaction temperature, the reaction tube was quickly evacuated to remove the gas phase hydrogen and then the reactant (ethylene or the mixture of ethylene and hydrogen) was admitted by opening the cock located on the top of the reaction tube.

The product was collected from the circulation system into a gas sampler and transferred to the gas chromatograph. The isotopes of hydrogen were analyzed by a Hitachi, Model RMU-7M, mass spectrometer.

Results and Discussion

The hydrogenation of ethylene was first conducted at -78 °C over 0.40 g of the LaNi₅H_{2.4} catalyst (containing 2.23 atom of H) by admitting only ethylene (8.5 cmHg, 1.35 mmol). Almost no change of pressure was observed, but analysis of samples by gas chromatography showed ethane was being formed at a very high speed (see Table II). It was also confirmed that samples contained only a trace of hydrogen. Therefore, it may be said that all the hydride that come out from the alloy react with ethylene to form ethane.

The hydrogenation of ethylene was next conducted at -78 °C over 0.40 g of the same catalyst using the same pressure of hydrogen (37.0 cmHg, 5.87 mmol) and various pressures of ethylene (4.8 cmHg, 0.76 mmol; 8.5 cmHg, 1.35 mmol; and 14.5 cmHg, 2.30 mmol). The results obtained

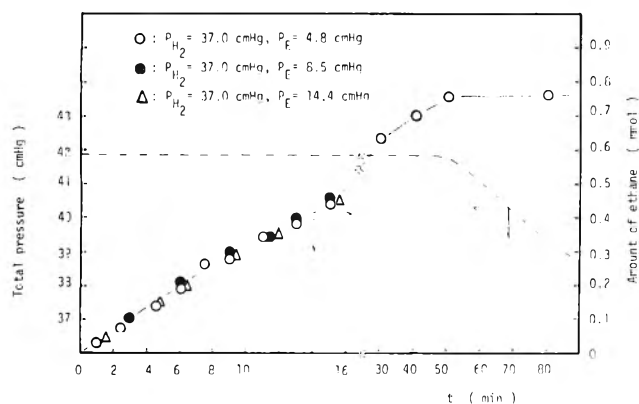


Figure 1. Typical time courses for the hydrogenation. Reactions were conducted at -78°C over 0.40 g of $\text{LaNi}_5\text{H}_{2.4}$. The dotted line shows the pressure change during the reaction when hydrogen (37.0 cmHg) and ethylene (4.8 cmHg) were admitted.

TABLE I: Distribution of Hydrogen Isotopes in the Resulting Ethane^a

Time, min	Convsn, ^b %	Distribution, %			
		$\text{C}_2\text{H}_3\text{D}_3$	$\text{C}_2\text{H}_4\text{D}_2$	$\text{C}_2\text{H}_5\text{D}$	C_2H_6
6	10.0	0	2.2	7.6	90.2
15	28.5	0	1.8	8.1	90.1
30	45.9	0	1.8	7.8	90.4
60	72.4	0.5	1.9	8.6	89.0

^a The reaction was conducted at -78°C over 0.40 g of $\text{LaNi}_5\text{H}_{2.4}$ using a mixture of ethylene (8.5 cmHg) and deuterium (20.5 cmHg). ^b Based on the hydride.

are shown in Figure 1. The total pressure remained unchanged until most of ethylene was converted into ethane, then it decreased gradually. The hydrogenation of ethylene was then conducted at -78°C over 0.40 g of the same catalyst (containing 2.23 atom of H) by admitting a mixture of deuterium (20.5 cmHg, 3.26 mmol) and ethylene (8.5 cmHg, 1.35 mmol), and the ethane formed was analyzed by mass spectrometry. Table I shows the results obtained, which indicates that most of ethane formed was C_2H_6 .

These results strongly imply that absorption of gaseous hydrogen into the alloy hardly takes place in the presence of a considerable amount of ethylene and that most of the hydrogen which participates in the reaction comes from the hydride. [The hydrogenation of ethylene of course proceeded by using gaseous deuterium. However the rate was much slower as compared with the rate when using the hydride. The slower reaction may be considered to proceed via the same mechanism as operates in the hydrogenation over LaNi_5 which will be shown later (via the surface reaction between the adsorbed ethylene and the adsorbed deuterium molecule).] Thus, the following equation can approximately be applied for the present hydrogenation:

$$y = \frac{1}{2}(C_0 - C_t) \quad \text{or} \quad C_t = C_0 - 2y \quad (1)$$

where y , C_t , and C_0 denote the amount of the resulting ethane (mmol of $\text{C}_2\text{H}_6/\text{g}$ of LaNi_5) at time t , the concentration of the hydride (atom of H/g LaNi_5) at time t and zero, respectively. By using the data shown in Figure 1, C_t was calculated according to eq 1 and $\ln C_t$ was plotted against the reaction time t (Figure 2), which leads to

$$\ln C_t = -k_0 t + \ln C_0$$

or

$$r = \frac{dy}{dt} = -\frac{1}{2} \frac{dC_t}{dt} = \frac{1}{2} k_0 C_t = k_1 C_t \quad (2)$$

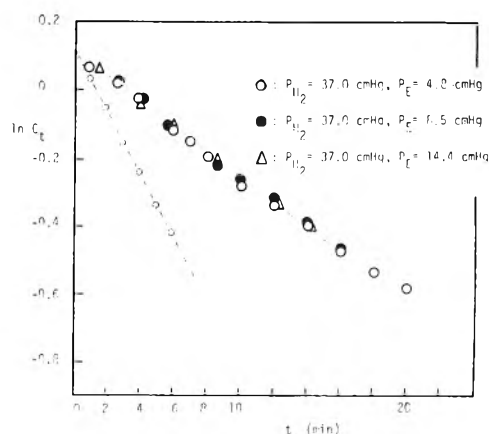


Figure 2. Plots of $\ln C_t$ vs. the reaction time t . C_t represents the concentration of the hydride at t . The hydrogenation experiments were conducted at -78°C over 0.40 g of $\text{LaNi}_5\text{H}_{2.4}$. The dotted line shows the time course of desorption of the hydride at -78°C over 0.40 g of $\text{LaNi}_5\text{H}_{2.4}$.

TABLE II: Rate Constants (k_1 in Eq 2) Obtained with Various Pressures of Ethylene and Hydrogen^a

P_{H_2} , cmHg	P_{E} , cmHg	k_1 , (g of LaNi_5) ⁻¹ min ⁻¹
1.1	8.5	3.45×10^{-1}
2.0	8.5	2.03×10^{-1}
9.5	8.5	3.33×10^{-2}
12.6	8.5	3.10×10^{-2}
20.5	8.5	3.41×10^{-2}
37.0	8.5	3.54×10^{-2}
37.0	2.1	3.10×10^{-2}
37.0	4.6	3.51×10^{-2}
37.0	14.3	3.36×10^{-2}
0	8.5	5.20×10^{-1}

^a The reactions were conducted at -78°C over 0.40 g of $\text{LaNi}_5\text{H}_{2.4}$.

where r is the rate of the formation of ethane (mmol of $\text{C}_2\text{H}_6/\text{g}$ of LaNi_5 min) at time t , and k_0 and k_1 denote the rate constants (g^{-1} of LaNi_5 min⁻¹) for the consumption of hydride and of the formation of ethane, respectively. It is immediately obvious from Figure 2 that the rate constant, k_1 , is independent of ethylene pressure under the experimental conditions.

The hydrogenation of ethylene was conducted at -78°C over 0.40 g of the same catalyst (containing 2.23 atom of H) using the same pressure of ethylene (8.5 cmHg, 1.35 mmol) and various pressures of hydrogen (1.1 cmHg, 0.17 mmol; 2.0 cmHg, 0.32 mmol; 9.5 cmHg, 1.51 mmol; 12.6 cmHg, 2.00 mmol; 20.6 cmHg, 3.27 mmol; and 37.0 cmHg, 5.87 mmol). The time course of the hydrogenation obeyed eq 2. The values of the rate constant, k_1 , obtained with various hydrogen pressures are summarized in Table II, which gives roughly eq 3 with k_2 and a being constants.

$$k_1 = k_2 / (1 + aP_{\text{H}_2}) \quad (3)$$

From eq 2 and 3 the rate of the formation of ethane over the $\text{LaNi}_5\text{H}_{2.4}$ catalyst is roughly given by

$$r = dy/dt = k_2 C_t / (1 + aP_{\text{H}_2}) \quad (4)$$

The hydrogenation of ethylene was then conducted at various temperatures over 0.40 g of the same catalyst using the same pressures of hydrogen (40.2 cmHg) and ethylene (8.5 cmHg). The values of k_1 obtained at various temperatures are shown in Table III. These values were close to a single line on the Arrhenius plot and approximately 5.7 kcal/mol was obtained as the apparent activation energy.

TABLE III: Rate Constants (k_1 in Eq 2) Obtained in the Cases of Both the Hydrogenation and Desorption of Hydride^a

	Temp, °C	k_1 , (g of LaNi ₅) ⁻¹ min ⁻¹	E , kcal/mol
Hydrogenation of C ₂ H ₄ over LaNi ₅ H _{2.4}	-65	7.73×10^{-2}	5.7
	-73	4.74×10^{-2}	
	-83	2.13×10^{-2}	
Desorption of the hydride	-60	3.82×10^{-1}	5.3
	-69	2.15×10^{-1}	
	-78	1.10×10^{-1}	
	-84	6.74×10^{-2}	

^a The hydrogenation experiments were conducted over 0.40 g of LaNi₅H_{2.4} using a mixture of hydrogen (40.2 cmHg) and ethylene (8.5 cmHg). The desorption experiments were conducted over 0.40 g of LaNi₅H_{2.4}.

TABLE IV: Rate Constants (k_1 in Eq 2) Obtained with the Various Concentrations of the Hydride (n)^a

n	k_1 , g ⁻¹ of LaNi ₅ min ⁻¹	n	k_1 , (g of LaNi ₅) ⁻¹ min ⁻¹
0.62	2.83×10^{-1}	2.1	2.29×10^{-2}
0.92	5.10×10^{-1}	2.4	3.54×10^{-2}
1.5	1.42×10^{-2}		

^a $n = 0.62, 0.92, 1.5, 2.1,$ and 2.4 . The reactions were conducted at -78°C over 0.40 g of each catalyst using a mixture of hydrogen (37.0 cmHg) and ethylene (8.5 cmHg).

Here, the hydrogenation of ethylene was conducted at -78°C using the same pressures of hydrogen (37.0 cmHg, 5.87 mmol) and ethylene (8.5 cmHg, 1.35 mmol) over 0.40 g of various catalysts (LaNi₅H _{n} ; $n = 0.62$, containing 0.58 matom of H; $n = 0.92$, 0.85 matom of H; $n = 1.5$, 1.39 matom of H; $n = 2.1$, 1.95 matom of H; and $n = 2.4$, 2.23 matom of H). These catalysts were prepared by exposure to various hydrogen pressures after the preactivated alloy was heated at 400°C under vacuum for 3 h. The time course of the hydrogenation obeyed eq 2 with every value of n . The rate constants (values of k_1) obtained (Table IV), however, depended on the value of n ; it decreased considerably with a decrease in n .

On the other hand, the hydrogenation of ethylene was also conducted at -78°C by admitting the mixture of hydrogen (5.7 cmHg, 0.91 mmol) and ethylene (5.4 cmHg, 0.86 mmol) over the LaNi₅ catalyst which was heated at 400°C for 3 h under vacuum (ca. 4×10^{-5} mmHg) and cooled quickly to a reaction temperature in the absence of gaseous hydrogen. In this case, the total pressure in a gas phase decreased gradually during the reaction.

The number of moles of ethane formed (followed by gas chromatography) exactly coincided with the decrease in the number of moles in the gas phase (estimated from the pressure drop of a gas phase) during the reaction.

From this result it may be said that gaseous hydrogen was hardly absorbed into the alloy in the presence of a considerable amount of ethylene. Thus, the catalyst is considered to be free from the hydride (absorbed hydrogen atom).

The hydrogenation of ethylene was conducted at -78°C over 6.0 g of the same catalyst using various pressures of hydrogen and ethylene, and the rate of the hydrogenation was followed by gas chromatography. In Table V are summarized the initial rates obtained, which leads to

$$r = k_3 P_{\text{H}_2}^{1.0} P_{\text{E}}^0 \quad (5)$$

where r is the initial rate of the hydrogenation, k_3 the rate constant, and P_{H_2} and P_{E} the initial pressures of hydrogen

TABLE V: Rates of the Hydrogenation Obtained with Various Pressures of Ethylene and Hydrogen^a

P_{H_2} , cmHg	P_{E} , cmHg	r , mmol of C ₂ H ₆ /g of LaNi ₅ , min
4.0	8.5	4.12×10^{-4}
7.7	8.5	8.93×10^{-4}
11.7	8.5	1.17×10^{-3}
19.0	8.5	1.95×10^{-3}
5.7	2.6	6.53×10^{-3}
5.7	4.0	6.78×10^{-3}
5.7	8.1	6.69×10^{-3}
5.7	15.8	6.60×10^{-3}

^a The reactions were conducted at -78°C over 6.0 g of LaNi₅.

TABLE VI: Rate Constants (k_3 in Eq 6) Obtained at Various Temperatures^a

Temp, °C	k_3 , (g of LaNi ₅) ⁻¹ min ⁻¹	E , kcal/mol
-60	9.42×10^{-4}	6.8
-69	4.17×10^{-4}	
-78	2.05×10^{-4}	
-83	1.35×10^{-4}	

^a The reactions were conducted over 6.0 g of LaNi₅ using a mixture of hydrogen (5.7 cmHg) and ethylene (5.4 cmHg).

and ethylene, respectively. The time course of the hydrogenation was confirmed to obey

$$\ln P_{\text{H}_2}^t = -k_3 t + \ln P_{\text{H}_2}^0$$

or

$$r = -dP_{\text{H}_2}^t/dt = k_3 P_{\text{H}_2}^t \quad (6)$$

which is an identical form with eq 5, where r is the rate of the hydrogenation (mmol of C₂H₆/g of LaNi₅ min), k_3 the rate constant (g⁻¹ of LaNi₅ min⁻¹), and $P_{\text{H}_2}^t$ and $P_{\text{H}_2}^0$ are the pressures of hydrogen at time t and zero, respectively.

The rate constants (values of k_3) obtained from the hydrogenation over the LaNi₅ catalyst at $-60, -69, -78,$ and -83°C using the same pressures of ethylene (5.4 cmHg) and hydrogen (5.7 cmHg) are shown in Table VI. These values were close to a single line on the Arrhenius plot and approximately 6.8 kcal/mol was obtained as the apparent activation energy.

It should be noted here that k_1 obtained over the LaNi₅H_{2.4} catalyst (Table III) is far greater than k_3 obtained over the LaNi₅ catalyst under similar experimental conditions.

In order to elucidate why gaseous hydrogen was hardly absorbed into the alloy in the presence of ethylene, the hydrogen-deuterium equilibration reaction was carried out using an equimolar mixture ($[\text{H}_2] = [\text{D}_2] = 9.2$ cmHg, 1.46 mmol) at -78°C for 2 h over 6.0 g of the same catalyst in the presence of ethylene (4.1 cmHg, 0.65 mmol). The isotopes of hydrogen were analyzed with the same method as reported by Yasumori et al.,⁸ the eluted hydrogen samples were converted into water vapor on a cupric oxide column heated at 500°C and were analyzed by gas chromatography using an alumina column at -196°C . The hydrogenation of course took place, but hydrogen deuteride was hardly detectable under these condition.

On the other hand, as reported in another paper,⁷ the equilibration reaction took place at a high speed at -78°C over the same catalyst in the absence of ethylene.

These results may be explained as follows. Dissociative adsorption of gaseous hydrogen hardly takes place in the presence of a considerable amount of ethylene. Atomic

species may of course be produced as a result of the surface reaction between the adsorbed ethylene and the adsorbed hydrogen (or deuterium) molecule, but they react quite readily with adsorbed ethylene. Consequently, there exists only molecular species on the surface, which may be the reason why gaseous hydrogen was hardly absorbed into the alloy.

We are concerned here with the mechanism for the hydrogenation of ethylene. It is clear from the results obtained that the hydrogenation reaction over the LaNi₅H_n catalyst operates via a different mechanism from that over the LaNi₅ catalyst. The mechanism of the hydrogenation over the LaNi₅H_n catalyst is first discussed.

It is obvious from the experimental results that the hydrogenation proceeded mainly by using the hydride (adsorbed hydrogen atom).

As described before, gas phase samples contained only a trace of hydrogen during the hydrogenation reaction over LaNi₅H_{2.4} where only ethylene was admitted. This suggests that all the hydride that came out of the alloy reacted immediately with ethylene to produce ethane. Therefore, the surface reaction between adsorbed ethylene and the hydride is not rate determining. The rate equation (eq 2) suggests that the migration of the hydride from the bulk to the surface sites is rate determining, which leads to

$$r = k_4 C_t C_s \quad (7)$$

where r , k_4 , C_t , and C_s represent the rate of the hydrogenation (rate of the migration of the hydride from the bulk to the surface sites), the rate constant, the concentration of the hydride, and the concentration of the effective surface sites where the hydride comes out from the alloy. The results shown in Table II suggest that C_s is independent of ethylene pressure and that it decreases with an increase in hydrogen pressure. Accordingly, it might be taken for granted to assume that hydrogen and ethylene are adsorbed on two separate parts of the surface and that one set of sites which adsorbs ethylene is almost completely covered with ethylene under the present conditions. Both hydrogen atom which comes out from the alloy and molecular hydrogen which comes from gaseous hydrogen may be competing for adsorption on the another set of sites. (As described before, dissociative adsorption of gaseous hydrogen hardly takes place under these conditions.) Since the surface reaction between adsorbed ethylene and hydrogen atom (hydride) is fast, the hydride is consumed as soon as it comes out from the alloy. Accordingly, there exist only molecular hydrogen species under these experimental conditions. Thus, the fraction of the vacant part of this set of sites can be expressed as $(1 - \theta_{H_2})$, and the rate of the hydrogenation (rate of the migration of the hydride from the bulk to this set of sites), r , can be represented by

$$r = k_4 C_t (1 - \theta_{H_2}) \quad (8)^{10}$$

where k_4 , C_t , and θ_{H_2} denote the rate constant, the concentration of hydride, and the fraction of second set of sites covered with molecular hydrogen. If the Langmuir isotherm were obeyed, θ_{H_2} is given by

$$\theta_{H_2} = K_{H_2} P_{H_2} / (1 + K_{H_2} P_{H_2}) \quad (9)$$

Equations 8 and 9 lead to

$$r = k_4 C_t / (1 + K_{H_2} P_{H_2}) \quad (10)$$

which is an identical form with the experimentally obtained eq 4, where P_{H_2} and K_{H_2} denote the hydrogen pressure and its adsorption coefficient. [If ethylene and hydrogen are competing for adsorption on the same sites,

it may be readily shown that

$$\theta_E = K_E P_E / (1 + K_E P_E + K_{H_2} P_{H_2}) \quad (11)$$

and

$$\theta_{H_2} = K_{H_2} P_{H_2} / (1 + K_E P_E + K_{H_2} P_{H_2}) \quad (12)$$

(As shown above, equilibrium is not established between the hydride in the alloy and the surface hydrogen atom. Thus, the term, $K_H C_t$, is neglected in eq 11 and 12). Therefore eq 8 takes the form

$$r = k_4 C_t (1 - \theta_E - \theta_{H_2}) \\ = k_4 C_t / (1 + K_E P_E + K_{H_2} P_{H_2}) \quad (13)$$

where P_E and P_{H_2} are the partial pressures of ethylene and hydrogen, and K_E and K_{H_2} are their adsorption coefficients, respectively. Since it may be considered that hydrogen adsorption is very weak and ethylene very strong, $K_{H_2} P_{H_2} \ll 1 \ll K_E P_E$, eq 13 is simply given by

$$r = k_4 C_t / K_E P_E \quad (14)$$

Equation 14 is far different from the experimentally obtained eq 4. Consequently, this mechanism is denied.]

Equation 10 can be explained on the assumption that less reactive molecular hydrogen species reduce the concentration of the effective sites where the hydride comes out from the alloy.

We are briefly concerned with a plausible reason why dissociative adsorption of gaseous hydrogen hardly takes place in the presence of ethylene while the hydride can easily come out from the alloy. It may be supposed that dual sites are necessary for gaseous hydrogen to be adsorbed dissociatively while such sites are not necessary for the hydride to come out from the alloy. Namely, it might be considered that such dual sites are almost completely lost by adsorbed ethylene which covers most of the surface. However the precise reason is open to discussion at present.

The apparent activation energy is given by

$$E_{app} = RT^2 \frac{\partial \ln r}{\partial T} = E_{k_4} \\ - \left[\frac{a^0 P_{H_2} e^{\Delta H/RT}}{1 + a^0 P_{H_2} e^{\Delta H/RT}} \right] \Delta H \quad (15)$$

where E_{k_4} , ΔH , and a^0 are the activation energy for the migration of the hydride from the bulk to the surface, the heat of adsorption of molecular hydrogen, and a constant independent of temperature.

It is known⁹ that the heat of adsorption of molecular hydrogen is usually very small. Therefore, the activation energy for the migration of the hydride can be estimated approximately as 5 kcal/mol.

To examine the validity of the mechanism proposed above, the following experiments were performed.

About 0.40 g of the LaNi₅H_{2.4} catalyst was prepared at -60, -69, -78, and -84 °C in the same reactor according to normal procedures. It was briefly evacuated at each temperature to remove the gas phase hydrogen and the pressure was continuously measured. The time course of desorption of the hydride obeyed eq 2 as shown in Figure 2. The rate constants, k_1 (in eq 2), for desorption of the hydride obtained at various temperatures are shown in Table III. These values are greater to some extent when compared with the values obtained in the hydrogenation experiments, which can be explained on the basis of eq 10. Besides, the apparent activation energy of desorption of the hydride is very close to that of the hydrogenation. These results strongly support the mechanism proposed above.

Kuijpers¹ measured in some detail the lattice parameters of LaCo_5 and LaCo_5H_n by x-ray diffraction analysis and it was found that the lattice parameters of LaCo_5H_n expand with an increase in the concentration of the hydride (n). Such a phenomenon can easily be expected also in the present alloy. It can also be considered that many of the characteristic physical properties of the alloy, such as, concentration of defects, distribution of porosity, etc., depend on the content of the hydride (n).

The experimental result that the rate of the hydrogenation depends considerably on the initial concentration of the hydride (n) may be attributable to these physico-chemical properties of the alloy. However the precise reason is open to discussion at the present.

Then, the mechanism of the hydrogenation of ethylene over the LaNi_5 catalyst is briefly discussed. Since this catalyst is free from hydride, it is obvious that the hydrogenation of ethylene proceeds by using gaseous hydrogen.

Many workers⁹ have obtained the same result as eq 5 in the hydrogenation of ethylene more especially for nickel catalyst, which has been explained on the basis of the following general mechanism.

Hydrogen and ethylene are reversibly adsorbed on two separate parts of the surface and interaction occurs at the interline, which leads to

$$r = k_5 \frac{a_{\text{H}_2} P_{\text{H}_2}}{(1 + a_{\text{H}_2} P_{\text{H}_2})} \frac{a_{\text{E}} P_{\text{E}}}{(1 + a_{\text{E}} P_{\text{E}})} \quad (16)$$

and if the hydrogen adsorption is weak and the ethylene strong, $a_{\text{H}_2} P_{\text{H}_2} \ll 1 \ll a_{\text{E}} P_{\text{E}}$, we can obtain

$$r = (k_5 a_{\text{H}_2}) P_{\text{H}_2} \quad (17)$$

which is identical with eq 5, where k_5 is the rate constant, P_{H_2} and P_{E} are the pressures of hydrogen and ethylene, and a_{H_2} and a_{E} are their adsorption coefficients, respectively.

As described before, dissociative adsorption of gaseous hydrogen hardly took place under the experimental conditions. Besides, the apparent activation energy obtained in this work (6.8 kcal/mol) is very close to those obtained by many authors.

From this, it may be considered that the above general mechanism can be applied also to the present case.

References and Notes

- (1) For example, R. L. Beck, quoted by E. A. Aitken, in "Intermetallic Compounds", J. H. Westbrook, Ed., Wiley, New York, N.Y., 1967, p 511; R. van Houten and S. Bartram, *Metall. Trans.*, **2**, 527 (1971); F. A. Kuijpers, *Philips Res. Rep.*, **2** (1973).
- (2) H. H. Neumann, Ph.D. Thesis, Technische Hochschule, Darmstadt, 1969.
- (3) J. H. N. van Vucht, F. A. Kuijpers, and H. C. M. Bruning, *Philips Res. Rept.*, **25** (1970).
- (4) F. A. Kuijpers and H. H. van Mal, *J. Less-Common Metal*, **23**, 395 (1971).
- (5) V. T. Coon, T. Takeshita, W. E. Wallace, and R. S. Craig, *J. Phys. Chem.*, **80**, 1878 (1976).
- (6) K. Soga, H. Imamura, and S. Ikeda, *Chem. Lett.*, 1387 (1976).
- (7) K. Soga, H. Imamura, and S. Ikeda, *Nippon Kagaku Kaishi*, submitted for publication.
- (8) I. Yasumori and S. Ohno, *Bull. Chem. Soc. Jpn.*, **39** (6), 1302 (1966).
- (9) For example, C. C. Bond, "Catalysis by Metal", Academic Press, London, 1962; P. H. Emmett, "Catalysis", Vol. 3, Reinhold, New York, N.Y., 1955.
- (10) r is of course a function of the surface area, and eq 8 must be expressed as

$$r = k_5' C_t (1 - \theta_{\text{H}_2}) S \quad (8')$$

in precise, where S and k_5' are the surface area of the catalyst and the rate constant per unit surface area. However eq 8 was used here in place of eq 8', because the surface area was constant.

Interaction of *p*-Nitrosalicylic Acid with Ethylenediamine in the Presence of Cetyltrimethylammonium Bromide, Sodium Dodecyl Sulfate, Triton X 100, Polyethylene Glycol, and Their Binary Mixtures. A Proton Donor-Acceptor Equilibrium in Micellar Solution

S. P. Moulik,* S. Ray, and A. R. Das¹

Department of Chemistry, Jadavpur University, Calcutta 700032, India (Received August 19, 1976; Revised Manuscript Received February 22, 1977)

Results of a spectrophotometric investigation on the proton donor-acceptor complexing equilibrium between *p*-nitrosalicylic acid and ethylenediamine in the presence of cetyltrimethylammonium bromide, sodium dodecyl sulfate, Triton X 100, polyethylene glycol, and their binary mixtures have been reported. The reaction has been observed to be enhanced by cetyltrimethylammonium bromide and sodium dodecyl sulfate, and suppressed by Triton X 100 and polyethylene glycol. The equilibrium constants have been determined and the standard thermodynamic quantities, ΔG° , ΔH° , and ΔS° , evaluated. The process has shown a linear enthalpy-entropy compensation effect.

Introduction

Proton transfer complexing equilibria of *p*-nitrophenol, *p*-nitrosalicylic acid, violuric acid, and reducing sugars with ethylenediamine in aquo-organic mixed solvent media have been recently reported.²⁻⁸ An extension of these studies in micellar and mixed micellar solutions would be worthwhile as micelles are known to affect various kinetic and equilibrium processes,⁹⁻¹⁴ which in turn would become

useful in understanding the nature of such reactions in an organized lipid phase such as membranes.

In this paper, we have reported proton transfer complexation between *p*-nitrosalicylic acid and ethylenediamine in cationic (cetyltrimethylammonium bromide, CTAB), anionic (sodium dodecyl sulfate, SDS), and nonionic (*p*-*tert*-alkylphenoxypolyoxyethanol, Triton X 100, abbreviated as TX 100) surfactants and their binary

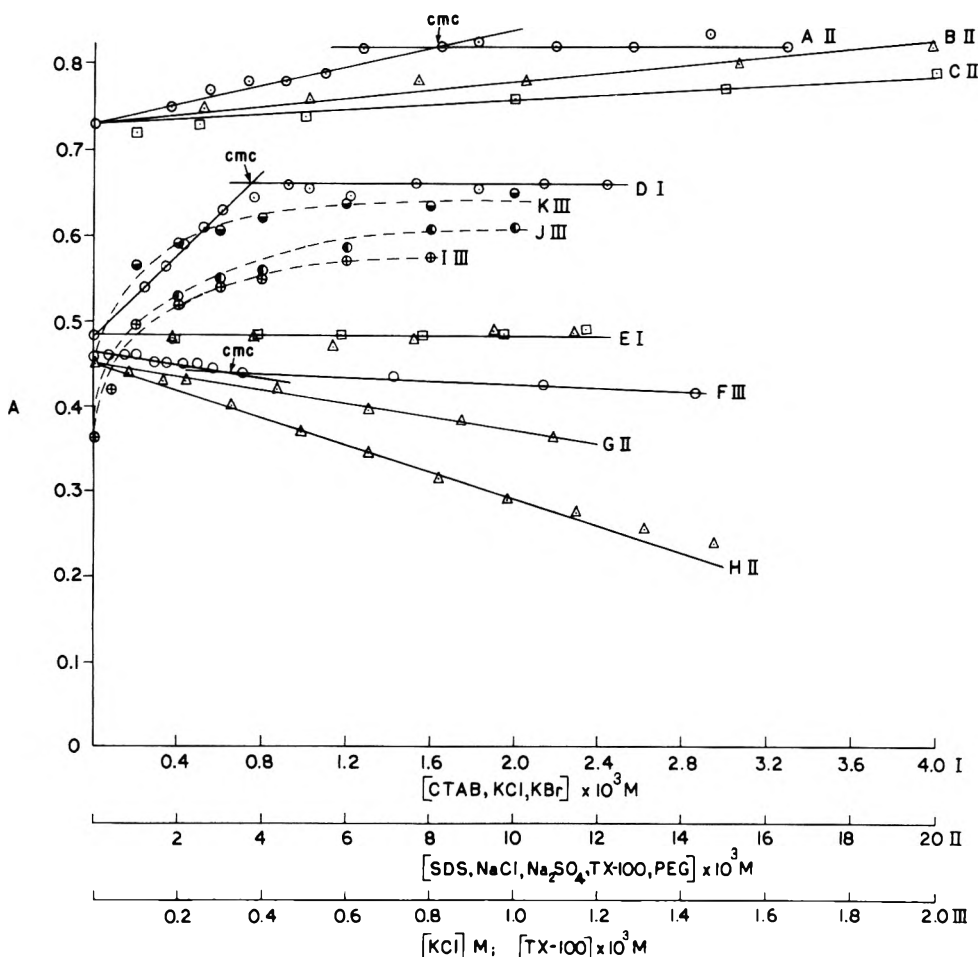


Figure 1. Influence of additives on the proton transfer from PNSA to EN: (A) 5.76×10^{-5} M PNSA plus 4.12×10^{-3} M EN with varying SDS; (B) same with varying Na_2SO_4 ; (C) same with varying NaCl; (D) 3.84×10^{-5} M PNSA plus 4.12×10^{-3} M EN with varying CTAB; (E) same with varying KCl (Δ) and KBr (\square); (F) 3.37×10^{-5} M PNSA plus 5.6×10^{-3} M EN with varying TX-100; (G) 3.5×10^{-5} M PNSA plus 4.3×10^{-3} M EN with varying TX-100; (H) same with varying PEG; (I) same plus 10.9×10^{-3} M TX-100 with varying KCl; (J) same plus 6.56×10^{-3} M PEG with varying KCl; (K) same with varying KCl.

mixtures. The report also includes results obtained with a polymer (polyethylene glycol, PEG) having a composition identical with the hydrophilic part of the nonionic surfactant, TX 100.

Experimental Section

Materials and Method. For the source of PNSA and EN, and their purity we refer to our previous publications.^{1,4} CTAB used was GR, E. Merck quality. SDS was a gift sample from Dr. B. N. Ghosh of Calcutta University. The standard of purity was that reported by Ghosh et al.¹⁵ The purity of CTAB and SDS was further checked by elemental analysis of C, N, and H. The calculated and the observed values agreed within 0.2%. TX 100 was a product of Rohm & Haas Co., USA, of average molecular weight 624, containing an average chain length of about 9.5 oxyethylene units. The reported cmc ¹⁶ was $2-3 \times 10^{-4}$ M. PEG was of BDH pure grade of average molecular weight 4000. This and TX 100 were used without further purification. Triple distilled conductivity water was used throughout the experiments (specific conductance, 1.2×10^{-6} mho cm^{-1} at 25 °C).

The cmc values of both CTAB and SDS were determined conductometrically using an ELICO conductivity bridge, made at Hyderabad in India, and were found to be 0.75×10^{-3} and 8.0×10^{-3} M, respectively. The best values reported in literature¹⁷ agree very closely with these. That of TX 100 as referred to above was not independently checked.

The spectral measurements were taken in a Beckman DU spectrophotometer. The details of measurements and experimental conditions were the same as described earlier.^{1,4}

Results

Spectral Characteristics and the Influence of Additives. The additives were observed not to affect the band positions of PNSA (320 nm) and the PNSA-EN complex (414 nm). The band intensity of the complex, on the other hand, was increased by CTAB and SDS, and diminished by TX 100 and PEG. Spectrophotometric measurements showed a linear variation of the absorbance with additive concentration yielding a sharp break at a concentration corresponding to the cmc of the additive. At comparable concentrations, salts were also observed to influence the absorbance but to a much lesser degree. A representation in this way corresponded nicely with the literature given values^{16,17} as well as those obtained for CTAB and SDS from conductometric measurements. No cmc giving break was observed for PEG.

Following exactly the same procedure as was done earlier,^{1,4} the equilibrium constant of the complex in various concentrations of CTAB and SDS were determined. In addition to this, equilibrium constants for systems having constant SDS and varying CTAB as well as constant CTAB and varying SDS were also determined. The results are given in Figure 2. Here also sharp breaks

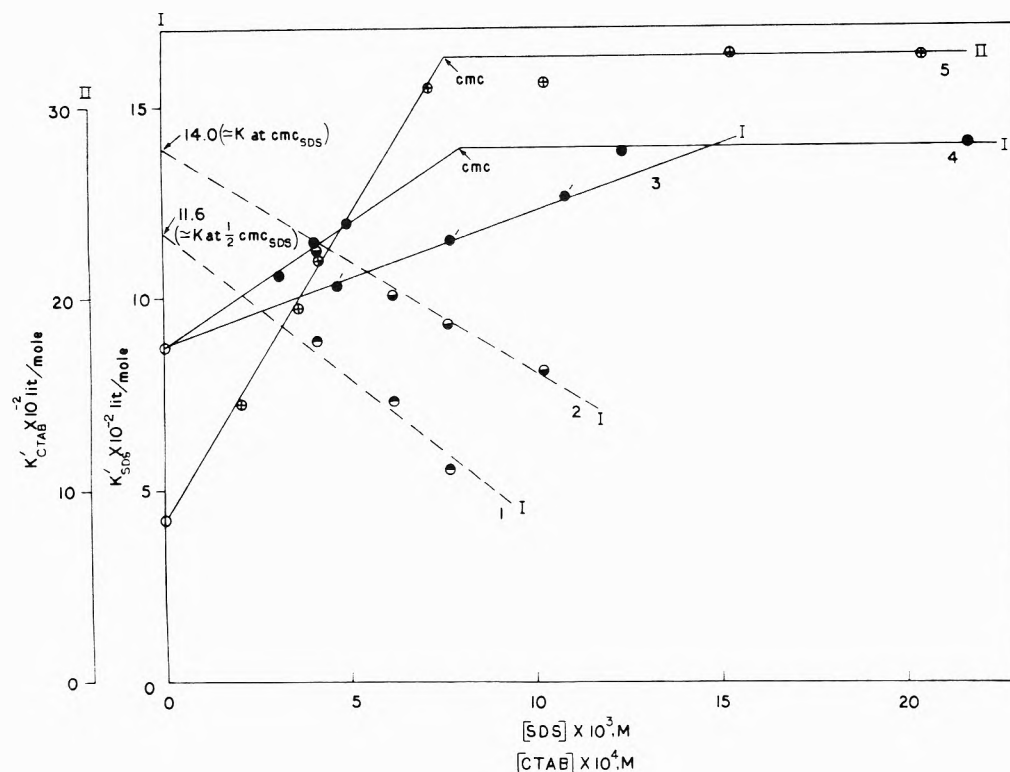


Figure 2. Influence of the additives, CTAB, SDS, and their mixtures on the stability constant of the complex determined using 3.5×10^{-5} M PNSA and EN in the range $2.16\text{--}10.07 \times 10^{-3}$ M at 303 K: (1) effect of CTAB in presence of 4.03×10^{-3} M SDS ($1/2$ cmc); (2) effect of CTAB in presence of 8.06×10^{-3} M SDS (cmc); (3) effect of SDS in presence of 7.17×10^{-4} M CTAB (cmc); (4) effect of SDS in absence of CTAB; (5) effect of CTAB in absence of SDS.

TABLE I: Thermodynamics of the Complex at 303 K in the Presence of Additives^a

Additives (M $\times 10^3$)	ΔG° , kJ/mol	ΔH° , kJ/mol	ΔS° , J/deg mol
0	-17.02 ± 0.08	-25.56 ± 0.36	-28.62 ± 1.25
CTAB (14)	-18.29 ± 0.17	-14.86 ± 0.34	$+11.51 \pm 1.68$
SDS (32)	-17.87 ± 0.17	-31.77 ± 0.55	-46.55 ± 1.26
TX 100 (5.64)	-15.40 ± 0.01	-23.78 ± 0.84	-28.05 ± 2.81
PEG (3.94)	-14.73 ± 0.13	-9.00 ± 1.55	$+19.21 \pm 4.78$
SDS + TX 100 (31.9 + 9.76)	-17.33 ± 0.13	-15.40 ± 0.34	$+6.45 \pm 0.72$
CTAB + TX 100 (14.0 + 9.76)	-15.90 ± 0.09	-14.69 ± 0.21	$+4.06 \pm 0.42$

^a PNSA = 3.5×10^{-5} M; EN = $5\text{--}25 \times 10^{-3}$ M.

were obtained at micellar concentrations.

Thermodynamics of Complexation. To derive ΔG° , ΔH° , and ΔS° , equilibrium constants were obtained at 298, 308, 318, and 328 K. The temperature coefficient of $\log K'$ then yielded ΔH° which in conjunction with ΔG° at constant temperature (308 K) in the Gibbs equation yielded ΔS° . The standard states were considered to be the hypothetical states of ideal solutions of unit molarity. The concentrations of all the additives and their mixtures were well above their cmc values. The results are contained in Table I.

Discussion

The results incorporated in Figure 1 show that charged micelles facilitated proton transfer from PNSA to EN, whereas uncharged micelles suppressed it, and there occurred little additional change of the said transfer at concentrations above cmc. Moreover, at comparable concentrations, salts (NaCl, KCl, and Na_2SO_4) were much less effective than the ionic surfactants. An obvious conclusion could be that hydrophobic-hydrophilic com-

posite molecules and their clusters (micelles) produced a better environment for proton transfer. That TX 100 having hydrophobic-hydrophilic parts worked better than PEG strengthened this view. The observed order of efficiency was CTAB > SDS > water > TX 100 > PEG. Suppressions by TX 100 and PEG were due to the hydrogen bonding of the -OH group of PNSA with the oxygen center of the polyoxyethanol chain present in each of them, which prevented efficient proton transfer to the amine.

Effects of micelles and polyelectrolytes have been reported^{18,19} to affect the apparent pK of the indicators. Both charge and nonelectrostatic (hydrophobic) effects were considered to alter the pK, which fell in line with our observations of efficient proton donation to the base in presence of composite hydrophobic-hydrophilic charged surfactant molecules.

Earlier reports showed that the proton transfer process would be partly guided by the solvent structure.^{1,4,20} It was likely that the PNSA, incorporated in the micelle, would be kinetically stabilized, and its link with the amine would take place in the vicinal microenvironment of the micellar

boundary and depend on its structure (we neglect any proton transfer in the interior of the micelles having low dielectric constant, since ten units lowering of it than water was observed to lower the complexation significantly under the present experimental conditions⁴). The ΔS° values given in Table I varied in the order SDS < water < TX 100 < (CTAB + TX 100) < (SDS + TX 100) < CTAB < PEG. The environment for the reaction was then most ordered in SDS, much less in CTAB, and the least in PEG. The free energy changes for the individual additives followed the order PEG < TX 100 < water < SDS < CTAB. Appearance of PEG and CTAB at the two extreme ends and that of SDS just before CTAB advocated the significant roles of charge and other specific effects^{1,4} than the water structure. The effects of micellar charge, the environmental dielectric, changed pK , water structure, and the partition of the species between the micelle and the bulk would all work in conjunction, whose dissection at present would not be meaningful.

In conclusion we make a statement that in spite of accepting the error related possibility of a linear enthalpy-entropy correlation,²¹ we observed such a nice extra-thermodynamic compensation for the present proton transfer process in the presence and absence of different additives including the hydroxylic nonaqueous solvents reported earlier.⁴

Acknowledgment. We thank Professor M. N. Das, Head of the Department of Chemistry for use of laboratory facilities.

References and Notes

- (1) Present Address: Department of Chemistry, Clarkson College of Technology, Potsdam, N.Y.
- (2) S. P. Moulik, A. K. Chatterjee, and K. K. Sen Gupta, *Spectrochim. Acta, Sect. A*, **29**, 363 (1973).
- (3) S. P. Moulik, A. K. Chatterjee, and K. K. Sen Gupta, *Ind. J. Chem.*, **12**, 92 (1974).
- (4) S. P. Moulik, S. Ray, and A. R. Das, *J. Phys. Chem.*, **80**, 157 (1976).
- (5) S. P. Moulik, S. Ray, and A. R. Das, *Ind. J. Chem.*, **14A**, 921 (1976).
- (6) S. P. Moulik, C. R. Sahu, and A. K. Mitra, *Carbohydr. Res.*, **25**, 197 (1972).
- (7) S. P. Moulik, A. K. Mitra, and K. K. Gupta, *Carbohydr. Res.*, **19**, 416 (1971).
- (8) S. P. Moulik and A. K. Mitra, *Carbohydr. Res.*, **23**, 65 (1972).
- (9) J. H. Fendler and E. J. Fendler, "Catalysis in Micellar and Macromolecular Systems", Academic Press, New York, N.Y., 1975.
- (10) L. M. Casilio, E. J. Fendler, and J. H. Fendler, *J. Chem. Soc. B*, 1377 (1971).
- (11) C. A. Bunton and M. J. Minch, *J. Phys. Chem.*, **78**, 1490 (1974).
- (12) R. L. Reeves, *J. Am. Chem. Soc.*, **97**, 6025 (1975).
- (13) C. J. O'Connor, E. J. Fendler, and J. H. Fendler, *J. Org. Chem.*, **38**, 3371 (1973).
- (14) C. J. O'Connor, E. J. Fendler, and J. H. Fendler, *J. Am. Chem. Soc.*, **96**, 370 (1974).
- (15) L. Kundu and B. N. Ghosh, *Ind. Chem. Soc.*, **46**, 462 (1969).
- (16) R. H. Crook, D. B. Fordyce, and G. F. Trebbi, *J. Phys. Chem.*, **67**, 1987 (1963).
- (17) P. Mukherjee and K. J. Mysels, *Natl. Stand. Ref. Data Ser., Natl. Bur. Stand.*, No. 36 (1971).
- (18) E. Baumgartner, R. Fernandes-Prini, and D. Turyn, *J. Chem. Soc., Faraday Trans. 1*, **70**, 1518 (1974).
- (19) J. V. Moller and U. Kragh-Hansen, *Biochemistry*, **14**, 2312 (1975).
- (20) S. N. Vinogradov, R. A. Hudson, and R. M. Scott, *Biochim. Biophys. Acta*, **214**, 6 (1970).
- (21) R. R. Krug, W. G. Hunter, and R. A. Grieger, *Nature (London)*, **281**, 567 (1976).

Observation of Quasilinear Fluorescence Spectra (the "Shpol'skii Effect") in Matrix-Isolated Polycyclic Aromatic Hydrocarbons

P. Tokousbalides, E. L. Wehry,* and Gleb Mamantov*

Department of Chemistry, University of Tennessee, Knoxville, Tennessee 37916 (Received May 16, 1977)

Publication costs assisted by the National Science Foundation and the Electric Power Research Institute

Quasilinear "Shpol'skii" fluorescence spectra of polycyclic aromatic hydrocarbons can be observed by matrix isolation, employing an n -alkane as the matrix, if the vapor-deposited sample is annealed at elevated temperature (ca. 140 K) prior to observation of the spectrum at low temperature (16 K). Quasilinear spectra obtained by matrix isolation compare closely to those obtained by conventional frozen-solution techniques in Shpol'skii matrices. Temperature variations of vapor-deposited samples after deposition but before spectral measurements reveal the presence of matrix "memory effects".

Introduction

Broad absorption or emission bands in the electronic spectra of polycyclic aromatic hydrocarbons (PAH) observed in liquid solutions of certain n -alkanes reduce to very narrow features ("quasilines") upon freezing at low temperature (the Shpol'skii effect¹). The quasilines correspond to purely electronic transitions, i.e., to transitions in which the vibrational state of the lattice does not change.^{2,3} In cases of weak coupling of the electronic and lattice vibrational transitions, the quasilines are accompanied (on the long-wavelength side of the fluorescence band and on the short-wavelength side of the absorption band) by a diffuse band, the "phonon wing". The phonon wing arises from electronic transitions in the PAH accompanied by concomitant changes in the vibrational state of the lattice. In the case of strong coupling between the

electronic transitions of the PAH and the vibrational transitions of the lattice, only the phonon wing is observed.² The existence of several slightly different, but well defined, types of molecular sites (impurity-host) in the alkane matrix, corresponding to different rotational isomers of the alkane molecule, is thought to be responsible for the "multiplet" structures of quasilines in many Shpol'skii spectra.¹

While the fluorescence spectroscopy of PAH in frozen solutions has received extensive study,^{1,2,4-9} very few spectral studies of PAH in vapor-deposited matrices¹⁰ have been described, and no reports of matrix isolation fluorescence spectra of PAH in Shpol'skii solvents have appeared. Matrices formed by deposition of vapors on a cold target usually possess a large number of poorly defined multiple sites.¹¹ This condition results in the appearance

of very broad bands in the luminescence spectra of guest molecules in vapor-deposited samples. Annealing of such a sample can reduce the extent of matrix imperfections, leading, in some cases, to substantial sharpening of spectra. Depending upon the relative sizes of guest and host molecules, annealing at temperatures close to the matrix melting point can also greatly facilitate guest-guest recombination, resulting in broad spectra characteristic of guest aggregates.

We now report the observation that quasilinear fluorescence spectra can be observed for PAH in *n*-alkane matrices if proper annealing procedures are employed; the present study pertains specifically to the fluorescence of benz[*a*]anthracene in such matrices.

Experimental Section

Benz[*a*]anthracene (purum) was obtained from Fluka AG and used without further purification. Spectroquality solvents (*n*-hexane and *n*-heptane, Matheson Coleman and Bell) were purified by treatment with sulfuric acid followed by distillation over anhydrous sodium sulfate.

The apparatus described previously^{12,13} for performing matrix isolation spectroscopy of PAH in "conventional" matrices (e.g., nitrogen) by Knudsen effusion-vacuum sublimation was modified by incorporation of a delivery system for *n*-alkane vapor. The apparatus was designed to permit degassing of the liquid *n*-alkane by the freeze-thaw method. Samples were deposited on a sapphire window mounted in the head of a closed-cycle refrigerator (Spectrim, CTI Cryogenics, Waltham, Mass.), with a matrix deposition rate of ca. 10^{-7} mol s⁻¹. The mole ratio of benz[*a*]anthracene to alkane ranged from 1:10⁵ to 1:10⁶. Annealing of deposits was accomplished by increasing the temperature of the deposit (which had been collected at a window temperature of 16 K) to the desired temperature (which was usually maintained for 5 min or less), then allowing the deposit to return to 16 K at the maximum cooling rate of the refrigerator (ca. 10 K/min). The brief annealing, at temperatures as much as 50 K below the matrix melting point, ensures that no significant diffusion of guest molecules occurs.

For frozen-solution spectroscopy, a 6-mm sealed cylindrical quartz cell was used. The cell was placed in a copper holder which was attached to the cold tip of the cryostat. The samples were frozen to the desired temperature in an elapsed time of approximately 5 min. All fluorescence spectra were obtained with a spectrometer constructed in this laboratory.¹⁴

Results and Discussion

The fluorescence spectrum of benz[*a*]anthracene (BaA) in frozen solutions of *n*-heptane (Figure 1A) exhibits a band centered at 384 nm which consists of three well-resolved quasilines. The quasilines occur at 383.6, 384.3, and 384.7 nm, in close agreement with previous results for BaA in frozen solutions of *n*-heptane.¹⁵ The central quasiline exhibits a half-width of 12 cm⁻¹. A broad band appears in the frozen-solution spectrum at ca. 405 nm; the intensity of this band increases, relative to that of the quasilines, as the BaA concentration in the solution is increased. This band may accordingly originate, at least in part, from emission of microcrystalline aggregates formed during freezing.

The fluorescence spectrum of BaA, matrix isolated in *n*-heptane at 16 K, is shown in Figure 1B; as anticipated, none of the well-defined features of the frozen-solution spectrum are observed. However, if the matrix-isolated sample, deposited at 16 K, is annealed at 140 K prior to measurement of the spectrum at 16 K, the spectrum shown

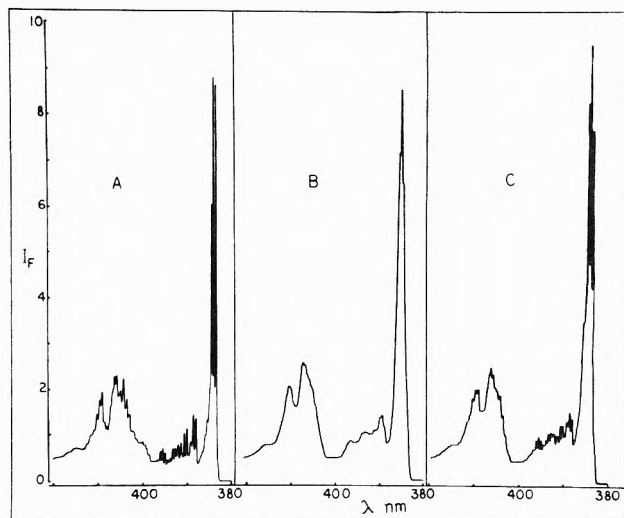


Figure 1. Fluorescence spectra of benz[*a*]anthracene in *n*-heptane at 16 K: A, in frozen solution ($C = 1.4 \times 10^{-5}$ M); B, matrix isolated (benz[*a*]anthracene:heptane mole ratio = 1:200 000) before annealing; C, after annealing B at 140 K. Excitation wavelength = 278 nm in all cases.

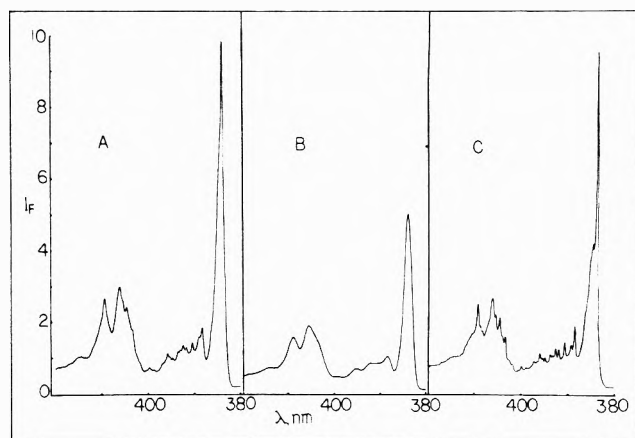


Figure 2. Fluorescence spectra of benz[*a*]anthracene in *n*-hexane at 16 K: A, in frozen solution ($C = 1.0 \times 10^{-6}$ M); B, matrix isolated (benz[*a*]anthracene:hexane mole ratio = 1:500 000) before annealing; C, after annealing B at 140 K. Excitation wavelength = 278 nm in all cases.

in Figure 1C is obtained. In the spectrum of the annealed matrix-isolated sample, the structureless band at 384 nm in Figure 1B is resolved into three well-defined quasilines, the wavelength maxima and half-widths of which coincide with those observed in a frozen solution (compare Figures 1A and 1C).

Frozen-solution spectra of BaA in *n*-hexane at 16 K, although much narrower than those observed at room temperature, do not exhibit quasilinear structure (Figure 2A). Thus, crystalline *n*-hexane does not act as a specific Shpol'skii solvent for BaA, at least under the freezing conditions of our cryostat. As anticipated, spectra of matrix-isolated samples in *n*-hexane, deposited at 16 K, are very broad, as shown in Figure 2B. Once again, however, annealing of such a matrix-isolated sample provides a quasilinear spectrum of BaA (Figure 2C), with a single sharp line of 22-cm⁻¹ half-width at 383.8 nm. Consequently, under certain conditions it appears possible to observe Shpol'skii spectra in matrix-isolated samples even in solvents in which frozen-solution spectra do not exhibit quasilinear structure.

As shown in Figure 3, evolution of quasilines from the broad band at 384 nm in a vapor-deposited BaA:*n*-heptane sample does not occur gradually with increasing annealing

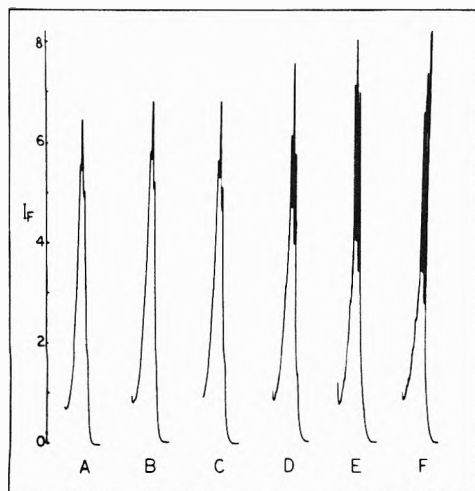


Figure 3. Effect of annealing temperature upon the 384-nm fluorescence band system of benz[a]anthracene in vapor-deposited *n*-heptane matrices: A, 16 K; B, 120 K; C, 130 K; D, 135 K; E, 140 K; F, 150 K.

temperature, but appears rather suddenly at annealing temperatures of 135 K or greater. (For *n*-hexane matrices, the onset of quasilines in the BaA fluorescence spectrum appears at an annealing temperature of 125 K.) The intensity ratio for the quasilines in *n*-heptane changes significantly as the annealing temperature is varied in the 135–150 K range but, at annealing temperatures between 150 and 170 K, the relative intensities of the three quasilines remain constant. (The melting point of *n*-heptane is 182.5 K.) Although there is no known phase change in crystalline hexane or heptane at such temperatures,¹⁶ it is conceivable that packing rearrangements or slight rotations of the carbon chains of the heptane molecules may conceivably occur at temperatures in the 125–150 K region. Such small matrix rearrangements appear sufficient to allow the guest (BaA) molecules to accommodate themselves in the “specific” types of lattice sites required for observation of quasilinear spectra. It is likely that the PAH molecule itself determines the nature of these “specific” sites.¹ For annealing temperatures greater than 150 K, the distribution of quasilines in the BaA fluorescence spectrum is independent of the duration of annealing; annealing times ranging from 3 min to 3 h were employed, with no detectable effect upon the relative intensities of the quasilines. This result indicates that the number of possible types of rotational or packing rearrangements in the alkane matrix is quite limited. Moreover, this result, coupled with the fact that quasilinear spectra are produced upon very brief (<5 min) annealing at temperatures as low as 50 K below the matrix melting point, signifies that diffusion of BaA molecules from one lattice site to another cannot play a significant role in the observed phenomena.

Our hypothesis on the effect of annealing upon the hindered rotation and mobility of *n*-alkane molecules in vapor-deposited matrices is supported by observation of a “memory” effect in the fluorescence spectra of BaA. As shown in Figure 4, if a matrix is annealed at, for example, 140 K and then cooled to 16 K, a quasilinear spectrum is obtained. If that sample is subsequently heated to any temperature less than 140 K, the spectrum loses its quasilinear character at the higher temperature, but re-cooling the matrix to 16 K restores the quasilinear structure, and the intensity ratio for the quasilines is virtually identical with that obtained prior to the heating step (Figures 4B and 4C). If, however, an annealed sample is subsequently heated to a temperature greater than the

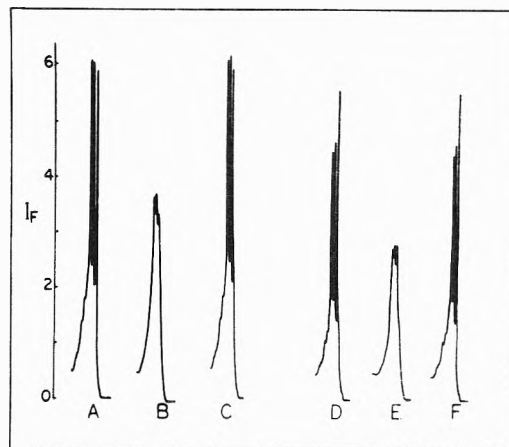


Figure 4. Preservation of “memory” in matrix-deposited spectra of benz[a]anthracene in *n*-heptane. Fluorescence band system at 384 nm recorded at: A, 16 K after annealing at 140 K; B, sample A at 100 K; C, after cooling B back to 16 K; D, 16 K after annealing at 150 K; E, sample D at 100 K; F, after cooling E back to 16 K.

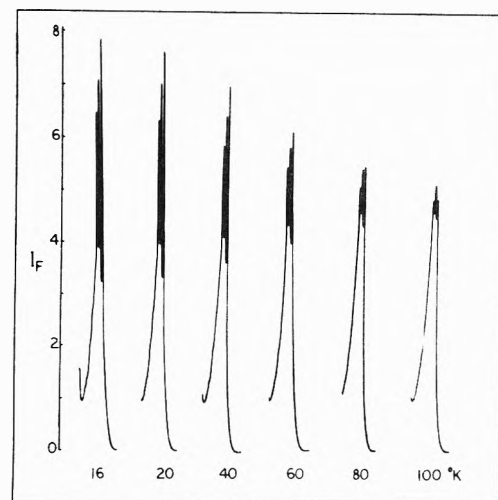


Figure 5. Dependence of quasiline intensity and structure for benz[a]anthracene in *n*-heptane matrices upon temperature.

original annealing temperature, and then cooled back to 16 K, a different quasilinear spectrum is obtained (compare Figures 4A and 4D). The “new” quasilinear spectrum is then unaffected by subsequent heating steps, so long as the “second” annealing temperature is never exceeded (cf. Figure 4D–F). Presumably the second annealing produces a different distribution of BaA microenvironments, which is “remembered” by the matrix so long as that annealing temperature is never exceeded in later annealing steps.

The intensity of quasilinear fluorescence is very sensitive to the temperature at which fluorescence of BaA is measured (Figure 5); this temperature dependence is virtually identical in frozen solutions and in vapor-deposited matrices. However, the total fluorescence intensity for BaA (quasilines + phonon wing) in vapor-deposited matrices remains virtually constant as the temperature is increased.

The results described herein imply the origins of quasilinear fluorescence of large organic molecules in frozen solutions and vapor-deposited *n*-alkane matrices to be the same. However, while annealing has a profound effect upon matrix-isolated Shpol'skii spectra, spectra obtained in frozen solutions are virtually unaffected by annealing. Accordingly, careful studies of the influence of annealing upon quasilinear fluorescence spectra obtained by matrix isolation may ultimately prove useful in probing conformational changes in solid *n*-alkanes (and other “Shpol'skii

solvents^{8,17}), as well as providing increased insight into the origins of quasilinear electronic spectra of complex molecules.

Acknowledgment. This work was supported in part by the Electric Power Research Institute (Contract 741011-RP-332-1) and the National Science Foundation (Grant MPS75-05364).

References and Notes

- (1) E. V. Shpol'skii, *Sov. Phys. Usp.*, **3**, 372 (1960); **5**, 522 (1962); **6**, 411 (1963).
- (2) K. K. Rebane, "Impurity Spectra of Solids", Plenum Press, New York, N.Y., 1970, p 35.
- (3) B. D'Albano and R. C. Powell, "Phonons and Resonances in Solids", Wiley, New York, N.Y., 1976, p 348.
- (4) J. L. Richards and S. A. Rice, *J. Chem. Phys.*, **54**, 2014 (1971).
- (5) E. V. Shpol'skii and T. N. Bolotnikova, *Pure Appl. Chem.*, **37**, 183 (1974).
- (6) C. Pfister, *Chem. Phys.*, **2**, 171, 181 (1973).
- (7) R. I. Personov, E. D. Godyaev, and O. N. Korotaev, *Sov. Phys. Solid State*, **13**, 88 (1971).
- (8) G. F. Kirkbright and C. G. de Lima, *Analyst*, **99**, 338 (1974).
- (9) I. S. Osad'ko, R. I. Personov, and E. V. Shpol'skii, *J. Lumin.*, **6**, 369 (1973).
- (10) B. Meyer and J. L. Metzger, *Spectrochim. Acta, Part A*, **28**, 1563 (1972).
- (11) B. Meyer, "Low Temperature Spectroscopy", American Elsevier, New York, N.Y., 1971, p 59.
- (12) E. L. Wehry, G. Mamantov, R. R. Kemmerer, H. O. Brotherton, and R. C. Stroupe in "Polynuclear Aromatic Hydrocarbons: Chemistry, Metabolism, and Carcinogenesis", R. Freudenthal and P. W. Jones, Ed., Raven Press, New York, N.Y., 1976, p 299.
- (13) G. Mamantov, E. L. Wehry, R. R. Kemmerer, and E. R. Hinton, *Anal. Chem.*, **49**, 86 (1977).
- (14) R. C. Stroupe, P. Tokousbalides, R. B. Dickinson, Jr., E. L. Wehry, and G. Mamantov, *Anal. Chem.*, **49**, 701 (1977).
- (15) N. A. Fenina, *Opt. Spectrosc.*, **20**, 428 (1966).
- (16) A. A. Schaerer, G. G. Bayle, and W. M. Mazee, *Recl. Trav. Chim. Pays-Bas*, **75**, 513 (1956).
- (17) G. F. Kirkbright and C. G. de Lima, *Chem. Phys. Lett.*, **37**, 165 (1976).

The Position of the Reaction Site and the Relative Reactivities of Simple Outer- and Inner-Sphere Electrode Reactions. The Reduction of Some Cr(III) Amine Complexes at Mercury Electrodes

Michael J. Weaver* and Thomas L. Satterberg

Department of Chemistry, Michigan State University, East Lansing, Michigan 48824 (Received February 7, 1977)

The electroreduction kinetics of a number of ammine and ethylenediamine complexes of Cr(III) have been studied at the mercury-aqueous interface as a function of the double layer structure in the absence and presence of specific anionic adsorption in order to identify the reduction mechanisms involved and to compare the reactivity patterns with those of previously studied aquo complexes. For most of the ammine complexes studied, anomalously large apparent transfer coefficients and rate responses to anionic specific adsorption were obtained which provide strong evidence that the outer-sphere transition state lies closer to the electrode than for the corresponding aquo reactants, and within the outer Helmholtz plane when this is formed by simple aquo cations. These differences are considered to be due to the presence of secondary hydration between the primary hydration layers surrounding the electrode and the aquo cations at their distance of closest approach, which is largely absent for the corresponding ammine cations. Such differences are in harmony with the markedly larger hydrated radii estimated for some aquo as compared with ammine complexes in bulk solution. The resulting greater enhancements of the electroreduction rate of Cr(III) ammine complexes at negative electrode potentials which arise from more favorable double layer work terms are considered to be responsible for the observed greater reluctance of acidopentaammine Cr(III) complexes to follow anion-bridged electroreduction pathways in comparison with the corresponding acidopentaquo systems.

Introduction

Studies of redox reactions involving Cr(III/II) couples in homogeneous solution have played a central role in characterizing the nature of inner-sphere electron-transfer reactions.¹ Although the nature of the analogous heterogeneous (i.e., electrochemical) electron-transfer reactions is much less well understood at the present time, kinetic studies of Cr(III/II) redox reactions at electrode surfaces also offer special opportunities for understanding the nature of these processes. In recent reports,^{2,3} experimental methods for distinguishing between certain inner- and outer-sphere electrode reactions have been described and applied to the reduction of a series of acidopentaquo Cr(III) complexes at mercury electrodes. An anion-bridged reduction mechanism was found to be rate determining for all the complexes that contained anions that are known to be significantly specifically adsorbed at the electrode

potentials concerned, and the very large differences in electroreduction rates observed between the various complexes were traced to variations in the intrinsic as well as the thermodynamic contributions⁴ to the free energy of activation.³ It is desirable to extend these studies to metal amine reactants. Such complexes are featured in the large majority of simple inorganic redox reactions that have been studied in homogeneous solution, and it is therefore of interest to scrutinize the behavior of typical members of this class at the well-defined mercury-aqueous interface, particularly in anticipation of kinetic studies involving metal amine complexes at solid electrode surfaces. Various Cr(III) ammine and ethylenediamine complexes, including those containing potential bridging anions, were chosen for this purpose. Such systems allow a direct comparison to be made with existing kinetic data for the corresponding pentaquo Cr(III) systems,³ and with

the kinetics of the corresponding homogeneous reactions that are known to follow inner-sphere pathways.¹ The results of these experiments form the basis of the present report.

Experimental Section

Materials. Analytical grade reagents were used without further purification. All solutions were prepared with water purified by a Milli-Q water purification system (Millipore Corp.). Synthesis of the Cr(III) ammine complexes followed standard published procedures. The double salt aquopentaamminechromium(III) ammonium nitrate⁵ was used as the starting point for the preparation of $\text{Cr}(\text{NH}_3)_5\text{OH}_2^{3+}$,⁵ $\text{Cr}(\text{NH}_3)_5\text{Br}^{2+}$,⁵ $\text{Cr}(\text{NH}_3)_5\text{Cl}^{2+}$,⁵ $\text{Cr}(\text{NH}_3)_5\text{NO}_3^{2+}$,⁵ $\text{Cr}(\text{NH}_3)_5\text{F}^{2+}$,⁶ $\text{Cr}(\text{NH}_3)_5\text{NCS}^{2+}$,⁷ and $\text{Cr}(\text{NH}_3)_5\text{N}_3^{2+}$.⁸ $\text{Cr}(\text{OH}_2)_5\text{NH}_3^{2+}$ was prepared as described in ref 9 and 10 and eluted from a Bio-Rad AG 50W-X8 cation column (H^+ form) using 3 M HClO_4 . The remaining complexes were gifts from Professor Fred Anson. All solid complexes were recrystallized from acidified water by precipitation as the perchlorate or chloride salts. A stock solution of sodium perchlorate used as supporting electrolyte was prepared from sodium carbonate and perchloric acid.

Apparatus and Techniques. Conventional two-compartment electrochemical cells (solution volume ca. 15 mL) were employed for the kinetic measurements. Solutions were deoxygenated by bubbling with prepurified nitrogen which had passed through a V(II) solution. A commercial calomel electrode (Sargent-Welch) was employed that contained saturated sodium chloride, but all potentials are reported with respect to the usual (KCl) saturated calomel electrode (SCE). Most heterogeneous electron transfer rates were determined using conventional dc polarography. This technique is especially suited to the present reactions which exhibit very slow reduction rates, allowing most of the systems to be scrutinized at potentials positive of -800 mV where the effect of the specific adsorption of simple nonreacting anions could be accurately evaluated. Polarographic data were obtained using a PAR 174 polarographic analyzer (Princeton Applied Research Corp.) and a Hewlett-Packard 7045A X-Y recorder. A dropping mercury electrode was used that had a natural drop time of ca. 4.5 s over the relevant potential range and a flow rate of 2.10 mg s^{-1} .

Kinetic data were extracted from the polarograms by means of the conventional Koutecky analysis,¹¹ without a correction for the possible effects of electrode sphericity (the inclusion of such a correction appears to be inappropriate under the experimental conditions employed here¹²). Cognizance was taken of possible corrections to the Koutecky analysis arising from the presence of anodic back-reactions. A procedure slightly modified from that outlined in the Appendix of ref 12 was employed due to the fact that most of the reactions studied here involve the back-reaction $\text{Cr}(\text{II}) - e^- \rightarrow \text{Cr}(\text{III})$ to yield $\text{Cr}(\text{OH}_2)_6^{3+}$ rather than the original Cr(III) complex. Essentially, the method consists of constructing cathodic and anodic Tafel lines using the cathodic polarograms and kinetic data for $\text{Cr}^{2+} - e^- \rightarrow \text{Cr}^{3+}$ obtained separately.^{3,12} The potential of intersection defined an "effective standard potential" E°_{eff} that was then employed in the normal analysis¹² in place of E° . This analysis led to the conclusion that anodic back reaction corrections were wholly negligible for each reaction under the conditions employed. A check that $\text{Cr}(\text{OH}_2)_6^{3+}$ was the only significant product of the reoxidation reaction on the polarographic time scale was obtained by inspecting the form of the reverse (anodic) scan for cyclic voltammograms obtained at a hanging mercury drop. For a few

reactions, polarographic maxima were encountered, whereupon data analysis was restricted to lower overpotentials and usually to the foot of the polarographic wave where the correction of the reduction current for concentration polarization is minimal. Kinetic data for the more rapidly reduced $\text{Cr}(\text{NH}_3)_5\text{Br}^{2+}$ complex were obtained in the laboratory of Professor Fred Anson by means of rapid chronocoulometry under computer control.¹²

The reactant concentrations were usually ca. 1 mM and the pH of the solution was kept at 1.8 or below to ensure that the amine and other basic ligands set free upon the formation of Cr(II) did not induce significant increases in the pH in the vicinity of the electrode surface. The reduction rates were found to be essentially independent of pH at least in the range 1–2 for solutions held at a fixed ionic strength. All measurements were made at 25.0 ± 0.1 °C using a Braun Melsungen circulating water bath for thermostatic control.

Results

In accordance with the approach taken in an earlier report,³ the reduction rates of each Cr(III) complex were examined as a function of electrode potential both in the absence and in the presence of anionic specific adsorption of the supporting electrolyte in order to identify the reduction mechanism as either inner- or outer-sphere.

Previously,³ acidified 1 M NaClO_4 (in which the effects of anionic specific adsorption can be neglected beyond ca. -700 mV) was used as the supporting electrolyte. However, a number of the present Cr(III) ammine complexes exhibit only a limited solubility in perchlorate media. Consequently, these complexes were examined in acidified 40 mM $\text{La}(\text{ClO}_4)_3$ and/or 40 mM LaCl_3 ; these electrolytes also exhibit only negligible anion specific adsorption under the experimental conditions employed. Double layer effects for lanthanum as well as sodium-based electrolytes have been extensively investigated for the outer-sphere reduction of Cr^{3+} and Eu^{3+} .¹²⁻¹⁴ The reduction rates for each complex measured at (or extrapolated to) -700 mV vs. SCE are given in Table I. Where the reduction kinetics could be examined both in 1 M NaClO_4 and 40 mM $\text{La}(\text{ClO}_4)_3$ or 40 mM LaCl_3 , the rate constants generally agreed to within ca. 10–25% (cf. ref 12).

The dependence of the apparent rate constant $k_{\text{app}}^{3,12}$ upon the electrode potential E for each complex was evaluated in the form of an apparent transfer coefficient $\alpha_{\text{app}} = -(2.3RT/F)(\partial \log k_{\text{app}}/\partial E)_\mu$ ^{3,12} at a constant electrolyte composition μ . This coefficient was then corrected for the presence of the diffuse layer to yield a "corrected transfer coefficient" α_{corr} (see Appendix II) given by

$$\alpha_{\text{corr}} = \left[\frac{\alpha_{\text{app}} - Z_r(\partial \phi_d/\partial E)_\mu}{1 - (\partial \phi_d/\partial E)_\mu} \right] \quad (1)$$

$(\partial \phi_d/\partial E)_\mu$ denotes the dependence of the average diffuse layer potential ϕ_d upon the electrode potential E at a constant electrolyte composition μ , and $Z_r F$ is the net charge residing on the reactant. For reaction sites at the outer Helmholtz plane³ (oHp) in the absence of discreteness-of-charge effects, α_{corr} can be identified with the intrinsic transfer coefficient α_1 .^{15,16} The experimental values of α_{app} , and values of α_{corr} obtained by applying eq 1 are listed in Table I for the Cr(III) complexes studied here and in previous work.^{3,17} The values of $(\partial \phi_d/\partial E)_\mu$ employed were obtained previously¹² from studies of double layer effects on the electroreduction kinetics of Cr^{3+} and Eu^{3+} (see Discussion section). As the (Tafel) plots of $\log k_{\text{app}}$ vs. E were found to be essentially linear¹⁸ and values of $(\partial \phi_d/\partial E)_\mu$ do not change markedly¹² over the

TABLE I: Summary of Kinetic Data for the Electroreduction of Various Cr(III) Complexes at Mercury Electrodes

Complex	K_{app}^{-700} , $\text{cm}^2 \text{s}^{-1}$	α_{app}^j	α_{corr}^k	Potential range $-E$, mV	$\frac{k_{app} \text{NH}_3^e}{k_{app} \text{OH}_3^{-700}}$	$\frac{\Delta \log k_{app} \text{Cr}^{3+}}{\Delta \log k_{app} \text{Cr}^{3+}}$	obsd m	calcd q	Indicated mechanism h
$\text{Cr}(\text{OH})_6^{3+}$, $^{3+}$, b	2.0^f , $1.8^g \times 10^{-5}$	0.58^f , 0.58^g	0.49^f , 0.49^g	700-1000		1.0	1.0		o.s.
$\text{Cr}(\text{OH})_5(\text{NH}_3)^{3+}$, a	4.5×10^{-5}	0.62^f	0.53^f	700-900		1.5 ± 0.2^n	0.99^n		o.s.
$\text{Cr}(\text{NH}_3)_2(\text{OH})_2^{3+}$, a	1.9×10^{-5}	0.70^f , 0.73^g	0.61^f , 0.64^g	700-900		2.0 ± 0.2^n	0.96^n	0.94^o	o.s.
$\text{Cr}(\text{NH}_3)_3(\text{OH})_2^{3+}$, a , d	6.2^f , 8.0^g , $h \times 10^{-6}$	0.73^f , 0.79^g , h	0.64^f , 0.70^g , h	700-950	0.31	2.3 ± 0.2^n	0.94^n	0.92^o , p	o.s.
$\text{Cr}(\text{NH}_3)_6^{3+}$, a	1.2×10^{-6} , g , h	0.84^g , h	0.76^g , h	800-950		2.3 ± 0.4^p	0.89^o		o.s.
$\text{Cr}(\text{OH})_5(\text{F})_2^{3+}$, c	1.3^f , $1.1^g \times 10^{-7}$	0.59^f , 0.57^g	0.54^f , 0.54^g	800-1250		0.55 ± 0.1^n	0.58^n		o.s.
$\text{Cr}(\text{NH}_3)_5(\text{F})_2^{3+}$, c	$\sim 4 \times 10^{-8}$	$\sim 0.65^f$	$\sim 0.60^f$	950-1150	0.31				o.s.
$\text{Cr}(\text{OH})_5(\text{Cl})_2^{3+}$, c	6.5×10^{-3}	0.37^f	0.31^f	600-900		-0.1 ± 0.1^n	0.68^n		i.s.
$\text{Cr}(\text{NH}_3)_5(\text{Cl})_2^{3+}$, a	5.5^f , $7.8^g \times 10^{-5}$	0.49^f , 0.54^g	0.43^f , 0.48^g	650-950	0.0085	$1.0-2.0^n$	$0.6-1.0^p$		o.s./i.s.
$\text{Cr}(\text{OH})_5(\text{Br})_2^{3+}$, c	13^f	0.43^f	$\sim 0.37^f$	200-450					i.s.
$\text{Cr}(\text{NH}_3)_5(\text{Br})_2^{3+}$, a	2.6×10^{-7}	0.40^f	0.34^f	500-700	0.002	-0.2 ± 0.1^n	0.66^n		i.s.
$\text{Cr}(\text{OH})_5(\text{N}_3)^{3+}$, c	1.05×10^{-4}	0.42^f	0.36^f	650-1100		-0.1 ± 0.05^n	0.66^n		i.s.
$\text{Cr}(\text{NH}_3)_5(\text{N}_3)^{3+}$, a	6×10^{-6} , 1.0×10^{-5} , g	0.56^f , 0.58^g	0.50^f , 0.53^g	750-900	0.055	$1.3-1.8^n$	0.60^n		o.s./i.s.
$\text{Cr}(\text{OH})_5(\text{NCS})_2^{3+}$, c	3.2×10^{-3}	0.38^f	0.32^f	650-900		-0.2 ± 0.1^n	0.67^n		i.s.
$\text{Cr}(\text{NH}_3)_5(\text{NCS})_2^{3+}$, a	5.5×10^{-5} , h	0.45^h	0.39^h	650-850	~ 0.015	-0.4 ± 0.2^p	0.64^p		i.s.
$\text{Cr}(\text{OH})_5(\text{NO}_3)^{3+}$, c	4.6×10^{-4}	0.41^f	0.35^f	700-1000		-0.1 ± 0.1^n	0.66^n		i.s.
$\text{Cr}(\text{NH}_3)_5(\text{NO}_3)^{3+}$, a	8.5×10^{-5} , 1.0×10^{-4} , g	0.55^f , 0.58^g	0.49^f , 0.53^g	600-800	0.18	1.0 ± 0.2^n	0.8 ± 0.2^p		o.s.
$\text{Cr}(\text{en})_3^{3+}$, c	1.1×10^{-6}	0.90^f	0.82^f	750-900		0.9 ± 0.1^n	0.87^n		o.s.
$\text{c-Cr}(\text{en})_2(\text{Cl})_2^{3+}$, a	4.2×10^{-4}	0.61^f	0.60^f	600-750		0 ± 0.1^n	0.16^n		i.s.
$\text{c-Cr}(\text{en})_2(\text{N}_3)_2^{3+}$, a	4.9×10^{-3}	0.56^f	0.54^f	550-650		0 ± 0.1^n	0.18^n		i.s.
$\text{c-Cr}(\text{en})_2(\text{NCS})_2^{3+}$, d	1.3×10^{-3}								i.s.

^a Data obtained in this work; $T = 25^\circ\text{C}$. ^b Data from ref. ¹² and ¹³; extrapolated to $T = 25^\circ\text{C}$. ^c Data from ref. ¹⁷. ^e k_{app} is apparent rate constant¹² evaluated at -700 mV vs. SCE. ^f Determined in 1 M NaClO_4 (acidified to pH $\sim 1.5-2$ with HClO_4). ^g Determined in $40\text{ mM La}(\text{ClO}_4)_3$ (acidified to pH $\sim 1.5-2$ with HClO_4). ^h Determined in 40 mM LaCl_3 (acidified to pH $\sim 1.5-2$ with HCl). ⁱ Determined in $0.32\text{ M Na}_2\text{SO}_4 + 0.031\text{ M NaHSO}_4$ (pH 2.2). ^j Defined by $\alpha_{app} = -(2.3RT/F)(\Delta \log k_{app}/\Delta E)_\mu$. See text and ref. ¹². ^k Determined from α_{app} using eq. 1. For $40\text{ mM La}(\text{ClO}_4)_3$ and 40 mM LaCl_3 ($\partial \phi_2/\partial E)_\mu$ was estimated from Gouy-Chapman-Stern theory. For 1 M NaClO_4 , experimental estimates of $(\partial \phi_2/\partial E)_\mu$ were employed as described in ref. 12. ^l Ratio of reduction rate for $\text{Cr}(\text{III})(\text{NH}_3)_6^{3+}$ compared with corresponding $\text{Cr}(\text{III})(\text{OH})_6^{3+}$ complexes at -700 mV vs. SCE. Where possible, data in 1 M NaClO_4 employed; otherwise $40\text{ mM La}(\text{ClO}_4)_3$ or 40 mM LaCl_3 . ^m Ratio of change in k_{app} for reduction of given complex compared to change in k_{app} for $\text{Cr}(\text{OH})_6^{3+}$ reduction brought about by specific ionic adsorption at a constant ionic strength. See text. ⁿ Coefficient determined for $(1-x)\text{ M NaClO}_4 + x\text{ M NaI}$ with varying x . ^o Coefficient determined for $(40-x)\text{ mM La}(\text{ClO}_4)_3 + (100-x)\text{ mM NaClO}_4 + x\text{ mM NaI}$ with varying x . ^p Coefficient determined for $(40-x)\text{ mM LaX}_3 + (180-x)\text{ mM NaX} + x\text{ mM NaBr}$ for $\text{X} = \text{ClO}_4^-$ or Cl^- with $x = 0, 180\text{ mM}$. ^q Calculated from eq. 3. ^r o.s. denotes outer-sphere mechanism; i.s. denotes inner-sphere (anion-bridged) mechanism. o.s./i.s. denotes probable mixed mechanism. See text.

relatively limited potential range investigated for each complex, single values of α_{app} and α_{corr} are listed for each complex in a given supporting electrolyte.

Inspection of Table I reveals that, as previously noted,^{3,12,18} the values of α_{corr} for $\text{Cr}(\text{OH}_2)_6^{3+}$ and $\text{Cr}(\text{OH}_2)_5\text{F}^{2+}$ that are thought to reduce via outer-sphere mechanisms are close to 0.5, which is the expected result for simple reactions with approximately symmetrical free energy barriers to electron transfer ($\alpha_1 \approx 0.5$) and reaction sites close to the oHp such that $\alpha_{\text{corr}} \approx \alpha_1$. However, for the mixed aquoammine complexes $\text{Cr}(\text{NH}_3)_x(\text{OH}_2)_{6-x}^{3+}$ which also are expected to undergo outer-sphere electroreduction and hence exhibit similar values of α_{corr} , monotonically increasing values of α_{corr} in the range 0.49–0.76 were observed as x increased from zero to six. A high value of α_{corr} (0.82) was also observed for the reduction of $\text{Cr}(\text{en})_3^{3+}$.

As has been previously noted,³ for the reduction of $\text{Cr}(\text{CH}_2)_5\text{X}^{2+}$ where $\text{X} = \text{Cl}^-, \text{Br}^-, \text{N}_3^-, \text{NCS}^-, \text{NO}_3^-$, the values of α_{app} and hence α_{corr} (Table I) are consistently and markedly less than 0.5. This result has been taken as evidence that these reductions proceed via dominating inner-sphere pathways involving ligand bridging by these anions.³ However, for the reduction of the corresponding $\text{Cr}(\text{NH}_3)_5\text{X}^{2+}$ complexes studied in the present work, values of α_{corr} that are sizably below 0.5 were only observed for $\text{X}^- = \text{Br}^-$ and NCS^- (0.34 and 0.39), the remaining complexes yielding $\alpha_{\text{corr}} \geq 0.5$ (Table I).

Such differences in the electroreduction behavior of otherwise analogous pentaquo and pentaammine Cr(III) complexes were also noted for the responses of the reaction rate to the addition of specifically adsorbed halide ions at a constant total ionic strength. The advantages of using supporting electrolytes of high constant ionic strength for these measurements have been previously discussed.¹³ For complexes that were sufficiently soluble in perchlorate and iodide media, the reduction rate was measured in the series of acidified electrolytes $(1-a) \text{ M NaClO}_4 + a \text{ M NaI}$ with $a = 0, 0.02, 0.05, 0.1, 0.33 \text{ M}$. Some complexes were additionally scrutinized in the electrolytes $0.04 \text{ M La}(\text{ClO}_4)_3 + (0.1-b) \text{ M NaClO}_4 + b \text{ M NaI}$ with $b = 0, 0.01, 0.05, 0.1 \text{ M}$; and/or $0.04 \text{ M La}(\text{ClO}_4)_3 + (0.18-c) \text{ M NaClO}_4 + c \text{ M NaBr}$ with $c = 0, 0.18 \text{ M}$. The appropriate double layer parameters for all these electrolytes have been previously determined.¹³ The study of some complexes was limited for reasons of solute solubility to the lanthanum-based electrolytes with LaCl_3 replacing $\text{La}(\text{ClO}_4)_3$. These two electrolytes have practically identical double layer properties at the electrode potentials of interest in this study,¹² and essentially identical kinetic behavior was observed for complexes which could be scrutinized in both electrolytes.

Previously,^{3,13} the change in $\log k_{\text{app}}$ at constant electrode potential, $(\Delta \log k_{\text{app}})_E$, for the outer-sphere electroreduction of various aquo complexes brought about by the addition of specifically adsorbed halide anions were found to be in accord with the relation^{3,13}

$$2.3(\Delta \log k_{\text{app}})_E = (\alpha_{\text{corr}} - Z_r)f(\Delta\phi_d)_E \quad (2)$$

where $f = F/RT$. $(\Delta\phi_d)_E$ is the change in the average potential at the reaction site which was assumed to be at the oHp (see Discussion section). For the pentaquo reactants $\text{Cr}(\text{OH}_2)_5\text{F}^{2+}$ and $\text{Cr}(\text{OH}_2)_5\text{OSO}_3^+$ as well as the tripositive reactants $\text{Cr}(\text{OH}_2)_6^{3+}$ and $\text{Eu}_{\text{aquo}}^{3+}$, the variations in $(\Delta \log k_{\text{app}})_E$ between these reactant systems could be simply accounted for by variations in Z_r and α_{corr} , the latter quantity being determined from eq 1.

It was therefore convenient to test the applicability of eq 2 in describing the effects of specific ionic adsorption

upon the reduction rates of the present complexes by comparing the experimental ratios of these rate changes to those observed for the "parent" $\text{Cr}(\text{OH}_2)_6^{3+}$ reduction at the same electrode potential E , i.e., $(\Delta \log k_{\text{app}}/\Delta \log k_{\text{app}}^{\text{Cr}^{3+}})_E^{\text{obsd}}$, with the corresponding calculated ratios $(\Delta \log k_{\text{app}}/\Delta \log k_{\text{app}}^{\text{Cr}^{3+}})_E^{\text{calcd}}$ expected on the basis of eq 2. This latter ratio was obtained from

$$\left(\frac{\Delta \log k_{\text{app}}}{\Delta \log k_{\text{app}}^{\text{Cr}^{3+}}} \right)_E^{\text{calcd}} = \frac{(\alpha_{\text{corr}} - Z_r)}{(\alpha_{\text{corr}} - Z_r)^{\text{Cr}^{3+}}} \quad (3)$$

where the numerator and the denominator on the right-hand side are $(\alpha_{\text{corr}} - Z_r)$ for the complex under consideration and for $\text{Cr}(\text{OH}_2)_6^{3+}$ reduction, respectively. For most complexes $(\Delta \log k_{\text{app}}/\Delta \log k_{\text{app}}^{\text{Cr}^{3+}})_E^{\text{obsd}}$ was found to be approximately independent of the extent of anion adsorption and the electrode potential, so that the extent of anion catalysis can be represented by a single such coefficient in Table I. However, for the reduction of $\text{Cr}(\text{NH}_3)_5\text{N}_3^{2+}$ and particularly $\text{Cr}(\text{NH}_3)_5\text{Cl}^{2+}$, a marked increase in this coefficient was observed with increasing overpotential (Table I).

Inspection of Table I reveals that there are marked discrepancies between $(\Delta \log k_{\text{app}}/\Delta \log k_{\text{app}}^{\text{Cr}^{3+}})_E^{\text{calcd}}$ and $(\Delta \log k_{\text{app}}/\Delta \log k_{\text{app}}^{\text{Cr}^{3+}})_E^{\text{obsd}}$ for most of the systems listed. The qualitative discrepancies between these coefficients (i.e., the rate decreases observed upon anion adsorption) observed for the reduction of $\text{Cr}(\text{OH}_2)_5\text{X}^{2+}$ where $\text{X}^- = \text{Cl}^-, \text{Br}^-, \text{N}_3^-, \text{NCS}^-,$ and NO_3^- have previously been taken as further strong evidence for the presence of dominating anion-bridged pathways^{2,3} for these reactions. Of the $\text{Cr}(\text{NH}_3)_5\text{X}^{2+}$ complexes studied in the present work, such negative (or essentially zero) values of $(\Delta \log k_{\text{app}}/\Delta \log k_{\text{app}}^{\text{Cr}^{3+}})_E^{\text{obsd}}$ were only observed for $\text{X}^- = \text{Br}^-$ and NCS^- . In contrast, for the remaining acidopentaammine complexes where $\text{X}^- = \text{Cl}^-, \text{N}_3^-, \text{NO}_3^-$ (excepting $\text{X}^- = \text{F}^-$ for which anion adsorption effects could not be conveniently studied due to the very negative reduction potentials observed for this system), values of this coefficient were obtained which were markedly larger than $(\Delta \log k_{\text{app}}/\Delta \log k_{\text{app}}^{\text{Cr}^{3+}})_E^{\text{calcd}}$. Similarly, the observed coefficients for the reduction of the $\text{Cr}(\text{NH}_3)_x(\text{OH}_2)_{6-x}^{3+}$ complexes are markedly larger than the calculated coefficients and increasingly so for higher values of x (Table I). This result is illustrated in more detail in Figures 1 and 2 for the reduction of $\text{Cr}(\text{NH}_3)_5\text{OH}_2^{3+}$ in mixed $\text{NaClO}_4/\text{NaI}$ electrolytes. Figure 1 contrasts the experimental $\log k_{\text{app}}-E$ plots for the iodide-containing solutions (solid points) with the corresponding plots that are predicted from eq 3 in conjunction with the experimental data for $\text{Cr}(\text{OH}_2)_6^{3+}$ reduction previously gathered in the same electrolytes¹³ (dashed lines). In Figure 2, it is seen that the increases in $\log k_{\text{app}}$ for the iodide-containing solutions taken with respect to 1 M NaClO_4 at a series of constant electrode potentials, $(\Delta \log k_{\text{app}})_E$, plotted against the corresponding values observed for $\text{Cr}(\text{OH}_2)_6^{3+}$ reduction¹³ fall on a common straight line of slope, $(\Delta \log k_{\text{app}}/\Delta \log k_{\text{app}}^{\text{Cr}^{3+}})_E^{\text{obsd}} = 2.3$, which passes through the origin and is essentially independent of the electrode potential and the extent of iodide adsorption.

For the reduction of aquo- and acidopentaammine Cr(III) complexes, values of $(\Delta \log k_{\text{app}}/\Delta \log k_{\text{app}}^{\text{Cr}^{3+}})_E^{\text{obsd}}$ were observed that were ca. 1.5 to 4 times higher than predicted by eq 3. In contrast, good agreement was obtained between these observed and calculated coefficients for $\text{Cr}(\text{OH}_2)_5\text{F}^{2+}$ and $\text{Cr}(\text{en})_3^{3+}$ reduction. The other ethylenediamine complexes studied in the present work, $c\text{-Cr}(\text{en})_2\text{Cl}_2^+$ and $c\text{-Cr}(\text{en})_2(\text{N}_3)_2^+$, both yielded essentially zero values of $(\Delta \log k_{\text{app}}/\Delta \log k_{\text{app}}^{\text{Cr}^{3+}})_E^{\text{obsd}}$, although

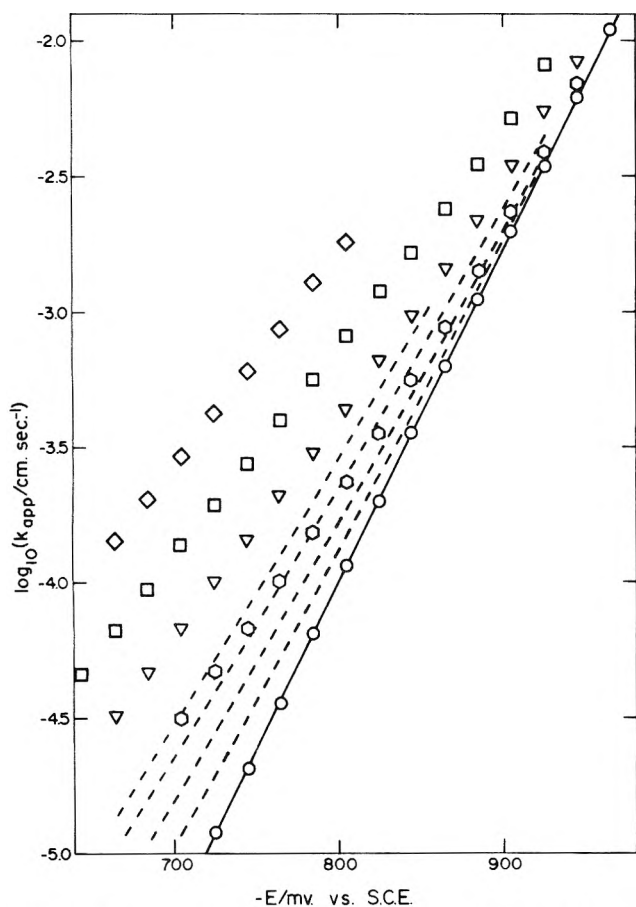


Figure 1. Comparison of the effect of specific iodide adsorption upon rate-potential plots for the electroreduction of $\text{Cr}(\text{NH}_3)_5\text{OH}_2^{3+}$ and $\text{Cr}(\text{OH}_2)_6^{3+}$ in mixed $\text{NaClO}_4 + \text{NaI}$ supporting electrolytes. k_{app} is the apparent electrochemical rate constant.^{3,12} Symbols are experimental points for $\text{Cr}(\text{NH}_3)_5\text{OH}_2^{3+}$ reduction in $(1-x)\text{M NaClO}_4 + x\text{M NaI}$ with $x = 0$ (\circ), 0.02 (\circ), 0.05 (∇), 0.10 (\square), 0.33 (\diamond). The dashed lines are the plots for the iodide-containing electrolytes predicted from eq 3 by using the experimental points for 1M NaClO_4 in conjunction with the experimental data previously gathered for $\text{Cr}(\text{OH}_2)_6^{3+}$ reduction in the same electrolytes.¹³

relatively small calculated values of this coefficient are predicted in view of the single positive charge carried by these complexes (eq 3).

In contrast to the marked disagreement of the observed rate responses for most complexes with the predictions of eq 2 and 3 in the presence of specific anion adsorption of the supporting electrolyte, good agreement was consistently obtained between the experimental rate responses of each complex to variations in the ionic strength of the supporting electrolyte in the absence of specific ionic adsorption and the responses calculated from eq 2. This point is illustrated for $\text{Cr}(\text{NH}_3)_5\text{OH}_2^{3+}$ reduction in Figure 3 where a comparison is made between the observed rate-potential plots for 1, 0.5, and 0.3 M NaClO_4 (experimental points) and the corresponding plots for 0.5 and 0.3 M NaClO_4 that were calculated with respect to the 1 M NaClO_4 plot using eq 3 and the data for $\text{Cr}(\text{OH}_2)_6^{3+}$ reduction obtained in these electrolytes¹² (dashed lines).

Qualitatively similar but less detailed results for some of these systems have been independently obtained by Anson et al.¹⁹ using normal pulse polarography, although they obtained quantitatively different rate responses to the addition of adsorbing iodide ions. This may be partly due to the restriction of their kinetic data to more negative potentials (ca. -900 mV) where large changes in the electrolyte composition were required in order to induce significant iodide specific adsorption.

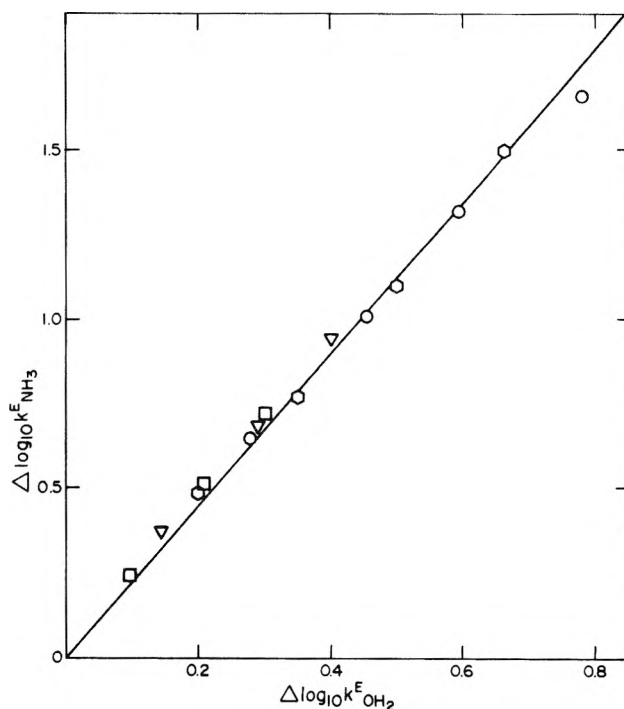


Figure 2. The increase in $\log k_{\text{app}}$ at a series of constant electrode potentials for $\text{Cr}(\text{NH}_3)_5\text{OH}_2^{3+}$ reduction, $\Delta \log k_{\text{NH}_3}^E$, plotted against the corresponding quantity for $\text{Cr}(\text{OH}_2)_6^{3+}$ reduction, $\Delta \log k_{\text{OH}_2}^E$, brought about by the addition of NaI to NaClO_4 at a constant total ionic strength of 1M . From data in Figure 1 and ref 13: -700 mV (\circ), -740 mV (∇), -780 mV (\square). The solid line has a slope of 2.26 and passes through the origin.

Discussion

The Position of the Reaction Site for Aquoammine Cr(III) Reactants. The sizable and systematic differences in the transfer coefficients and the extent of catalysis by adsorbed anions for the present acidopentaammine and aquoammine $\text{Cr}(\text{III})$ complexes compared with the hexaquo and acidopentaquo $\text{Cr}(\text{III})$ complexes that were previously scrutinized^{2,3,12-14} suggest that significant differences in the reaction site and/or mechanism attend the electroreduction of these otherwise similar reactants. In particular, the failure of the diffuse layer analysis embodied in eq 1-3 to account for the observed double layer effects in the aquoammine series $\text{Cr}(\text{NH}_3)_x(\text{OH}_2)_{6-x}^{3+}$ as x varies from zero to six suggests that the reaction sites for these complexes that are all expected to exhibit outer-sphere electroreduction may differ significantly from the oHp.

Irrespective of the reaction pathway, the double layer effects upon the apparent transfer coefficient α_{app} can generally be treated through the following "quasi-thermodynamic" relation^{3,16} for a one-electron reduction:

$$\alpha_{\text{app}} = \frac{\alpha_{\text{I}}}{F} \left(\frac{\partial \Delta G_{\text{AD}}^{\circ}}{\partial E} \right) + \frac{(1 - \alpha_{\text{I}})}{F} \left(\frac{\partial \Delta G_{\text{AR}}^{\circ}}{\partial E} \right) + \alpha_{\text{I}} \quad (4)$$

where $\Delta G_{\text{AR}}^{\circ}$ and $\Delta G_{\text{AD}}^{\circ}$ are the standard free energies of adsorption of the reactant and product in the configurations immediately prior to, and following electron transfer, respectively. Equation 4 is generally applicable inasmuch as it allows for the presence of interactions of a chemical as well as an electrostatic nature between the reactant and the double layer region. However, for the aquo and ammine complexes, only electrostatic interactions are expected which allows eq 4 to be written in the form:

$$\alpha_{\text{app}} = \alpha_{\text{I}} - (\alpha_{\text{I}} - Z_{\text{r}})(\partial \phi_{\text{r}} / \partial E) \quad (5)$$

TABLE II

Complex	$(\partial\phi_r/\partial E)_\mu^a$	$(\partial\phi_r/\partial q^m)_\mu,^b$ $\mu F^{-1} \text{ cm}^2 \times 10^3$	$(\partial\phi_r/\partial q')_E,^c$ $\mu F^{-1} \text{ cm}^2 \times 10^3$
$\text{Cr}(\text{OH}_2)_6^{3+}$	0.035 ^{d,e}	1.7 ^{d,e}	1.8, ^g 1.6, ^h 1.7 ⁱ
$\text{Cr}(\text{OH}_2)_5\text{NH}_3^{3+}$	0.05 ^d	2.4 ^d	2.7 ^g
c- $\text{Cr}(\text{NH}_3)_4(\text{OH}_2)_2^{3+}$	0.08, ^d 0.09 ^e	3.8, ^d 4.5 ^e	3.6, ^g 3.5 ^h
$\text{Cr}(\text{NH}_3)_5\text{OH}_2^{3+}$	0.09, ^d 0.115 ^{e,f}	4.3, ^d 5.8 ^{e,f}	4.1, ^g 4.8, ^h 3.9 ⁱ
$\text{Cr}(\text{NH}_3)_6^{3+}$	0.135 ^{e,f}	6.8 ^{e,f}	6.4 ^h
$\text{Cr}(\text{en})_3^{3+}$	0.16 ^d	7.6 ^d	1.6 ^g
GCS prediction ^j	0.055-0.085 ^d		3.1-4.0 ^{d,g}
	0.025-0.045 ^e		1.5-2.3 ^{e,h}

^a Determined from eq 5 assuming $Z_e = 3$, $\alpha_1 = 0.5$ (see text); values of α_{app} from Table I. ^b Determined from $(\partial\phi_r/\partial q^m)_\mu = (1/C)(\partial\phi_r/\partial E)_\mu$, where C is the average differential electrode capacitance in the appropriate electrolyte over the potential range where α_{app} was determined (C determined from charge-potential data in ref 12). q^m is the excess electrode charge density. ^c Determined from eq 7 using the responses in reduction rate, $(\Delta \log k_{\text{app}})_E$, brought about by a charge density q'_x of specifically adsorbed X^- anions at a constant ionic strength. q' is the net change in charge density at the electrode surface at a given electrode potential resulting from X^- specific adsorption which equals $(q'_x + \Delta q^m)_E$. Data for $\text{Cr}(\text{OH}_2)_6^{3+}$ reduction and X^- specific adsorption taken from ref 13. ^d 1 M NaClO_4 . ^e 40 mM $\text{La}(\text{ClO}_4)_3$ or 40 mM $\text{La}(\text{ClO}_4)_3 + 100$ mM NaClO_4 . ^f 40 mM LaCl_3 . ^g $(1-x)$ M $\text{NaClO}_4 + x$ M NaI . ^h $(40-x)$ mM $\text{La}(\text{ClO}_4)_3 + (100-x)$ mM $\text{NaClO}_4 + x$ mM NaI . ⁱ $(40-x)$ mM $\text{LaX}_3 + (180-x)$ mM $\text{NaX} + x$ mM NaBr for $X = \text{ClO}_4^-$ or Cl^- . ^j Predicted coefficients using the Gouy-Chapman-Stern theory²³ and assuming that the reaction site lies at the oHp, i.e., $\phi_r = \phi_d$. Limits of values given are for the range $6 < -q^m < 11 \mu\text{C cm}^{-2}$ (see Table II of ref 12).

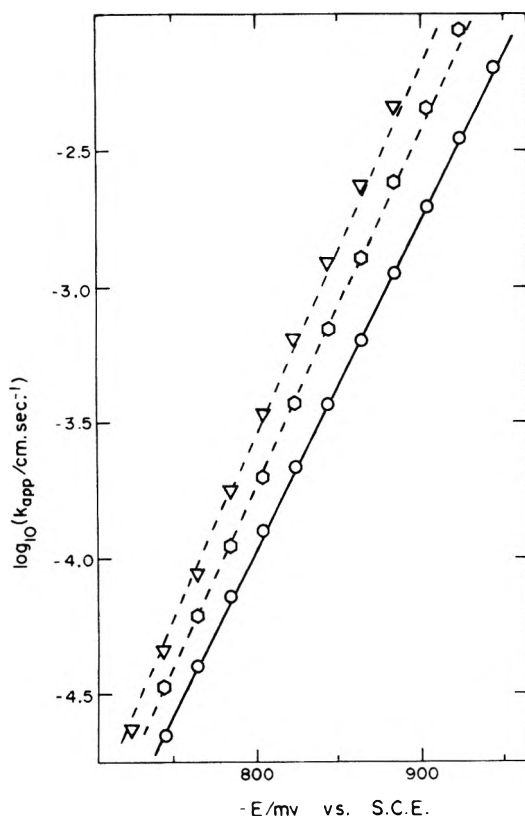


Figure 3. Comparison of the response of the rate-potential plots for $\text{Cr}(\text{NH}_3)_5\text{OH}_2^{3+}$ and $\text{Cr}(\text{OH}_2)_6^{3+}$ reduction to changes in the ionic strength in NaClO_4 electrolytes. Symbols are experimental points for $\text{Cr}(\text{NH}_3)_5\text{OH}_2^{3+}$ reduction in 1 M (O), 0.5 M (○), and 0.3 M NaClO_4 (▽). The dashed lines are the rate-potential plots constructed for 0.5 and 0.3 M NaClO_4 by calculating the rate increases $(\Delta \log k_{\text{app}})_E$ with respect to the experimental data for 1 M NaClO_4 (solid line) by using eq 3 and the corresponding experimental data for $\text{Cr}(\text{OH}_2)_6^{3+}$ reduction.¹²

as $\Delta G^\circ_{\text{Ar}} = Z_r F \phi_r$ and $\Delta G^\circ_{\text{Ap}} = (Z_r - 1) F \phi_r$, where ϕ_r is the average potential at the reaction plane, and $Z_r F$ is the electrostatic charge on the reactant.

Similarly, changes in the apparent rate constant at a constant electrode potential, $(\Delta \log k_{\text{app}})_E$, induced by changes in the electrolyte composition can be generally written as^{3,16}

$$(\Delta \log k_{\text{app}})_E = -\frac{1}{2.3RT} \{ \alpha_1 [\Delta(\Delta G^\circ_{\text{Ap}})_E - \Delta(\Delta G^\circ_{\text{Ar}})_E] + \Delta(\Delta G^\circ_{\text{Ar}})_E \} \quad (6)$$

which for $\Delta(\Delta G^\circ_{\text{Ar}})_E = Z_r F(\Delta\phi_r)_E$, $\Delta(\Delta G^\circ_{\text{Ap}})_E = F(Z_r - 1)(\Delta\phi_r)_E$ becomes (cf. eq 9 of ref 3)

$$2.3(\Delta \log k_{\text{app}})_E = f(\alpha_1 - Z_r)(\Delta\phi_r)_E \quad (7)$$

Equations 1 and 2 employed above to analyze the kinetic data are therefore special cases of eq 5 and 7 that only fully account for the double layer effects when the reaction site lies at the oHp. It therefore seems likely that the behavioral differences between the $\text{Cr}(\text{III})$ aquo and ammine complexes have their origin in differing values of ϕ_r sensed by these reactants. As there is good reason to expect that α_1 will be close to 0.50 for simple electron transfer reactions,²⁰ both eq 5 and 7 can in principle be used to locate the position of the reaction site within the double layer region. The effects of varying the electrode potential (and hence the electrode charge q^m), the ionic strength μ in the absence of specific adsorption, and the extent of specific anionic adsorption q'_x at a constant ionic strength upon the electroreduction rates of $\text{Cr}(\text{OH}_2)_6^{3+}$ and Eu^{3+} were previously analyzed using eq 1 and 2.^{12,13} As predicted by the simple Frumkin treatment,²² the derived quantities $(\partial\phi_d/\partial q^m)_\mu$ and $(\partial\phi_d/\partial q')_E$ (where $q' = q'_x + \Delta q^m$ is the net change in charge density at the metal surface resulting from the specific adsorption of X^- at a given electrode potential E) were found to be very similar for these two reactions in both 40 mM lanthanum perchlorate and 1 M sodium perchlorate-based electrolytes for the added anions $X^- = \text{I}^-$ and Br^- .^{12,13}

Values of $(\partial\phi_r/\partial E)_\mu$, $(\partial\phi_r/\partial q^m)_\mu$, and $(\partial\phi_r/\partial q')_E$ obtained from eq 5 and 7 for the series of complexes $\text{Cr}(\text{NH}_3)_x(\text{OH}_2)_{6-x}^{3+}$ and for $\text{Cr}(\text{en})_3^{3+}$ are summarized in Table II. The listed values of $(\partial\phi_r/\partial E)_\mu$ were obtained from the relation $(\partial\phi_r/\partial q^m)_\mu = (1/C_{\text{dl}})(\partial\phi_r/\partial E)_\mu$, where C_{dl} is the average differential electrode capacitance over the relevant potential range in the appropriate electrolyte.¹² The values of $(\partial\phi_r/\partial q')_E$ in Table II were obtained from eq 7 using the experimental values of $(\Delta \log k_{\text{app}}/\Delta \log k_{\text{app}}^{\text{Cr}^{3+}})_E^{\text{obsd}}$ given in Table I coupled with the experimental adsorption data for I^- and Br^- given in ref 13. Inspection of Table II reveals that considerable increases in each of the coefficients $(\partial\phi_r/\partial E)_\mu$, $(\partial\phi_r/\partial q^m)_\mu$, and $(\partial\phi_r/\partial q')_E$ are obtained as x increases from zero to six in the series $\text{Cr}(\text{NH}_3)_x(\text{OH}_2)_{6-x}^{3+}$. Nevertheless, the corresponding values of $(\partial\phi_r/\partial q^m)_\mu$ and $(\partial\phi_r/\partial q')_E$ for each member of this series are consistently similar.

These marked increases in $(\partial\phi_r/\partial q^m)_\mu$ and $(\partial\phi_r/\partial q')_E$ can most simply be explained by progressive change in the

position of the reaction site toward the electrode surface as the number of ammine ligands bound to the Cr(III) center are increased. In the lanthanum-based electrolytes, the reasonable agreement of these coefficients for Cr(OH₂)₆³⁺ (and Eu_{aq}³⁺) reduction with the corresponding values of $(\partial\phi_d/\partial q)$ calculated from the Gouy-Chapman-Stern (GCS) theory²³ (Table II) has been taken as good evidence that the reaction site for these reactants in La³⁺ electrolytes lies at the oHp.^{12,13} Such a circumstance is expected as the position of the oHp at potentials negative of the pzc will be determined by a hydrated rather than the bare ionic radius of the supporting electrolyte cation,²⁴⁻²⁶ and the hydrated radii of Cr³⁺ and La³⁺ are probably very similar^{27,28} (see below). Consequently, the reduction of the Cr(III) ammine complexes probably takes place inside the oHp in these electrolytes.

The interpretation of the results obtained in sodium-based electrolytes is less clearcut. Thus the experimental values of $(\partial\phi_r/\partial q^m)_\mu$ and $(\partial\phi_r/\partial q)_E$ for Cr(OH₂)₆³⁺ (and Eu_{aq}³⁺^{12,13}) reduction are uniformly a factor of 1.5–2 less than the GCS predictions in 1 M NaClO₄-based electrolytes (Table II) which could be taken as evidence that the reaction site lies significantly outside the oHp. Such a notion is supported by the likelihood that the effective hydrated radius of Cr³⁺ is expected to be somewhat larger than that of Na⁺ (e.g., the hydrated radii r_h given by Nightingale^{28a} are $r_h(\text{Cr}^{3+}) = 4.61 \text{ \AA}$, $r_h(\text{Na}^+) = 3.58 \text{ \AA}$). However, similar discrepancies have also been observed between the corresponding experimental and GCS values of $(\partial\phi_r/\partial\mu)_E$ in the absence of specific ionic adsorption, and the magnitude of $(\partial\phi_r/\partial\mu)_E$ is expected to be insensitive to the position of the reaction site if this lies in the diffuse layer within the vicinity of the oHp.¹² Also, we have observed that the values of α_{app} for Cr(OH₂)₆³⁺ reduction are essentially identical (± 1 –2%) in 1 M LiClO₄, NaClO₄, and NH₄ClO₄. As the hydrated radii of these three cations are significantly different (e.g., $r_h(\text{Li}^+) = 3.82 \text{ \AA}$, $r_h(\text{Na}^+) = 3.58 \text{ \AA}$, $r_h(\text{NH}_4^+) = 3.31 \text{ \AA}$ ^{28a}), such essentially identical discrepancies between the experimental and GCS values of $(\partial\phi_r/\partial E)_\mu$ for these three systems are unlikely to be due to the presence of a reaction site outside the oHp. Therefore, we favor the explanation given previously^{12,13} which attributes the major source of this discrepancy to the failure in the GCS theory at the high (1 M) ionic strengths employed. (The GCS theory is expected to overestimate ϕ_d under these conditions.¹²) Therefore we regard the experimental values of $(\partial\phi_r/\partial E)_\mu$ given in ref 12 for NaClO₄ electrolytes as approximating the true diffuse layer parameters $(\partial\phi_d/\partial E)_\mu$ which supports the use of these parameters in computing α_{corr} from eq 1 for the various complexes listed in Table I, and suggests that the reduction of at least the higher Cr(III) ammine complexes also takes place significantly within the oHp in sodium-based electrolytes. Unaffected by these considerations, however, is the basic conclusion that the distance of the reaction site from the electrode is decreased as the number of ammine groups in the complex is increased.

The close similarity of $(\Delta \log k_{\text{app}})_E$ resulting from changes in ionic strength in the absence of specific ionic adsorption for complexes of a given charge type, such as Cr(OH₂)₆³⁺ and Cr(NH₃)₅OH₂³⁺ (Figure 3) is not in conflict with the widely differing values of $(\partial\phi_r/\partial q^m)_\mu$ and $(\partial\phi_r/\partial q)_E$ given in Table II. As shown in Appendix II, in the absence of specific adsorption eq 7 can be rewritten as:

$$2.3(\Delta \log k_{\text{app}})_E = f(\alpha_{\text{corr}} - Z_r)(\Delta\phi_d)_E \quad (\text{A.13})$$

As $-(\alpha_{\text{corr}} - Z_r) = 2.36$ and 2.51 for Cr(NH₃)₅OH₂³⁺ and Cr(OH₂)₆³⁺ reduction, respectively, in NaClO₄ (Table I), eq A.13 can account for the absence of significant dif-

ferences in the rate responses for these two complexes (Figure 3).

It is of particular interest to extract from the values of $(\partial\phi_r/\partial E)_\mu$ information on the spatial position of the reaction site for a given complex within the double layer region. For this purpose, it is useful to define a quantity λ such that in the absence of specific ionic adsorption

$$\phi_r = \phi_d + \lambda(\phi_m - \phi_d) \quad (8)$$

where ϕ_m is the Galvani metal-solution potential difference. If λ is independent of electrode potential, then

$$(\partial\phi_r/\partial E)_\mu = (1 - \lambda)(\partial\phi_d/\partial E)_\mu + \lambda \quad (9)$$

Taking $(\partial\phi_d/\partial E)_\mu$ to equal the coefficients $(\partial\phi_r/\partial E)_\mu$ measured for Cr(OH₂)₆³⁺ reduction, from the values of $(\partial\phi_r/\partial E)_\mu$ given for each complex in Table II and eq 9, λ is deduced to vary in the range 0–0.10 as x varies between one and six. Thus, it appears that the differences in reaction site are encompassed within a relatively small fraction of the total potential difference across the inner layer. However, the quantitative relationship between λ and the spatial position of the reaction site depends on the dielectric constant profile within the inner layer.^{29,30} The commonly accepted model of the inner layer for aqueous systems in the absence of specific ionic adsorption consists of a "primary hydration layer" of oriented water molecules immediately adjacent to the electrode surface, and a "secondary hydration layer" consisting of the solvation sheath of the ions residing at the oHp, and bound by the charge centers of these ions.²⁵ A marked increase in the dielectric constant ϵ is expected within the secondary as compared to the primary inner layer.^{24,25,30} For the purpose of estimating the distance of the reaction site from the electrode surface x_r in relation to the overall thickness of the inner layer x_d , a simple method of accounting for this nonconstancy of ϵ is to assume that the regions $0 < x < x_r$ and $x_r < x < x_d$ are associated with the average dielectric constants ϵ_{mr} and ϵ_{rd} so that²⁹

$$\lambda = \frac{\epsilon_{\text{mr}}(x_d - x_r)}{[\epsilon_{\text{mr}}(x_d - x_r) + \epsilon_{\text{rd}}x_r]} \quad (10)$$

As for the present systems $\lambda \ll 1$, eq 10 can be further simplified to yield

$$\lambda \approx \left(\frac{\epsilon_{\text{mr}}(x_d - x_r)}{\epsilon_{\text{rd}}x_r} \right) \quad (11)$$

Experimental estimates of x_d have been made in the absence of ionic specific adsorption by comparing the experimental ionic surface excesses for concentrated electrolytes with the predictions of diffuse layer theory.³¹⁻³⁴ The resulting values of x_d on the negative side of the pzc vary both with the excess electrode charge density q^m ³¹ and the hydrated radius of the supporting electrolyte cation.³² Thus in concentrated NaH₂PO₄ solutions in the potential region considered here (ca. -650 to -1000 mV vs. SCE, $q^m = -4$ to $-12 \mu\text{C cm}^{-2}$) where Na⁺ is the dominant component of the diffuse layer, the "inner layer thickness" (assumed to be the distance from the oHp to the center of the water molecules forming the primary layer^{31,35}) is ca. 4 Å, which yields $x_d \sim 5.5 \text{ \AA}$. (Given that the thickness of the primary inner layer will be close to the diameter of a water molecule, 3.1 Å, this result lends some support to the suggested existence of a secondary hydration layer.)

Using eq 11 and these estimates of x_d , limits may be placed on the values of $(x_d - x_r)$ that correspond to our experimental result $\lambda \lesssim 0.1$. Thus the ratio $\epsilon_{\text{rd}}/\epsilon_{\text{mr}}$ will be greater than one but is unlikely to exceed four^{31,32} in which

case for $x_d \sim 5.5 \text{ \AA}$, $\lambda = 0.1$: $0.5 \text{ \AA} < (x_d - x_r) < 1.5 \text{ \AA}$.

However, eq 5 and 7 ignore the possible presence of discreteness-of-charge effects which cause the actual (or micro-) potential at the reaction site in the presence of the reactant (or activated state) to differ from ϕ_r .^{29,30} In the absence of specific ionic adsorption of the supporting electrolyte, the sole discreteness-of-charge term for a reactant residing in the inner layer is the self-image potential which arises from the attractive images formed by the reacting ion in the electrode and in the diffuse layer.^{29,30} Although the magnitude of the self-image potential for ions located within the diffuse layer is probably small due to the screening effect of other ions,³⁶ for reactions that occur within the primary and (to a lesser extent) the secondary inner layer, these terms may provide large contributions to the overall double layer effects.^{29,30} Although quantitative estimates cannot be made with confidence at the present time, for cation electroreduction in the potential region under consideration here (ca. -650 mV to -1000 mV , Table I) the presence of these effects will almost certainly act to increase the observed values of α_{app} and hence $(\partial\phi_r/\partial E)_\mu$. Consequently, the above estimates of $(x_r - x_d)$ should be taken as upper limits.

In the presence of specific ionic adsorption of the supporting electrolyte, an important additional contribution to the discreteness-of-charge terms is provided by the "exclusion disk potential" which results from the fact that the charge density provided by the specifically adsorbed ions is discrete and these ions occupy a finite area within the inner layer.³⁷⁻³⁹ As shown in Appendix I, markedly larger values of $(\partial\phi_r/\partial q)_E$ compared with $(\partial\phi_r/\partial q^m)_\mu$ are predicted if the reaction site lies significantly inside the oHp. Therefore the consistently close agreement between the apparent values of $(\partial\phi_r/\partial q^m)_\mu$ and $(\partial\phi_r/\partial q)_E$ for all the aquoammine Cr(III) complexes studied (Table II) suggests that such discreteness-of-charge effects may be significant. Although no complete theoretical treatment has yet appeared for the present cases where the reaction sites almost undoubtedly lie further away from the electrode than the inner Helmholtz plane, this result may be qualitatively rationalized on this basis as the exclusion disk potential will act to decrease these apparent values of $(\partial\phi_r/\partial q)_E$ obtained from eq 7 below their true values.^{38,39} Nevertheless, although the values of α_{app} and $(\Delta \log k_{\text{app}})_E$ induced by changes in ionic specific adsorption are both very sensitive to the position of the reaction site and yield compatible results, the former measurements yield more direct estimates of λ and hence x_r .

These relatively minor changes in the spatial position of the reaction site x_r , as water is replaced by ammonia in the coordination shell of Cr(III) are most simply accounted for by changes in the effective hydrated radii of these reactant ions. The crystallographic radii of these complexes are likely to be very similar as the size of the ammonia and water ligands are almost equal.⁴⁰ However, the Cr^{3+} ion and other small trivalent ions such as La^{3+} are extensively hydrated, not only by the primary coordination sheath of six water molecules but also by a tightly held secondary layer of "frozen" water⁴¹ which leads to large values for the Stokes and other hydrated radii for such cations.²⁸ However, there is some evidence that otherwise similar ammine complexes are less hydrated. Thus the Stokes radii r_s for $\text{Cr}(\text{NH}_3)_6^{3+}$ and $\text{Co}(\text{NH}_3)_6^{3+}$ (2.80 and 2.77 \AA , respectively⁴²) are ca. 1–1.5 \AA smaller than for $\text{Cr}(\text{OH}_2)_6^{3+}$ (4.12 \AA ^{28a}) and other tripripositive aquo ions. Such a difference may result from less extensive hydrogen bonding between the NH_3 ligands and surrounding water molecules compared with OH_2 ligands. Therefore the

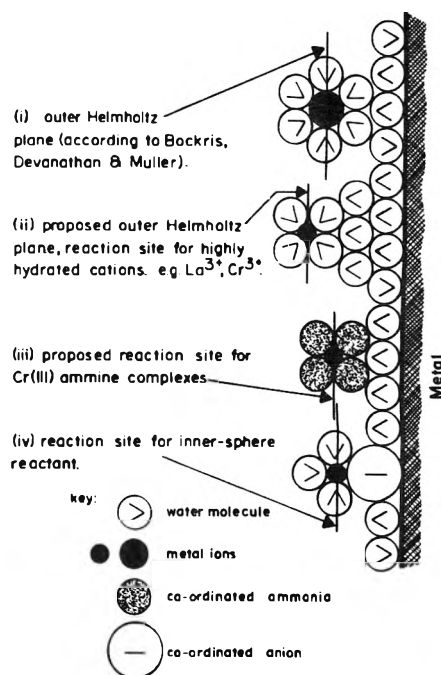


Figure 4. Proposed structure of the mercury-aqueous solution double layer and the reaction sites for aquo and ammine Cr(III) complexes at negative values of the excess electrode charge density.

observed monotonic increases in $(\partial\phi_r/\partial E)_\mu$, $(\partial\phi_r/\partial q^m)_\mu$, and $(\partial\phi_r/\partial q)_E$ as x increases within the series $\text{Cr}(\text{NH}_3)_x(\text{OH}_2)_{6-x}^{3+}$ can reasonably be ascribed to the ability of the ammine complexes to approach the electrode progressively more closely than either the $\text{Cr}(\text{OH}_2)_6^{3+}$ reactant, or the supporting electrolyte cations Na^+ and (particularly) La^{3+} that form the oHp. This notion is illustrated schematically in Figure 4. (i) in Figure 4 depicts the inner layer structure on the negative side of the pzc as discussed above:²⁵ both the cation at the oHp, and the electrode surface are considered to retain their primary hydration sheaths. (ii) depicts the corresponding structure for small polyvalent aquo cations that is suggested by the present results: in addition to the primary hydration shells surrounding the cation at the oHp and the electrode surface some secondary hydration is considered to be partially or completely wedged in between these layers. In contrast, this secondary hydration is considered to be largely absent for Cr(III) ammine complexes at their distance of closest approach to the electrode surface as shown in (iii). A possible alternative structure of (iii) for Cr(III) ammine complexes involves penetration of the primary layer by the ammine ligands. Although this possibility cannot be entirely discounted, we consider that it is unlikely as the Cr(III) center would then penetrate a region of low dielectric constant which would be expected to yield values of λ that would be markedly larger than those observed here.

Such a model also provides a simple explanation for the consistently higher values of $(\partial\phi_r/\partial E)_\mu$, $(\partial\phi_r/\partial q^m)_\mu$, and $(\partial\phi_r/\partial q)_E$ that are observed for Cr(III) ammine reduction in lanthanum as compared with sodium-based electrolytes (Table II) as x_d is expected to be larger for the more extensively hydrated La^{3+} ion²⁸ leading to larger values of λ and hence these coefficients via eq 11. The sensitivity of electrode kinetics to the nature of the supporting electrolyte cation in the absence of specific adsorption has been previously noted.²⁶

The Relative Rates of Inner- and Outer-Sphere Pathways for the Electroreduction of Acido Cr(III) Complexes. The substitution of a single water ligand in

$\text{Cr}(\text{OH}_2)_6^{3+}$ by coordinated anions was previously shown to produce profound changes in the electroreduction kinetics of $\text{Cr}(\text{III})$.³ The dominating influence of inner-sphere mechanisms involving ligand-bridging by these coordinated anions was found in most cases to be accompanied by considerable increases in the reduction rate. Two primary methods were developed for mechanism diagnosis. First, cationic reactants that were reduced via dominating ligand-bridging mechanisms were found to yield small rate decreases upon addition of adsorbed, nonreacting anions instead of the large rate increases expected on the basis of eq 7.^{2,3} Secondly, these ligand-bridged reactions also exhibit values of α_{app} that are markedly below 0.5, in contrast to the prediction of eq 5 for outer-sphere reactants with $\alpha_1 = 0.5$.³ These two anomalies can be explained by taking into account the interactions between the bridging anions and the nonreacting adsorbed anions, and the electrode surface, respectively.^{2,3} Thus for such ligand-bridged pathways, the reacting cation can no longer be considered as a point charge and eq 4 and 6 no longer reduce to eq 5 and 7. Instead, the interactions involving the bridging anion predominate as this part of the complex ion reactant is now situated within the primary inner layer in a region of extremely low dielectric constant.^{2,3,43} Using these criteria, rate-dominating inner-sphere mechanisms were found for $\text{Cr}(\text{OH}_2)_5\text{X}^{2+}$ complexes when $\text{X}^- = \text{Cl}^-, \text{Br}^-, \text{NCS}^-, \text{N}_3^-,$ and NO_3^- , as evidenced by the low values of α_{app} and α_{corr} and the small negative (or essentially zero) values of $(\Delta \log k_{\text{app}}/\Delta \log k_{\text{app}}^{\text{Cr}^{3+}})_E^{\text{obsd}}$ listed for these complexes in Table I. Outer-sphere mechanisms with a reaction site close to the oHp were only found for $\text{X}^- = \text{F}^-$ and SO_4^{2-} (as well as for $\text{Cr}(\text{OH}_2)_6^{3+}$) as evidenced by values of α_{corr} close to 0.5 and good agreement between $(\Delta \log k_{\text{app}}/\Delta \log k_{\text{app}}^{\text{Cr}^{3+}})_E^{\text{obsd}}$ and $(\Delta \log k_{\text{app}}/\Delta \log k_{\text{app}}^{\text{Cr}^{3+}})_E^{\text{calcd}}$ (see Table I and ref 3).

In contrast, rate-determining anion bridged mechanisms for the reduction of $\text{Cr}(\text{NH}_3)_5\text{X}^{2+}$ complexes studied in the present work are only indicated on the basis of these criteria for $\text{X}^- = \text{Br}^-$ and NCS^- (Table I). When $\text{X}^- = \text{F}^-, \text{Cl}^-, \text{N}_3^-,$ and NO_3^- , positive values of $(\Delta \log k_{\text{app}}/\Delta \log k_{\text{app}}^{\text{Cr}^{3+}})_E^{\text{obsd}}$ are obtained which are considerably larger than $(\Delta \log k_{\text{app}}/\Delta \log k_{\text{app}}^{\text{Cr}^{3+}})_E^{\text{calcd}}$ that are predicted on the basis of eq 3 (Table I). This behavior is similar to that found for the aquoammine complexes considered above, and therefore can be reasonably interpreted in terms of rate-dominating outer-sphere electroreduction pathways with reaction sites inside the oHp.

It is tempting to suggest that this relative reluctance of the acidopentaammine complexes to follow anion-bridged electroreduction mechanisms results from a relative stabilization of competing outer-sphere transition states which arises from the ability of the pentaammine complexes to approach the electrode more closely prior to electron transfer than is possible for the corresponding pentaquo complexes. Support for this notion comes from the comparison of the relative reduction rates of corresponding acidopentaammine and pentaquo $\text{Cr}(\text{III})$ complexes at a fixed electrode potential. These rate ratios determined (for convenience) at -700 mV are listed in Table I. For simple adiabatic outer-sphere reactions when the work terms are negligible (or cancel), Marcus has shown⁴⁴ that the ratio of rate constants for the homogeneous reduction or oxidation of a pair of reactants by a given reagent should be the same as the ratio of rate constants for the corresponding electrochemical reactions involving these reactants measured at a fixed electrode potential. A similar relationship may also be expected to apply to pairs of

inner-sphere reactions⁴⁵ such as the $\text{Cr}(\text{NH}_3)_5\text{X}^{2+}$ and $\text{Cr}(\text{OH}_2)_5\text{X}^{2+}$ systems considered here where only the nonbridging ligands are altered and the differences in the work terms for formation of the precursor and successor complexes should approximately cancel when the chemical and electrochemical rate ratios are compared. The homogeneous inner-sphere reduction of $\text{Cr}(\text{NH}_3)_5\text{X}^{2+}$ and $\text{Cr}(\text{OH}_2)_5\text{X}^{2+}$ by Cr^{2+} has been studied for $\text{X}^- = \text{F}^-, \text{Cl}^-, \text{Br}^-$ and N_3^- , and from published data the ratio of these rate constants $k^{\text{NH}_3}/k^{\text{OH}_2}$ are found to be 1.2×10^{-2} (F^-), 1.8×10^{-3} (Cl^-), $<9 \times 10^{-4}$ (Br^-), and 3×10^{-3} (N_3^-).⁴⁶ The comparison of these ratios with the corresponding electrochemical ratios $(k_{\text{app}}^{\text{NH}_3}/k_{\text{app}}^{\text{OH}_2})_{-700}$ given in Table I reveals that markedly larger values of the latter coefficients are characteristically obtained except when $\text{X}^- = \text{Br}^-, \text{NCS}^-,$ and Cl^- , which again indicates that a more favorable competing electroreduction mechanism is available to the ammine complexes. The disparities between these chemical and electrochemical rate ratios increase with increasing negative electrode potentials, as seen from the relative values of α_{app} for these ammine and aquo complexes (Table I). In spite of the large positive values of $(\Delta \log k_{\text{app}}/\Delta \log k_{\text{app}}^{\text{Cr}^{3+}})_E^{\text{obsd}}$ obtained for the reduction of $\text{Cr}(\text{NH}_3)_5\text{Cl}^{2+}$, the similarity of $k^{\text{NH}_3}/k^{\text{OH}_2}$ and $(k_{\text{app}}^{\text{NH}_3}/k_{\text{app}}^{\text{OH}_2})_{-700}$ for this system (1.8×10^{-3} and 8.5×10^{-3} , respectively) suggests that the ligand-bridged pathway may contribute significantly to the measured electroreduction rate. As the ligand-bridged pathway is expected to exhibit a markedly lower value of α_{corr} , the rate via this pathway should become increasingly competitive in comparison with the outer-sphere rate as the cathodic overpotential decreases. This is in harmony with the marked decreases in $(\Delta \log k_{\text{app}}/\Delta \log k_{\text{app}}^{\text{Cr}^{3+}})_E^{\text{obsd}}$ that are observed with decreasing cathodic overpotential for this system, as well as for the reduction of $\text{Cr}(\text{NH}_3)_5\text{N}_3^{2+}$. Values of α_{corr} for these two reactants that are intermediate between those expected for dominating anion-bridged and outer-sphere mechanisms (Table I) also suggest the presence of mixed electroreduction mechanisms. Therefore the simple mechanistic criterion based on the sign of the rate responses to the addition of specifically adsorbed anions may not give clearcut results when the rates of the competing inner- and outer-sphere pathways are comparable.

The absence of dominating anion-bridged pathways for $\text{Cr}(\text{NH}_3)_5\text{X}^{2+}$ complexes when $\text{X}^- = \text{N}_3^-, \text{NO}_3^-,$ and Cl^- is not surprising as the rate analysis described in ref 3 indicates that the rate-determining inner-sphere pathways observed for the reduction of the corresponding $\text{Cr}(\text{OH}_2)_5\text{X}^{2+}$ complexes are favored by less than 10–100-fold over the competing outer-sphere pathways. An analysis of the relative rates of electrochemical and chemical $\text{Cr}(\text{III})|(\text{II})$ exchange reactions given elsewhere⁴⁷ indicates that such anion-bridged electrochemical reactions are considerably less favored over the competing outer-sphere pathways than is the case for the corresponding homogeneous self-exchange reactions. When $\text{X}^- = \text{Br}^-$ or NCS^- , the ligand-bridged pathways are favored to a greater extent due to the strong adsorption of these anions to the mercury surface as well as a probable lowering of the intrinsic barrier to electron transfer when $\text{X}^- = \text{Br}^-$,^{3,47} so that these pathways remain dominant even in the presence of a relatively more favorable outer-sphere pathway.

The relatively larger rates for outer- vs. inner-sphere electroreduction for $\text{Cr}(\text{NH}_3)_5\text{X}^{2+}$ complexes compared with the corresponding $\text{Cr}(\text{OH}_2)_5\text{X}^{2+}$ systems are indeed expected from the differences in the position of the reaction site noted above for the outer-sphere electro-

duction of ammine and aquo complexes. Thus in the electrode potential region of interest, the sign of the potential drop within the inner layer region is negative,⁴⁸ so that smaller values of x_r will yield larger negative values of ϕ_r , and hence a more favorable pathway for the reduction of cationic reactants (eq 7). Another important factor is the decrease in the solvent reorganization energy for an outer-sphere electrode reaction that is expected for smaller values of x_r .²¹

The Electroreduction of Cr(III) Ethylenediamine Complexes. The effects of varying the double layer structure upon the electroreduction kinetics of $\text{Cr}(\text{en})_3^{3+}$ provide an interesting contrast to the behavior of the aquoammine complexes considered above. Thus the high value of α_{app} (0.90) contrasts with the close similarity of $(\Delta \log k_{\text{app}}/\Delta \log k_{\text{app}}^{\text{Cr}^{3+}})_E^{\text{obsd}}$ and $(\Delta \log k_{\text{app}}/\Delta \log k_{\text{app}}^{\text{Cr}^{3+}})_E^{\text{calcd}}$ for this system (Table I) which results in apparent values of $(\partial\phi_r/\partial q^m)_\mu$ that are markedly larger than $(\partial\phi_r/\partial q)_E$ (Table II). A discrepancy between these coefficients in the opposite direction would be expected on the basis of an average potential model of the inner layer (see Appendix I). The relatively low value obtained for $(\partial\phi_r/\partial q)_E$ is expected as the larger size of the ethylenediamine ligands would seem to necessitate a reaction site further from the electrode surface for $\text{Cr}(\text{en})_3^{3+}$ (Stokes radius $r_s = 3.75 \text{ \AA}^{42}$) compared with Cr(III) ammine complexes, unless the complex can effectively replace water molecules in the primary inner layer (i.e., be specifically adsorbed). We believe that this discrepancy between $(\partial\phi_r/\partial q^m)_\mu$ and $(\partial\phi_r/\partial q)_E$ is probably due to a value of α_1 markedly above 0.5: the assumption $\alpha_1 = 0.5$ was made in extracting $(\partial\phi_r/\partial q^m)_\mu$ from α_{app} using eq 5. A high value for α_1 (0.8) has previously been obtained for isothiocyanate-bridged electroreduction of $\text{c-Cr}(\text{en})_2(\text{NCS})_2^+$ where α_1 could be directly evaluated from experimental data.¹⁷ The reduction kinetics of $\text{c-Cr}(\text{en})_2\text{Cl}_2^+$ and $\text{c-Cr}(\text{en})_2(\text{N}_3)_2^+$ that appear to follow anion-bridged pathways on the basis of the essentially zero values of $(\Delta \log k_{\text{app}}/\Delta \log k_{\text{app}}^{\text{Cr}^{3+}})_E^{\text{obsd}}$ (Table I) also exhibit relatively high values of α_{app} and α_{corr} in comparison with other similar anion-bridged electrode reactions (Table I), which suggests that α_1 is also markedly above 0.5 for these reactions. Such anomalously high values of α_1 indicate that the elementary barrier to electron transfer is asymmetrical. This could arise from the large distortions of the chelating ethylenediamine ligands necessary to stretch a pair of axial ligands in order to accommodate the incoming electron in an antibonding e_g orbital. Such distortions will not be necessary for the complexes containing the unidentate ammine ligands. It is interesting to note that a value of α_1 equal to 0.5 was obtained using purely experimental data¹⁷ for the inner-sphere reduction of $\text{t-Cr}(\text{en})_2(\text{NCS})_2^+$ where it would be expected that only the two Cr(III)-isothiocyanate bonds that lie along the bridging axis would be required to be markedly stretched prior to electron transfer.

Conclusions

The chief conclusion from the present study is that the distance of closest approach of cationic reactants as well as for the supporting electrolyte cations can vary markedly depending on the extent of secondary hydration as well as the primary hydration or ligation surrounding the ion. Simple aquo cations that are extensively hydrated in bulk solution also appear to retain some secondary hydration between the primary hydration layers surrounding the ion and the electrode surface. Reductions in this effective size of the reactant, as seen when ammonia replaces water in the coordination sphere of Cr(III), produce significant

decreases in the distance of the reaction plane from the electrode surface which, at least at potentials negative of the pzc can result in a sizable catalysis of the electrode reaction even though the mechanism remains of the outer-sphere type. This stabilization of the outer-sphere transition state can result in rates for this pathway that can be comparable to or greater than the rates of alternative anion-bridged pathways even for bridging anions that exhibit moderate specific adsorption, and especially at far negative potentials where the close approach of the cationic rather than the anionic center of the complex ion to the electrode surface will be strongly favored on electrostatic grounds.

Studies of the extent of the catalysis of the reaction rate by specifically adsorbed anions, particularly when coupled with accurate measurements of the apparent transfer coefficients, appear to be an extremely promising tool not only for the distinction between inner- and outer-sphere electrode reaction mechanisms^{2,3} but also for making more subtle distinctions between different reaction sites for reactions within a given mechanistic type.

Acknowledgments. A number of the Cr(III) complexes were synthesized by Noel Demers and Paul Tyma provided valuable computing expertise. Helpful discussions with Professor W. R. Fawcett aided the preparation of the final form of this paper. We are grateful to Hercules Inc. and to the Research Corporation for supporting this work through a Hercules Incorporation Research Grant of the Research Corporation.

Appendix

The Relation between $(\Delta \log k_{\text{app}})_E$ and the Position of the Reaction Site. (I) **Rate Responses to Changes in Specific Ionic Adsorption.** If the reaction site lies at the oHp or within the diffuse layer, the quantities $(\partial\phi_r/\partial q^m)_\mu$ and $(\partial\phi_r/\partial q)_E$ derived from α_{app} and $(\Delta \log k_{\text{app}})_E$ using eq 5 and 7 in the absence and presence, respectively, of specific ionic adsorption of the supporting electrolyte are expected to be identical in the absence of discreteness-of-charge effects.¹³ However, if the reaction site lies inside the oHp, $(\partial\phi_r/\partial q^m)_\mu$ and $(\partial\phi_r/\partial q)_E$ are generally expected to differ, as demonstrated by the following argument.

Equation 9 which applies in the absence of specific ionic adsorption can be rewritten as

$$\left(\frac{\partial\phi_r}{\partial q^m}\right)_\mu = \left(\frac{\partial\phi_d}{\partial q^m}\right)_\mu (1 - \lambda) + \frac{\lambda}{C_{\text{dl}}} \quad (\text{A.1})$$

where C_{dl} is the differential double layer capacitance at the appropriate value of q^m .

In the presence of specific ionic adsorption of the supporting electrolyte we can write (eq 9 of ref 29):

$$\phi_r = \phi_d + \lambda_1(\phi_m - \phi_a) \quad (\text{A.2})$$

where ϕ_a is the average potential in the plane of the adsorbed anions at a distance x_a from the electrode surface. Equation A.2 can also be written as (eq 10 of ref 29):

$$\phi_r = \phi_d + \lambda_1(\phi_m - \phi_d) - \frac{\lambda_1 q^m}{K_{\text{ma}}} \quad (\text{A.3})$$

where K_{ma} is the integral capacitance of the region between the metal surface and x_a . Then

$$\left(\frac{\partial\phi_r}{\partial q^m}\right)_E = (1 - \lambda_1) \left(\frac{\partial\phi_d}{\partial q^m}\right)_E - \frac{\lambda_1}{K_{\text{ma}}} \left(\frac{\partial q^m}{\partial q^m}\right)_E \quad (\text{A.4})$$

If $x_a < x_r < x_d$, $\lambda_1/\lambda = K_{\text{md}}/K_{\text{ad}}$ where K_{md} and K_{ad} are the

integral capacitances of the inner layer regions $x < x_d$ and $x_a < x < x_d$ then

$$\left(\frac{\partial \phi_r}{\partial q'}\right)_E = \left(1 - \lambda \frac{K_{ad}}{K_{md}}\right) \left(\frac{\partial \phi_d}{\partial q'}\right)_E - \frac{\lambda K_{ad}}{K_{ma} K_{md}} \left(\frac{\partial q^{ra}}{\partial q'}\right)_E \quad (\text{A.5})$$

If $\lambda > 0$, and $x_a < x_r < x_d$, it is generally expected that the right-hand side of eq A.1 would be larger than the right-hand side of eq A.5, which reflects the fact that the adsorbed anions are located closer to the reaction plane than the electrode charge q^m . For example, for Γ^- adsorption in concentrated (~ 1 M) electrolytes: $(\partial q^m / \partial q)_E \approx -0.65$ [as $(\partial q^m / \partial q'_x)_E = -0.40^{13}$], $K_{ad} \approx 60 \mu\text{F cm}^{-2}$, K_{md} , $C_{dl} \approx 25 \mu\text{F cm}^{-2}$, $K_{ma} \approx 17.5 \mu\text{F cm}^{-2}$.⁵⁰ For the typical values $\lambda = 0.1$, $(\partial q^m / \partial \phi_d)_\mu = 500 \mu\text{F cm}^{-2}$, we obtain from eq A.1 and A.5 $(\partial \phi_r / \partial q^m)_\mu = 6 \times 10^{-3} \mu\text{F}^{-1} \text{cm}^2$, $(\partial \phi_r / \partial q)_E = 1 \times 10^{-2} \mu\text{F}^{-1} \text{cm}^2$.

(II) *Rate Responses to Changes in Ionic Strength.* It as been noted previously¹² that measurements of the reaction rate response to changes in ionic strength in the absence of specific ionic adsorption are expected to be insensitive to the position of the reaction site if this lies within the diffuse layer. A similar conclusion (although for different reasons) may be reached when the reaction site lies within the inner layer from the following argument. A general form of the rate law for a one-electron reduction reaction is (cf. eq 4 and 6)^{3,16}

$$2.3RT \log k_{app} = K_1 - \alpha_I(\Delta G^\circ_{Ap} - \Delta G^\circ_{Ar} + FE) + \Delta G^\circ_{Ar} \quad (\text{A.6})$$

where K_1 is a constant that is independent of electrode potential.

For reactions that occur within the inner layer region, eq A.1 can be written as:

$$2.3RT \log k_{app} = K_1 - \alpha_I[(\Delta G^\circ_{Ap})^i - (\Delta G^\circ_{Ar})^i - F\phi_d + FE] + Z_r F\phi_d + (\Delta G^\circ_{Ar})^i = K_{11} - \alpha_{corr}(FE - F\phi_d) + Z_r F\phi_d \quad (\text{A.8})$$

where K_{11} is another potential-independent constant and α_{corr} is the "diffuse-layer corrected" transfer coefficient which is the value of α_{app} that would be observed in the absence of a diffuse layer effect. Thus as $\alpha_{app} = (2.3RT/F)(\partial \log k_{app}/\partial E)_\mu$ ^{3,12} then from eq A.8 it follows that $\alpha_{app} = \alpha_{corr} - (\alpha_{corr} - Z_r)(\partial \phi_d/\partial E)_\mu$ which leads to eq 1 above.

When the reaction site lies within the inner layer at an average potential ϕ_r , in the absence of nonelectrostatic and discreteness-of-charge effects we can write eq A.7 in the form

$$2.3RT \log k_{app} = K_1 - \alpha_I F[E - (\phi_r - \phi_d) - \phi_d] + Z_r F(\phi_r - \phi_d) + Z_r F\phi_d \quad (\text{A.9})$$

Comparing eq A.8 and A.9 yields

$$\alpha_{corr} = \alpha_I - (\alpha_I - Z_r)\lambda \quad (\text{A.10})$$

with λ as defined in eq 8 above. If the composition of the inner layer region remains constant, then the change in ϕ_r at constant electrode potential, $(\Delta \phi_r)_E$, brought about by a change in the diffuse layer potential, $(\Delta \phi_d)_E$, will be related by

$$(\Delta \phi_r)_E = (1 - \lambda)(\Delta \phi_d)_E \quad (\text{A.11})$$

Then the corresponding rate response at a constant

electrode potential, $(\Delta \log k_{app})_E$, will from eq 7 to be equal to:

$$2.3(\Delta \log k_{app})_E = f[(\alpha_I - Z_r)(1 - \lambda)(\Delta \phi_d)_E] \quad (\text{A.12})$$

Combination of eq A.10 and A.12 yields

$$2.3(\Delta \log k_{app})_E = f(\alpha_{corr} - Z_r)(\Delta \phi_d)_E \quad (\text{A.13})$$

Note that eq A.13 is identical with the corresponding relation derived for a reaction site at the oHp (eq 3 of ref 12) except for the replacement of α_I by α_{corr} . Therefore the differences in the rate response $(\Delta \log k_{app})_E$ obtained in the absence of specific ionic adsorption resulting from differences in the position of the reaction site within the inner layer region can be completely accounted for by changes in α_{corr} . As for the present systems $\alpha_{corr} \ll Z_r$, such measurements will therefore be insensitive to the position of the reaction site, the evaluation of α_{app} and α_{corr} from the potential dependence of the rate in the absence of specific ionic adsorption yielding the same information with much greater sensitivity.

However, eq A.13 will not generally apply to rate responses induced by changes in the inner layer composition, such as those arising from the effects of specifically adsorbed anions as eq A.11 will then be invalid if $\lambda > 0$. Consequently, these latter measurements provide additional information not provided by measurements of α_{corr} and are extremely sensitive to the position of the reaction site, as is demonstrated by the results described above.

References and Notes

- H. Taube, "Electron Transfer Reactions of Complex Ions in Solution", Academic Press, New York, N.Y., 1970.
- M. J. Weaver and F. C. Anson, *J. Am. Chem. Soc.*, **97**, 4403 (1975).
- M. J. Weaver and F. C. Anson, *Inorg. Chem.*, **15**, 1871 (1976).
- N. Sutin, *Acc. Chem. Res.*, **1**, 225 (1968).
- M. Mori, *Inorg. Syn.*, **5**, 132 (1954).
- A. E. Ogard and H. Taube, *J. Am. Chem. Soc.*, **80**, 1084 (1958).
- D. L. Gay and G. C. Lalor, *J. Chem. Soc. A*, 1179 (1966).
- M. Linhard and W. Berthold, *Z. Anorg. Chem.*, **279**, 173 (1955).
- M. Ardon and B. E. Mayer, *J. Chem. Soc.*, 2816 (1962).
- J. H. Espenson and D. W. Carlyle, *Inorg. Chem.*, **5**, 586 (1966).
- J. Koutecky, *Collect. Czech. Chem. Commun.*, **18**, 597 (1953); J. Weber and J. Koutecky, *ibid.*, **20**, 980 (1955).
- M. J. Weaver and F. C. Anson, *J. Electroanal. Chem.*, **65**, 711 (1975).
- M. J. Weaver and F. C. Anson, *J. Electroanal. Chem.*, **65**, 737 (1975).
- M. J. Weaver and F. C. Anson, *J. Electroanal. Chem.*, **65**, 759 (1975).
- R. Parsons, *Croat. Chem. Acta*, **42**, 281 (1970).
- M. J. Weaver and F. C. Anson, *J. Electroanal. Chem.*, **58**, 81 (1975).
- M. J. Weaver and F. C. Anson, *J. Electroanal. Chem.*, **58**, 95 (1975).
- M. J. Weaver and F. C. Anson, *J. Phys. Chem.*, **80**, 1861 (1976).
- F. C. Anson, M. G. Finn, and A. Yamada, *Inorg. Chem.*, in press.
- Thus α_I is predicted to be close to 0.5 at most accessible overpotentials from modern theories of electron transfer, such as that of Marcus.²¹ Experimental values of α_{corr} very close to 0.5 have been observed over a wide range of overpotentials for the electroreduction of some aquo Cr(III) complexes¹⁸ for which the double layer effects are small and/or the reaction site should be close to the oHp¹² so that α_{corr} may be approximately identified with α_I .
- R. A. Marcus, *J. Chem. Phys.*, **43**, 679 (1965).
- P. Delahay, "Double Layer and Electrode Kinetics", Interscience, New York, N.Y., 1965, Chapter 9.
- Reference 22, Chapter 3.
- N. F. Mott, R. Parsons, and R. J. Watts-Tobin, *Phil. Mag.*, **Ser. 8**, **7**, 483 (1962).
- J. O'M. Bockris, M. A. V. Devanathan, and K. Muller, *Proc. R. Soc. (London)*, **Ser. A**, **274**, 55 (1963).
- W. R. Fawcett, *J. Electroanal. Chem.*, **22**, 19 (1969).
- The term "hydrated radius" denotes the average radius of the ion with both the primary and secondary hydration that can be regarded as forming an integral species in solution.²⁸ Although estimates of these hydrated radii inevitably vary somewhat with the method used to determine them, the relative values for most cations do not, for the most part, differ greatly.
- (a) E. R. Nightingale, *J. Phys. Chem.*, **63**, 1381 (1959); (b) C. B. Monk, "Electrolytic Dissociation", Academic Press, New York, N.Y., 1961, Chapter 14.
- W. R. Fawcett, *J. Chem. Phys.*, **61**, 3842 (1974).
- S. Levine, K. Robinson, and W. R. Fawcett, *J. Electroanal. Chem.*, **54**, 237 (1974).
- R. Parsons and F. G. R. Zobel, *J. Electroanal. Chem.*, **9**, 333 (1965).

- (32) (a) J. A. Harrison, J. E. B. Randles, and D. J. Schiffrin, *J. Electroanal. Chem.*, **25**, 197 (1970); (b) D. J. Schiffrin in "Specialist Periodical Reports—Electrochemistry", Vol. 2, The Chemical Society, London, 1972, p 175.
- (33) B. B. Damaskin, A. N. Frumkin, V. F. Ivanov, N. I. Melekhova, and V. F. Khonina, *Sov. Electrochem.*, **4**, 1200 (1968).
- (34) N. I. Melekhova, V. F. Ivanov, and B. B. Damaskin, *Sov. Electrochem.*, **5**, 569 (1969).
- (35) R. M. Reeves in "Modern Aspects of Electrochemistry", Vol. 9, B. E. Conway and J. O'M. Bockris, Ed., Plenum Press, New York, N.Y., 1974, p 262-264.
- (36) J. M. Hale, "Reactions of Molecules at Electrodes", N. S. Hush, Ed., Wiley-Interscience, New York, N.Y., 1971, Chapter 4.
- (37) S. Levine and K. Robinson, *J. Electroanal. Chem.*, **41**, 159 (1973).
- (38) W. R. Fawcett and S. Levine, *J. Electroanal. Chem.*, **43**, 175 (1973).
- (39) W. R. Fawcett and S. Levine, *J. Electroanal. Chem.*, **65**, 505 (1975).
- (40) See, for example, F. Basolo and R. G. Pearson, "Mechanisms of Inorganic Reactions", 2nd ed, Wiley, New York, N.Y., 1967, pp 62-64.
- (41) H. S. Frank and W.-Y. Wen, *Discuss. Faraday Soc.*, **24**, 133 (1957).
- (42) T. Takahashi and T. Koiso, *Bull. Chem. Soc. Jpn.*, **49**, 2784 (1976).
- (43) Fawcett and Gardner (*J. Electroanal. Chem.*, in press) have recently criticized this simple explanation and suggested an alternative approach treating the reactant as a dipole. Although this model is formally rigorous it does not consider the marked variation of dielectric constant across the inner layer region which leads to predictions that are in disagreement with some experimental data. This question will be considered in detail elsewhere.
- (44) R. A. Marcus, *J. Phys. Chem.*, **67**, 853 (1963).
- (45) R. A. Marcus, *J. Phys. Chem.*, **72**, 891 (1968).
- (46) Ratios obtained from rate constants measured at, or extrapolated to 25 °C. Data sources: $\text{Cr}(\text{OH})_2\text{X}^{2+}$ where $\text{X}^- = \text{F}^-$, Br^- : D. L. Ball and E. L. King, *J. Am. Chem. Soc.*, **80**, 1091 (1958); Cl^- : R. V. James and E. L. King, *Inorg. Chem.*, **9**, 1301 (1970); N_3^- : R. Snellgrove and E. L. King, *Inorg. Chem.*, **3**, 288 (1964). $\text{Cr}(\text{NH}_3)_5\text{X}^{2+}$ where $\text{X}^- = \text{F}^-$, Cl^- , Br^- : A. E. Ogard and H. Taube, *J. Am. Chem. Soc.*, **80**, 1084 (1958); N_3^- : R. Davies and R. B. Jordon, *Inorg. Chem.*, **10**, 1102 (1971).
- (47) M. J. Weaver, submitted for publication.
- (48) The potential region of interest here exhibits negative values of q^m ($-E > 650$ mV, $-q^m > 4 \mu\text{C cm}^{-2}$), and therefore the potential drop due to free charges⁴⁹ will be negative. At the potential of zero charge (i.e., where $q^m = 0$) there is a small negative contribution to the potential drop from orientated water dipoles (ca. -80 mV⁴⁹) but as the reaction site for Cr(III) ammine complexes is located outside the primary inner layer of water dipoles, $\phi_i \sim 0$ at the pzc.
- (49) B. B. Damaskin and A. N. Frumkin, *Electrochim. Acta*, **19**, 173 (1974); S. Trassati, *J. Electroanal. Chem.*, **64**, 128 (1975).
- (50) E. Dutkiewicz and R. Parsons, *J. Electroanal. Chem.*, **11**, 100 (1966).

Upper and Lower Bounds on the Thermal Conductivity of a Random, Two-Phase Material

Antonio L. DeVera, Jr., and William Strieder*

Department of Chemical Engineering, University of Notre Dame, Notre Dame, Indiana 46556 (Received February 25, 1977)

Publication costs assisted by the National Science Foundation

Reciprocal variational principles are applied to the thermal conductivity of a two phase, heterogeneous material. Rigorous upper and lower bounds on the thermal conductivity of a bed of randomly placed, freely overlapping spheres of one or more sizes are derived. When compared with the experimental values of a number of investigators, the bounds provide estimates of the thermal conductivity of freeze dried food, plastic insulating foam, and metal filled polymers.

Introduction

Rigorous upper and lower bounds on the effective thermal conductivity λ_e of a two-phase heterogeneous material in terms of the phase thermal conductivities λ_1 and λ_2 and the volume fractions ϕ_1 and ϕ_2 can be calculated from reciprocal variational principles. The best known of these, the parallel upper bound and series lower bound on λ_e , are obtained when a constant trial flux j^* and a linear trial temperature T^* are substituted into the variational principles (15)

$$[\phi_1\lambda_1^{-1} + \phi_2\lambda_2^{-1}]^{-1} \leq \lambda_e \leq \phi_1\lambda_1 + \phi_2\lambda_2 \quad (1)$$

Hashin and Shtrikman¹ have presented a better set of upper and lower bounds valid for any homogeneous, isotropic heterogeneous material of known volume fractions for $\lambda_2 > \lambda_1$

$$\lambda_1 \left[1 + \frac{3\phi_2(\lambda_2 - \lambda_1)}{3\lambda_1 + \phi_1(\lambda_2 - \lambda_1)} \right] \leq \lambda_e \leq \lambda_2 \left[1 + \frac{3\phi_1(\lambda_1 - \lambda_2)}{3\lambda_2 + \phi_2(\lambda_1 - \lambda_2)} \right] \quad (2)$$

We need only reverse the roles of the phases, and ultimately the inequality signs of (2), to obtain upper and lower bounds for the case $\lambda_2 < \lambda_1$. While the bounds of eq 2 are very valuable in their generality, when λ_1 and λ_2

differ widely these bounds become weak and separate. Hashin and Shtrikman also demonstrate, that to improve their bounds (2) additional statistical information on the spatial distribution of the two phases, besides the volume fractions, must be known. Improvement of the bounds of eq (2) for those cases where λ_1 and λ_2 differ widely will require some reasonable assumptions about the physical distribution of the two phases.

Weissberg² obtained substantial improvements over the Hashin-Shtrikman upper bound when he calculated the variational upper bound on the effective thermal conductivity through a bed of randomly placed, freely overlapping, insulating spheres. The sphere phase of thermal conductivity, $\lambda_2 = 0$, was distributed at random without regard to interpenetration throughout a continuous phase of finite thermal conductivity, $\lambda_1 (>> \lambda_2)$. Weissberg worked in the context of an equivalent problem, the effective diffusion coefficient in a porous solid. The apparent success of Weissberg's approach arises from the inclusion of the sum of the thermal microgradients about all of the neighboring spherical structural elements in the trial function. As the heat flux must pass around an insulating sphere, these thermal microgradients in the vicinity of the sphere are important in the limit $\lambda_2 \rightarrow 0$.

Weissberg did not calculate the reciprocal variational lower bound for the effective thermal conductivity because, for a randomly overlapping bed of insulating spheres, the

lower bound vanishes. In the present work we examine the opposite case of a bed of randomly overlapping, highly conducting spheres ($\lambda_1 \ll \lambda_2$ and $\lambda_2 \rightarrow \infty$). All the local flux tends to pass through conducting spheres, so thermal microgradients are again important to λ_e . However in contrast to Weissberg's insulating sphere results, we find the lower bound on the effective conductivity for conducting spheres is finite and provides the useful upper bound in the effective resistivity, whereas, the opposite bound, the lower bound on the resistivity, vanishes. We also calculate both the upper and lower bounds on λ_e of a randomly overlapping sphere bed for the more general case, that one often finds in heterogeneous materials, of finite, nonvanishing, but widely differing λ_1 and λ_2 . These results will be compared with the Hashin-Shtrikman bounds.

The model of randomly placed freely overlapping spheres of thermal conductivity λ_2 in a continuous matrix of thermal conductivity λ_1 lends itself to comparison with experimental data. Effective thermal conductivities measured in markedly different systems (freeze dried apple, freeze dried beef, and polyurethane foams all with various gases in the void, metal filled polymers, and granular suspensions) are compared with our upper and lower bound results. From this comparison the upper bound, an improvement over the parallel conduction upper bound of eq 1, estimates λ_e for experimental systems modeled with poorly conducting spherical voids. The lower bound, an improvement over the series conduction lower bound of (1), gives estimates for those systems modeled with conducting spheres. In each case, the opposite bound tends toward zero (infinity) and gives no useful information.

Effective Thermal Conductivity

Suppose the ends of a long heterogeneous slab of total volume V are coincident with the planes $x = 0$ and $x = l$, and that \mathbf{i} is a unit vector pointing across the slab in the positive x direction. At any point \mathbf{r} within the slab volume the local temperature gradient $\nabla T(\mathbf{r})$ and the local heat flux $\mathbf{j}(\mathbf{r})$ are divergence free in the steady state and related to one another by Fourier's law

$$\mathbf{j}(\mathbf{r}) = -\lambda(\mathbf{r})\nabla T(\mathbf{r}) \quad (3)$$

The local thermal conductivity $\lambda(\mathbf{r})$ will change as a function of the position within the heterogeneous material. If in addition, a constant temperature difference $T_l - T_0$ is maintained across the slab, then the average heat flux $\langle \mathbf{j}(\mathbf{r}) \rangle$ per unit cross-sectional area is related to that temperature difference by the effective thermal conductivity λ_e

$$\langle \mathbf{j}(\mathbf{r}) \rangle = -\lambda_e \alpha \quad (4)$$

or

$$= -\lambda_e (T_l - T_0) l^{-1} \mathbf{i} \quad (5)$$

The angular brackets denote a volume average over a representative sample of the random suspension

$$\langle \dots \rangle = V^{-1} \int_V \dots d\rho \quad (6)$$

To bound λ_e we first note the reciprocal variational principles^{3,4}

$$2\langle \mathbf{g}^* \cdot \nabla T \rangle - \langle \lambda^{-1} (\mathbf{g}^*)^2 \rangle \leq \langle \lambda (\nabla T)^2 \rangle \leq \langle \lambda (\nabla T^*)^2 \rangle \quad (7)$$

valid for any trial temperature T^* continuous with at least piecewise continuous first partial derivatives in V . The integrand being bounded in (7) is essentially the dot product of a flux and a gradient, one can show under the

applied thermal gradient α that

$$\langle \lambda (\nabla T)^2 \rangle = -\alpha \cdot \langle \mathbf{j}(\mathbf{r}) \rangle \quad (8)$$

A less obvious but more compact form of the lower limit is obtained when the lower bound containing the trial vector flux

$$\mathbf{g}^*(\mathbf{r}) = \epsilon \mathbf{j}^*(\mathbf{r}) \quad (9)$$

is optimized with respect to the parameter ϵ , we have (8)

$$\frac{\langle \mathbf{j}^* \cdot \nabla T \rangle^2}{\langle \lambda^{-1} (\mathbf{j}^*)^2 \rangle} \leq -\alpha \cdot \langle \mathbf{j} \rangle \leq \langle \lambda (\nabla T^*)^2 \rangle \quad (10)$$

That \mathbf{j}^* is divergence free with at least piecewise continuously differentiable components and continuous normal components at internal interfaces, after some manipulation and the use of (5), allows us to rewrite (7) as

$$\frac{\langle (\mathbf{j}^*) \cdot \mathbf{i} \rangle^2}{\langle \lambda^{-1} (\mathbf{j}^*)^2 \rangle} \leq \lambda_e \leq \frac{\langle \lambda (\nabla T^*)^2 \rangle}{\alpha^2} \quad (11)$$

For the randomly, overlapping sphere model, we require that \mathbf{j}^* have continuous normal components at the entire interface of every sphere.

As the slab is very long, the upper bound integral in (11) does not depend on the end values of T^* , and in place of the condition that T^* satisfy the end conditions we may substitute

$$\langle \nabla T^* \rangle = \alpha \quad (12)$$

and impose the slab symmetry conditions of homogeneity and isotropy of the volume averages to obtain

$$\frac{\langle \mathbf{j}^* \rangle^2}{\langle \lambda^{-1} (\mathbf{j}^*)^2 \rangle} \leq \lambda_e \leq \frac{\langle \lambda (\nabla T^*)^2 \rangle}{\langle \nabla T^* \rangle^2} \quad (13)$$

Both the numerator and denominator of the upper bound in (13) are quadratic in ∇T^* , hence any constant vector $\langle \nabla T^* \rangle$ across the slab will meet condition (12).

The integrals of inequality (13) can be written directly in terms of the thermal conductivities λ_1 and λ_2 of the two phase medium, if we define the random function $q(\mathbf{r})$

$$q(\mathbf{r}) = \begin{cases} 1 & \mathbf{r} \text{ in phase 1} \\ 0 & \mathbf{r} \text{ in phase 2} \end{cases} \quad (14)$$

and modify the form of (13) by the use of $q(\mathbf{r})$

$$\langle \mathbf{j}^* \rangle^2 [(\lambda_1^{-1} - \lambda_2^{-1}) \langle q(\mathbf{r}) (\mathbf{j}^*)^2 \rangle + \lambda_2^{-1} \langle (\mathbf{j}^*)^2 \rangle]^{-1} \leq \lambda_e \leq \langle \nabla T^* \rangle^{-2} [(\lambda_1 - \lambda_2) \langle q(\mathbf{r}) (\nabla T^*)^2 \rangle + \lambda_2 \langle (\nabla T^*)^2 \rangle] \quad (15)$$

Bed of Overlapping Spheres

One very simple model for a random two-phase material is generated when Vn spheres, all of the same radius a , are placed in a volume V without any correlation between the positions of different spheres. The final result of this process will be a random bed of spheres, some isolated and some overlapping one another. Now phase two of the corresponding heterogeneous two-phase material will consist of all those points lying in the interior of one or more spheres, all the remaining points in V not in the interior of any sphere are points in phase one. Thus the two-phase heterogeneous material consists of randomly overlapping spheres of phase two material distributed in a continuous bed of phase one. A discussion of the statistics of a bed of overlapping spheres can be found in ref 2; however, as additional results are presented here, a development is given in its entirety.

In spite of the complexity and asymmetry of its geometry, the statistics of this random model is sufficiently straightforward to allow ready evaluation of the necessary probabilities and as well the integrals of the variational inequalities. To obtain an expression for the volume fraction ϕ_1 in terms of the density of sphere centers n and the sphere radius a , we first calculate the probability P_v of placing N centers in a large volume V in such a way that a smaller volume v contains no centers. The random placement of each center is independent of the positions of the other centers, and the probability is

$$P_v = \left[\frac{V-v}{V} \right]^N = \left[1 - \frac{nv}{N} \right]^N \quad (16)$$

As N is made larger holding v and n fixed, the well-known sequential limit

$$P_v = e^{-nv} \quad (17)$$

is obtained.

The volume fraction ϕ_1 can be interpreted as the probability that a randomly chosen point in our material falls in phase one, or the probability that no sphere of phase two has its center within a distance a of the random point, or from P_v of (17)

$$\phi_1 = (1 - \phi_2) = \langle q(\mathbf{r}) \rangle = \exp[-(4\pi a^3/3)n] \quad (18)$$

The probability P_n that an infinitesimal volume $d\rho$ contains a sphere center is given by similar arguments to be

$$P_n = N \left[\frac{d\rho}{V} \right] = n d\rho \quad (19)$$

Upper Bounds on λ_e

The trial temperature gradient to be substituted into the upper bound of (15) is formulated by adding to a constant vector \mathbf{A} pointing in the direction of α directly across the slab, the sum of the microgradient disturbances from each sphere

$$\nabla T^* = \mathbf{A} + m \sum_i \nabla f(\rho_i) \quad (20)$$

The vector $\rho_i = \mathbf{r} - \mathbf{r}_i$ points away from the i th sphere center located at \mathbf{r}_i . For a sphere radius a the form of $f(\rho)$

$$f(\rho) = \mathbf{A} \cdot \rho (a/\rho)^3 \quad \rho > a \\ = \mathbf{A} \cdot \rho \quad \rho < a \quad (21)$$

is suggested by the solution of the thermal conduction problem in which a single sphere of phase two is placed in a large slab of phase one. The constant multiplier m is known for this special case of infinite dilution of spheres

$$m_\infty = (\lambda_1 - \lambda_2)/(\lambda_2 + 2\lambda_1) \quad (22)$$

however, for an arbitrarily dense sphere concentration and any volume fraction ϕ_1 , m is determined by optimization of the upper bound variational integral. Examining m_∞ of eq 22, we find that for infinite dilution of spheres whenever λ_1 and λ_2 differ significantly, the $\nabla f(\rho)$ term strongly influences the overall temperature gradient (20) in the vicinity of the sphere. We should expect then, in the general case of arbitrary sphere density, the most important improvements in the upper bound from the $\nabla f(\rho)$ term will occur when λ_1 and λ_2 differ widely.

When the trial temperature gradient (20) is inserted into the upper bound (15) several summations result

$$\lambda_e \leq \Gamma_1^{-1} \{ (\lambda_1 \phi_1 + \lambda_2 \phi_2) + 2m\Gamma_2 + m^2\Gamma_3 \} \quad (23)$$

where

$$A^2\Gamma_1 = \{ \mathbf{A} + m \langle \sum_i \nabla f(\rho_i) \rangle \}^2 \quad (24)$$

$$A^2\Gamma_2 = \mathbf{A} \cdot \{ (\lambda_1 - \lambda_2) \langle q \sum_i \nabla f(\rho_i) \rangle + \lambda_2 \langle \sum_i \nabla f(\rho_i) \rangle \} \quad (25)$$

and

$$A^2\Gamma_3 = \{ (\lambda_1 - \lambda_2) \langle q [\sum_i \nabla f(\rho_i)]^2 \rangle + \lambda_2 \langle [\sum_i \nabla f(\rho_i)]^2 \rangle \} \quad (26)$$

It is in the evaluation of these sums over sphere centers and pairs of sphere centers that the statistical properties of the bed of spheres must be considered.

The single summations in (24) and (25) are readily evaluated for a bed of randomly placed, freely overlapping spheres all of the same radius. The probability (19) that the infinitesimal volume $d\rho$ contains a sphere center is simply $n d\rho$, and

$$\langle \sum_i \nabla f(\rho_i) \rangle = n \int_{V_a} \nabla f(\rho) d\rho \quad (27)$$

For a very large slab inserting the form of $f(\rho)$ from (21) we find

$$\langle \sum_i \nabla f(\rho_i) \rangle = (4\pi n a^3/3) \mathbf{A} \quad (28)$$

The probability that a randomly selected point is in phase one is just the volume fraction ϕ_1 , thus

$$\langle q(\mathbf{r}) \sum_i \nabla f(\rho_i) \rangle = \phi_1 n \int_{V_a} \nabla f(\rho) d\rho \quad (29)$$

The presence of $q(\mathbf{r})$ in the integrand of (29) requires the probability that \mathbf{r} be outside of the volume of any sphere, ϕ_1 , and that we find a sphere in $d\rho$, in a bed of randomly placed, freely overlapping spheres these events are independent. A sphere of radius a located at the origin is excluded from the volume V_a in the integration of (29), since \mathbf{r} must be a point in phase one no sphere center can be a distance less than a from the phase one point. For the form (21) of $f(\rho)$ the integral (29) vanishes

$$\langle q(\mathbf{r}) \sum_i \nabla f(\rho_i) \rangle = 0 \quad (30)$$

Distinguishing between two types of terms appearing in the double sum, namely, those for which $i = j$ and those for which i and j are different, we have first an integral similar to (28)

$$\langle \sum_i [\nabla f(\rho_i)]^2 \rangle = n \int_{V_a} [\nabla f(\rho)]^2 d\rho \quad (31)$$

or with (21)

$$\langle \sum_i [\nabla f(\rho_i)]^2 \rangle = 4\pi n a^3 A^2 \quad (32)$$

The second diagonal term in the double sum is similar to (29)

$$\langle q(\mathbf{r}) \sum_i [\nabla f(\rho_i)]^2 \rangle = n \phi_1 \int_{V_a} [\nabla f(\rho)]^2 d\rho \quad (33)$$

and its evaluation with (21) gives

$$\langle q \sum_i [\nabla f(\rho_i)]^2 \rangle = 8\pi n a^3 \phi_1 A^2/3 \quad (34)$$

If the sphere centers are distributed at random regardless of their interpenetration, the coordinates ρ_i and ρ_j of the ij pair are completely uncorrelated, for those terms

terms of the double sum where $i \neq j$ we can write

$$\langle \sum_{\substack{i,j \\ i \neq j}} \nabla f(\rho_i) \cdot \nabla f(\rho_j) \rangle = n^2 \int_V \int_V \nabla f(\rho_1) \cdot \nabla f(\rho_2) d\rho_1 d\rho_2 \quad (35)$$

or with (21)

$$\langle \sum_{\substack{i,j \\ i \neq j}} \nabla f(\rho_i) \cdot \nabla f(\rho_j) \rangle = 16\pi^2 n^2 a^6 A^2 / 9 \quad (36)$$

and

$$\langle \mathbf{q}(\mathbf{r}) \sum_{\substack{i,j \\ i \neq j}} \nabla f(\rho_i) \cdot \nabla f(\rho_j) \rangle = \phi_1 n^2 \int_{V_a} \int_{V_a} \nabla f(\rho_1) \cdot \nabla f(\rho_2) d\rho_1 d\rho_2 \quad (37)$$

which vanishes upon evaluation with (21)

$$\langle \mathbf{q} \sum_{\substack{i,j \\ i \neq j}} \nabla f(\rho_i) \cdot \nabla f(\rho_j) \rangle = 0 \quad (38)$$

Equations 27-38 are now substituted into the Γ terms (24) through (26), and the optimum value of m is obtained by differentiation of the upper bound (23), the optimizing value of m is

$$m_0 = \phi_1 (\lambda_1 - \lambda_2) / [2\phi_1 (\lambda_1 - \lambda_2) + 3\lambda_2] \quad (39)$$

When this value of m is substituted back into the upper bound (23), the optimum upper bound is

$$\lambda_e < (\phi_1 \lambda_1 + \phi_2 \lambda_2 - m_0 \lambda_2 \ln \phi_1) (1 - m_0 \ln \phi_1)^{-1} \quad (40)$$

where (18) has been used to eliminate n from the final results.

Lower Bounds on λ_e

As has already been pointed out, the simplest trial flux for the lower bound variational principle, the constant flux across the slab, leads to a series conduction arrangement of the two phases as a lower bound on the effective conductivity. To improve this result we reformulate the trial temperature (20) into a complementary trial flux

$$\mathbf{j}^*(\mathbf{r}) = \lambda_1 \mathbf{A} + \omega \sum_i \lambda_1^{-1} \nabla h(\rho_i) \quad (41)$$

for spheres of radius a

$$\begin{aligned} h(\rho) &= \mathbf{A} \cdot \rho (a/\rho)^3 & \rho > a \\ &= -2\mathbf{A} \cdot \rho & \rho < a \end{aligned} \quad (42)$$

The divergence of \mathbf{j} must vanish, and in addition the normal component of \mathbf{j} must be continuous across any sphere interface within the random bed of overlapping spheres. In the limit of an infinitely dilute bed of spheres the true flux is known and

$$\omega_\infty = (\lambda_1 - \lambda_2) / (\lambda_2 + 2\lambda_1) \quad (43)$$

The trial flux is identical with that obtained from the trial temperature (20) in the same infinitely dilute limit. Then as with the trial temperature gradient, the $h(\rho)$ contribution to the trial flux (41) will be most effective when λ_1 and λ_2 differ widely. In general the constant ω in (41) will be selected to obtain the best bounds. Also as with the upper bound, we sum contributions of the microgradients not only of the nearest sphere, but those of neighboring spheres as well to obtain results for any sphere density or void fraction.

When substitution of (41) is made into the lower bound variational principle (15) on the thermal conductivity, or the upper bound on the effective resistivity λ_e^{-1} , we obtain

$$\lambda_e^{-1} \leq \Omega_1^{-1} \{ \phi_1 \lambda_1^{-1} + \phi_2 \lambda_2^{-1} + 2\omega \Omega_2 + \omega^2 \Omega_3 \} \quad (44)$$

where

$$A^2 \Omega_1 = \{ \mathbf{A} + \omega \langle \sum_i \nabla h(\rho_i) \rangle \}^2 \quad (45)$$

$$\begin{aligned} A^2 \Omega_2 &= (\lambda_1^{-1} - \lambda_2^{-1}) \mathbf{A} \cdot \langle \mathbf{q}(\mathbf{r}) \sum_i \nabla h(\rho_i) \rangle \\ &+ \lambda_2^{-1} \mathbf{A} \cdot \langle \sum_i \nabla h(\rho_i) \rangle \end{aligned} \quad (46)$$

and

$$\begin{aligned} A^2 \Omega_3 &= (\lambda_1^{-1} - \lambda_2^{-1}) \langle \mathbf{q}(\mathbf{r}) [\sum_i \nabla h(\rho_i)]^2 \rangle \\ &+ \lambda_2^{-1} \langle [\sum_i \nabla h(\rho_i)]^2 \rangle \end{aligned} \quad (47)$$

The integrals of (45) to (47) are in fact identical in form with eq 27, 29, 31, 33, 35, and 37, and their evaluation for the specific form of h given in (42) is also similar to the corresponding integrals of the upper bound calculation. We obtain

$$\Omega_1 = \{ 1 - 8\pi n \omega a^3 / 3 \}^2 \quad (48)$$

$$\Omega_2 = -(8\pi n a^3) / (3\lambda_2) \quad (49)$$

and

$$\begin{aligned} \Omega_3 &= (\lambda_1^{-1} - \lambda_2^{-1}) 8\pi n a^3 \phi_1 / 3 + \lambda_2^{-1} 64\pi^2 n^2 a^6 / 9 \\ &+ \lambda_2^{-1} 8\pi a^3 n \end{aligned} \quad (50)$$

The value of ω that gives the variational bound (44) its smallest value

$$\omega_0 = \phi_1 (\lambda_2^{-1} - \lambda_1^{-1}) / [3\lambda_2^{-1} - \phi_1 (\lambda_2^{-1} - \lambda_1^{-1})] \quad (51)$$

gives the optimized bound

$$\begin{aligned} \lambda_e^{-1} &\leq (\phi_1 \lambda_1^{-1} + \phi_2 \lambda_2^{-1} + 2\omega_0 \lambda_2^{-1} \ln \phi_1) \\ &\times (1 + 2\omega_0 \ln \phi_1)^{-1} \end{aligned} \quad (52)$$

Non-Uniform Spheres

The same reciprocal variational principles used to derive the upper bound (40) and the lower bound (52) for uniform spheres can also be applied to a bed of overlapping spheres of phase two of several sizes. It is interesting to note that the same bounds (40) and (52) are obtained for the mixture of spheres. If the sphere bed can be regarded as a superposition of separately constructed sphere beds each of sphere radius a_μ for $\mu = 1, 2, 3, \dots$ and sphere density n_μ , then the statistics for each of the beds are independent. For any one of the sphere beds of radius a_μ the probability that a randomly chosen point in that bed is in phase one is just the volume fraction of phase one for that bed given by (18), and the obvious extension to a bed of overlapping spheres of several sizes is

$$\phi_1 = \exp[-(4\pi/3)(n_1 a_1^3 + n_2 a_2^3 + \dots)] \quad (53)$$

The generalized derivations of the upper and lower bounds on λ_e are a straightforward repetition of the procedure used for uniform spheres, we need only mention the forms of the trial functions. The trial function which replaces (20) is

$$\nabla T^* = \mathbf{A} + m_1 \sum_{i_1} \nabla f_1(\rho_{i_1}) + m_2 \sum_{i_2} \nabla f_2(\rho_{i_2}) + \dots \quad (54)$$

where

$$\begin{aligned} f_\mu(\rho) &= \mathbf{A} \cdot \rho (a_\mu/\rho)^3 & \rho > a_\mu \\ &= \mathbf{A} \cdot \rho & \rho < a_\mu \\ \mu &= 1, 2, \dots \end{aligned} \quad (55)$$

TABLE I: Tabulation of Hashin-Shtrikman Upper and Lower Bounds on $\lambda_e/(\lambda_1\lambda_2)^{1/2}$ from Eq 2^a

ϕ_1	$\beta \rightarrow 0$	$\beta = 0.01$	$\beta = 0.05$	$\beta = 0.1$	$\beta = 10$	$\beta = 50$	$\beta = 100$	$\beta \rightarrow \infty$
0.1	0.0690 $\beta^{-1/2}$	0.786	0.523	0.522	2.77	6.09	8.59	0.857 $\beta^{1/2}$
	1.33 $\beta^{1/2}$	0.132	0.287	0.393	2.29	2.51	2.17	28.0 $\beta^{-1/2}$
0.3	0.222 $\beta^{-1/2}$	2.31	1.19	0.973	2.08	4.38	6.14	0.609 $\beta^{1/2}$
	2.28 $\beta^{1/2}$	0.223	0.458	0.592	1.36	0.964	0.756	8.00 $\beta^{-1/2}$
0.5	0.400 $\beta^{-1/2}$	4.07	1.95	1.49	1.49	2.93	4.07	0.400 $\beta^{1/2}$
	4.00 $\beta^{1/2}$	0.383	0.733	0.885	0.885	0.519	0.383	4.00 $\beta^{-1/2}$
0.7	0.609 $\beta^{-1/2}$	6.14	2.83	2.08	0.973	1.69	2.31	0.222 $\beta^{1/2}$
	8.00 $\beta^{1/2}$	0.736	1.25	1.36	0.592	0.309	0.223	2.29 $\beta^{-1/2}$
0.9	0.857 $\beta^{-1/2}$	8.59	3.88	2.77	0.522	0.624	0.786	0.0690 $\beta^{1/2}$
	28.0 $\beta^{1/2}$	2.17	2.56	2.29	0.393	0.186	0.132	1.33 $\beta^{-1/2}$

^a For each volume fraction ϕ_1 the upper row lists the upper bound and the lower row lists the lower bound values for given $\beta = \lambda_2/\lambda_1$.

TABLE II: Tabulation of Randomly Overlapping Sphere Model Upper and Lower Bounds on $\lambda_e/(\lambda_1\lambda_2)^{1/2}$ from Eq 40 and 52^a

ϕ_1	$\beta \rightarrow 0$	$\beta = 0.01$	$\beta = 0.05$	$\beta = 0.1$	$\beta = 10$	$\beta = 50$	$\beta = 100$	$\beta \rightarrow \infty$
0.1	0.0465 $\beta^{-1/2}$	0.595	0.482	0.515	2.86*	6.32*	8.92*	0.891 $\beta^{1/2}$ *
	1.13 $\beta^{1/2}$ *	0.113*	0.252*	0.353*	2.20*	3.11	3.14	56.0 $\beta^{-1/2}$
0.3	0.187 $\beta^{-1/2}$	1.99	1.09	0.932	2.18*	4.63*	6.51*	0.647 $\beta^{1/2}$ *
	1.69 $\beta^{1/2}$ *	0.168*	0.361*	0.490*	1.40	1.20	0.969	11.4 $\beta^{-1/2}$
0.5	0.371 $\beta^{-1/2}$	3.80	1.86	1.45	1.49	2.91	4.03	0.395 $\beta^{1/2}$
	3.24 $\beta^{1/2}$ *	0.314*	0.626*	0.782*	0.915	0.591	0.445	4.77 $\beta^{-1/2}$
0.7	0.594 $\beta^{-1/2}$	6.00	2.79	2.06	0.875	1.36	1.82	0.171 $\beta^{1/2}$
	9.44 $\beta^{1/2}$	0.847	1.35	1.42	0.603	0.326	0.237	2.45 $\beta^{-1/2}$
0.9	0.855 $\beta^{-1/2}$	8.57	3.87	2.77	0.432	0.327	0.346	0.0228 $\beta^{1/2}$
	93.9 $\beta^{1/2}$	4.56	3.36	2.60	0.394	0.187	0.133	1.34 $\beta^{-1/2}$

^a For each volume fraction ϕ_1 the upper row lists the values of the upper bound and the lower row lists the corresponding values of the lower bound for given values of $\beta = \lambda_2/\lambda_1$. The Hashin-Shtrikman bound gives a better result for those bounds marked with an asterisk.

and the trial flux for a mixture of spheres that replaces (41) is

$$j^* = \lambda_1 A + \omega_1 \sum_{i_1} \lambda_{i_1} \nabla h_1(\rho_{i_1}) + \omega_2 \sum_{i_2} \lambda_{i_2} \nabla h_2(\rho_{i_2}) + \dots \quad (56)$$

where

$$h_\mu(\rho) = A \cdot \rho (a_\mu / \rho)^3 \quad \rho > a_\mu \\ = -2A \cdot \rho \quad \rho < a_\mu \quad (57) \\ \mu = 1, 2, \dots$$

Discussion of Results

That the resulting upper and lower bounds are clear improvements over the parallel and series results (1) is guaranteed by the trial functions (20) and (41) themselves for one could always set the parameters m and ω to zero at any stage of the calculations. The previously cited theorem of Hashin and Shtrikman asserts that the upper and lower bounds (2) provide respectively the least and greatest bounding values on the effective thermal conductivity that can be derived without considering statistical descriptions of the medium other than the void fraction. The success of our calculations then must be measured by the degree to which the randomly overlapping sphere bounds improve on the Hashin-Shtrikman bounds (2), and to this end we have listed some results from inequalities (2) in Table I. For each volume fraction ϕ_1 the upper row lists the upper bound and the lower row gives lower bound values for eight selected values of λ_2/λ_1 .

It has already been pointed out that the trial functions (20) and (41) used to calculate the upper (40) and lower bounds (52) will give the best results for the many important cases where the thermal conductivities λ_1 and λ_2 differ widely. With this in mind, in Table II we present those values for the upper and lower bounds on the thermal conductivity for a bed of randomly overlapping

spheres of phase two immersed in a matrix of phase one, that correspond to the values listed in Table I. For each volume fraction again the upper row lists the upper bounds and the lower row gives the lower bounds for a range of values of $\beta (= \lambda_2/\lambda_1)$. For those points marked with an asterisk, the Hashin-Shtrikman results give the better bound.

The upper bounds for randomly overlapping insulating spheres ($\beta \rightarrow 0$), originally presented by Weissberg,² are listed in the upper rows of the first column of Table II. For all values of the matrix fraction ϕ_1 , they show a clear improvement over the corresponding Hashin-Shtrikman results listed in Table I. The improvement of the upper bounds of Table II increases with decreasing ϕ_1 ; the best example is the decrease of the upper bound by 0.66 for the largest listed sphere fraction $\phi_1 = 0.1$. However we find in addition to Weissberg's bounds that the upper bound continues to give significant improvements even when $\beta = 0.01$ or 0.05. This result is of some importance for freeze-dried foods and insulating foams.

The lower bounds near the limit $\beta \rightarrow 0$ are only improved if the volume fraction ϕ_1 lies above 0.5. However, there are very strong improvements at low sphere fractions, indeed, for the case $\phi_1 = 0.9$ the lower bound of Table II is increased by a factor of 3.36 over the corresponding value in Table I. Again these trends continue to hold for $\beta = 0.01$ and 0.05. The practical effect of these improvements on the lower bound near $\beta \rightarrow 0$ is not great, because the lower bound, no matter how good, must vanish for insulating spheres. One possible outcome of the randomly overlapping sphere placement is that they completely block the slab, thus the lower bound on λ_e is zero for perfectly insulating spheres. The lower bound, concerned with fluctuations, must lie far below λ_e in the limit $\beta \rightarrow 0$, while the upper bound provides the estimate of λ_e .

A most interesting result is found when the lower bounds of Table II are examined near the limit of highly conducting spheres $\beta \rightarrow \infty$ and compared with the corre-

sponding lower bound results in the lower rows and last column of Table I. In contrast to Weissberg's upper bounds for insulating spheres, we find the lower bound on the conductivity (upper bound on the resistivity) gives large improvements over the Hashin-Shtrikman lower bounds for highly conducting spheres for all values of ϕ_1 . This improvement in the lower bound by Table II increases with decreasing ϕ_1 , the best value is a twofold increase at $\phi = 0.1$. Equation 52 still gives significant improvement when $\beta = 50$.

The reciprocal sense between the high and low thermally conducting spheres continues for the upper bound. Upon examination of the last column of Table II, we find the λ_e upper bound becomes very large for very highly conducting spheres (the lower bound on the resistivity vanishes for λ_2 very large), again this is due to fluctuations in the sphere distribution. Then only the lower bound can give an estimate of λ_e for perfectly conducting spheres. Furthermore, improvements in the upper bound for randomly overlapping spheres over the Hashin-Shtrikman bounds of Table I are only possible if the continuous phase volume fraction ϕ_1 lies above 0.3, and very strong improvements in the upper bounds, decreased by a factor of 3.03, are found near $\phi_1 = 0.9$.

For the larger values of ϕ_1 listed, both the upper and the lower bound are improved over those of Table I. As discussed in the introduction, trial thermal microgradients and the resulting bounds (40) and (52) will be most effective when the phase thermal conductivities differ widely (i.e., $\beta < 0.1$ and $\beta > 10$), and where the Hashin-Shtrikman bounds are weak. With the exception of the point $\beta = 10$, $\phi = 0.1$, bounds (40) and (52) always improve on either one or both of the Hashin-Shtrikman bounds within this region of interest.

The randomly overlapping sphere model has been assumed in order to obtain the additional statistical information to improve the Hashin-Shtrikman bounds.¹ Such a procedure is particularly meaningful if the model bears some resemblance to some important physical systems. It is expected that the use of sufficient statistical information would provide bounds on the effective thermal conductivity, which are sufficiently close to furnish useful predictions of some experimental results. Weissberg² demonstrated that the randomly overlapping sphere upper bound could give estimates of void diffusivities in a mixture of solid spheres. Another case of insulating spheres is freeze-dried food whose internal pore structure has been described⁵ as having "the appearance of an assembly of ping pong balls with smaller spheres imbedded in their surface to permit a continuous void phase". Freeze-dried food gains this appearance due to ice crystals that are sublimed out of the material.

For freeze-dried food or insulating plastic foams, the spheres (phase two) of the model are given the role of air voids, while the continuous phase (phase one) represents the solid. Variational results along with some values of the effective thermal conductivity of several freeze-dried foods and a polyurethane foam measured by Harper and El Sahrighi⁶ are listed for comparison in Table III. The measurements of Harper and El Sahrighi were taken at an average temperature T_{av} of 308 K. Radiative energy transport is rather small and is usually neglected at this temperature, however, when the gas phase conductivity is very low and the void fraction is high, radiation can make a second-order contribution to the effective thermal conductivity. Radiative transport was not included explicitly in the analysis, but in those instances where it should be included and its effects are not dominant, the

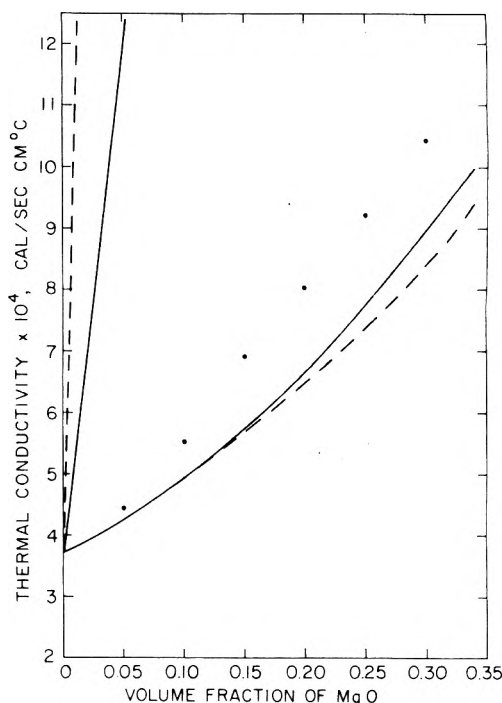


Figure 1. Thermal conductivity of a MgO-polystyrene suspension. The data points were taken by Sundstrom and Lee.⁷ The phase conductivity ratio, $\lambda_2/\lambda_1 = 354$. Upper and lower bound curves (—) from eq 40 and 52 as well as the Hashin-Shtrikman upper and lower bound curves (---) from eq 2 are also included on the plots.

addition to the gas phase conductivity of a simple Damkohler⁵-type radiation contribution

$$\lambda_r = 1.35 \times 10^{-12} \frac{4\epsilon \bar{d}}{2 - \epsilon} T_{av}^3 \frac{\text{cal}}{\text{cm}^2 \text{ s K}^4} \quad (58)$$

where the radiation emissivity ϵ is assumed to be 0.80, and \bar{d} , the average pore diameter is given in Table III, should approximately include radiation within the present model. These corrections are included within the sphere phase conductivities of Table III.

When the sphere phase is insulating the lower bound on the effective thermal conductivity must tend toward zero and vanish in the limit. We find as expected in Table III that the lower bound is not a good estimate of λ_e . However, the agreement of the upper bound within an average of 3.9% is good, particularly in the light of difficulties in the measurement of the air volume fraction and the solid conductivity. Comparison with the Hashin-Shtrikman upper bound (2) gives an average agreement of only 12.0%. The randomly overlapping sphere bounds successfully estimate the thermal conductivity in the difficult and extreme case $\lambda_2 \ll \lambda_1$ for the dense sphere problem, i.e., for sphere volume fractions as high as 0.86, 0.85, and 0.76.

Metal filled polymers provide an important case in the opposite extreme, where the sphere phase is highly conducting. Experimental data points taken by Sundstrom and Lee⁷ for MgO particles suspended in a polystyrene matrix with a phase thermal conductivity ratio $\lambda_2/\lambda_1 = 354$, and CaO dispersed in polyethylene with a ratio $\lambda_2/\lambda_1 = 45$ are shown in Figures 1 and 2, respectively. The solid lines refer to eq 40 and 52, the dashed lines represent the Hashin-Shtrikman bounds of eq 2. While both upper and lower bounds on the effective thermal conductivity are drawn, the upper bounds move rapidly off scale and, in contrast to insulating spheres, it is the lower bounds that give an estimate of the value. Both eq 52 and 2 predict the correct result for the pure polymer, as the CaO or MgO

TABLE III: Comparison of Random Sphere Model Bounds on the Effective Thermal Conductivity from Eq 40 and 52, and the Hashin-Shtrikman Upper Bound of Eq 2 with Measured Values for Insulating Spheres ($\lambda_2/\lambda_1 < 1$)^a

System	Obsd pore diameter, μm	Fraction sphere phase ϕ_2	Conductivity				System conductivity			% deviation	
			Sphere phase		Upper bound ^b $\lambda_{eu} \times 10^5$ (cal/cm)(s)(°C)	Lower bound ^c $\lambda_e \times 10^5$ (cal/cm)(s)(°C)	Hashin-Shtrikman upper bound ^d $\lambda_{eHS} \times 10^5$ (cal/cm)(s)(°C)	Measd $\lambda_e \times 10^5$ (cal/cm)(s)(°C)	Upper bound ^b $(\lambda_e - \lambda_{eu}) / (\lambda_e \times 100)$	Hashin-Shtrikman upper bound ^d $(\lambda_e - \lambda_{eHS}) / (\lambda_e \times 100)$	
			$\lambda_2 \times 10^5$ (cal/cm)(s)(°C)	$\lambda_1 \times 10^5$ (cal/cm)(s)(°C)							
N ₂ -freeze-dried beef	30-120	0.76	6.45	62	15.9	8.91	16.5	15.6	-1.8	-5.9	
CO ₂ -freeze-dried beef	30-120	0.76	4.20	62	13.5	5.92	14.5	13.4	-0.8	-8.4	
Freon 12-freeze-dried beef	30-120	0.76	2.42	62	11.5	3.47	12.9	11.9	+3.1	-8.8	
Vacuum-freeze-dried beef	30-120	0.76	0.08	62	8.78	0.12	10.9	8.93	+1.7	-21.6	
CO ₂ -freeze-dried apple	130-300	0.86	4.35	62	9.58	5.17	10.2	9.59	+0.1	-6.1	
Freon 12-freeze-dried apple	130-300	0.86	2.57	62	7.55	3.08	8.50	7.90	+4.5	-7.6	
Vacuum-freeze-dried apple	130-300	0.86	0.23	62	4.68	0.28	6.29	5.37	+12.9	-17.1	
Freon 12-polyurethane foam	200-600	0.85	2.76	23	4.93	3.29	5.00	5.08	+3.0	+1.5	
Vacuum-polyurethane foam	200-600	0.85	0.42	23	2.30	0.51	2.82	2.15	-7.1	-31.0	

^a Measurements are taken from Harper and El Sahrighi, ref 6. ^b Equation 40. ^c Equation 52. ^d Equation 2.

TABLE IV: Comparison of Random Sphere Model Bounds on the Effective Thermal Conductivity from Eq 40 and 52, and the Hashin-Shtrikman Lower Bound of Eq 2 with Measured Values for Conducting Spheres ($\lambda_2/\lambda_1 > 1$)

System	Fraction sphere phase ϕ_2	Conductivity				System conductivity			% deviation	
		Sphere phase		Upper bound ^a $\lambda_{eu} \times 10^2$ (cal/cm)(s)(°C)	Lower bound ^b $\lambda_{el} \times 10^5$ (cal/cm)(s)(°C)	Hashin-Shtrikman lower bound ^c $\lambda_{eHS} \times 10^5$ (cal/cm)(s)(°C)	Measd $\lambda_e \times 10^5$ (cal/cm)(s)(°C)	Lower bound ^b $(\lambda_e - \lambda_{el}) / (\lambda_e \times 100)$	Hashin-Shtrikman lower bound ^c $(\lambda_e - \lambda_{eHS}) / (\lambda_e \times 100)$	
		$\lambda_2 \times 10^2$ (cal/cm)(s)(°C)	$\lambda_1 \times 10^5$ (cal/cm)(s)(°C)							
Copper-epoxy suspension	0.45	91	54	30.5	215	186	240	+11	+22.5	8
Copper-epoxy suspension	0.60	91	54	47.4	380	296	390	+2.6	+24.1	9
H ₂ O-liquid lead shot packed bed	0.600	8.43	153.0	4.48	907	758	831	-9.1	+8.8	10
Glycerine-liquid lead shot packed bed	0.510	8.43	68.0	3.54	318	270	489	+35	+44.7	10
H ₂ -lead shot packed bed	0.600	8.43	46.0	4.41	308	245	335	+8.1	+26.9	10
Air-lead shot packed bed	0.690	8.43	6.24	5.35	66.5	47.6	162	+59	+70.6	10

^a Equation 40. ^b Equation 52. ^c Equation 2.

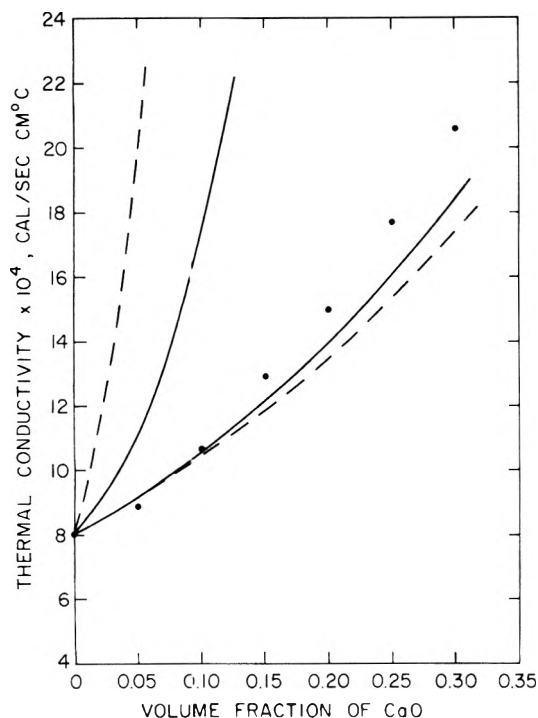


Figure 2. Thermal conductivity of a CaO-polyethylene suspension. The data points were taken by Sundstrom and Lee.⁷ The phase conductivity ratio $\lambda_2/\lambda_1 = 45$. Upper and lower bound curves (—) from eq 40 and 52 as well as the Hashin-Shtrikman upper and lower bound curves (---) from eq 2 are also included on the plots.

concentration increases the difference between the two curves increases. At a concentration of 30% eq 52 lies 11.0% below the data for CaO-polyethylene and 13.8% below the data of MgO-polystyrene, whereas the Hashin-Shtrikman result lies below the data by 15.5 and 19.3%, respectively, in each case. The difference is cut by about one-third for each curve.

Some additional thermal conductivity data for metal-filled polymers, and a few representative values for packed beds are given in Table IV. The lower bound continues to provide the best estimate of λ_e . For the copper-epoxy suspension data, the thermal conductivity ratios are very high $\lambda_2/\lambda_1 = 1.7 \times 10^3$, the right-hand column of Table II should provide values of λ_e . The agreement of eq 52 with experiment for these cases is apparent. With the exception of the H₂O liquid-lead shot system, eq 52 always predicts the effective thermal conductivity more accurately than the lower bound of Hashin and Shtrikman. The lead shot packed bed data are included to illustrate that the rigorous lower bounds of eq 52 continue to furnish useful estimates of λ_e in granular systems. However, for granular packings where the void conductivity is very small, contacts between the grains dominate heat transport. That our overlapping spheres model is not appropriate for such cases is evidenced by the large percent deviation of the air-lead shot data. Dul'nev and Sigalova¹¹ and Chan and Tien¹² among others have treated this problem in the literature.

The use of eq 40 and 52 to estimate effective thermal conductivities need not be restricted to the classes of experimental systems that we have considered. Van Kreveld and Van den Hold¹³ have successfully used randomly overlapping spheres to model silica gels for gel permeation chromatography. Amberlite resin beads¹⁴ prepared by controlled suspension polymerization appear

to be made up of overlapping solid spheres of precipitate of diameters as small as 10^{-4} mm. Van Eeklen¹⁵ argues the advantages of the randomly overlapping spheres as a model for catalysts. For these systems and others we would expect a useful estimate of λ_e from (52). Indeed the basic method of placing well defined shapes at random in a volume can be used in other geometries as well. For example, long copper wires of random orientation in a continuous phase of epoxy should model the data of Hansen and Tomkiewicz¹⁶ for the λ_e of their copper wire-epoxy suspensions. As is evidenced in the calculations that we have done, the method of placing well-defined shapes at random is simple and straightforward, yet the model is realistic enough to apply with reasonable success to experimental situations. In addition, the results presented here for thermal conductivity are also relevant to diffusion, magnetic permeabilities, and dielectric constants of heterogeneous materials.

The reciprocal upper (40) and lower bound (52) equations provide a unified theory of the effective thermal conductivity for certain two phase materials whose phase thermal conductivities differ widely. Estimates of the thermal conductivity through a bed of insulating spheres are provided by the upper bound, and good approximate values of the thermal resistivity through a bed of conducting spheres are given by the reciprocal lower bound. The bound that estimates λ_e is usually substantially better than the result of eq 2. Prager,¹⁷ Brown,¹⁸ and Beran¹⁹ have also suggested methods to improve on the bounds of Hashin and Shtrikman (2), based on three point correlations. The forms²⁰ of the necessary correlations for a randomly overlapping bed of spheres are known and could be used to calculate bounds for λ_e , but they are rather cumbersome.²¹ On the other hand, by reformulating the problem as we have done, the statistics required is greatly simplified. An application of the method of Brown and Beran to the random bed of overlapping spheres is in progress.

Acknowledgment. The authors express their appreciation to the National Science Foundation for support of this work under NSF Grant ENG 76-80783.

References and Notes

- (1) Z. Hashin and S. Shtrikman, *J. Appl. Phys.*, **33**, 3125 (1962).
- (2) H. L. Weissberg, *J. Appl. Phys.*, **34**, 2636 (1963).
- (3) R. Courant and D. Hilbert, "Methods of Mathematical Physics", Vol. 1, Interscience, New York, N.Y., 1953.
- (4) S. Prager, *J. Chem. Phys.*, **50**, 4305 (1969).
- (5) J. M. Smith, "Chemical Engineering Kinetics", McGraw-Hill, New York, N.Y., 1970.
- (6) J. C. Harper and A. F. El Sahrighi, *Ind. Eng. Chem., Fundam.*, **3**, 318 (1964).
- (7) D. W. Sundstrom and Y. Lee, *J. Appl. Polym. Sci.*, **16**, 3159 (1972).
- (8) J. Delmonte, "Metal Filled Plastics", Reinhold, New York, N.Y., 1961.
- (9) W. Colletti and L. Rebori, *Insulation (Libertyville, Ill.)*, **27** (1965).
- (10) T. E. W. Schumann and V. Voss, *Fuel*, **13**, 249 (1934).
- (11) G. M. Dul'nev and Z. V. Sigalova, *Int. Chem. Eng. Process Ind.*, **5**, 218 (1965).
- (12) C. K. Chan and C. L. Tien, *J. Heat Trans. ASME*, **95**, 302 (1973).
- (13) M. E. Van Kreveld and N. Van den Hold, *J. Chromatog.*, **83**, 111 (1973).
- (14) B. W. Stevens and J. W. Kerner, *Chem. Eng.*, **82**, 85 (1975).
- (15) H. A. M. Van Eekelen, *J. Catal.*, **29**, 75 (1973).
- (16) D. Hansen and R. Tomkiewicz, *Polym. Eng. Sci.*, **15**, 353 (1975).
- (17) S. Prager, *Physica*, **29**, 129 (1963).
- (18) W. F. Brown, *Trans. Soc. Rheology*, **9**, 35 (1965).
- (19) M. Beran, "Statistical Continuum Theories", Wiley, New York, N.Y., 1968.
- (20) W. Strieder and R. Aris, "Variational Methods Applied to Problems of Diffusion and Reaction", Springer-Verlag, Berlin, 1973.
- (21) M. Hori, *J. Math. Phys.*, **16**, 1772 (1975).

Superoxide Generation in the Photolysis of Aqueous Cadmium Sulfide Dispersions. Detection by Spin Trapping¹

John R. Harbour* and Michael L. Hair

Xerox Research Centre of Canada, 2480 Dunwin Drive, Mississauga, Ontario L5L 1J9, Canada (Received October 12, 1976; Revised Manuscript Received May 13, 1977)

Publication costs assisted by the Xerox Research Centre of Canada

Photoinduced electron transfer reactions of aqueous cadmium sulfide (CdS) dispersions in the presence of electron acceptors have been investigated. The technique of spin trapping has been successfully applied to the detection of the photoinduced formation of the superoxide ion which is formed when the CdS dispersion is irradiated. In addition, direct confirmation of electron transfer has been obtained by detection of the methyl viologen (MV) cation radical upon irradiation of the CdS dispersions containing MV^{2+} . In both cases substantial increases in radical production were observed when EDTA was present. Only light with $h\nu > E_{\text{band gap}}$ was effective in bringing about the photoreductions. The effect of surfactant adsorption on the photochemistry was also investigated. The results are interpreted using the band model for semiconductors.

Introduction

The interaction of light with semiconducting particles dispersed in a liquid medium can lead to useful photochemistry. The photochemical synthesis of hydrogen peroxide through illumination of aqueous zinc oxide dispersions is a well studied example in photocatalysis.² In addition, solar energy conversion systems have been demonstrated in which a semiconductor such as cadmium sulfide interfaces with an aqueous medium.³⁻⁵ In these systems light is absorbed by the semiconductor and this results in electron transfer across the solid-liquid interface which in conjunction with a second electrode (such as platinum) constitutes a cell capable of direct optical to electrical energy conversion. Although single crystals are mostly used for this technique, working cells have also been demonstrated using a film made from zinc oxide particles.⁶ The photographic imaging characteristics of photoactive pigments suspended in insulating fluids have also received commercial attention in the past decade and there are numerous references in the patent literature.⁷ Finally, biological systems such as chloroplast suspensions also undergo electron transfer across the solid-liquid interface upon illumination with light.⁸ All the above described systems involve an interfacial photochemistry resulting directly from the absorption of light by the particles in suspension.

Although the final products in many of the above systems are well identified, very little detail is known about the intermediates involved in the processes. Since photochemistry often proceeds through radical intermediates, ESR spectroscopy offers (in principle) an ideal method for the study of this type of interfacial photochemistry. Unfortunately, the lifetimes of many of the radicals produced are short-lived and this precludes their direct detection by conventional techniques. However, if a molecule can be determined which will react with the short-lived radical to form a more stable radical adduct, then such a molecule can be added to the system and the intermediate detected indirectly. This technique is known as "spin trapping"⁹ and it has been successfully applied to the study of photoinduced reactions between chloroplasts and molecular oxygen.⁸

It is the major objective of this work to demonstrate the feasibility of employing spin traps in the study of the photochemistry of pigment dispersions. Cadmium sulfide

was chosen as the pigment because of its well established photoactivity. Aqueous dispersions were studied both in the presence and absence of anionic and cationic surface active agents.

Experimental Section

The cadmium sulfide powder was received from both Fisher Scientific Co. (99.2%) and from Ventron (ultrapure) and used without further treatment. Methyl viologen (ICN-K&K Laboratories, Inc.) and ethylenediaminetetraacetic acid, disodium salt, EDTA (The British Drug Houses, Ltd.) were also used as received. Distilled water was redistilled from an all glass apparatus. 5,5-Dimethyl-1-pyrroline 1-oxide (DMPO)¹⁰ was used as spin trap and received from C. A. Evans and J. R. Bolton. It was purified prior to use by bulb-to-bulb distillation on a vacuum system and added directly to the dispersion (~0.1 M).

In all cases, the CdS particles were dispersed ultrasonically. The CdS concentration was varied from 1 to 5% by weight with greater concentrations giving rise to larger ESR signals. Illumination was accomplished in situ with a tungsten quartz-iodide lamp described elsewhere¹¹ or with a Hanovia Model 997B-1 KW Hg-Xe lamp in a Schoeffel Model LH 151N lamp housing with appropriate filters. ESR spectra were obtained on a Varian E12 electron spin resonance spectrometer.

Results

The aqueous CdS dispersion gave no ESR signals on addition of the spin trap (DMPO); however, upon illuminating with light ($\lambda < 520$ nm) a small ESR signal due to a spin adduct was observed. This signal is shown in Figure 1 and has $a^N = 14.1$ G, $a_\beta^H = 11.3$ G, $a_\gamma^H = 1.25$ G, and $g = 2.0061$. This is identical with the signal assigned to the O_2^-/O_2H adduct of DMPO.¹² If the same sample was exposed to O_2 gas rather than air an increase in signal intensity was observed upon illumination. When nitrogen purging was carried out, no photoinduced signal was observable. Hence a light induced reduction of oxygen to superoxide is occurring with the O_2^- being trapped by the DMPO.

Under the above conditions CdS surface is negatively charged (i.e., it has a negative surface potential as determined using a Rank Brothers microelectrophoresis

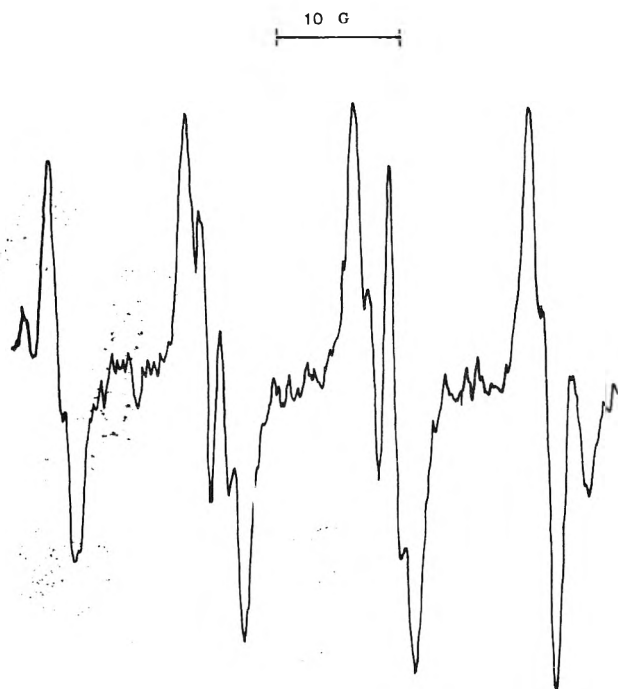


Figure 1. ESR spectrum generated upon illumination of an aqueous CdS dispersion in the presence of both DMPO and O_2 . The signal intensity is seen to increase with time (approximately 1 min has elapsed from the onset of illumination). Instrument settings are microwave power 10 mW; modulation amplitude 1.0 G; time constant 0.3 s, scan time 2 min.

apparatus). It is also negatively charged when an anionic surfactant, bis(2-ethylhexyl) sodium sulfosuccinate (AOT) is added to the suspension to improve dispersibility. However, addition of a cationic surfactant, cetyl trimethylammonium bromide (CTMAB), brings about a reversal of polarity. In an effort to determine if this surface potential is important in controlling the photochemistry, the initial experiments were repeated using either CTMAB or AOT as a surfactant in the dispersions. In both cases an oxygen-dependent, photoinduced O_2^- adduct was observed suggesting that the particle charge is not playing a key role in controlling this photoreduction. However, it is noted that when CTMAB was used as surfactant the ESR signals were more intense. Neither surfactant significantly altered the efficiency of O_2^- production (although increasing the dispersability) thus implying that adsorption of surfactant at the interface does not inhibit the photochemistry.

It was noted that addition of a good electron donor (EDTA) to the system caused a substantial increase in the photoproduction of O_2^- . As with the previous experiments the superoxide production was oxygen dependent and occurred only when molecular oxygen was present.

In order to directly detect the one electron reduction product in the CdS/ H_2O system it is necessary that molecular oxygen is replaced by a molecule whose reduced form is relatively stable. Methyl viologen is a water soluble substance which exists as a colorless dication in aqueous media and can form a stable blue radical cation¹³ upon one electron reduction, provided oxygen is absent. The redox potential of methyl viologen is -0.44 V (vs. NHE). When methyl viologen was added to the CdS dispersion under nitrogen purging conditions, illumination did indeed give rise to the MV^+ signal. If EDTA was also added to this system, the photoproduction of the MV^+ was significantly increased.

In all cases light of frequency less than the band gap (2.4 eV) of CdS was ineffective in bringing about this pho-

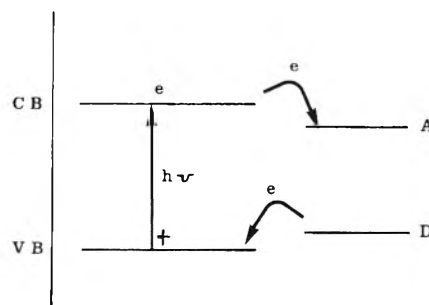


Figure 2. A photon ($h\nu$) of light causes the excitation of an electron from the valence band (VB) to the conduction band (CB). If the energy level of the acceptor (A) is below that of the CB then electron transfer can occur as indicated by the arrow. Similarly, if the donor (D) state is above that of the VB electron transfer to the hole can occur.

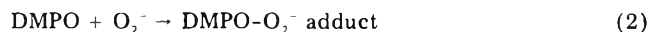
tochemistry. When light of $\lambda > 400$ nm was used with CdS absent, no radicals were observed upon illumination of either methyl viologen or DMPO (colorless) as expected. UV illumination of MV brought about MV^+ formation as already well documented.

Discussion

The results presented can be interpreted in terms of the band model for semiconductors. Light of wavelength less than the band gap (520 nm) excites an electron from the valence band (VB) to the conduction band (CB) giving rise to an electron-hole pair (Figure 2). If an acceptor (A) has an energy level less than that of the conduction band, then electron transfer from CB to A is possible. Such is the case for either O_2 or MV:



In the case where A is O_2 , then O_2^- is generated and subsequently trapped by the DMPO (eq 2). This implies



that the positive charge (hole) remains with the particle. When EDTA was added to the dispersion there was enhancement in the formation of A^- suggesting that this hole is neutralized through oxidation of EDTA. This returns the system to its original state thus allowing the particle to again be functional in the photoproduction of A^- . Hence, the CdS particles are acting in a catalytic role and in fact can be considered as a photocatalytic pump in which electrons are transferred from EDTA to O_2 or MV. Since no radicals were trapped from the oxidation of EDTA, either DMPO has a rate constant for reaction with this radical that is slow compared to the lifetime of the radical or the resulting adduct is inherently unstable. The mechanism probably involves decarboxylation.

It is interesting that surfactant adsorption does not prevent the electron transfer. In fact the primary charge on the surface as a result of surfactant adsorption does not significantly alter the efficiency of the photochemistry. However, the fact that apparent efficiencies are higher with a positive surface charge suggest that band bending¹⁴ may play a subsidiary role in the photochemistry (band bending creates a space charge region within the semiconductor which acts to separate the charges and can either enhance or retard electron transfer depending on the polarity of the surface charge).

Direct detection of a stable radical (MV^+) was also possible when O_2 was replaced with MV^{2+} . The fact that it behaves similarly to the O_2^- production as conditions are varied adds support to the fact that superoxide anions are indeed being generated. The redox potential of MV (-0.44 V)¹⁵ is more negative than that of O_2^- (-0.15 V)¹⁶ and in

fact O_2 will react spontaneously with MV^+ to form O_2^- . Both are lower than the energy level of the conduction band of CdS (-1.0 V)¹⁷ which is consistent with the mechanism outlined in Figure 2. In fact MV^+ production through visible light has been shown to be a means of hydrogen production with the aid of the enzyme hydrogenase.¹⁸ Hence it is noted that the present type of particulate system, with a suitable oxidizable species, could be used for photogeneration of hydrogen.

Conclusions

It has been demonstrated that spin trapping is a useful technique for the photochemical studies of pigment dispersions. Superoxide formation can be detected when CdS is used as pigment. EDTA enhances the photoformation of O_2^- and the results are consistent with the band model for semiconductors. In effect, CdS acts as a photocatalytic pump transferring electrons from EDTA to oxygen. Direct detection of the photoreduction of MV^{2+} is also possible and parallels the photochemistry of superoxide formation as conditions are varied. This system can, in fact, be used for the photoproduction of hydrogen. This technique has future application in mechanistic studies of photocatalysis and solar energy conversion devices using semiconductor electrodes as well as other systems (such as imaging devices) which employ photoactive pigments dispersed in liquid media.

Acknowledgment. We thank Professor James R. Bolton and the University of Western Ontario for the use of the ESR facilities.

References and Notes

- (1) Parts of this work were presented at the 173rd National Meeting of the American Chemical Society, New Orleans, La., Mar 20-25, 1977.
- (2) T. Freund and W. P. Gomes, *Catal. Rev.*, **3**, 1 (1969).
- (3) H. Gerisher, *J. Electro Anal. Chem. Interfacial Electrochem.*, **58**, 263 (1975).
- (4) M. S. Wrighton, D. S. Ginley, P. T. Wolczanski, A. B. Ellis, D. L. Morse, and A. Linz, *Proc. Natl. Acad. Sci. USA*, **72**, 1578 (1975).
- (5) A. B. Ellis, S. W. Kaiser, and M. S. Wrighton, *J. Am. Chem. Soc.*, **98**, 6855 (1976).
- (6) L. R. Weisberg, C. F. Grain, and R. R. Addiss Jr., *Appl. Phys. Lett.*, **27**, 440 (1975).
- (7) F. W. Schmidlin, *IEEE Trans. Electron Devices*, **ED-19**, 448 (1972).
- (8) J. R. Harbour and J. R. Bolton, *Biochem. Biophys. Res. Commun.*, **64**, 803 (1975).
- (9) E. G. Janzen, *Acc. Chem. Res.*, **4**, 31 (1971).
- (10) E. G. Janzen and J. I-Ping Liu, *J. Mag. Reson.*, **9**, 510 (1973).
- (11) J. T. Warden and J. R. Bolton, *J. Am. Chem. Soc.*, **95**, 6435 (1973).
- (12) J. R. Harbour, V. Chen, and J. R. Bolton, *Can. J. Chem.*, **52**, 3549 (1974).
- (13) J. S. Bellin, R. Alexander, and R. D. Mahoney, *Photochem. Photobiol.*, **17**, 17 (1973).
- (14) J. R. Harbour and M. L. Hair, manuscript in preparation.
- (15) A. A. Krasnovskii and G. P. Brin, *Dokl. Akad. Nauk, SSSR*, **16**, 761 (1965).
- (16) D. Meisel, *Chem. Phys. Lett.*, **34**, 263 (1975).
- (17) H. Meier, "Spectral Sensitization", Focal Press, New York, N.Y., 1968.
- (18) S. Markiewicz, M. S. Chan, R. H. Sparks, C. A. Evans, and J. R. Bolton, International Conference on the Photochemical Conversion and Storage of Solar Energy, London, Ontario, Canada, 1976.

COMMUNICATIONS TO THE EDITOR

Anion Radical of 2-Chlorothiophene. A σ^* Radical

Publication costs assisted by the Japan Atomic Energy Research Institute

Sir: In the course of our ESR studies of radicals produced by γ -irradiation of thiophene and its related compounds, we have detected the anion radical of 2-chlorothiophene which we believe is the first observation of a σ^* radical of the type >C-hal^- .

Single crystals of 2-chlorothiophene (mp -71.9°C) were grown at -110°C in Suprasil tubes using a technique which has been described previously.² As far as we are aware, the crystal structure of 2-chlorothiophene is not known. The single crystals and polycrystalline samples of 2-chlorothiophene were irradiated with cobalt-60 γ -rays in the dark at 77 K to a dose of 6 Mrd. ESR spectra were recorded at x-band with a Varian E-9 instrument.

Single crystals of 2-chlorothiophene after γ -irradiation showed a markedly anisotropic spectrum in the dark at 77 K. Figure 1 shows typical spectra obtained at two crystal orientations with respect to the magnetic field differing 90° in the rotation plane perpendicular to the tube axis (z). The strong signals present in the central part are mostly due to the defects produced in the sample tube, and not discussed here. Spectrum a in Figure 1 consists of a quartet at $g = 2.0064$ with a hyperfine splitting value of 35.5 G, the width of each line being 11~13 G. Spectrum

b is the best-resolved one in the rotation plane and consists of four groups with substructures. The substructures present in the outer groups are different from those in the inner groups, indicating that the spectrum consists of at least two sets of quartets with different primary splitting values and with additional splittings. By assuming that spectrum b consists of two sets of quartets and each line of the quartets is split to a quartet which is seen in the outer groups, primary splitting values of 84 and 70 G can be obtained for both quartets as shown by the stickplot below the spectra in Figure 1. The ratio of these splitting values (1.2) agrees well with that of the magnetic moments of ^{35}Cl and ^{37}Cl nuclei, and the quartet splittings are ascribed to the hyperfine interaction with chlorine nuclei. The intensity ratio of both quartets is roughly 3, which is also in good agreement with the ratio of the natural abundance of the two nuclei (3.07).

In other orientations, the observed spectra were very complex and ill-resolved partly due to the presence of two nonequivalent sites. The angular variation of the spectrum, however, indicates that the primary splitting values of 35 and 84 G obtained from spectra a and b in Figure 1 are the minimum and maximum, respectively, for the ^{35}Cl splitting in the rotation plane. Moreover, these values are found to be the principal values, A_\perp and A_\parallel , of the axially symmetric hyperfine tensor of ^{35}Cl by comparison with the

PHYSICAL PHENOMENA

spectroscopy,
thermodynamics,
reaction kinetics,
and other areas
of experimental
and theoretical
physical chemistry
are covered
completely in

THE JOURNAL OF PHYSICAL CHEMISTRY

The biweekly JOURNAL OF PHYSICAL CHEMISTRY includes over 25 papers an issue of original research by many of the world's leading physical chemists. Articles, communications, and symposia cover new concepts, techniques, and interpretations. A "must" for those working in the field or interested in it, the JOURNAL OF PHYSICAL CHEMISTRY is essential for keeping current on this fast moving discipline. Complete and mail the coupon now to start your subscription to this important publication.

AVAILABLE IN HARD COPY
OR MICROFICHE.

The Journal of Physical Chemistry American Chemical Society

1155 Sixteenth Street, N.W.
Washington, D.C. 20036

1977

Yes, I would like to receive the JOURNAL OF PHYSICAL CHEMISTRY at the one-year rate checked below:

	U.S.	Foreign and Canada	Latin America
ACS Member*	<input type="checkbox"/> \$24.00	<input type="checkbox"/> \$34.00	<input type="checkbox"/> \$33.00
Nonmember	<input type="checkbox"/> \$96.00	<input type="checkbox"/> \$106.00	<input type="checkbox"/> \$105.00
Bill me <input type="checkbox"/>	Bill company <input type="checkbox"/>	Payment enclosed <input type="checkbox"/>	

Air freight rates available on request.

Name _____

Street _____

Home
Business

City _____

State _____

Zip _____

Journal subscriptions start in January '77.
Allow 60 days for your first copy to be mailed.

*NOTE: Subscriptions at ACS member rates are for personal use only.

Chemical and Biochemical Applications of Lasers

VOLUME 2

Edited by C. BRADLEY MOORE

CONTENTS: *D. H. Levy*, Laser Spectroscopy in Supersonic Jets. *F. Legay*, Vibrational Relaxation in Matrices. *A. Laucereau and W. Kaiser*, Picosecond Investigations of Dynamic Processes in Polyatomic Mole-

cules in Liquids. *R. D. Levine and A. Ben-Shaul*, Thermodynamics of Molecular Disequilibrium. *B. R. Ware*, Applications of Laser Velocimetry in Biology and Medicine. *J. J. Ewing*, New Laser Sources.

1977, 298 pp., \$15.00/£10.65 ISBN: 0-12-505402-5

Advances in Magnetic Resonance

VOLUME 9

Edited by JOHN S. WAUGH

CONTENTS: *P. D. Sullivan and E. M. Menger*, Temperature-Dependent Splitting Constants in the ESR Spectra of Organic Free Radicals. *T. A. Miller and R. S. Freund*, Magnetic Resonance Induced by Electrons: Studies of the Simplest Atomic and Molec-

ular Systems. *L. G. Werbelow and D. M. Grant*, Intramolecular Dipolar Relaxation in Multispin Systems. *C. L. Khetrapal and A. C. Kunwar*, NMR Studies of Molecules Oriented in Thermotropic Liquid Crystals.

1977, 448 pp., \$44.00/£31.25 ISBN: 0-12-025509-X; also available
Library Edition with Microfiche, \$57.00/£40.45 ISBN: 0-12-025577-6
Microfiche only, \$31.00/£22.00 ISBN: 0-12-025577-4

Advances in Quantum Chemistry

VOLUME 10

Edited by PER-OLOV LOWDIN

CONTENTS: *P. Coppens and E. D. Stevens*, Accurate X-Ray Diffraction and Quantum Chemistry: the Study of Charge Density Distributions. *P. Kaijser and V. H. Smith, Jr.*, Evaluation of Momentum Distributions and Compton Profiles for Atomic and Molecular Systems. *H. Kleinpoppen*, Analysis

of Electron-Atom Collisions. *J. Katriel and R. Pauncz*, Theoretical Interpretation of Hund's Rule. *B. H. Brandow*, Linked-Cluster Perturbation Theory for Closed- and Open-Shell Systems. *B. Pullman*, Quantum-Mechanical Approach to the Conformational Basis of Molecular Pharmacology.

1977, 352 pp., \$34.50/£24.50 ISBN: 0-12-034810-1

Advances in Physical Organic Chemistry

VOLUME 14

Edited by V. GOLD

Associate Editor: D. BETHELL

CONTENTS: *T. W. Bentley and P. von R. Schleyer*, Medium Effects on the Rates and Mechanisms of Solvolytic Reactions. *A. Pross*, The Reactivity-Selectivity Principle and its Mechanistic Applications. *E. Bunce and H.*

Wilson, Physical Organic Chemistry of Reactions in Dimethyl Sulphoxide. *M. J. Blandamer*, Kinetics of Organic Reactions in Water and Aqueous Mixtures.

1977, 384 pp., \$31.25/£16.00 ISBN: 0-12-033514-X

Journal of Magnetic Resonance

Editor: WALLACE S. BREY, JR.

Since it first appeared in 1969, the *Journal of Magnetic Resonance* has established itself as a leading source of up-to-date, authoritative information on the theory, techniques, methods of spectral analysis, and results of magnetic resonance spectroscopy.

It presents important original papers not only in both nuclear and electron magnetic resonance, but also in such related fields as quadrupole resonance, cyclotron resonance, the Mössbauer effect, and magnetic properties of the solid state.

Volume 25-28, 1977 (Monthly) Institutional subscription rate.
U.S.A. \$186.00; All other countries: \$215.00 (Prices include postage)
All journal subscriptions are payable in advance.

Send payment with book order and save postage plus 50¢ handling charge.
Prices are subject to change without notice.

ACADEMIC PRESS, INC.

A Subsidiary of Harcourt Brace Jovanovich, Publishers
111 FIFTH AVENUE, NEW YORK, N.Y. 10003
24-28 OVAL ROAD, LONDON NW1 7DX